UNIVERSITY OF ALBERTA

MODELLING BREAKUP ON THE MACKENZIE RIVER NEAR FORT PROVIDENCE, NWT

BY

WEI CUI ©

A THESIS
SUBMITTED TO THE FACULTY OF GRADUATE AND RESEARCH IN
PARTIAL FULFILLMENT OF THE REQUIREMENT FOR THE DEGREE
OF MASTER OF SCIENCE
IN
WATER RESOURCES ENGINEERING

DEPARTMENT OF CIVIL ENGINEERING

EDMONTON, ALBERTA
SPRING, 1996

National Library
of Canada

Acquisitions and
Bibliographic Services Branch

395 Wellington Street
Ottawa, Ontario
K1A 0N4

Bibliothèque nationale
du Canada

Direction des acquisitions et
des services bibliographiques

395, rue Wellington
Ottawa (Ontario)
K1A 0N4

Your file Votre référence

Our file Notre référence

The author has granted an irrevocable non-exclusive licence allowing the National Library of Canada to reproduce, loan, distribute or sell copies of his/her thesis by any means and in any form or format, making this thesis available to interested persons.

L'auteur a accordé une licence irrévocable et non exclusive permettant à la Bibliothèque nationale du Canada de reproduire, prêter, distribuer ou vendre des copies de sa thèse de quelque manière et sous quelque forme que ce soit pour mettre des exemplaires de cette thèse à la disposition des personnes intéressées.

The author retains ownership of the copyright in his/her thesis. Neither the thesis nor substantial extracts from it may be printed or otherwise reproduced without his/her permission.

L'auteur conserve la propriété du droit d'auteur qui protège sa thèse. Ni la thèse ni des extraits substantiels de celle-ci ne doivent être imprimés ou autrement reproduits sans son autorisation.

ISBN 0-612-10701-9

Canada

UNIVERSITY OF ALBERTA

RELEASE FORM

NAME OF AUTHOR: WEI CUI

TITLE OF THESIS: MODELLING BREAKUP ON THE MACKENZIE RIVER NEAR FORT PROVIDENCE, NWT

DEGREE: MASTER OF SCIENCE

YEAR THIS DEGREE GRANTED: 1996

Permission is hereby granted to the University of Alberta library to reproduce single copies of this thesis and to lend or sell such copies for private, scholarly or scientific research purposes only.

The author reserves all other publication and other rights in association with the copyright in the thesis, and except as herein before provided, neither the thesis nor any substantial portion thereof may be printed or otherwise reproduced in any material form whatever without the author's prior written permission.

Wei Cui

Wei Cui

#103, 10710-85th Avenue
Edmonton, Alberta
Canada T6E 2K8

Date: Dec. 21, 1995

UNIVERSITY OF ALBERTA

FACULTY OF GRADUATE STUDIES AND RESEARCH

The undersigned certify that they have read, and recommend to the faculty of Graduate Studies and Research for acceptance, a thesis entitled MODELLING BREAKUP ON THE MACKENZIE RIVER NEAR FORT PROVIDENCE, NWT submitted by WEI CUI in partial fulfillment of the requirements for the degree of MASTER OF SCIENCE in WATER RESOURCES ENGINEERING.

F.E. Hicks

Dr. F. E. Hicks (Supervisor)

Martin Sharp

Dr. Martin Sharp (External Examiner)

Gan Thian Yew

Dr. T.Y. Gan

Date: Dec. 20, 1995

Abstract

Our present knowledge of forecasting river ice breakup is still relatively site specific and the most effective models are still heavily dependent upon documented patterns of breakup empirically correlated with meteorological and hydraulic data.

This investigation considered the site just downstream of Great Slave Lake where spring breakup delays recommissioning of the ferry of Fort Providence crossing the Mackenzie River. This leads to an interruption in service after the winter ice bridge closes. Upstream of the ferry crossing breakup is predominantly thermal and in the ferry reach itself, breakup is dynamic.

Useing data collected in 1992 to 1995, the thermal breakup in the upstream reach was modelled with an energy budget and a conceptual, linear heat transfer approaches. With limited data, the simpler, conceptual approach provided excellent results with calibrated parameters that are consistent from year to year.

Four mechanisms of ice cover failure under imposed loads were considered in the dynamic reach. The results show that none of these dynamic models of breakup has much application potential and until more sophisticated models of breakup are developed, forecasts will likely continue to be largely based on site specific breakup patterns.

ACKNOWLEDGMENTS

The author would like to thank Mr. Tony MacAlpine, Director of Marine Operations, Marine Services Division, Government of the Northwest Territories, who supervised the contract and who provided guidance and support in its performance. Thanks are also extended to Mr. Greg Whitlock, Marine Superintendent, Marine Services Division, Mr. Michel Lanteigne, Project Engineer, Transportation Engineering Division and Ms. Robyn McGregor, Transportation Planning Engineer, Transportation Planning Division, for their assistance in the field and their advice on the project. The author would also like to thank the ferry captains and staff, who provided information on conditions, in particular Mr. Audi Steinwand and Mr. Come Deshaies, who provided assistance in the field throughout both the spring breakup observations and the summer surveys in 1992.

Thanks are also extended the following people who supplied data and/or equipments for this study. They are Mr. Murray Jones of NWT Programs, Inland Water Directorate, Ft. Smith, Mr .Paul Squires of NWT Programs, Inland Water Directorate, Yellowknife. Mr. R. Scott MacDonald, Head of Operations for Water Survey of Canada, NWT Programs, Inland Water Directorate, Yellowknife. Mr. Gerard Langevin of the Atmospheric Environment Service, Ms. Evelyn Krutko of the Natural Resources Department of the GNWT, Dr. Terry Prowse of the National Hydrology Research Institute (NHRI), Saskatoon, Saskatchewan, Mr. Ted Malewski of Air Providence Ltd., Mr. Bruce Wentzell, Line Pilot with Aero Arctic Helicopter Services and Mr. Bob O'Conner of Aero Arctic.

The author would also like to thank Mr. Sheldon Lovell of Civil Engineering Department, University of Alberta for field data collection, Mr. David, D. Andres, President of Trillium Engineering and Hydrographics Inc., for his valuable advice, Mr. Xiaobing Chen, former Graduate Student and Dr. Thian Yew Gan, Associate Professor of the Civil Engineering Department, University of Alberta, for their advice and help. The author would like to thank his thesis external examiner Dr. M. Sharp, Associate Professor of the Department of Earth and Atmospheric Sciences, University of Alberta, for his kindly help. Thanks are also extended to Mr. Bermard Trevor of Trillium Engineering and Hydrographics Inc., Dr. Arbind Mainali, Research Associate and Sessional Lecturer, Dept. of Civil Engineering, University of Alberta, Lianne Lefsrud, John Take, Greg Sikora, Lisa Pooke and Stacy Mikolajczyk.

The author would like to thank his thesis supervisor and graduate program advisor, Dr. Faye E. Hicks, in a special way. The countless hours and the untiring effort she spent in guiding my research to a successful completion is much appreciated.

Lastly but not the least, I wish to acknowledge my heart felt gratitude to my beloved wife, Anjiang Wang, for her unfailing support and love, and for always being around when time is bleak.

TABLE OF CONTENTS

ABSTRACT

ACKNOWLEDGMENTS

TABLE OF CONTENTS

LIST OF TABLES

LIST OF FIGURES

LIST OF SYMBOLS

1.0 INTRODUCTION 1

2.0 REACH DESCRIPTION AND DATA COLLECTION PROGRAM 4

2.1 Description of Study Reach 4

2.2 Historical Data 5

2.2.1 Introduction 5

2.2.2 Streamflow Data 5

2.2.3 Meteorological Data 6

2.2.4 Ice Regime 6

2.2.5 Ferry and Ice Bridge Operation 7

2.2.6 Discussion of Historical Data 7

2.3 Field Observation Program 7

2.3.1 Introduction 7

2.3.2 Meteorological Data 8

2.3.2.1 Introduction 8

2.3.2.2 Solar Insolation 9

2.3.2.3 Air Temperature 11

2.3.2.4 Relative Humidity 12

2.3.2.5 Wind Speed 13
2.3.3 Other Data Related to Open Water Development 13
2.3.3.1 Introduction 13
2.3.3.2 Water Temperature Data 13
2.3.3.3 Ice Characteristics and Snow Depths 16
2.3.4 Hydraulic Data 18
2.3.4.1 General 18
2.3.4.2 Geometric Data 18
2.3.4.3 Discharge Data 21
2.3.4.4 Water Level Measurements 22
2.3.4.5 Indirect Discharge Determination 25
2.3.4.6 Estimating Discharge during Breakup 28
2.3.4.7 Calibration of the Pre-Breakup Ice Roughness through Providence Rapids 29
2.3.5 Nature of Breakup 30
2.3.5.1 Introduction 30
2.3.5.2 Breakup in the Ferry Reach 30
2.3.5.3 Breakup in Beaver Lake 33

3.0 FORMULATION OF THE BREAKUP MODELS 76
3.1 Introduction 76
3.2 Modelling the Development of Open Water at Great Slave Lake/Beaver Lake 76
3.2.1 Introduction 76
3.2.2 Energy Budget Approach 77
3.2.2.1 Introduction 77
3.2.2.2 Formulation 78
3.2.2.3 Model Application 93

3.2.2.4 Discussion of Results 96
3.2.3 Conceptual (Radiation-Temperature) Approach 97
3.2.3.1 Formulation 97
3.2.3.3 Model Application 101
3.2.3.3 Discussion of Results 102
3.3 Modelling the First Movement of Ice at Providence Narrows 103
3.3.1 Introduction 103
3.3.2 Quantifying Ice Deterioration 104
3.3.2.1 Introduction 104
3.3.2.2 Nature of Solar Radiation Absorption by an Ice Cover 105
3.3.2.3 Quantifying the Porosity of the Ice C 107
3.3.2.4 Ice Strength Reduction 109
3.3.3 Forces Acting on the Ice Cover 113
3.3.3.1 Introduction 113
3.3.3.2 Shear Stress on the Underside of the Ice Cover 113
3.3.3.3 Weight of the Ice Cover 116
3.3.4 Compression Failure 117
3.3.4.1 Formulation 117
3.3.4.2 Model Application 118
3.3.5 Shear Failure 120
3.3.5.1 Formulation 120
3.3.5.2 Model Application 122
3.3.6 Buckling Failure 123
3.3.6.1 Formulation 123
3.3.6.2 Model Application 125
3.3.7 Discussion of Results 126
3.3.7.1 Introduction 126

3.3.7.2 Variation in Measured Variables 126
3.3.7.3 Failure Criteria 127
3.3.7.4 Summary 129

4.0 CONCLUSIONS AND RECOMMENDATIONS 170
4.1 Thermal Models of Breakup: Beaver Lake Reach 170
4.1.1 Energy Budget Approach 170
4.1.2 Conceptual Linear Heat Transfer Approach 171
4.2 Dynamic models of Breakup: Ferry Reach 172
4.2.1 Models of Ice Deterioration 172
4.2.2 Criteria for Ice Cover Failure 173

REFERENCES 175

LIST OF TABLES

Table 2.1 Ice records for the Mackenzie River at Ft. Providence (Lat. 61°20', Long. 117°40') 35

Table 2.2 Spring ice bridge and ferry operations (1962–1995) 36

Table 2.3 Mean daily insolation measured at Ft.Providence, 1992 to 1995 37

Table 2.4 Mean daily temperatures measured at Ft.Providence, 1992 to 1995 38

Table 2.5 Mean daily RH measured at Ft.Providence, 1992 to 1995 39

Table 2.6 Mean daily wind speed measured at Ft.Providence, 1992 to 1995 40

Table 2.7 (a) Temperature profiles measured in Great Slave Lake, 1992 41

(b) Estimate of corrected emperature rofiles in Great Slave Lake, 1992 41

Table 2.8 Water temperatures measured in the downstream reach, 1993 and 1994 42

Table 2.9 (a) Depth of snow on the rough ice cover (m) - Mackenzie River, 1992 43

(b) Depth of snow on the border ice cover (m) - Mackenzie River, 1992 43

Table 2.10 (a) Depth of snow on the rough ice cover (m) - Mackenzie River, 1993 44

(b) Depth of snow on the border ice cover (m) - Mackenzie River, 1993 44

Table 2.11 (a) Depth of snow on the rough ice cover (m) - Mackenzie River, 1994 45

(b) Depth of snow on the border ice cover (m) - Mackenzie River, 1994 45

Table 2.12 Depth of snow on the rough ice cover (m) - Mackenzie River, 1995 46

Table 2.13 (a) Rough ice thickness (m) - Mackenzie River, 1992 47

(b) Border ice thickness (m) - Mackenzie River, 1992 47

Table 2.14 (a) Rough ice thickness (m) - Mackenzie River, 1993 48

(b) Border ice thickness (m) - Mackenzie River, 1993 48

Table 2.15 (a) Rough ice thickness (m) - Mackenzie River, 1994 49

(b) Border ice thickness (m) - Mackenzie River, 1994 49

Table 2.16 (a) Rough ice thickness (m) - Mackenzie River, 1995 50

(b) Border ice thickness (m) - Mackenzie River, 1995 50

Table 2.17 Key water levels at the ferry crossing, 1992 to 1994. 51

Table 2.18 Calibration of hydraulic model for the Mackenzie River between Great Slave Lake and Mills Lake, 11-Jul-92..........................52

Table 2.19 Verification of hydraulic model for the Mackenzie River between Beaver Lake and Ft. Prov., 29-Aug-91. 52

Table 2.20 Calibration of hydraulic model for the Mackenzie River between Great Slave Lake and Big River, April 1992. 53

Table 2.21 Calibration of hydraulic model for the Mackenzie River between Great Slave Lake and Big River, April 1993. 53

Table 2.22 Calibration of hydraulic model for the Mackenzie River between Great Slave Lake and Big River, April 1994. 54

Table 2.23 Calibration of hydraulic model for the Mackenzie River between Great Slave Lake and Big River, April 1995. 54

Table 2.24 Timing of key breakup events, 1992 to 1995. 55

Table 2.25 Development of open water area on the Mackenzie River upstream of Burnt Point, 1992 to 1995..56

Table 3.1 Albedo of various surface for short-wave radiation (Maidment, 1993)..... 130

Table 3.2 Various values of constants for Brunt's formula (Anderson, 1954). 130

Table 3.3 Values of the fraction of sky cover used in this study....................... 131

Table 3.4 Roughness heights on different surfaces (Eagleson, 1970). 131

Table 3.5 Twenty year average atmospheric pressures for NWT sites (DFO, 1981). 131

Table 3.6 Typical value of snow density (Maidment, 1993). 132

Table 3.7 Nature ice density at ice bridge cross section (Department of Transportation, NWT, 1992). 132

Table 3.8 The values of constants in simulation. 133

Table 3.9 Initial conditions in thermal breakup simulation. 133

Table 3.10 Measured late winter ice thickness and initial ice thicknesses used in simulation. 134

Table 3.11 Variances of simulations under different h_i and h_w. 135

Table 3.12 Values of μ and ν as functions of the state of ice. 136

Table 3.13 Ice strength measured in the natural ice adjacent to the ice bridge in 1989 and 1991. 137

Table 3.14 Strength ratio at Providence rapids, apportioned solar radiation used. 138

Table 3.15 Compression force calculation. 139

Table 3.16 Compression strength and stress ratio, based on apportioned soalr radiation used. 140

Table 3.17 Shear force calculation by the crack shear resistance approach. 141

Table 3.18 The ratio of the crack shear resistance to the shear stress. 142

Table 3.19 Shear force calculation by the reuced shear strength approach. 143

Table 3.20 The ratio of shear strength and shear stress, based on apportioned solar radiation. 144

Table 3.21 Buckling failure calculation. 145

Table 3.22 The ratio of the buckling resistance to the load forces. 146

LIST OF FIGURES

Figure 2.1 Location of study reach 57

Figure 2.2 Location of cross sections and temporary benchmarks on the Mackenzie River near Ft. Providence. 58

Figure 2.3 (photograph) The Mackenzie River looking upstream to the Ft. Providence ferry crossing. 59

Figure 2.4 (photograph) The WSC gauge house on the berm at the south bank at the ferry crossing. 59

Figure 2.5 Comparison of daily insolation values obtained with hourly measurements to those based on a measurement interval of 30 minutes 60

Figure 2.6 Duration of bright sunshine vs. daily insolation at Ft. Providence, spring 1992 and 1993 61

Figure 2.7 Comparison of mean daily temperatures measured at various sites near Ft. Providence, spring 1992 62

Figure 2.8 Comparison of mean daily temperatures obtained with hourly measurements to those based on a measurement interval of 30 minutes 63

Figure 2.9 Comparison of mean daily temperatures obtained with the sheltered thermistor and those measured with the temperature sensor internal to the datalogger, spring 1992 and 1993 64

Figure 2.10 Automated water temperature measurements at the Great SLave Lake TBM, 1992 65

Figure 2.11 (a) Water temperature profile measured in Great Slave Lake, 7-Apr-93. 66

(b) Water temperature profile measured in Great Slave Lake, 16-Mar-94. 66

(c) Water temperature profile measured in Great Slave Lake, 20-Apr-95 66

Figure 2.12 RAMSET® nail penetrations in the border and rough ice, 1992 and 1993 67

Figure 2.13 Stage hydrographs measured at the ferry crossing, 1991 to 1994 68

Figure 2.14 Calibration of hydraulic model for the Mackenzie River between Great Slave Lake and Mills Lake, 11-Jul-92. 69

Figure 2.15 Verification of hydraulic model for the Mackenzie River between Beaver Lake and Ft. Prov., 29-Aug-91 69

Figure 2.16 Measured and calculated discharges through the breakup period, 1992 to 1995. 70

Figure 2.17 Great Slave Lake spring water levels, 1992 to 1995. 71

Figure 2.18 (photograph) Overflow from open water leads, looking upstream to Providence Island 72

Figure 2.19 (photograph) Initial movement of ice in the ferry reach, looking downstream to Providence Narrows. 72

Figure 2.20 (photograph) Looking south to the Mackenzie River at the ferry crossing. The path of the ferry passage channel is evident in the ice cover texture 73

Figure 2.21 (photograph) Looking north shortly after failure of the ferry passage channel, May 1992. 73

Figure 2.22 (photograph) Typical pattern of open water development in the South Channel. 74

Figure 2.23 (photograph) Typical pattern of open water development in the North Channel. 74

Figure 2.24 Development of open water area on the Mackenzie River upstream of Burnt Point, 1992 to 1995. 75

Figure 3.1 Heat components acting on ice surface and water body 147

Figure 3.2 Surface albedo calibration of the Energy Budget approach by individual year, 1993 148

Figure 3.3 Surface albedo calibration of the Energy Budget approach by individual year, 1994 149

Figure 3.4 Surface albedo calibration of the Energy Budget approach by individual year, 1995 150

Figure 3.5 Variances, Δ^2, for the calibration of the Energy Budget approach by individual year 151

Figure 3.6 Typical Surface albedo calibration, E. B. approach Case A 152

Figure 3.7 Typical Surface albedo calibration, E. B. approach Case B 153

Figure 3.8 Typical Surface albedo calibration, E. B. approach Case C. 154

Figure 3.9 Variances, Δ^2, for the calibration of the E. B. approach, albedo. 155

Figure 3.10 (a) Longwave radiation heat change with the temperature difference between the air and the surface. 156

(b) Convective heat change with the temperature difference between the air and the surface. 156

Figure 3.11 (a) Simulation of open water area development by conceptual model, Case A ($h_i = 8$; $h_w = 20$). 157

(b) Simulation of open water area development by conceptual model, Case A ($h_i = 12$; $h_w = 10$). 158

Figure 3.12 (a) Simulation of open water area development by conceptual model, Case B ($h_i = 8$; $h_w = 20$). 159

(b) Simulation of open water area development by conceptual model, Case B ($h_i = 12$; $h_w = 10$). 160

Figure 3.13 (a) Simulation of open water area development by conceptual model, Case C ($h_i = 8$; $h_w = 20$). 161

(b) Simulation of open water area development by conceptual model, Case C ($h_i = 12$; $h_w = 10$). 162

Figure 3.14 The relationship of Ferry channel breakup and Providence rapids breakup. 163

Figure 3.15 Solar radiation absorbed in an ice cover, Borisenkov (1970). 164

Figure 3.16 Solar radiation penetrating an ice cover, Bulatov (1970). 164

Figure 3.17 Absorbed radiation in different depth of ice cover. 165

Figure 3.18 Strength reduction with increase in absorbed radiation, Bulatov (1970). 166

Figure 3.19 (a) Strength reduction with increase of porosity. 167

(b) Comparison of strength reduction models with field measurements. 167

Figure 3.20 The reduction of the strength ratio, based on apportioned solar radiation. 168

Figure 3.21 Comparison of the ratios obtained by the various failure mechanisms. 169

Figure 3.22 Lead time provide by the various approaches. 169

LIST OF SYMBOLS

A_w = The total open water area at end of day, in m^2;

$\tilde{A}_w$ = average open water area, in m^2;

A_w^j = the total open water area at end of day j, in m^2;

A_w^{j-1} = open water area at the end of day which is one day before simulated day, in m^2;

a = constant in Brunt's equation;

b = constant in Brunt's equation;

c = empirical parameter in Bulatov's radiation penetration equation;

c_1 = psychrometric constant;

C = a fraction of sky covered;

C_p = specific heat of water, in J/kg °C;

E_{ei} = the heat loss or gain by evaporation or condensation on per unit area of ice .cover;

E_{hi} = the convective heat on per unit area of ice cover, in J/m^2;

E_{li} = the longwave radiation heat exchange between the ice surface and the atmosphere on per unit area of ice cover, in J/m^2

E_R = the accumulated radiation heat absorbed in unit volume of ice, in J/m^3;

E_{Ro} = total heat absorbed in unit volume of ice at the time current strength reaching to zero, in J/m^3;

E_{si} = the short-wave radiation heat on per unit area of ice cover, in J/m^2;

e_a = vapor pressure of air, in millibar;

e_{tw} = the vapor pressure on water surface, in millibar;

e_{ti} = the vapor pressure on ice surface, in millibar;

F_b = limited buckling force on per unit width of ice cover, in N/m;

F_l = the force due to the loads on per unit width of ice cover, in N/m;

F_n = the force difference between the applied forces and the bank reactions per unit length, in N/m;

F_w = the force due to weight of ice cover, in Newton;

F_τ = the force due to shear stress underside of ice cover, in Newton;

g = acceleration of gravity, (9.81 m/s^2);

h_i = heat transfer coefficient between air and ice surface, in W/m^2 °C;

h_w = heat transfer coefficient between air and water surface, in W/m^2 °C;

I = incoming solar radiation, in W/m^2;

I_a = solar insolation absorbed by the ice cover, in W/m^2;

I_p = solar insolation penetrating the ice cover, in W/m^2;

I_o = solar insolation at the surface of the ice cover, in W/m^2;

k = an empirical constant in Bolz's equation;

L = length of free ice cover, in metres;

L_m = latent heat of fusion, in J/kg;

L_v = latent heat of vaporization, in J/kg;

n_i = Manning's roughness coefficient for ice underside;

n_b = Manning's roughness coefficient for river bed;

P = atmospheric pressure, in millibar;

Q = channel discharge, in m^3/s;

Q_{ai} = advection heat on ice (or snow) surface carried by snow or rain, in joule;

Q_{aw} = advection heat on water surface carried by snow or rain, in joule;

Q_{ei} = the heat loss or gain by evaporation or condensation from ice (or snow) surface, in joule;

Q_{ew} = the heat loss or gain by evaporation or condensation from water surface, in joule;

Q_f = the heat created by flow fraction, in joule;

Q_g = the heat energy conducted from river bed, in joule;

Q_{hi} = the convective heat exchange between ice (or snow) surface and atmosphere, in joule;

Q_{hw} = the convective heat exchange between water surface and atmosphere, in joule;

Q_{lake} = the heat energy carried by warm water coming from upstream, in joule;

Q_{li} = the longwave radiation hear exchange between water surface and the atmosphere, in joule;

Q_{lw} = the longwave radiation hear exchange between ice (or snow) surface and the atmosphere, in joule;

Q_{si} = the solar radiation hear incident to ice (or snow) surface, in joule;

Q_{sw} = the solar radiation hear incident to water surface, in joule;

R_{bo} = Bowen's ratio;

R_h = relative humidity, in percentage.

R = hydraulic radius, in metre;

R_b = hydraulic radius caused by bed roughness, in metre;

R_i = hydraulic radius caused by ice roughness, in metre;

R_l = longwave radiation flux, in W/m^2;

R_{lf} = long wave radiation flux reflect from the atmosphere, in W/m^2;

$R_{lf\,clear}$ = longwave radiation reflected from atmosphere under clear sky in W/m^2;

R_{lw} = the net longwave radiation flux from water surface to the atmosphere, in W/m^2;

R_s = solar insolation, in W/m^2;

S_f = the slope of the energy grade line for the river;

S_w = water surface slope of river channel;

T_a = air temperature measured at height of 2 metres above surface in °C

T_{lake} = the water temperature in the lake, in °C;

T_t = surface temperature, in °C;

T_{ti} = temperature at ice surface, in °C;

T_{tw} = temperature at water surface, in °C;

T_w = the average water temperature in the open water area, in °C

T_{wup} = water temperature at upstream end of open water area, in °C;

t_i = the ice thickness, in metre;

t_{ia} = average value of the ice cover thickness, in metre;

t_i^j = ice thickness at the end of day j, in metre;

t_{io} = the initial ice thickness include t_{SIE}, in metre;

t_o = the initial ice thickness not include t_{SIE}, in metre;

t_{sa} = average snow depth at simulation area, in metre;

t_{SIE} = snow ice equivalent depth, in metre;

u_2 = windspeed measured at height of two metres above the surface, km/day;

$u_{6.4}$ = windspeed measured at height of 6.4 metres above the surface, in m/s;

u^* = shear velocity, in m/s;

V_b = mean velocity for the bed zone, in m/s;

V_i = mean velocity for the ice zone, in m/s;

V_{por} = the porous volume of the ice cover, in m^3;

V_{total} = the total volume of the ice cover, in m^3;

W = width of ice cover

w_i = downslope force due to the weight per unit area of ice cover, in Pa;

z = variable of depth, in cm or m;

z_o = roughness length, in metre;

α_i = the albedo of ice;

α_w = the albedo of the water surface;

Δ^2 = variance;

ΔA_w^j = the new open water area developed in day j, in m^2;

Δt = time interval, in second;

Δt_i = ice thickness deduction, in metre;

ε = emittance coefficient;

Φ = porosity of the ice cover;

Φ_o = the porosity of the ice cover associated with a value of Young's modulus equal to zero;

Φ_{top} = porosity of top 0.3 m of the ice cover;

κ = von Karman's constant (0.4);

μ = empirical parameter in Koptev's radiation absorption equation;

ν = empirical parameter in Koptev's radiation absorption equation;

ρ_i = density of ice, in kg/m^3;

ρ_s = density of snow, in kg/m^3;

ρ_w = density of water, in kg/m^3;

σ = currently ice strength, in Pa;

σ_l = the compress stress of ice cover caused by loads, in Pa;

σ_o = ice strength before reduction, in Pa;

τ = shear stress acting on the boundary due to flow drag, in Pa;

τ_f = shear stress underside of ice cover, in Pa;

τ_m = Crack shear strength of ice cover, in Pa;

τ_o = initial shear strength of the intact ice cover, before reduction, in Pa;

τ_s = shear stress transmitted to the bank across each shore, in Pa;

τ_t = shear strength of intact ice cover, in Pa;

ω = Stefan-Boltzmann constant, ($5.67\text{x}10^{-8}$ W/m^2 °K^4);

ξ = coefficient in the relationship between Young's modulus and porosity;

1.0 INTRODUCTION

The term *river breakup* describes the deterioration and breaking of an intact ice cover in response to thermal inputs such as warm air and solar radiation, and dynamic forces such as flow drag (Ashton, 1986). When the deterioration is dominated by heat effects, the breakup is described as thermal. In the extreme case, the ice cover simply melts in place. When the ice cover breaks into large sheets or smaller pieces (called ice floes) before significant thermal deterioration has occurred, the breakup is described as dynamic.

The exact timing of breakup for any particular river site depends on a precise definition of what constitutes breakup (Ashton, 1986). Thermal breakup may occur over a period of days to weeks, and in this case breakup is generally considered to be complete once the river is clear of ice. In contrast, a dynamic breakup may occur over as short a time as one day (Ashton, 1986) and consequently it is usually the initial movement of ice which constitutes the onset of breakup.

At the present level of knowledge, forecasting breakup on a river is still relatively site specific, although a number of approaches have been applied with varying success for both thermally dominated events (Andres, 1970), and for dynamic breakups (Ashton, 1986; Ferrick, 1989). Thermal breakup is more amenable to transposable techniques, as only heat inputs are important in quantifying breakup. Dynamic breakup models must consider the effects of heat input on ice strength deterioration, as well as the increasing loads (due to increasing discharge in response to snowmelt in the catchment) acting on the deteriorating ice cover during the breakup period. Therefore, it is much more difficult to forecast than thermal breakup. As is the case in many aspects of river engineering, complex natural variations and the lack of data are the two limiting factors in forecasting either type of breakup.

The site considered in this investigation was the reach affecting the Fort Providence ferry crossing of the Mackenzie River, approximately 65 km downstream of Great Slave Lake. This ferry operates during the summer and a portion of the winter, and an ice bridge is used for the remainder of the winter. A critical period at this crossing is during breakup, after the ice bridge has been decommissioned for the season but before the river is clear of ice. At this time the ferry is not operational and goods and vehicles must be transported across the river by helicopter, causing considerable inconvenience and expense. It has between this time and the time of the initial movement of ice at the ferry crossing by cutting a passage channel through the ice cover. Under this proposal, ferry operations would cease during the period in which the ice in the ferry reach breaks up and clears out. Operations would resume after this, with brief interruptions during the passage of ice from upstream.

This proposed operation scheme would only be feasible if these major ice movements could be reliably forecast, using limited field observations each year and readily available hydrometeorological data, with sufficient lead time to enable the ferry to retreat to safety. Therefore, the Government of the Northwest Territories (GNWT), Department of Transportation, initiated a preliminary research program with the University of Alberta in 1991, which evolved into a comprehensive three year research investigation (1992 to 1994) to develop a better understanding of the breakup processes on this particular reach of the Mackenzie River and ultimately to develop a forecasting tool for breakup. Preliminary results for each of the three years of the observation program have been presented in annual reports (Hicks *et al.*, 1992, 1994, 1995).

Based on these field observations, two key sub-reaches were identified, in terms of the dominant factors controlling breakup. In the reach of the river where the ferry crosses the channel, breakup is predominantly dynamic. Upstream of this reach, breakup is predominantly thermal. From a research perspective, this study site provides an ideal situation for assessing current breakup modelling techniques. Calibration of a breakup model in the predominantly thermal upstream reach has the potential to define the parameters in the thermal model of ice strength deterioration in the ferry reach. Furthermore, because the study reach is located downstream of a large lake, discharge increases through the breakup period would be expected to be much more gradual than in a typical dynamic breakup scenario. This means that the loads on the ice cover would be expected to remain fairly constant over the breakup period, allowing for a more controlled examination of the strength deterioration and possible failure mechanisms.

The data from this three year study has been supplemented with an additional year of data collected by GNWT staff in 1995. Also, Chen (1993) conducted a detailed investigation of the effects of ice on the hydraulics of this reach of the Mackenzie River, based on hydraulic data collected early in the three year data collection program. In this thesis, Chapter 2 presents the reach description and summarizes all of the available data, including the pertinent results of Chen's analyses. In Chapter 3 breakup models in the two sub-reaches are examined. This begins with the modelling of the thermal breakup in the upstream reach, using two approaches: the energy budget approach and a conceptual linear heat transfer approach. Breakup modelling for the ferry reach is then examined, first with a review of the available literature on strength deterioration in ice covers, followed by the formulation and application of the dynamic breakup models. Failure of the ice cover in compression, shear and buckling are considered in the dynamic breakup model. Conclusions and recommendations are presented in Chapter 4.

2.0 REACH DESCRIPTION AND DATA COLLECTION PROGRAM

2.1 Description of the Study Reach

Figure 2.1 illustrates the study reach on the Mackenzie River which is located just downstream of Great Slave Lake, in the Northwest Territories (NWT). The reach of interest extends from Great Slave Lake past Ft. Providence to Mills Lake. The Mackenzie River is the twelfth largest river in the world by drainage area and eleventh in terms of mean annual discharge (Foerstel, 1981). Great Slave Lake, the fourth largest lake in Canada with a surface area of 26,900 km^2, has a dominating influence on this upper reach of the Mackenzie River, moderating both low and high flows (Foerstel, 1981).

Figure 2.2 illustrates the study reach in more detail. At the outlet of Great Slave Lake, Big Island divides the flow between the South Channel, which discharges the majority of the flow, and the shallow North Channel. The Mackenzie River widens significantly downstream of Big Island through the reach known as Beaver Lake, where the Kakisa River joins the Mackenzie River from the south. Just downstream of this confluence, the width of Mackenzie River gradually decreases through Burnt Point down to Providence Narrows (located at the upstream end of Meridian Island in the vicinity of the Big River site noted on the map). At this point the river takes on an anastomosing characteristic with numerous large islands and distributaries splitting the flow. One particularly large distributary, the Big Snye, leaves the main channel here rejoining downstream at Mills Lake. The Town of Ft. Providence is located on the north bank of the main channel in the vicinity of the RCMP and Dock sites noted on the map in Figure 2.2. The main channel in this reach is known as Providence Rapids. Between Great Slave Lake and Mills Lake, the river "...has a low lying, nearly flat topography covered with muskeg, pothole lakes, and relatively slow meandering streams." (Foerstel, 1981) Overbank vegetation is comprised mainly of coniferous trees. The area is remote, with access to the river by ground transportation limited to the area in the immediate vicinity of Ft. Providence.

The Yellowknife Highway crosses the Mackenzie River approximately 12 km upstream of the town of Ft. Providence. Figure 2.3 presents a photograph of the ferry crossing, looking upstream. There is a short berm at the south bank landing and a long approach berm (through the shallow portion of the channel) at the north landing. The channel width between the berm tips is approximately 1 kilometer (km).

2.2 Historical Data

2.2.1 Introduction

A perusal of the available data (Hicks *et al.*, 1992) suggests that there has been little systematic investigation of the ice and flow regime of the Fort Providence reach of the Mackenzie River, particularly the former. Most attention has been focused on the portion of the Mackenzie below the Liard River confluence, primarily in connection with an assessment of the potential regime changes cause by potential hydroelectric developments in the Liard catchment.

2.2.2 Streamflow Data

There are two Water Survey of Canada (WSC) hydrometric stations located in the upper reach of the Mackenzie River. One (WSC10FB001) was located at Dory Point, just upstream of the ferry crossing until the fall of 1992, at which time it was relocated to the south berm at the ferry crossing, as shown in Figure 2.4. The second WSC gauge (WSC10GC001) is located near Ft. Simpson, approximately 350 km downstream. In addition, there is a station on the Liard River near its confluence with the Mackenzie River at Ft. Simpson (WSC10ED002). All three gauges measure stage (water level) which is then converted to discharge through the use of stage-discharge (rating) curves developed based on a program of direct discharge measurement using current meters. Although WSC includes winter measurements of discharge, varying ice conditions make it impossible to develop a simple rating curve at any gauging site under ice conditions, particularly during freezeup and breakup.

With the exception of the 1972-73 winter season, the Ft. Providence gauge was operational only during the summer months prior to being relocated to the ferry crossing in 1992. Since that time it has been operational on a year round basis. At Ft. Simpson, the Mackenzie and Liard River gauges are operational throughout the year. Although streamflow data at the Ft. Simpson gauges have been useful for confirming discharges in the study reach for open water analyses, the complex interactions of ice and water flow during the breakup period precludes their use as a tool in breakup forecasting.

2.2.3 Meteorological Data

At the time the study was initiated in 1991, there was no meteorological station at Ft. Providence. Limited data available from the Natural Resources station in Ft. Providence included: minimum, maximum and mean daily temperatures, relative humidity, wind speed and direction, and descriptions of cloud cover, measured three times daily (0900h, 1200h and 1700h). However, the Natural Resources station is operated only seasonally for fire hazard assessment, starting the first of May each spring.

An extensive historical record of meteorological data was assembled for this site in the preliminary study (Hicks *et al.*, 1992). This information was based on measurements of air temperature, precipitation and bright sunshine data obtained from Atmospheric Environment Services (AES) in Edmonton, Alberta. Due to the dearth of meteorological data at Ft. Providence, values from the surrounding AES stations at Yellowknife, Hay River, Ft. Smith and Ft. Simpson were used to synthesize supplemental records for the study site by weighting station data according to its distance from Ft. Providence. The resulting historical record assembled for Ft. Providence was presented in the appendices to the preliminary study report (Hicks *et al*, 1992).

2.2.4 Ice Regime

Available information provided by Environment Canada on the ice regime in the study reach seems to be limited to dates of freezeup and breakup and maximum ice thicknesses at Fort Providence over a limited time period: 1956–1961 and 1972–1974. This information is reproduced in Table 2.1. The 13 year record indicates that "complete freeze over" can occur from November 19 to January 31, while the date on which the river was clear of ice has ranged from April 22 to June 19. As will be discussed later, the range of dates for freezeup is representative, with the variation dependent upon the nature of freezeup. However, the large range for breakup can likely be attributed to a lack of distinction between the clearing of river ice (typically during the latter half of May) and the ice run from Great Slave Lake (which generally occurs in June).

2.2.5 Ferry and Ice Bridge Operations

Records of ferry operations are available since 1962. Table 2.2 presents this data along with information on the date the ice bridge closed, as provided by Marine Transportation, Ft. Providence, NWT. As the table indicates, service interruption at the crossing has ranged from 15 to 35 days since 1980. The Yellowknife Chamber of Commerce estimates that it costs residents of that city alone over $250,000 each week when neither the ferry nor ice bridge are operational (Gerard, Sego and Hrudey, 1990).

2.2.6 Discussion of Historical Data

The variability in hydrologic and meteorological conditions explains the wide range of breakup timing observed from year to year. Thus, to develop a model of breakup, one would need simultaneous measurement of heat inputs to the ice cover (*e.g.* temperature and solar insolation), ice characteristics, discharges, water levels and open water development. Unfortunately there is insufficient data regarding the latter three, to compile an adequate historical record for breakup forecasting.

2.3 Field Observation Program

2.3.1 Introduction

In 1991-92, a three year observation program was initiated to study the nature of breakup at the Ft. Providence ferry crossing. The field observation program was particularly comprehensive in that first year, involving freezeup monitoring, mid-winter surveys of ice characteristics and snow cover, detailed breakup observations and summer surveys (to define channel geometry). At that time the WSC gauge (10FB001) was located upstream of the ferry crossing at Dory Point and was not operational during the winter. Therefore, a pressure transducer, linked to a datalogger, was installed at the south berm of the ferry crossing during the late winter of 1992 to measure the water level. Instrumentation for measuring solar insolation and air temperature were installed and connected to the same datalogger. Additional dataloggers, equipped to measure water and air temperature, were installed upstream at the Kakisa River and Great Slave Lake sites noted on the map in Figure 2.2. Water levels were monitored in the remote areas upstream and downstream of the ferry reach by installing staff gauges in and beside the ice cover, and in the reach accessible by road using a rod and level. Discharge measurements were conducted in the ferry reach as well.

Based on the extensive data collected during the 1991-92 season, a hydraulic model was developed for the early breakup period. The observational program was refined, limiting data collection to those key factors identified as crucial to the development of the ice breakup forecasting model. The WSC gauge was moved to the south berm of the ferry crossing in the fall of 1992, and became operational year round. WSC staff reactivated the program of discharge measurements, including mid-and late-winter measurements providing key data for the refinement of the hydraulic model. During the 1992-93 mid-winter site visit, the research team established a more comprehensive meteorological station at the airport in Ft. Providence. The observation program continued in the 1993-94 season with only minor refinements. GNWT Transportation staff continued the monitoring program in 1994-95. Because of the significant value of the additional year of data to the model development, the 1994-95 data are included in this report, as well.

2.3.2 Meteorological Data

2.3.2.1 Introduction

It was considered essential to establish a meteorological station at Ft. Providence for a number of reasons. First, it is undoubtedly more accurate to obtain such data directly at the site than to use data measured at surrounding stations, particularly when consideration is taken of the local scale of meteorological events such as snow squalls and cloud cover and the distance to the surrounding stations. Second, there is a time delay in obtaining the records from Environment Canada and compiling them to synthesize the record for Ft. Providence. "Real-time" meteorological observations are indispensable when conducting breakup observations, as decisions on the breakup data measurements to be obtained are closely related to the prevailing meteorological conditions. Finally, real time data collection is essential if breakup forecasting is to be facilitated.

As stated earlier, for the 1992 breakup program, a meteorological station was installed on the south bank at the ferry crossing to measure insolation and air temperature. This site was chosen, for the most part, in consideration of the fact that the scope of this study included the training of GNWT Transportation staff to continue data collection once the 3 year program was complete and the staff involved at that time were stationed on the south side of the river at the ferry camp. However, this meteorological station was moved to the Ft. Providence airport on 9-May-92 after ice damaged the datalogger. At that time it was decided that the Ft. Providence airport was a more suitable site for the study portion of the project, since the south bank of the river is inaccessible during breakup (except by helicopter). This has not been a disadvantage for the GNWT staff who have taken over the monitoring program, as ferry staff are no longer involved.

In February 1993, the research team established a more comprehensive meteorological station at the airport in Ft. Providence, installing air temperature and relative humidity probes in a standard instrument shelter and adding a wind anemometer to the tower used for the solar insolation measurement device. Details of the devices used and the results obtained are provided in the following sections.

2.3.2.2 Solar Insolation

Incoming solar radiation contributes to the thermal decay of the ice in a number of ways. Initially, it causes snowmelt on the ice surface and in the catchment draining to the stream. The snow on the ice cover tends to have a high albedo (reflectance) during the early part of the breakup season, and consequently much of the incoming energy is reflected rather than absorbed. However, as the snow melts, its albedo decreases dramatically, leaving the ice surface very dark and capable of absorbing further incoming energy much more efficiently. Therefore, snowmelt has a positive feedback effect on ice melt. Once the snow is melted, incoming energy penetrates the ice cover and begins the thermal deterioration process. The ice first melts along the interface between crystals which in columnar ice, leads to the candle structure so commonly observed in well rotted ice. The third way in which solar insolation contributes to the thermal decay of ice is somewhat indirect, as heat absorbed by the river flow in open water areas causes melt on the underside of the downstream ice cover. Clearly these three processes are interrelated and cumulative.

Measurement of Solar Insolation

In the past, the input solar radiation (insolation) was usually determined indirectly, based on measurements of the duration of bright sunshine received at a site. This measurement was often achieved using a sunshine ball, a glass ball which focuses the suns rays onto a cardboard card. A hole is burned through the card whenever the sun is not obscured by cloud. As the sun moves across the sky, the burn mark traces a path across the card which is marked in increments indicating the duration of the burn. This approach to measuring insolation is labour intensive as the card must be replaced daily and the burned cards need to be interpreted manually.

For the purpose of this study, and to facilitate the ultimate use of the results of this study in a forecasting situation, automated measurements were preferable. The device used was a model LI-200SA pyranometer sensor manufactured by LI-Cor, Inc/LI-Cor, Ltd, which was calibrated by the manufacturer against an Eppley Precision Spectral Pyranometer under natural daylight conditions and found to have an absolute error of ±5% (maximum), with the typical error being ±3%.

The pyranometer was interfaced to a Lakewood datalogger. As stated earlier, the pyranometer was initially installed at the south berm at the ferry crossing, but was moved to the instrument tower at the Ft. Providence airport on 9-May-92 for the duration of the study. The current instrument height at the Ft. Providence airport is 5.74 m above ground level as it was installed on the existing instrument tower. Both sites were free of shade effects.

Table 2.3 presents the measured insolation during the late winter and breakup periods for the three years of study. 1995 data is also included. With the exception of the 1992 data, the reported values are based on the average of 24 (hourly) measurements, expressed in term of Watts per square meter (W/m^2). Data were obtained on 30 minute intervals in 1992, with the daily value computed as the average of the 48 daily readings. As the plot in Figure 2.5 illustrates, the results based on a 30 minute sampling interval are not significantly different from those obtained using the hourly interval. The one hour sampling rate was more practical in terms of the total data storage capacity of the datalogger. The measured results presented in Table 2.3 are consistent with average daily insolation values presented by Gray (1970) for this time of year.

Relationship Between Hours of Bright Sunshine and Solar Insolation

In addition to the automated insolation measurements, the duration of bright sunshine was measured at Ft. Providence during 1992 and 1993 breakup seasons, using a sunshine ball on loan from the National Hydrology Research Institute (NHRI). These measurements were conducted to provide a relationship between the data collected with the pyranometer as well as with bright sunshine data collected by Environment Canada at surrounding stations. Figure 2.6 illustrates the total daily insolation measured at the site versus the measured duration of bright sunshine, both expressed in terms of a percentage of the maximum possible values for the date of observation. Based on this 1993 data, a relationship between solar insolation and duration of bright sunshine was obtained by least squares regression:

$$\%\ Solar\ Insolation = 46.762 + 0.590\ (\%\ Bright\ Sunshine) \quad [2.1]$$

The coefficient of determination, r^2, for this regression was 0.900. (A value of r^2 = 1.0 would indicate a perfect correlation between bright sunshine and insolation measurements.) The values of the regression constants obtained are consistent with those reported at other sites in Canada (Gray, 1970). Equation 2.1 was used to fill in missing insolation data for the period from 4 to 8-May-92, when the datalogger connected to the pyranometer was damaged by ice and no insolation data was obtained.

2.3.2.3 Air Temperature

As with the insolation data, an automated measurement device was used to measure air temperature. During the first year of the study, air temperature was measured using Lakewood temperature sensors mounted internal to the dataloggers installed at the ferry crossing (south berm) as well as at the Great Slave Lake and Kakisa sites shown in Figure 2.2. Figure 2.7 illustrates the comparison of the mean daily temperatures at the latter two sites to those obtained at the ferry crossing. The differences noted at the Kakisa River site are likely due to exposure conditions, as the probes were not sheltered. Based on this comparison, all air temperature measurements taken near Ft. Providence were considered representative of the entire study area. This temperature sensor was moved with the pyranometer to the Ft. Providence airport on 9-May-92 for the duration of the study.

In 1992, measurements were obtained on 30 minute intervals, and the 48 daily measurement were averaged to obtain mean daily temperatures. The measurement interval was increased to one hour starting in 1993 with the mean daily temperature then calculated by averaging the 24 daily measurements. Figure 2.8 shows a comparison of mean daily air temperatures obtained with the datalogger's internal sensor based on 48 and 24 readings per day. As the figure illustrates, the effect of increasing the sampling interval from 30 minutes to 1 hour was negligible.

The most significant change between 1992 and subsequent years, was the fact that a high accuracy thermistor was obtained and installed in a standard instrument shelter at the Ft. Providence airport in February 1993. The device used was a Lakewood model YSI 46043 thermistor with a temperature range of -80°c to 200°C and an accuracy of ±0.05°C. The thermistor was interfaced to a Lakewood datalogger sampling on hourly intervals. Figure 2.9 illustrates a comparison of the mean daily temperatures obtained with the sheltered thermistor to those measured with the temperature sensor internal to the datalogger during spring, 1992 and 1993. As the figure indicates, there is a systematic error obtained with the internal sensor, which is likely primarily due to solar heating of the datalogger case. To make the 1992 data record consistent with the data collected since 1993, a linear regression was employed. The resulting equation:

$$\textit{sheltered temperature} = -1.698 + 0.992\ \textit{(internal temperature)} \qquad [2.2]$$

was used to correct the 1992 record. The coefficient of determination, r^2, for this regression was 0.987, indicating an excellent fit.

Table 2.4 presents the mean daily temperatures record for the late winter and breakup periods for the three years of study. 1995 data is also included.

2.3.2.4 Relative Humidity

A relative humidity (RH) probe was installed in the standard instrument shelter at the Ft. Providence airport in February 1993. The device used was a Vaisala model HMP 35A (HUMICAP® H-sensor, 0062HM) probe manufactured by Hoskin Scientific. This device has an accuracy of ±2% in the range of 0 to 90% RH and ±3% in the range of 90 to 100% RH, with a repeatability better than 1% RH/year. The RH probe was interfaced to a Lakewood datalogger sampling on hourly intervals. Table 2.5 presents mean daily values of relative humidity based on an average of the 24 daily readings. Data collected at the Natural Resources station in Ft. Providence in 1992 is presented as well. These mean daily values were based on an average of the three measurements made daily by Natural Resources staff.

2.3.2.5 Wind Speed

A wind anemometer was installed on the instrument tower at the Ft. Providence airport in February 1993. The device used was an 18 cm diameter, 4-blade helicoid propeller with a threshold sensitivity of 1.0 m/s (model 05103 Wind Monitor) manufactured by R. M. Young Company. it was installed at a height of 6.4 m above the ground surface and interfaced to a Lakewood datalogger sampling both wind speed and direction on an hourly basis. The 0° wind direction indicator was aligned with magnetic north.

Table 2.6 presents mean daily values of wind speed based on an average of the 24 daily readings. Data collected at the Natural Resources station in Ft. Providence in 1992 is presented as well. These mean daily values were based on an average of the three measurements made daily by Natural Resources staff.

2.3.3 Other Data Related to Open Water Development

2.3.3.1 Introduction

Other data pertinent to the development of a breakup forecasting tool, includes: water temperature; snow depth, ice thickness and ice strength. All of these variables were measured as a part of the field data collection program.

2.3.3.2 Water Temperature Data

Water temperature is especially significant to the ice processes in this reach because of the release of warm water from Great Slave Lake in late winter. This occurs because of the unique density characteristics of water (Ashton, 1986). As with other fluids, water density varies with temperature. However, water density is maximum at 4°C, and decreases with temperatures both below and above 4°C. In deep lakes containing water at temperatures in excess of 4°C, the cooler, denser water is found at greater depths than the warmer, less dense water. This vertical stratification is stable because further heating of the surface layers of water only leads to reduced density in these upper layers. However, as a water body cools below 4°C, it develops an inverse temperature gradient. Initially, surface heat loss lowers the water temperature in the upper layers towards 4°C and this denser water then moves to the lower levels. As the temperature cools the water further, the water density decreases and the colder (but less dense) water remains nearer the surface. The resulting profile is at 0°C near the surface and 4°C at the lake bed. Further heat loss through the winter season has the potential to cool the water through the entire depth. However, there will still be a temperature gradient until all of the water has been cooled to 0°C. There are two reasons why a temperature gradient persists through the winter in some lakes. First, an ice cover forms, insulating the lake water from cold air temperatures. Snow accumulations on the ice cover enhance this insulating effect. Second, considerable energy is released in the formation and growth of the ice cover and consequently much of the heat lost from the lake during cold weather occurs in the upper layers. It is important to note that the vertical temperature gradient does not persist once the water enters the river, due to the turbulent nature of the flow. Consequently, temperature measurements in the river would be expected to be homogeneous through the flow depth.

The release of warm water from Great Slave Lake into the Mackenzie River has the potential to affect the ice regime in three ways. First, it could inhibit the early formation of an ice cover in the upper reach of the river (near the lake outlet). Second, it could limit the thermal growth of ice in the channel downstream of the lake. Third, it could lead to the early melt of river ice in the spring. All three effects, are, of course closely interrelated especially near the lake.

Great Slave Water Temperature Data

To quantify the source of heat from the lake, automated water temperature measurements were conducted in the spring of 1992 using a Lakewood model YSI 46043 thermistor (temperature range: -80°C to 200°C; accuracy: ±0.05°C) interfaced to a Lakewood datalogger located at the Great Slave Lake TBM. The measurements, conducted on 30 minute intervals, were then smoothed by calculating a 12 hour moving mean water temperature to facilitate interpretation of the data as the 30 minute readings displayed a high degree of natural variation. The results, illustrated in Figure 2.10, show that water released to the Mackenzie River was consistently in excess of 0°C though only in the order of 0.05 to 0.25 °C. It is interesting to note the increase in water temperatures observed during the first few days of May at the time when the mean daily air temperature was between 10 and

20°C, as there was open water at this site at the time. This probe was lost on 10-May-92, likely due to ice movement.

In an attempt to quantify the heat at its source, manual water temperature profiles were measured through the lake depth, just upstream of the outlet, on three occasions in 1992: 25-Apr, 29-Apr and 4-May. This was done with a Resistance Temperature Detector (RDT) interfaced with two wires to a standard ohm meter. The results of these measurements, shown in Table 2.7 (a), are somewhat difficult to interpret due to difficulties encountered in calibrating the temperature probes to 0°C[1]. Measured temperature differences are considered quite accurate, but absolute values are unknown. As Table 2.7 (a) shows, a temperature gradient was measured in Great Slave Lake on all three occasions, with warmer water near the bed, as is consistent with the theory. Given that the minimum possible water temperature is 0°C (near the top, adjacent to the ice), it was possible to determine the minimum possible temperatures within each profile as presented in Table 2.7 (b). Based on an integration of these adjusted temperature through the depth, minimum possible average lake outflow temperatures could be estimated for 1992. As the table show, there is excellent consistency by this approach. Consequently, it can be said with some confidence, that the average water temperature in the lake upstream of the outlet was at least 0.4°C.

In the subsequent years of the study, the precision of the temperature measurement was improved by eliminating wire resistance effects. This was done by introducing a switch between the wires and the ohm meter, facilitating the measurement of the wire resistance. Figure 2.11 presents the water temperature profiles obtained in 1993, 1994 and 1995 using the improved device. Average temperatures were again determined through integration, with values of 0.49, 0.22 and 0.22°C obtained for 1993, 1994 and 1995, respectively.

---

[1] The reason for this difficulty is related to the resistance of the wires connecting the probe to the meter, the effect of which is a function of ambient temperature and the length of the wires. This effect becomes important when attempting to obtain precision in the order of tenths or hundreds of a degree.

Other Water Temperature Data

Manual water temperature measurements were also conducted further downstream in the study reach during 1993 and 1994. These data, shown in Table 2.8, were measured under the undisturbed ice cover.

2.3.3.3 Ice Characteristics and Snow Depths

Depth of Snow on the Ice Cover

Accumulated snowfall affects breakup in two ways. First, early snow cover has an insulating effect, inhibiting the thermal growth of ice during the winter period. In the spring, this insulating effect inhibits thermal decay of the ice. This effect is enhanced by the (typically) high albedo of the snow cover, such that the snow not only insulates the ice against heat input, it reflects much of the incoming solar radiation as well.

Tables 2.9 through 2.12 present the measured snow depths obtained from 1992 to 1995, respectively. Snow depths were measured on both the border ice and the rough ice, where ever possible. Values presented represent the average of three individual snow depth measurements at the site in question.

Ice Thickness

Ice thickness is a key variable in any breakup model. If the ice cover deteriorates primarily by melting, then theoretically, when sufficient heat has been absorbed to cause the ice thickness to become zero, breakup is complete. In the case where breakup is more dynamic, with increasing or fluctuating water levels lifting and breaking an ice cover weakened by heat input, knowledge of the ice thickness is critical to the determination of the forces involved and the rate of ice weakening. Hydraulic analyses, which are important to the determination of flow rates during breakup, also require knowledge of ice thickness values.

In 1992, measurements of ice thickness were obtained in both the rough ice and border ice (where ever possible) at 19 stations between Great Slave Lake and Mills Lake. These measurements were first conducted in late winter (late March and early April) and then repeated 3 times during the initial period of the breakup season. Measurements were discontinued once the initial movement of the ice cover occurred. Tables 2.9 (a) and (b) present a summary of the measurements obtained in the rough ice and the border ice, respectively.

This measurement program was continued in the following three years, with 1995 data collected by GNWT staff. Tables, 2.10 to 2.12 present the measured data for 1993 to 1995, respectively.

Ice Strength Measurements

In situ ice strengths were estimated at 17 stations throughout the study reach in 1992 and 1993. Measurements were conducted by firing a nail vertically into the ice with a RAMSET® nail driver using a No. 6 charge, and then measuring the depth of penetration in millimeters (mm). Three test points were used at each location and then averaged to obtain an indication of strength (the deeper the penetration the lesser the ice strength). Gerard (1975) discusses the interpretation of this test in terms of the compressive strength of the ice. However, because of changes in the types of nails manufactured since that time, the measured penetration was taken as an index of strength in this study.

Two problems associated with this strength test were noted during the 1992 breakup observations. First, measurements in the rough accumulation were hampered by the surface irregularities of the accumulation. Where possible, measurements were taken in the center of a pan. However, for particularly rough accumulations, the only flat surfaces were in the thermal ice between the floes. The second difficulty was associated with extending measurements through the breakup period. By late April there was sufficient water on the ice surface (from the melting snow), to render the nail driver inoperable. Nevertheless, the data do provide valuable information on the consistency of ice resistance to penetration form year to year and between ice types.

As spatial variations were found to be insignificant, representative average values were plotted as a function of time in Figure 2.12 for both the border and rough ice in 1992 and 1993. As the figure shows, there appears to be a measurable change in ice strength between late March and late April. However, as the early April measurements illustrate, variations from year to year and between border and rough ice were not significant.

2.3.4 Hydraulic Data

2.3.4.1 General

The onset of breakup in a particular river reach is strongly dependent upon the discharge in the river. In terms of the thermal component of breakup, it is the heat contained within the flow which melts the underside of the ice cover. In terms of the dynamics of breakup, it is the increasing water levels due to snowmelt runoff which increases the drag on the underside of the ice cover and also lifts the ice cover free of retaining ice frozen to the banks. Therefore, knowledge of the discharge throughout the breakup period is essential to the development a breakup forecasting model.

Typically, for open water conditions, variations in streamflow are determined by water level measurements which are related to discharge from an established rating curve at the measurement site. This rating curve is developed by conducting simultaneous water level and discharge measurements over a wide range of stream flows. Although this is a well researched problem in open channel flow situations, at present this relationship is poorly defined and extremely variable under ice conditions, particularly when partial ice covers and/or ice jams are involved The relationships tend to be not only site specific but "situation specific" as well. If major ice movements are underway and/or if ice jams are forming and releasing, it is generally not possible to obtain direct discharge measurements. Consequently, discharge estimates for this period requires the development of an hydraulic model which considers ice effects on the flow.

2.3.4.2 Geometric Data

To develop a reliable model of the hydraulics of the Mackenzie River, a database of appropriate channel characteristics had to be developed. Although much of this information was already available in the form of hydrographic charts, it had been some years since the surveys on which the charts were based, were conducted. Furthermore, the charts provided no information on the channel geometry above the low water profile and considerable difficulty was encountered in relating the single chart elevation to geodetic levels. Therefore, cross section soundings were undertaken in July of 1992. All cross section surveys were extended up onto the bank to facilitate the hydraulic analysis at high water levels. In total, 18 cross sections were surveyed between Great Slave Lake and Mills Lake. In addition, soundings were conducted in the North Channel at the outlet of Great

Slave Lake and in the Big Snye near the upstream end of Meridian Island. Figure 2.2 illustrates the location and alignment of these cross sections. Details of the cross section surveys are presented by Chen (1993).

Horizontal control was achieved for most of the cross sections with the use of a portable Global Positioning System (GPS) which provides locations in terms of universal coordinates by triangulation on orbiting satellites. During each channel crossing, a series of coordinates were obtained, with a corresponding notation placed on the depth sounding chart. These coordinates were used in combination with the sounding chart to apportion distances across the channel width. In all cases, an effort was made to keep the boat on a straight course, approximately perpendicular to the flow.

Generally the absolute horizontal accuracy attained with a single GPS device is about 10 to 20 meters (Leick, 1990). Therefore, in order to minimize error, positioning should be conducted with a minimum of two receivers (Canada Centre for Surveying (CCS), 1992). This is particularly important at high latitudes, such as at this study site, because of the increased potential for fluctuations in the earth's magnetic field (CCS, 1992). When measurements are taken with only one receiver, it is recommended that relative positioning be examined to ensure data consistency (CCS, 1992). For this study, linear regression analyses were conducted between the latitudes and longitudes measured at the GPS data points at each cross section to evaluate the consistency of the data obtained in the moving boat. Although these regressions did not facilitate quantification of the horizontal error of the GPS, most points plotted on a near perfect straight line, indicating a measure of consistency between readings at each cross section. Details of this consistency analysis are provided by Chen (1993) and Hicks *et al.* (1995).

Vertical control was achieved by referencing temporary benchmarks (TBM) which had been set up at each of the cross section sites, into the system of monuments established by the Geodetic Survey of Canada (GSC). These monuments are located adjacent to roads and highways and, consequently, only short level circuits were required to establish geodetic elevations for the temporary benchmarks located between the Ice Bridge section and the dock in Ft. Providence in August, 1991 and May, 1992.

On the other hand, relating temporary benchmarks to the GSC datum for the other, more remote, cross section sites was considerably more difficult, due to the paucity of geodetic benchmarks, lack of road access, and the difficult nature of the terrain. The only practical time for surveying over such long distances was during winter, when a clear line of site was available along the ice cover. Therefore, upstream of the Ice Bridge section, the TBMs at Burnt Point and Beaver Lake were tied into the system by closed level circuit (approximately 12 km each way) in December of 1991.

The TBMs further upstream, at Kakisa River, the South Channel and at Great Slave Lake were tied in during March 1992, by surveying up to the lake (a distance of approximately 45 km) without closing the circuit. Because this level circuit was not closed, it was essential to attempt to validate the survey by some alternate method. This was achieved by examining Water Survey of Canada (WSC) measurements of Great Slave Lake water levels at Hay River and Yellowknife Bay in comparison to water levels measured at the Great Slave Lake TBM (based on the unclosed level circuit) site during the spring of 1992. Although the WSC measurements of Great Slave Lake water levels at Hay River and Yellowknife Bay were normally within 10 to 15 cm of each other, both were approximately 1 m different from the water levels measured at the Great Slave Lake TBM. For this reason, the unclosed level circuit to the Great Slave Lake TBM was rejected, and the elevation of the TBM at this site was estimated based on the assumption that the water level at the Great Slave Lake TBM site was the same as that recorded at Hay River. To maximize consistency, this estimate was based on water levels measured at the two sites over a period of more than one month (late March to early May 1992). Given that the variation in Great Slave Lake water levels between Hay River and Yellowknife were in the order of 10 to 15 cm, the error in the estimated TBM elevation at Great Slave Lake section is likely of the same order. This error was considered acceptable as it represents only about 4% of the water surface elevation difference between the Great Slave Lake and Beaver Lake cross sections.

Once the elevation of the Great Slave Lake TBM was established, the TBM elevations at the Kakisa River and South Channel sections were checked by assuming a constant water surface slope between the Beaver Lake and Great Slave Lake sections. The TBM elevation obtained at the South Channel section by this method was within 10 cm of the elevation determined in the unclosed level circuit, while the TBM elevation obtained at the Kakisa River section was nearly identical to the elevation determined in the unclosed level circuit. Consequently, the Kakisa River and South Channel TBM elevations were accepted as surveyed.

Downstream of Ft. Providence, the research team was fortunate to find a Public Works benchmark near the TBM set up on the navigation tower adjacent to the Mills Lake cross section, enabling it to be tied into the system in July of 1992.

Figure 2.2 illustrates the location of all of the TBMs which have been established in the study reach to date. It should be noted that, in some instances, more than one TBM has been established at a site to facilitate measurements at low and high stages.

2.3.4.3 Discharge Data

1992 Breakup Season

During the 1992 breakup season, approximate discharge measurements were obtained at the ferry crossing on 27-Apr-92 and 1-May-92 and downstream of Ft. Providence at the Orange Cabin section on 6-May-92. The discharge was estimated from velocity measurements at approximately 0.2 and 0.8 of the depth at five holes across the channel, integrated over the area of the surveyed cross section. Velocities were measured using an electromagnetic flow meter aligned to provide zero secondary velocity on the meter scale.

Normally, 20 or more measurement stations are used to evaluate the discharge. To estimate the error associated with using only 5 stations, a comparison of the discharge values obtained using 5 stations versus 22 and 25 stations was conducted using WSC discharge measurements taken the following year on 7 and 20- Apr-93, respectively (also under late winter ice conditions). These calculations showed that the discharge was underestimated by only 8 to 9% when only 5 stations were used.

1993 Breakup Season

Water Survey of Canada (WSC) staff conducted winter discharge measurements at the ferry crossing on 5 occasions between 12-Jan-93 and 20-Apr-93. These are summarized below.

Date of Measurement	Discharge (m^3/s)
12-Jan-93	2150
17-Feb-93	2370
11-Mar-93	2240
7-Apr-93	2410
20-Apr-93	3090

These dates provided excellent coverage of the winter period and the 20-Apr-93 measurement was taken only two days before the initial movement of ice in the study reach.

1994 Breakup Season

WSC staff (assisted by the University of Alberta field team) conducted a late winter discharge measurement at the ferry crossing on 19-Apr-94. The measured discharge was 2390 m^3/s.

1995 Breakup Season

WSC staff measured a discharge of 1980 m^3/s at the ferry crossing on 19-Apr-95.

2.3.4.4 Water Level Measurements

1992 Breakup Season

As the WSC stage recorder at Dory Point was not operational during the 1991-92 winter period, a temporary continuous recorder was set up at the ferry crossing to monitor stage changes during the late winter of 1992. These stage measurements were obtained using a pressure transducer housed in a steel pipe welded to the sheet piling on the dyke at the south bank. The data were recorded on the same datalogger used for air temperature and incoming solar radiation records. Because of constraints on the cable length for the effective use of the pressure transducer, the datalogger had to be placed right on the berm at the south bank of the ferry crossing.

During late March, prior to installation of the pressure transducer, intermittent measurements were made by DOT staff. These were continued through early April to facilitate calibration of the continuous recorder. Upon commencement of breakup observations in late April, the research team began routine surveys of water surface profiles through the study reach. As breakup progressed and ice movements increased, these water surface profile measurements were increased in frequency from 1 per day, to 3 or 4 per day. In total, more than 45 water surface profiles were measure in the study reach between 5-Apr and 20-May-92. These are reproduced in Appendix B (in Volume II) of the 1992 data report.

1993 Breakup Season

The WSC gauge was moved to the ferry crossing in 1992 and the stage recorder was operational throughout the winter period, providing a continuous record of water level at the ferry cross section during that period. Water surface profiles were measured by University of Alberta researchers on the following dates:

Date of Measurement	Reach Covered
16 &17-Dec-92	Great Slave Lake to Mills Lake
23 to 25-Feb-93	Ice Bridge to Ft. Prov. dock
7 & 8-Apr-93	Great Slave Lake to Mills Lake
23-Apr-93	Ice Bridge to Ft. Prov. dock
9-May-93	Great Slave Lake to Ft. Prov. dock

Upon commencement of breakup observations in late April, the research team began routine surveys of water surface profiles through the study reach extending from the Ice Bridge section to the dock in Ft. Providence. Again, as breakup progressed and ice movements increased, these water surface profile measurements were increased in frequency. In total, 24 water surface profiles were measured in the study reach between 16-Dec-92 and 9-May-93. Figures illustrating these water surface profiles are presented in Appendix A of the 1993 data report.

In 1993, water level measurements were limited to the reach between the Ice Bridge section and the dock in Ft. Providence during the breakup period, due to the expense associated with conducting measurements at the remote sites upstream and downstream (which must be done by helicopter). This was considered a reasonable approach since the measurements made during the 1992 breakup period showed that water levels at the remote sites upstream were well approximated by assuming a linear decrease in water surface elevation between the Great Slave Lake and Ice Bridge cross sections, even during periods of major ice movement.

Water levels were obtained at Great Slave Lake when complete water surface profiles were measured on 17-Dec-92 and 7-Apr-93. Values of 156.79 m and 156.95 m were recorded on the respective dates. A water level of 156.80 m was measured on 9-May-93, by accessing the site by float plane, once the majority of the Beaver Lake ice had moved downstream. The average of the pre- and post-breakup water levels at Great Slave Lake was 156.87 m, with the total drop in water level at the site between 7-Apr and 9-May-93 being only 0.15 m (15 cm). As this variation is within the accuracy of the temporary benchmark (TBM) elevation at this site (Hicks, Andres *et al*, 1993) the average value of 156.87 m was considered representative for this breakup period. Great Slave Lake water levels measured by WSC on Great Slave Lake at Yellowknife and Hay River were also used to evaluate the reasonableness of this estimate.

1994 Breakup Season

The WSC stage recorder at the ferry crossing was again operational throughout the winter, providing a continuous record of water level at the ferry cross section during that period. Water surface profiles were measured by University of Alberta researchers on the following dates:

Date of Measurement	**Reach Covered**
14 to 16-Mar-94	Great Slave Lake to Ft. Prov. dock
12 to 14-Apr-94	Great Slave Lake to Mills Lake

On 22-Apr-94 the research team began routine surveys of water surface profiles through the study reach extending from the Ice Bridge section to the dock in Ft. Providence. As breakup progressed and ice movements increased, these water surface profile measurements were increased in frequency from 1 per day, to 3 per day (as varying conditions dictated). Figures illustrating these water surface profiles are presented in Appendix A of the 1994 data report.

Again, as in 1993, water level measurements were limited to the reach between the Ice Bridge section and the dock in Ft. Providence during the breakup period. Water levels were obtained at Great Slave Lake on 16-Mar-94 and 12-Apr-94 (when complete water surface profiles were measured). Values of 156.75 m and 156.87 m were recorded on the respective dates. A water level of 157.02 m was measured on 16-May-94, once the majority of the Beaver Lake ice had moved downstream. These measured water levels represent a near linear increase in the water level at Great Slave Lake over the breakup period. Water levels measured on Great Slave Lake (by WSC) at Yellowknife and Hay River, displayed a comparable gradual increase.

1995 Breakup Season

Water surface profiles were measured by GNWT staff throughout the breakup period, including a full profile (to Great Slave Lake) on 19-Apr-95.

Figure 2.13 illustrates the stage hydrographs at the ferry crossing for the spring and breakup periods for all three years compiled from the WSC gauge record and the manual measurements by the University of Alberta field team. A summary of key water levels at the ferry crossing is provided in Table 2.17. More detailed hydrographs, including details of related ice movements are available in the yearly data reports.

2.3.4.5 Indirect Discharge Determination

Determination of river discharge throughout the breakup period requires an hydraulic model, as direct measurements cannot be obtained, for safety reasons. The first step in understanding the hydraulics of the Mackenzie River downstream of Great Slave Lake was to develop a hydraulic model of the channel under open water conditions. This calibration was then used with late winter water level, ice thickness and discharge measurements, to calibrate an hydraulic model for the early breakup period each year.

Open Water Calibration

Two water surface profiles were available, allowing for both calibration and verification of the open water model. One open water profile was measured between Beaver Lake and the RCMP section in Ft. Providence on 29-Aug-91 to 1-Sep-91. A second profile, extending from Great Slave Lake to Mills Lake, was measured on 11-Jul-92. Measured discharges were not available for either of these dates. Instead the discharge was determined from a rating curve established by a power law regression of the measured stage-discharge data at the WSC station at Dory Point (Chen, 1993). Based on this analysis, the estimated discharges for the 1991 and 1992 profiles were 7000 m^3/s and 8500 m^3/s, respectively. These discharge estimates were compared to those published by WSC for the Mackenzie River at Ft. Simpson (less the flow in the Liard River) based on an estimated travel time of 48 hours between Ft. Providence and Ft. Simpson. The results were within 2% of the rating curve discharge for the 1991 discharge estimate and within 1% for the 1992 estimate.

There are also numerous small tributaries which contribute streamflow throughout the modeled reach, as well as one large one: the Kakisa River. Based on estimated peak flows from the small tributaries (observed to be in the order of 1 m^3/s during spring runoff) their total input to the flow in the modeled reach would be in the order of 100 m^3/s. The Kakisa River has recorded peak floods in the order of 100 to 200 m^3/s, based on published WSC records. Therefore, if all tributaries were peaking simultaneously (an unlikely occurrence, and certainly not the case at the time the open water profiles were measured) the combined inflow would be in the order of 300 m^3/s, (approximately 4% of the Mackenzie River discharge) which is of the order of the accuracy of the discharge estimate itself. Therefore, these inflows were not considered in the model.

The study reach presents a unique problem because the channel splits at Meridian Island, thereby limiting the applicability of standard one-dimensional models. However, by using the surveyed cross section in the Big Snye channel, an estimate was made for the distribution of flow between the two channels, assuming uniform flow in the Big Snye (Chen, 1993). This discharge was subtracted from the discharge upstream of the split. This allowed the north channel of the river to be modeled, at least approximately, using a standard one-dimensional gradually varied flow model. The slope through the Big Snye was estimated using the difference in the water surface elevation between the Big River section and the Mills Lake section (where the Big Snye rejoins the main channel). The channel roughness, expressed in terms of Mannings *n*, was estimated to be 0.025 on the basis of practical experience and sensitivity analyses (Chen, 1993; and Hicks *et al.*, 1995). The resulting estimates for the flow in the Big Snye were in the order of 10% of the total discharge. A similar approach was used to account for the split between the north and south channels at Great Slave Lake. In that case, the south channel was modeled (Chen, 1993).

The more extensive 1992 profile was selected for the calibration of bed roughness. The calibration was carried out using the U.S. Corps of Engineers Water Surface Profile (HEC-2) program, and proceeded by successive trial runs until a suitable match between the observed and computed water surface profile was obtained. Table 2.18 and Figure 2.14 present the results of this calibration. The calibrated bed roughness values ranged from 0.020 to 0.030 (Chen, 1993; and Hicks *et al.*, 1995). The larger roughness values, calculated for the Providence Rapids (between the Big River section and the dock in Ft. Providence), can be attributed to the lower depths evident in this steep reach. Both the mean bed material size and relative roughness effects would be expected to be larger in the rapids than in the milder sloped reaches upstream and downstream.

To verify this calibration, the same roughness values were used with the discharge corresponding to the 1991 profile, and then the computed water levels were compared to the measured values. Table 2.19 and Figure 2.15 present the results of this verification for which good agreement was obtained. Although the verification discharge is less than 20% different from the calibration discharge, it must be remembered that streamflows are significantly regulated by Great Slave Lake and, therefore, extreme fluctuations in flow are rare (WSC recorded open water flows only range from about 4500 to 8500 m^3/s over the period of record).

Calibration with an Ice Cover

In each year of the study, a calibration of the model for the late winter ice cover was conducted based on the measured ice thicknesses, water levels and discharges. The Big River section was taken at the downstream boundary of the hydraulic model, because the distribution of flow between the Big Snye and the Providence Rapids channel was unknown at this time of year. Average ice thicknesses at each section were obtained by weighting the border ice and rough ice thicknesses based on their relative extent of coverage. The calibrated composite roughness values were found by adjusting the roughness values until the computed water surface profile matched the measured one at the corresponding measured discharge.

Separation of the composite roughness, n, into the ice roughness, n_i, and the bed roughness, n_b, was based on the Sabeneev equation (Nezhikhovskiy, 1964):

$$n = \left(\frac{n_i^{3/2} + n_b^{3/2}}{2} \right)^{2/3} \qquad [2.3]$$

and based on the results of the open water calibration.

The calibration procedure for the late winter ice cover was repeated in each of the three years of the study, as well as in 1995 (based on data collected by GNWT). Tables 2.20 to 2.23, summarize the results of the hydraulic ice model calibration for the years 1992 to 1995, respectively.

2.3.4.6 Estimating Discharge During Breakup

Using the calibrated ice model extending from the Big River Section to the Ice Bridge section, an iterative procedure was used to estimate the discharge using measured water surface profiles. This procedure was used through the early breakup period in each year, until ice movement rendered the calibrated models inapplicable.

An indirect discharge measurement was obtained from the open water rating curve, once all of the ice had cleared each year. Together with the direct measurements, and early breakup (calculated) discharges, this provided adequate data to estimate the discharge throughout the breakup period. The resulting hydrographs, presented in Figure 2.16, illustrate that discharge increased in the reach through the breakup period, in all four years from 1992 to 1995.

At present the reason for this increase in discharge during the breakup period is unclear as lateral inflows downstream of the lake are typically small in comparison to the total streamflow at this time of year, as discussed earlier. Also, discharge fluctuations in this reach of the Mackenzie River would be expected to be mitigated by the storage effects of Great Slave Lake as snowmelt from the upstream catchment is largely captured by the lake. Nevertheless, as Figure 2.17 illustrates, a gradual increase in lake level was observed over the breakup period in three of the four years, and this increase is sufficient to cause the increase in discharge observed, based on the hydraulic analysis of the lake outlet (Chen, 1993; Hicks *et al.*, 1995). However, this was not the case in 1995, where both the WSC data and the water levels measured by GNWT staff at the Great Slave Lake TBM indicate a decrease in lake level over the breakup period, while the discharge hydrograph indicates an increase in flow rate from about 2000 to 7000 m^3/s over this same period.

It is possible that increased flows during the breakup period could be attributed to the development of open water at the lake outlet, which results in the increased hydraulic efficiency of the outlet and corresponding increases in the discharge released to the downstream channel. However, although a systematic trend supporting this theory was evident in the data collected from 1992 and 1993, the 1994 data indicated the opposite effect. One possibility for this discrepancy is that development of open water at the lake outlet, while it does have the potential to increase the hydraulic efficiency of the outlet, also exposes the lake outlet to wind effects. Thus in a manner analogous to lake seiching, outflow from the lake could be restricted when there is a strong wind against the flow (i.e. from the west). This is supported by the fact that anecdotal evidence provided by GNWT staff, based on experiences reported by barge pilots operating in the reach, suggests that wind plays an important role in the lake outlet hydraulics, although this has never been documented.

2.3.4.7 Calibration of the Pre-Breakup Ice Roughness through Providence Rapids

When the calibration for the ice cover was initially conducted for the 1992 ice conditions, the Big River section was chosen as the starting cross section because of a lack of information on the proportion of flow carried in the Big Snye under ice conditions. However, after discharge estimates were developed for late April and early May 1992 and it was determined that little or no flow was passing down the Big Snye, an assessment of the composite roughness of the pre-breakup ice cover along Ft. Providence Rapids became possible. Three water surface profiles, measured on 27-Apr, 29-Apr and 4-May-92, were used for this analysis. The ice thicknesses used in the model, which ranged from 1.2 to 1.9 m, were obtained by averaging measured ice thicknesses in a manner similar to that done for the calibration of the reach upstream of the Big River section. The calculated composite roughness for the 27-Apr-92 water surface profile varied from 0.023 at the Big River section to 0.041 further downstream. These calibrated composite roughness values were used along with the discharge values computed for 29-Apr and 4-May-92 to calculate water surface profiles through the Providence Rapids. The computed profiles showed good agreement to measured water levels on these 2 days, validating the roughness values obtained.

Based on Sabeneev's equation and the bed roughness values obtained from the open water calibration, the calibrated ice roughness through Providence Rapids to the Dock at Ft. Providence was found to be 0.050. The ice cover was expected to be rougher in the Providence Rapids reach than in the channel upstream of the Big River section, given that an extremely rough accumulation had developed in this steeper reach during freezeup.

This analysis was repeated for the 1993 to 1995 conditions, inclusively. The roughness values obtained for the late winter ice roughness in the Providence Rapids were 0.070, 0.070, and 0.050 for these three years, respectively.

2.3.5 Nature of Breakup

2.3.5.1 Introduction

In general, the nature of breakup on a reach can vary from one in which the ice gradually deteriorates and more-or-less melts in place, to one in which breakup occurs suddenly due to the passage of a dynamic breakup front while the ice is still competent. The manner of breakup depends on a subtle trade-off between ice deterioration due to warm weather and tributary inflow, and an increased discharge due to snowmelt, rain or an ice jam failure upstream.

One of the main factors governing the manner of breakup is the competence of the ice cover. Ice strength at the onset of breakup will depend upon the ice type, thickness and in particular, the solar-radiation received prior to breakup. The competence of the ice cover is closely related to: the nature of freezeup; the meteorological circumstances over the previous winter: and the prevailing meteorological and hydrologic conditions during the spring.

Over the three years of this study, extensive observations of the sequence of ice deterioration and breakup were monitored by flying over the river and video-taping the reach on a daily basis. The information obtained on these flights were supplemented with detailed notes taken by the engineer in the field, on an ongoing basis. Together with the quantitative data described in the previous sections, this data permits the development of a description of the nature of breakup in the two key sub-reaches: the ferry reach and in the Beaver Lake area.

2.3.5.2 Breakup in the Ferry Reach

This reach extends upstream from the dock in Ft. Providence to the Ice Bridge section, upstream of the ferry crossing. Breakup in the ferry reach is of critical importance to late winter and early spring ferry operations, as major ice movements pose a serious threat to potential ferry operations. With the intent being to cut a ferry passage channel across the intact ice cover in the late winter, it is essential to be able to predict the initial movement of ice at the ferry crossing to permit the ferry to retreat behind the south berm in anticipation. Fortunately, a very consistent sequence of breakup events has been observed in the ferry reach. These are outlined in the following text.

In response to increasing outflows from Great Slave Lake in mid- to late April, water levels throughout the reach begin to rise gradually. Ice frozen to the ground near the banks is unable to float up with the rest of the ice cover and therefore this border ice becomes inundated with water. Also in mid- to late April open water leads begin to develop in the Providence Rapids, and as discharge increases, overflow of water onto the ice cover at the downstream end of these leads is observed. Figure 2.18 illustrates this with a photograph taken looking upstream over Providence Island which is typical of all three years (1992 to 1994).

Breakup in the ferry reach is primarily mechanical. The first ice movement typically occurs at Providence Narrows, likely for two reasons. First the channel steepens considerably into Providence Rapids here and, therefore, the flow is accelerating. Both gravity and drag effects on the ice cover are higher in this area than in the reach upstream. Second, the ice cover is typically thinner upstream of Providence Narrows than it is in the rapids and therefore, it is more susceptible to failure under gravity and drag effects than the ice cover downstream. Thermal deterioration also plays an important role in the timing of this initial ice movement. Figure 2.19, a photo taken looking downstream through the Providence Rapids, illustrates the typical pattern of this first ice movement. The ice cover in the upstream portion of the Providence Rapids collapses, followed by the ice sheet breaking away from the upstream ice cover near the Blue Quonset. This ice sheet then moves into Providence Narrows and leads to further shoving of the ice cover in the upstream portion of the Providence Rapids.

Thermal deterioration is also important because the ice lodged at Providence Narrows, once sufficiently weak, will fragment further and move into Providence Rapids. Such a movement typically results in a "shove" which fractures the ice cover in the rapids and consolidates the ice floes forming a thickened accumulation or "ice jam". The resulting accumulation may consist of ice floes ranging in size from small pieces (of the order of 10 m or less in diameter) tightly packed together (typically located in the downstream portions of the jam), to large sheets (1/4, or more, river widths in diameter) arranged edge to edge (typically located near the upstream end, or "head", of the accumulation). The formation of a jam decreases the hydraulic efficiency of the channel, due to the increased thickness and increased roughness (underside) of the ice cover, and often results in a rapid increase in water levels upstream of the "toe" (where the "toe" is the downstream limit of the accumulation). This response to the formation of the accumulation propagates upstream as a wave, increasing water levels well upstream of the jam: through the ferry crossing and into Beaver Lake, where its effect is diminished by the large width of the river there. It is likely that this wave precipitates the initial movement of ice at the ferry crossing, both by lifting the ice cover above a key (constraining) level and by fracturing the ice sheet as it passes.

The initial ice movement at the ferry crossing in three of the four years (1992, 1993 and 1995) was the crushing of the ferry passage channel. This did not occur in 1994 since, due to the late freezeup, no ferry passage channel was constructed. Figure 2.20 illustrates the ferry crossing in the early breakup period, where the path of the ferry passage channel is evident in the ice cover texture. Figure 2.21 illustrates the crossing shortly after collapse of the ferry passage channel in 1992. As presented in Table 2.17, for two of the three years in which there was a ferry passage channel failure, the water level at the ferry crossing was at or above 152 m at the time of this initial ice movement and the water level was 0.5 to 0.9 m above the freezeup water level. In 1995, however, the ferry passage channel failed when the ferry water level was still 0.3 m *below* the freezeup water level.

Breakup of the ice cover between the ferry crossing and Providence Narrows follows as ice movements and thermal deterioration between the ferry crossing and Providence Narrows result in repeated "shoves" in the Providence Rapids causing fluctuating water levels upstream. Breakup in Providence Rapids depends primarily on thermal effects: sufficient deterioration of the ice cover downstream of Ft. Providence to allow the ice to move downstream and/or sufficient heat absorbed in open water areas upstream to melt the ice in the accumulation. Breakup upstream of the ferry is also primarily dependent upon thermal input from heat absorbed in open water areas upstream. It may also be influenced by wind and, between the ice bridge and the ferry, water level fluctuations events in Providence Rapids.

It is important to note that the upstream propagation of a wave resulting from a "shove" in the Providence Rapids is not a necessary condition for breakup to occur in the ferry reach. In years where the breakup would be described as primarily thermal, dramatic fluctuations in water levels at the ferry crossing would not necessarily occur prior to breakup in the ferry reach. Consequently, although the initial movement of ice at the ferry crossing has on some occasions been preceded by a rapid or significant increase in water level at the ferry crossing and/or water levels at the ferry crossing rising in excess of the freezeup water level, the data to date proves neither is a necessary precedent for ice movement at the ferry crossing. Therefore, though either occurrence should be taken as warning of imminent ice movement at the ferry crossing, neither should be considered a necessary condition for such an occurrence.

Table 2.24 summarizes the timing of key events related to ice breakup in the study reach. In all four years of observations to date, the initial movement of ice, was consistently the failure of the ice cover in the upstream portion of Providence Rapids. In those same four years, the initial movement of ice at the ferry crossing occurred 1 to 6 days later. Although the timing is not precisely documented, the field observations made during 1991 confirm that the failure of the ice cover in the vicinity of the Big River section preceded the initial movement of ice at the ferry crossing. Clearly then, the initial movement of ice at Big River is a key indicator of imminent ice movement at the ferry crossing, and it is therefore a primary objective of this study to develop the framework of a model to forecast this occurrence.

2.3.5.3 Breakup in Beaver Lake

This reach extends from Great Slave Lake, through the North and South Channels around Big Island, and downstream to Burnt Point. Breakup in this reach is of importance in this study for two reasons. First of all, the nature of breakup in this area is predominantly thermal, with the development of open water progressing from small open water areas initiated at the upstream end of the outlet channels as a result of the release of warm water from the lake in the late winter period. Thus calibration of a thermal model in this reach would provide the thermal parameters for input into a model of breakup for the ferry reach, which would be comprised of thermal and dynamic components. The second reason for the importance of breakup in this reach to this study is that ice moving downstream from this reach typically interrupts spring ferry operations for 24 to 48 hours.

Warm water flowing under the ice cover tends to thin the ice, resulting in the downstream propagation of a melting front (thermal breakup). This is the type of breakup which is observed in the North and South Channels at Great Slave Lake each spring. Figures 2.22 and 2.23 illustrate the typical pattern of open water development in these two channels, respectively. Early breakup is primarily influenced by the issuance of warm water from Great Slave Lake which, because of its large storage capacity, can maintain water temperatures slightly above 0°C through the winter season, as discussed earlier. When heat from the overlying air mass or solar radiation is absorbed by the ice cover directly, the ice in the interstices between crystals melts often leaving behind the familiar "candled ice" which is, structurally, quite weak. Evidence from this, and other, studies suggests that most of this type of deterioration occurs near the ice surface (particularly in the top 30 cm or so), though not necessarily from the top down. It is important to note that the "candled ice" structure is merely the crystal structure of thermal ice, which has formed due to the vertical growth of the ice cover as heat is lost from the river water. The structure of frazil ice crystals is more granular in nature, and therefore the thermal deterioration of this type of ice does not result in candle-like remnants. Frazil ice is also more resistant to thermal deterioration.

As open water areas increase in the north and south channels at the lake outlet, heat from solar radiation and the overlying air mass begins to be absorbed by the water directly. This process quickly dominates the open water development at Great Slave Lake because the water surface has a much lower albedo than the ice cover. As the open water areas increase more heat can be absorbed. Therefore, the development of open water at the lake outlet accelerates through the breakup season. This is illustrated in Figure 2.24, which presents the measured open water areas in the reach upstream of Burnt Point. These areas were determined by drawing the open water areas (documented with video) onto scale maps of the reach and then planimetering the open water area.

It has consistently been observed that the breakup in the upper reach is predominantly thermal until both the North and South Channels are completely open. At this point the open water area is approximately 280 km^2. Subsequent open water development in the Beaver Lake area occurs as a result of cracking and breaking of ice in addition to thermal deterioration. As Figure 2.25 illustrates, the rate of open water development tends to become nearly linear at this time. With the exception of the 1994 breakup, in which dynamic effects occurred sooner than average, the rates of open water development after this point were also quite consistent: 37.4 km^2/day in 1992; 42.4 km^2/day in 1993; and 39.1 km^2/day in 1995.

Table 2.1 Ice records for the Mackenzie River at Ft. Providence (Lat. 61°20', Long. 117°40').
Source: Environment Canada, Ottawa

Ice Year	First Permanent Ice	Complete Freeze Over	Ice Safe for Traffic	Max. Ice Thickness	Ice Unsafe for Traffic	First Deterioration of Ice	Water Clear of Ice
1956	14-Oct	8-Dec		5'	10-Apr	10-May	
1957				6'		8-May	8-Jun
1958	11-Oct	12-Dec	15-Jan	3.5'	22-Apr	15-May	19-Jun
1959	6-Oct	31-Jan		5'		10-May	8-Jun
1960	22-Oct	29-Nov	20-Dec	5'	15-May	27-May	15-Jun
1961	9-Oct	7-Dec	12-Dec				
1972	25-Oct	30-Nov	30-Dec		20-Apr	12-Apr	5-May
1973	29-Oct	23-Nov	7-Dec		18-Apr	10-Apr	13-May
1974	29-Sep	9-Dec	4-Jan		19-Apr	8-May	14-May
1975	28-Oct	25-Nov	24-Jan		10-Apr	6-Apr	4-May
1976	22-Oct		14-Dec	7'	15-Apr	3-Apr	6-May
1977	2-Nov	5-Dec	29-Dec	7'	22-Apr	8-Apr	13-May
1978	30-Oct	28-Nov	8-Jan	6'	27-Apr	11-May	25-May
1979	3-Nov	5-Dec	20-Dec	7'	15-Apr	20-Apr	28-Apr
1980	27-Oct	19-Nov	9-Feb	7'	21-Apr	30-Apr	5-May
1981				7'	23-Apr	11-May	17-May
1984				10"	15-Apr	10-Apr	22-Apr

Table 2.2 Spring ice bridge and ferry operations (1962–1995).
Source: Marine Transportation, Ft Providence, NWT

Year	Ice Bridge Closed	Ferry Operations Resumed
1962		31-May
1963		17-May
1964		28-May
1965		20-May
1966		25-May
1967		29-May
1968		28-May
1969		25-May
1970		21-May
1971		11-May
1972		29-May
1973		14-May
1974		18-May
1975		14-May
1976		9-May
1977		8-May
1978		19-May
1979		25-May
1980	13-Apr	6-May
1981	21-Apr	6-May
1982	23-Apr	22-May
1983	19-Apr	20-May
1984	12-Apr	6-May
1985	22-Apr	19-May
1986	25-Apr	21-May
1987	16-Apr	9-May
1988	16-Apr	11-May
1989	15-Apr	20-May
1990	17-Apr	10-May
1991	19-Apr	12-May
1992	25-Apr	21-May
1993	14-Apr	6-May
1994	23-Apr	9-May
1995	25-Apr	13-May

Table 2.3 Mean daily insolation measured at Ft. Providence, 1992 to 1995.

Date	1992 (W/m²)	1993 (W/m²)	1994 (W/m²)	1995 (W/m²)
5-Apr		133	217	188
6-Apr	91	180	153	226
7-Apr	144	195	151	228
8-Apr	195	229	213	229
9-Apr	195	197	146	212
10-Apr	212	86	118	226
11-Apr	216	142	153	237
12-Apr	209	188	115	226
13-Apr	219	235	150	247
14-Apr	178	197	187	211
15-Apr	174	207	226	157
16-Apr	206	244	237	177
17-Apr	215	236	257	251
18-Apr	134	217	265	245
19-Apr	180	257	264	138
20-Apr	210	261	262	187
21-Apr	127	230	264	259
22-Apr	248	152	193	262
23-Apr	230	273	281	251
24-Apr	248	277	285	259
25-Apr	190	213	277	186
26-Apr	185	278	214	278
27-Apr	100	274	291	285
28-Apr	190	155	212	276
29-Apr	223	265	286	275
30-Apr	168	271	278	287
1-May	97	209	284	172
2-May	186	170	294	230
3-May	262	241	301	293
4-May	237	241	278	297
5-May	250	218	261	304
6-May	197	212	272	291
7-May	241	176	229	273
8-May	249	131	292	265
9-May	182	292	159	307
10-May	118	236	220	308
11-May	160	152	204	315
12-May	223	288	111	256
13-May	248	313	292	298
14-May	214	282	280	329
15-May	242	210	185	211
16-May	174	316	278	130
17-May	111	226	318	158
18-May	150	323	331	231
19-May	278	321	340	262
20-May	286	93	333	271

Note: shaded values calculated from sunshine ball data and Equation [2.1]

Table 2.4 Mean daily temperatures measured at Ft. Providence, 1992 to 1995.

Date	1992 (°C)	1993 (°C)	1994 (°C)	1995 (°C)
5-Apr			-5.4	-12.5
6-Apr			-2.8	-10.7
7-Apr	-9.7	-3.0	-3.9	-6.5
8-Apr	-17.5	0.1	-5.3	-5.5
9-Apr	-18.0	-3.1	-5.4	-1.4
10-Apr	-20.4	-1.6	-5.7	0.9
11-Apr	-15.9	0.5	-3.0	-0.1
12-Apr	-7.9	-0.3	-3.9	-3.1
13-Apr	-7.8	0.5	-5.1	-3.4
14-Apr	-11.0	2.1	-4.3	-4.1
15-Apr	-9.1	5.1	-1.5	-3.8
16-Apr	-5.7	3.0	2.4	-1.2
17-Apr	-6.9	1.5	2.4	1.2
18-Apr	-10.8	0.2	-2.1	2.6
19-Apr	-4.2	3.9	-1.4	1.6
20-Apr	-1.1	6.0	0.4	-0.2
21-Apr	1.9	7.4	3.1	0.6
22-Apr	0.6	2.4	2.0	3.8
23-Apr	-0.1	-2.8	-3.1	2.7
24-Apr	0.0	-5.0	-5.7	2.4
25-Apr	0.1	-3.2	-5.0	0.1
26-Apr	2.2	0.1	-3.1	2.3
27-Apr	0.1	3.5	-2.2	2.2
28-Apr	0.0	1.9	4.8	3.4
29-Apr	1.1	2.1	5.6	5.6
30-Apr	2.7	2.0	6.1	7.2
1-May	1.0	7.6	5.9	6.1
2-May	2.4	7.8	4.2	-0.6
3-May	6.1	5.3	5.8	0.4
4-May	9.4	2.0	8.7	7.9
5-May	-3.4	9.7	11.1	10.9
6-May	-3.9	12.8	11.8	8.6
7-May	-2.2	9.7	8.9	14.1
8-May	0.2	7.8	6.9	11.4
9-May	1.1	9.0	6.3	4.5
10-May	2.6	7.8	6.6	6.4
11-May	2.8	7.5	4.7	6.0
12-May	3.5	11.5	7.1	7.5
13-May	6.2	8.2	8.5	4.8
14-May	5.3	5.0	7.5	4.9
15-May	3.7	4.0	6.5	9.3
16-May	6.1	3.0	10.5	5.6
17-May	2.7	5.7	10.3	3.9
18-May	0.8	6.7	6.6	4.1
19-May	1.2	7.5	4.5	3.8
20-May	1.8	5.0	12.0	5.3

Note: 1992 data corrected with Equation [2.2]

Table 2.5 Mean daily RH measured at Ft. Providence, 1992 to 1995.

Date	1992 (%)	1993 (%)	1994 (%)	1995 (%)
5-Apr			53.3	46.4
6-Apr			73.5	48.6
7-Apr		50.0	76.7	50.9
8-Apr		63.2	61.8	45.9
9-Apr		64.0	63.9	63.8
10-Apr		86.5	79.1	69.7
11-Apr		78.0	82.4	72.4
12-Apr		77.5	72.6	65.1
13-Apr		78.0	73.6	59.9
14-Apr		77.3	73.2	55.2
15-Apr		69.7	71.0	80.1
16-Apr		74.0	54.0	79.1
17-Apr		77.3	51.8	74.0
18-Apr		80.1	45.1	69.5
19-Apr		60.4	47.1	70.1
20-Apr		53.6	53.1	69.0
21-Apr		51.8	63.7	72.2
22-Apr		73.2	55.1	61.2
23-Apr		55.4	42.9	56.9
24-Apr		60.0	62.6	65.0
25-Apr		51.6	71.6	54.3
26-Apr		56.7	71.2	54.5
27-Apr		54.2	68.1	49.7
28-Apr		65.2	52.8	65.6
29-Apr		60.8	61.1	57.2
30-Apr		68.0	62.3	49.3
1-May		65.8	63.9	65.5
2-May		76.5	64.4	70.0
3-May		66.0	49.0	59.7
4-May		68.3	42.7	44.1
5-May	*69.3*	58.1	48.6	37.5
6-May	*61.3*	57.2	42.3	50.2
7-May	*61.3*	73.6	56.9	40.9
8-May	*50.3*	68.0	59.8	50.5
9-May	*72.0*	52.5	71.3	68.8
10-May	*47.0*	51.1	74.8	63.6
11-May	*67.3*	78.2	76.9	53.7
12-May	*49.3*	57.1	82.0	50.5
13-May	*51.7*	56.9	74.6	46.1
14-May	*62.3*	53.5	69.0	37.2
15-May	*51.0*	55.0	70.5	51.4
16-May	*70.0*	64.0	50.5	79.1
17-May	*71.0*	64.2	51.4	73.2
18-May	*52.0*	59.2	51.1	56.7
19-May		56.0	62.6	54.0
20-May		79.3	48.5	47.4

Note: 1992 values were obtained from the Naural Resources station in Ft. Providence

Table 2.6 Mean daily wind speed measured at Ft. Providence, 1992 to 1995.

Date	**1992** **(m/s)**	**1993** **(m/s)**	**1994** **(m/s)**	**1995** **(m/s)**
5-Apr			0.6	1.6
6-Apr			1.2	2.0
7-Apr		2.0	1.3	1.6
8-Apr		1.4	1.4	1.4
9-Apr		1.4	1.7	1.1
10-Apr		0.9	0.9	0.7
11-Apr		0.5	0.7	1.1
12-Apr		1.8	2.7	1.2
13-Apr		1.4	1.4	1.6
14-Apr		1.5	1.9	1.3
15-Apr		1.3	1.5	1.4
16-Apr		1.4	1.2	1.8
17-Apr		1.6	2.6	2.4
18-Apr		1.2	1.7	1.8
19-Apr		1.4	1.8	1.6
20-Apr		1.3	1.5	1.2
21-Apr		1.6	1.1	1.2
22-Apr		1.8	1.5	1.5
23-Apr		1.4	1.9	1.6
24-Apr		1.6	1.1	1.3
25-Apr		1.4	1.5	1.6
26-Apr		1.5	1.4	1.5
27-Apr		1.3	1.8	1.5
28-Apr		1.5	1.6	1.6
29-Apr		1.7	1.4	1.8
30-Apr		1.7	1.4	1.5
1-May		1.6	1.4	1.3
2-May		1.8	2.0	1.6
3-May		1.7	2.0	1.4
4-May		2.1	1.6	1.3
5-May	*2.4*	1.3	2.1	1.4
6-May	*2.4*	1.0	2.1	1.6
7-May	*2.8*	1.5	2.7	2.0
8-May	*4.1*	2.2	1.3	1.6
9-May	*1.8*	3.0	1.9	1.8
10-May	*5.6*	2.3	1.6	1.6
11-May	*3.6*	1.6	1.8	1.6
12-May	*2.8*	1.4	1.4	1.1
13-May	*1.8*	1.4	2.1	1.5
14-May	*4.3*	1.8	1.5	1.6
15-May	*2.8*	1.3	1.4	1.6
16-May	*3.1*	1.6	1.5	1.9
17-May	*3.3*	1.2	1.8	1.9
18-May	*2.5*	1.6	1.6	2.3
19-May		1.8	1.9	1.4
20-May		1.0	1.8	1.4

Note: 1992 values were obtained from the Naural Resources station in Ft. Providence

Table 2.7 (a) Temperature profiles measured in Great Slave Lake, 1992.

Depth	25-Apr		Depth	29-Apr		Depth	4-May	
(m)	Ω	°C	(m)	Ω	°C	(m)	Ω	°C
2	101.05	-0.51	1.0	*101.1*	*-0.77*	1.0	101.17	-0.20
3	101.05	-0.51	1.5	*101.1*	*-0.77*	1.5	101.18	-0.18
4	101.36	0.28	2.0	*101.1*	*-0.77*	2.0	101.18	-0.18
5	101.39	0.36	2.5	*101.1*	*-0.77*	2.5	101.18	-0.18
6	101.40	0.38	3.0	*101.1*	*-0.77*	3.0	101.26	0.03
			3.5	*101.4*	*0.00*	3.5	101.45	0.51
			4.0	*101.4*	*0.00*	4.0	101.47	0.56
			4.5	*101.4*	*0.00*	4.5	101.48	0.59
			5.0	*101.4*	*0.00*	5.0	101.47	0.56
			5.5	*101.4*	*0.00*	5.5	101.45	0.51
			6.0	*101.4*	*0.00*	6.0	101.44	0.49
			6.44	*101.4*	*0.00*	6.5	101.44	0.49

Notes: 8060A ohmeter and 15.2 m probe

Fluke 87 ohmeter (reading at 0.1Ω precision) and 15.2 m probe

Table 2.7 (b) Estimate of corrected temperature profiles in Great Slave Lake, 1992.

Depth	25-Apr		Depth	29-Apr		Depth	4-May	
	Measured	Corrected		Measured	Corrected		Measured	Corrected
(m)	°C	°C	(m)	°C	°C	(m)	°C	°C
2	-0.51	0.00	1.0	-0.8	0.00	1.0	-0.20	0.00
3	-0.51	0.00	1.5	-0.8	0.00	1.5	-0.18	0.02
4	0.28	0.79	2.0	-0.8	0.00	2.0	-0.18	0.02
5	0.36	0.87	2.5	-0.8	0.00	2.5	-0.18	0.02
6	0.38	0.89	3.0	-0.8	0.00	3.0	0.03	0.23
			3.5	0.0	0.77	3.5	0.51	0.71
			4.0	0.0	0.77	4.0	0.56	0.76
			4.5	0.0	0.77	4.5	0.59	0.79
			5.0	0.0	0.77	5.0	0.56	0.76
			5.5	0.0	0.77	5.5	0.51	0.71
			6.0	0.0	0.77	6.0	0.49	0.69
			6.44	0.0	0.77	6.5	0.49	0.69
Integrated averages		**0.39**			**0.38**			**0.39**

Table 2.8 Water temperatures measured in the downstream reach, 1993 and 1994.

Location	**Date**	**Water temperature °C**
Ferry N	24-Apr-93	0.08
Ferry N	25-Apr-93	0.03
Ferry N	24-Apr-94	0.10
Dock	24-Apr-94	0.00
Boat Launch	24-Apr-94	0.05
Campground	24-Apr-94	0.00

Table 2.9 (a) Depth of snow on the rough ice cover (m) - Mackenzie River, 1992.

Location	Station (km)	22 to 25-Mar	5 to 9-Apr	25 to 28-Apr	29 to 30-Apr
Great Slave Lake	4.5	0.00	0.00	0.00	
Matheson Island	12.2		*0.26*	*0.08*	0.00
South Channel	16.8		*0.29*	*0.14*	0.00
d/s Range Island	24.8		*0.37*	0.23	0.25
North Channel	30.3		*0.38*	0.26	0.33
Kakisa River	34.7		0.56	0.34	0.37
d/s Kakisa River	41.1		0.49	0.48	
Beaver Lake	47.3		0.35	0.42	
Burnt Point	52.8	0.56	*0.36*	0.41	
Ice Bridge	59.2	0.42	0.52	0.25	
Dory Point	63.7		0.00	0.00	
Ferry	65.3		0.40	0.24	
Coast Guard	67.3		0.45	0.24	
Big River	72.7		0.29		
Blue House	76.7		0.61	0.26	
RCMP	77.9		0.54	0.13	
Ft. Prov. dock	79.5		0.49		
Averages		0.49	0.42	0.27	0.19

Italics indicate that the measurements were taken in pan ice adjacent to the rough ice

Table 2.9 (b) Depth of snow on the border ice (m) - Mackenzie River, 1992.

Location	Station (km)	22 to 25-Mar	5 to 9-Apr	25 to 28-Apr
Great Slave Lake	4.5	0.41		0.34
South Channel	16.8		0.37	0.26
Kakisa River	34.7	0.33		
Beaver Lake	47.3		0.38	0.17
Burnt Point	52.8	0.27		0.16
Ice Bridge	59.2	0.39		
Dory Point	63.7	0.46		0.00
Ferry	65.3	0.30		0.07
Coast Guard	67.3		0.45	0.18
Big River	72.7		0.38	
Ft. Prov. dock	79.5		0.45	
Mills Lake	103.9		0.50	
Averages		0.36	0.42	0.17

Table 2.10 (a) Depth of snow on the rough ice (m) - Mackenzie River, 1993.

Location	Station (km)	23-Feb-93	7 to 8-Apr-93	24 to 25-Apr-93
Great Slave Lake	4.2			
South Channel	16.7		0.00	
Kakisa River	34.2		0.04	
Beaver Lake	47.5		0.25	
Burnt Point	52.6		0.10	
Ice Bridge	59.2		0.07	
Dory Point	63.7			
Ferry	65.3		0.00	0.00
Coast Guard	67.3			
Blue Quonset	71.5		0.00	
Big River	72.7	0.19	0.00	
Campground	75.0	0.23	0.05	
Blue House	76.7	0.29	0.05	
Boat Launch	77.4	0.26	0.05	
RCMP	77.9	0.19		
Ft. Prov. dock	79.5	0.23	0.03	0.00
Orange Cabin	89.5		0.03	
Mills Lake	103.9		0.17	
Averages		0.23	0.06	0.00

Table 2.10 (b) Depth of snow on the border ice (m) - Mackenzie River, 1993.

Location	Station (km)	17-Dec-92	23-Feb	7 to 8-Apr
Great Slave Lake	4.2	0.07		0.03
South Channel	16.7	0.05		0.03
Kakisa River	34.2	0.01		0.00
Beaver Lake	47.5	0.04		0.00
Burnt Point	52.6	0.02		0.00
Ice Bridge	59.2	0.00	0.15	0.00
Dory Point	63.7	0.02	0.20	0.00
Ferry	65.3	0.02		
Coast Guard	67.3	0.02	0.19	0.00
Blue Quonset	71.5	0.03	0.18	0.00
Big River	72.7	0.03		
Campground	75.0	0.02		
Blue House	76.7			
Boat Launch	77.4			
RCMP	77.9	0.03		
Ft. Prov. dock	79.5	0.08		
Orange Cabin	89.5	0.03		
Mills Lake	103.9	0.08		0.02
Averages		0.03	0.18	0.01

Table 2.11 (a) Depth of snow on the rough ice (m) - Mackenzie River, 1994.

Location	Station (km)	14 to 16-Mar	12 to 14-Apr	19.Apr	24-Apr	27-Apr
Great Slave Lake	4.2					
South Channel	16.7	0.36				
Kakisa River	34.2					
Beaver Lake	47.5	0.35				
Burnt Point	52.6	0.43				
Ice Bridge	59.2	*0.30*	*0.27*			
Dory Point	63.7					
Ferry	65.3	0.11	0.82	*0.10*		
Coast Guard	67.3					
Blue Quonset	71.5	0.22				
Big River	72.7	0.19				0.08
Campground	75.0	0.35				
Blue House	76.7	0.32				
Boat Launch	77.4	0.12			0.08	0.08
RCMP	77.9	0.38	0.72			
Ft. Prov. dock	79.5					0.11
Orange Cabin	89.5					
Mills Lake	103.9		0.38			
Averages		0.28	0.55	0.10	0.08	0.09

Note: italized values are based on transverse profiles

Table 2.11 (a) Depth of snow on the border ice (m) - Mackenzie River, 1994.

Location	Station (km)	14 to 16-Mar	12 to 14-Apr	24-Apr	26-Apr
Great Slave Lake	4.2	0.46	0.51		
South Channel	16.7	0.46	0.45		
Kakisa River	34.2				
Beaver Lake	47.5	0.32	0.27		
Burnt Point	52.6	0.35	0.29		
Ice Bridge	59.2	*0.29*	*0.19*		0.09
Dory Point	63.7	0.38		0.17	
Ferry	65.3			0.00	
Coast Guard	67.3	0.32		0.22	
Blue Quonset	71.5		*open water*		
Big River	72.7		0.10	0.11	
Campground	75.0			0.13	
Blue House	76.7		*open water*		
Boat Launch	77.4				
RCMP	77.9				
Ft. Prov. dock	79.5	0.29	0.10	0.08	
Orange Cabin	89.5				
Mills Lake	103.9				
Averages		0.36	0.27	0.12	0.09

Table 2.12 Depth of snow on the ice cover (m) - Mackenzie River, 19 to 22-Apr-95.

Location	**Station (km)**	**on the rough ice**	**on the border ice**
Great Slave Lake	4.2	*open water*	0.51
South Channel	16.7	0.31	0.49
Kakisa River	34.2	0.44	0.38
Beaver Lake	47.5	0.37	0.41
Burnt Point	52.6	0.26	0.38
Ice Bridge	59.2	*0.31*	0.23
Dory Point	63.7		
Ferry	65.3	0.26	
Coast Guard	67.3		0.24
Blue Quonset	71.5		0.22
Big River	72.7	0.29	
Campground	75.0	0.36	
Blue House	76.7	0.28	
Boat Launch	77.4		0.28
RCMP	77.9	0.33	
Ft. Prov. dock	79.5	0.29	
Averages		0.32	0.35

Note: *on 4-May-95, zero snow depths were observed between the ice bridge and the dock in Ft. Prov.*

Table 2.13 (a) Rough ice thickness (m) - Mackenzie River, 1992.

Location	Station (km)	22 to 25-Mar	5 to 9-Apr	25 to 28-Apr	29 to 30-Apr	3 to 4-May
Great Slave Lake †	4.5	0.00	0.00	0.00	0.00	0.00
Matheson Island	12.2		*0.51*	*0.60*	0.00	0.00
South Channel	16.8		*0.75*	*0.45*	0.40	0.00
d/s Range Island	24.8		*0.87*	**1.11**	1.07	0.99
North Channel	30.3		*1.13*	**1.27**	1.30	1.04
Kakisa River	34.7		1.17	**1.26**	1.22	1.18
d/s Kakisa River	41.1		*0.59*	**1.38**	*0.78*	>1.4††
Beaver Lake	47.3		1.04	**1.63**	1.66	1.57
Burnt Point	52.8	1.55	*0.81*	**>1.7††**	1.75	>1.6††
Ice Bridge	59.2	>1.7††	**1.76**	1.70	**>1.7††**	>1.7††
Dory Point †	63.7	0.00	0.00	0.00		0.00
Ferry	65.3		1.04	**1.08**	1.03	
Coast Guard	67.3		1.07	1.30		
Blue Quonset	71.5					0.00
Big River	72.7		0.72			
Blue House	76.7		1.10	**1.19**		0.00
Boat Launch	77.4			1.22		
RCMP	77.9		1.42	**>1.7††**		
Ft. Prov. dock	79.5		1.57	1.50		

† Open lead at the centre of the channel at Dory Point and Great Slave Lake
†† ">" indicates that the actual ice thickness exceeded the thickness stated
Italics indicate that the measurements were taken in pan ice adjacent to the rough ice
Bold indicates that measurements were taken in a different hole from previous

Table 2.13 (b) Border ice thickness (m) - Mackenzie River, 1992.

Location	Station (km)	22 to 25-Mar	5 to 9-Apr	25 to 28-Apr	29 to 30-Apr	3 to 4-May
Great Slave Lake	4.5	0.8	0.64	0.62	0.75	0.51
South Channel	16.8		0.74	0.78	0.78	0.00
Kakisa River	34.7	0.7	0.69	1.04		0.00
Beaver Lake	47.3		1.57	1.10	0.98	0.00
Burnt Point	52.8	1.0	1.09	0.96	0.94	0.86
Ice Bridge	59.2	0.8				
Dory Point	63.7	0.6		0.66		
Ferry	65.3	0.9		0.94	0.92	
Coast Guard	67.3		0.76	0.70		
Big River	72.7		0.75			
Ft. Prov. dock	79.5		1.07	0.75		
Mills Lake	103.9			0.59		
Averages		0.79	0.91	0.81	0.87	0.69

Table 2.14 (a) Rough ice thickness (m) - Mackenzie River, 1993.

Location	Station (km)	23-Feb-93	7&8-Apr-93	25-Apr-93
Great Slave Lake	4.2			
South Channel	16.7		1.13	
Kakisa River	34.2		1.25	
Beaver Lake	47.5		1.12	
Burnt Point	52.6		1.36	
Ice Bridge	59.2		1.74	
Dory Point	63.7	0.90		
Ferry	65.3	0.47	1.03	0.82
Coast Guard	67.3	0.79		
Blue Quonset	71.5		0.65	
Big River	72.7	0.76	0.74	
Campground	75.0	1.11	1.90	
Blue House	76.7	1.93	1.87	
Boat Launch	77.4	1.83	1.83	
RCMP	77.9	0.93	0.96	
Ft. Prov. dock	79.5		0.90	0.75
Orange Cabin	89.5		0.96	
Mills Lake	103.9		1.18	

Table 2.14 (b) Border ice thickness (m) - Mackenzie River, 1993.

Location	Station (km)	16&17-Dec-92	23-Feb-93	7&8-Apr-93
Great Slave Lake	4.2	0.28		0.98
South Channel	16.7	0.49		1.12
Kakisa River	34.2	0.51		0.92
Beaver Lake	47.5			0.80
Burnt Point	52.6	0.30		0.79
Ice Bridge	59.2	0.41	0.90	1.06
Dory Point	63.7	0.20	0.90	0.76
Ferry	65.3			
Coast Guard	67.3	0.20	0.79	0.80
Blue Quonset	71.5	0.15	0.86	0.68
Big River	72.7	0.21		
Campground	75.0	0.28		
Blue House	76.7			
Boat Launch	77.4			
RCMP	77.9	0.18		
Ft. Prov. dock	79.5	0.44		1.20
Orange Cabin	89.5	0.68		
Mills Lake	103.9	0.49	0.72	0.78
Averages		0.34	0.84	0.90

Table 2.15 (a) Rough ice thickness (m) - Mackenzie River, 1994.

Location	Station (km)	14 to 16-Mar	12 to 14-Apr	19-Apr	24-Apr	27 to 29-Apr	1-May
Great Slave Lake	4.2						
South Channel	16.7	1.07					
Kakisa River	34.2						
Beaver Lake	47.5	1.43					
Burnt Point	52.6	1.07					
Ice Bridge	59.2	*0.92*	*1.01*				
Dory Point	63.7						
Ferry	65.3	0.79	0.88	*0.93*		0.70	0.76
Coast Guard	67.3						
Blue Quonset	71.5						
Big River	72.7	0.90				0.87	
Campground	75.0	0.63					
Blue House	76.7	0.69					
Boat Launch	77.4	0.51			0.91	1.04	
RCMP	77.9	1.08	1.14				
Ft. Prov. dock	79.5					1.46	
Orange Cabin	89.5						
Mills Lake	103.9		1.15				

Note: italized values are based on transverse ice profiles

Table 2.15 (b) Border ice thickness (m) - Mackenzie River, 1994.

Location	Station (km)	14 to 16-Mar	12 to 14-Apr	24-Apr	26-Apr	30-Apr	1-May
Great Slave Lake	4.2	0.82	0.79				
South Channel	16.7	0.85	0.88				
Kakisa River	34.2						
Beaver Lake	47.5	0.80	0.91				
Burnt Point	52.6	0.74	0.74				
Ice Bridge	59.2	*0.89*	*0.79*		0.87		
Dory Point	63.7	0.58		0.59			
Ferry	65.3			1.15		0.55	0.58
Coast Guard	67.3	0.61		0.46			
Blue Quonset	71.5		*open water*				
Big River	72.7			0.89			
Campground	75.0			0.69			
Blue House	76.7		*open water*				
Boat Launch	77.4						
RCMP	77.9						
Ft. Prov. dock	79.5	1.10	1.39	1.28			
Orange Cabin	89.5						
Mills Lake	103.9						
Averages		0.80	0.92	0.84	0.87	0.55	0.58

Table 2.16 (a) Rough ice thickness (m) - Mackenzie River, 1995.

Location	Station (km)	19 to 22-Apr	4-May
Great Slave Lake	4.2	*open water*	
South Channel	16.7	1.20	
Kakisa River	34.2	0.86	
Beaver Lake	47.5	1.37	
Burnt Point	52.6	1.22	
Ice Bridge	59.2	0.95	
Dory Point	63.7		
Ferry	65.3	1.18	
Coast Guard	67.3		
Blue Quonset	71.5		0.42
Big River	72.7	0.79	
Campground	75.0	1.34	
Blue House	76.7	>2	
Boat Launch	77.4		
RCMP	77.9	0.75	
Ft. Prov. dock	79.5	1.80	

Table 2.16 (b) Border ice thickness (m) - Mackenzie River, 1995.

Location	Station (km)	19 to 22-Apr	4-May
Great Slave Lake	4.2	0.87	
South Channel	16.7	1.03	
Kakisa River	34.2	0.91	
Beaver Lake	47.5	0.79	
Burnt Point	52.6	0.70	
Ice Bridge	59.2	0.80	
Dory Point	63.7		1.05
Ferry	65.3		
Coast Guard	67.3	0.70	
Blue Quonset	71.5	0.41	1.50
Big River	72.7		
Campground	75.0		1.80
Blue House	76.7		1.30
Boat Launch	77.4	0.75	0.38
RCMP	77.9		0.66
Ft. Prov. dock	79.5		2.00
Averages		0.77	1.24

Table 2.17 Key water levels at the ferry crossing, 1992 to 1995.

Year	**Water Level at the Ferry Crossing**		**Difference** (m)
	at freezeup (m)	**at the time of the initial ice movement**† (m)	
1992	152.24	152.7	0.5
1993	151.14	152.0	0.9
1994	151.38	152.4††	1.0
1995	151.66	151.4	-0.3

† *initial ice movement at the ferry crossing*

†† *ferry water level remained above the freezeup level throughout the winter in 1994*

Table 2.18 Calibration of hydraulic model for the Mackenzie River between Great Slave Lake and Mills Lake, 11-Jul-92.

Location	Station (km)	Thalweg elevation (m)	Surveyed water level 11-Jul-92 (m)	Calibrated bed roughness n_{bed}	Discharge (m^3/s)	Computed water level (m)	Calculated minus surveyed water level (m)
G. S. Lake	4.2	153.03	157.11	0.022	7990	157.10	-0.01
South Channel	16.7	151.57	156.11	0.022	7990	156.07	-0.04
Kakisa River	34.2	149.92	154.72	0.022	8500	154.55	-0.17
Beaver Lake	47.5	149.56	153.98	0.022	8500	154.06	0.08
Burnt Point	52.6	147.59	153.89	0.022	8500	153.90	0.01
Ice Bridge	59.2	146.70	153.69	0.022	8500	153.51	-0.18
Dory Point	63.7	145.10	152.46	0.020	8500	152.47	0.01
Ferry	65.3	144.79	151.80	0.020	8500	151.93	0.13
Coast Guard	67.3	142.97	151.59	0.020	8500	151.50	-0.09
Blue Quonset	71.5	143.19	150.60	0.020	8500	150.35	-0.25
Big River	72.7	141.37	150.03	0.030	7570	149.94	-0.09
Campground	75.0	139.61	147.85	0.030	7570	147.72	-0.13
Blue House	76.7	140.18	146.20	0.030	7570	146.12	-0.08
Boat Launch	77.4	139.06	145.93	0.025	7570	145.97	0.04
RCMP	77.9	139.57	145.70	0.025	7570	145.71	0.01
Ft. Prov. Dock	79.5	137.50	145.19	0.025	7570	145.35	0.16
Mills Lake	103.9	134.15	142.54	0.020	7570	142.54	--

Table 2.19 Verification of hydraulic model for the Mackenzie River between Beaver Lake and Ft. Prov., 29-Aug-91.

Location	Station (km)	Thalweg elevation (m)	Surveyed water level 29-Aug-91 (m)	Bed roughness n_{bed}	Discharge (m^3/s)	Computed water level (m)	Calculated minus surveyed water level (m)
Beaver Lake	47.5	149.56	153.80	0.022	7000	153.65	-0.15
Burnt Point	52.6	147.59	153.60	0.022	7000	153.48	-0.12
Ice Bridge	59.2	146.70	153.39	0.022	7000	153.10	-0.29
Dory Point	63.7	145.10	152.13	0.020	7000	151.96	-0.17
Ferry	65.3	144.81	151.48	0.020	7000	151.41	-0.07
Coast Guard	67.3	142.97	151.14	0.020	7000	151.01	-0.13
Blue Quonset	71.5	143.19		0.020	7000	149.93	
Big River	72.7	141.37	149.53	0.030	6450	149.53	0.00
Campground	75.0	139.61		0.030	6450	147.33	
Blue House	76.7	140.18	145.90	0.030	6450	145.75	-0.15
Boat Launch	77.4	139.06		0.025	6450	145.60	
RCMP	77.9	139.57	145.36	0.025	6450	145.36	--

Table 2.20 Calibration of hydraulic model for the Mackenzie River between Great Slave Lake and Big River, April 1992.
(measured discharge = 4350 m^3/s on 27-Apr-92)

Location	Station (km)	Thalweg elevation (m)	Surveyed water level 27-Apr-92 (m)	Calibrated bed roughness[1] n_{bed}	Weighted ice thickness (m)	Calibrated ice roughness n_{ice}	Computed water level (m)	Calculated minus surveyed water level (m)
Great Slave Lake	4.2	153.03	157.06	0.022	0.6	0.015	157.36	0.30
South Channel	16.7	151.57	156.59	0.022	0.8	0.015	156.59	0.00
Kakisa River	34.2	149.92	155.03	0.022	1.2	0.015	155.05	0.02
Beaver Lake	47.5	149.56	154.44	0.022	1.2	0.015	154.44	0.00
Burnt Point	52.6	147.59	154.30	0.022	1.2	0.015	154.28	-0.02
Ice Bridge	59.2	146.70	154.10	0.022	1.7	0.015	153.90	-0.20
Dory Point	63.7	145.10	152.77	0.020	1.2	0.015	152.74	-0.03
Ferry	65.3	144.79	152.10	0.020	1.2	0.015	152.26	0.16
Coast Guard	67.3	142.97	151.80	0.020	1.2	0.015	151.92	0.12
Blue Quonset	71.5	143.19		0.020	1.2	0.015	151.02	
Big River	72.7	141.37	150.54	0.030	1.2	0.015	150.54	–

Table 2.21 Calibration of hydraulic model for the Mackenzie River between Great Slave Lake and Big River, April 1993.
(measured discharge = 2410 m^3/s on 7-Apr-93)

Location	Station (km)	Thalweg elevation (m)	Surveyed water level 7 and 8-Apr-93 (m)	Calibrated bed roughness[1] n_{bed}	Weighted ice thickness (m)	Calibrated ice roughness n_{ice}	Computed water level (m)	Calculated minus surveyed water level (m)
G. S. Lake	4.2	153.03	156.95	0.022	0.8	0.015	156.86	-0.09
South Channel	16.7	151.57	155.90	0.022	1.1	0.015	156.10	0.20
Kakisa River	34.2	149.92	154.30	0.022	1.1	0.015	154.27	-0.03
Beaver Lake	47.5	149.56	153.52	0.022	1.1	0.015	153.46	-0.06
Burnt Point	52.6	147.59	153.37	0.022	1.1	0.015	153.33	-0.04
Ice Bridge	59.2	146.70	153.15	0.022	1.7	0.015	153.11	-0.04
Dory Point	63.7	145.10	151.80	0.020	1.0	0.015	151.52	-0.28
Ferry	65.3	144.79	150.92	0.020	1.0	0.015	150.78	-0.14
Coast Guard	67.3	142.97	150.48	0.020	0.7	0.015	150.55	0.07
Blue Quonset	71.5	143.19	149.77	0.020	0.7	0.015	149.68	-0.09
Big River	72.7	141.37	149.27	0.030	0.7	0.015	149.27	–

[1] *based on open water calibration*

Table 2.22 Calibration of hydraulic model for the Mackenzie River between Great Slave Lake and Big River, April 1994.
(measured discharge = 2390 m^3/s on 19-Apr-94)

Location	Station (km)	Thalweg elevation (m)	Surveyed water level 12-Apr-94 (m)	Calibrated bed roughness[1] n_{bed}	Weighted ice thickness (m)	Calibrated ice roughness n_{ice}	Computed water level (m)	Calculated minus surveyed water level (m)
G. S. Lake	4.2	153.03	156.87	0.022	0.8	0.015	156.77	-0.10
South Channel	16.7	151.57	155.80	0.022	1.0	0.015	155.97	0.17
Kakisa River	34.2	149.92		0.022	1.0	0.015	154.09	
Beaver Lake	47.5	149.56	153.24	0.022	1.0	0.015	153.13	-0.11
Burnt Point	52.6	147.59	153.08	0.022	1.0	0.015	152.98	-0.10
Ice Bridge	59.2	146.70	152.82	0.022	1.0	0.015	152.78	-0.04
Dory Point	63.7	145.10		0.020	1.0	0.015	151.76	
Ferry	65.3	144.79	151.37	0.020	1.0	0.015	151.41	0.04
Coast Guard	67.3	142.97		0.020	1.0	0.030	151.22	
Blue Quonset	71.5	143.19		0.020	1.0	0.030	149.91	
Big River	72.7	141.37	148.67	0.030	1.0	0.030	148.67	--

Table 2.23 Calibration of hydraulic model for the Mackenzie River between Great Slave Lake and Big River, April 1995.
(measured discharge = 1980 m^3/s on 19-Apr-95)

Location	Station (km)	Thalweg elevation (m)	Surveyed water level 19-Apr-95 (m)	Calibrated bed roughness[1] n_{bed}	Weighted ice thickness (m)	Calibrated ice roughness n_{ice}	Computed water level (m)	Calculated minus surveyed water level (m)
G. S. Lake	4.2	153.03	156.87	0.022	0.9	0.020	156.81	-0.06
South Channel	16.7	151.57	155.83	0.022	1.1	0.020	156.03	0.20
Kakisa River	34.2	149.92	154.23	0.022	1.1	0.020	154.16	-0.07
Beaver Lake	47.5	149.56	153.33	0.022	1.1	0.020	153.15	-0.18
Burnt Point	52.6	147.59	153.14	0.022	1.1	0.020	152.99	-0.15
Ice Bridge	59.2	146.70	152.94	0.022	1.1	0.020	152.80	-0.14
Dory Point	63.7	145.10	151.77	0.020	1.1	0.020	151.54	-0.23
Ferry	65.3	144.79	150.76	0.020	1.2	0.020	150.71	-0.05
Coast Guard	67.3	142.97	150.18	0.020	0.8	0.020	150.47	0.29
Blue Quonset	71.5	143.19	149.65	0.020	0.8	0.020	149.44	-0.21
Big River	72.7	141.37	149.04	0.030	0.8	0.020	149.04	--

[1] *based on open water calibration*

Table 2.24 Timing of key breakup events, 1992 to 1995.

Year	Freezeup front passed through the ferry crossing	Breakup - Initial Ice Movement			Ferry Reach clear	Prov. Rapids open
		at Big River	at the Ferry Crossing	difference (days)		
1992	29-Nov-91	3-May-92	4-May-92	1	11-May-92	21-May-92
1993	10-Dec-92	22-Apr-93	26-Apr-93	4	30-Apr-93	2-May-93
1994	15-Jan-94	1-May-95	7-May-94	6	8-May-94	7-May-94
1995	18-Nov-94	4-May-95	5-May-95	1	8-May-95	*unknown* [†]

Year	Ferry Reach snow mostly gone from ice cover	Noticable change in albedo on Beaver Lake		Beaver Lake open
		Date	open water area (km^2)	
1992	1-May-92	4-May-92	120	16-May-92
1993	*no snow on the ice cover prior to breakup*	26-Apr-93	76	9-May-93
1994	1-May-94	7-May-94	98	15-May-94
1995	29-Apr-95	6-May-95	128	*19-May-95* [††]

[†] *however, it is known that this occurred after 13-May-95*

[††] *this date was estimated from the WSC gauge record at the ferry crossing*

Table 2.25 Development of open water area on the Mackenzie River upstream of Burnt Point, 1992 to 1995.

1992		**1993**		**1994**		**1995**	
Date	**Area** (sq.km.)	**Date**	**Area** (sq.km.)	**Date**	**Area** (sq.km.)	**Date**	**Area** (sq.km.)
21-Mar	1	9-Apr	8	19-Apr	7	20-Apr	20
4-Apr	2	22-Apr	43	20-Apr	7	21-Apr	24
25-Apr	46	23-Apr	48	21-Apr	8	28-Apr	43
29-Apr	74	24-Apr	55	22-Apr	10	29-Apr	55
30-Apr	83	25-Apr	64	23-Apr	10	30-Apr	69
2-May	102	26-Apr	76	24-Apr	11	1-May	82
3-May	110	27-Apr	87	25-Apr	13	2-May	84
4-May	120	28-Apr	105	26-Apr	15	3-May	91
5-May	126	29-Apr	121	28-Apr	20	4-May	103
6-May	140	30-Apr	144	29-Apr	23	5-May	124
7-May	158	1-May	176	30-Apr	25	6-May	128
9-May	201	2-May	200	1-May	31	7-May	153
11-May	269	3-May	222	2-May	34	8-May	162
12-May	293	4-May	243	3-May	42	9-May	181
13-May	334	5-May	281	4-May	52	10-May	195
14-May	352	6-May	316	6-May	81	11-May	231
15-May	399	7-May	361	7-May	92	12-May	252
17-May	496	8-May	404	8-May	113	13-May	291
		9-May	450	9-May	159	*19-May*	*500*
				11-May	210		
				12-May	225		
				13-May	254		
				14-May	283		
				15-May	394		

Note: the italicized value was estimated from the WSC record

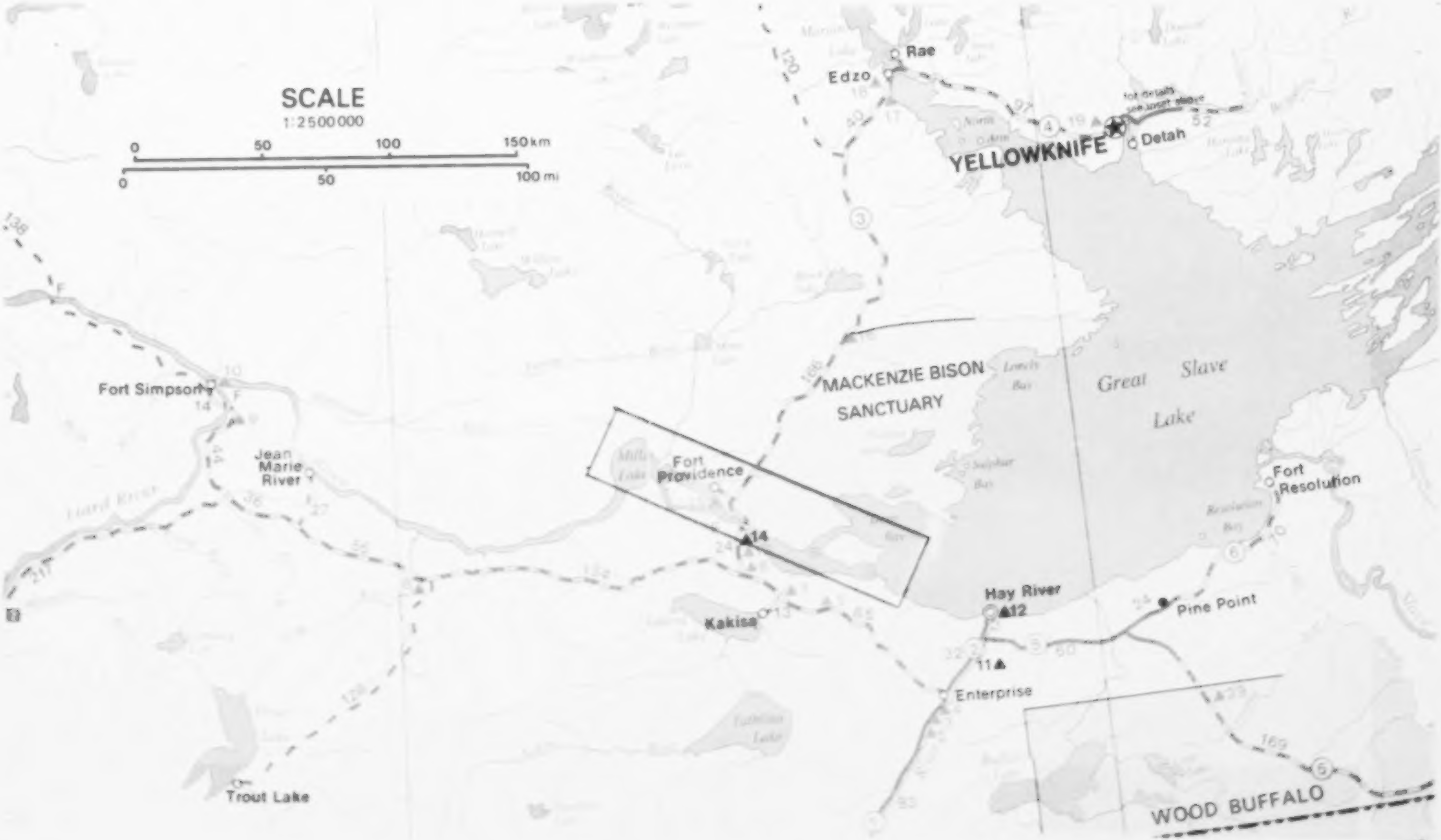
SCALE
1:2500000
0
50
100
150km
0
50
100 mi
Rae
Edzo
YELLOWKNIFE
Detah
for details see inset above
MACKENZIE BISON
SANCTUARY
Great Slave Lake
Fort Resolution
Pine Point
Hay River
12
11
Enterprise
Fort Providence
14
Kakisa
Fort Simpson
Jean Marie River
Trout Lake
WOOD BUFFALO

Figure 2.1 Location of study reach.

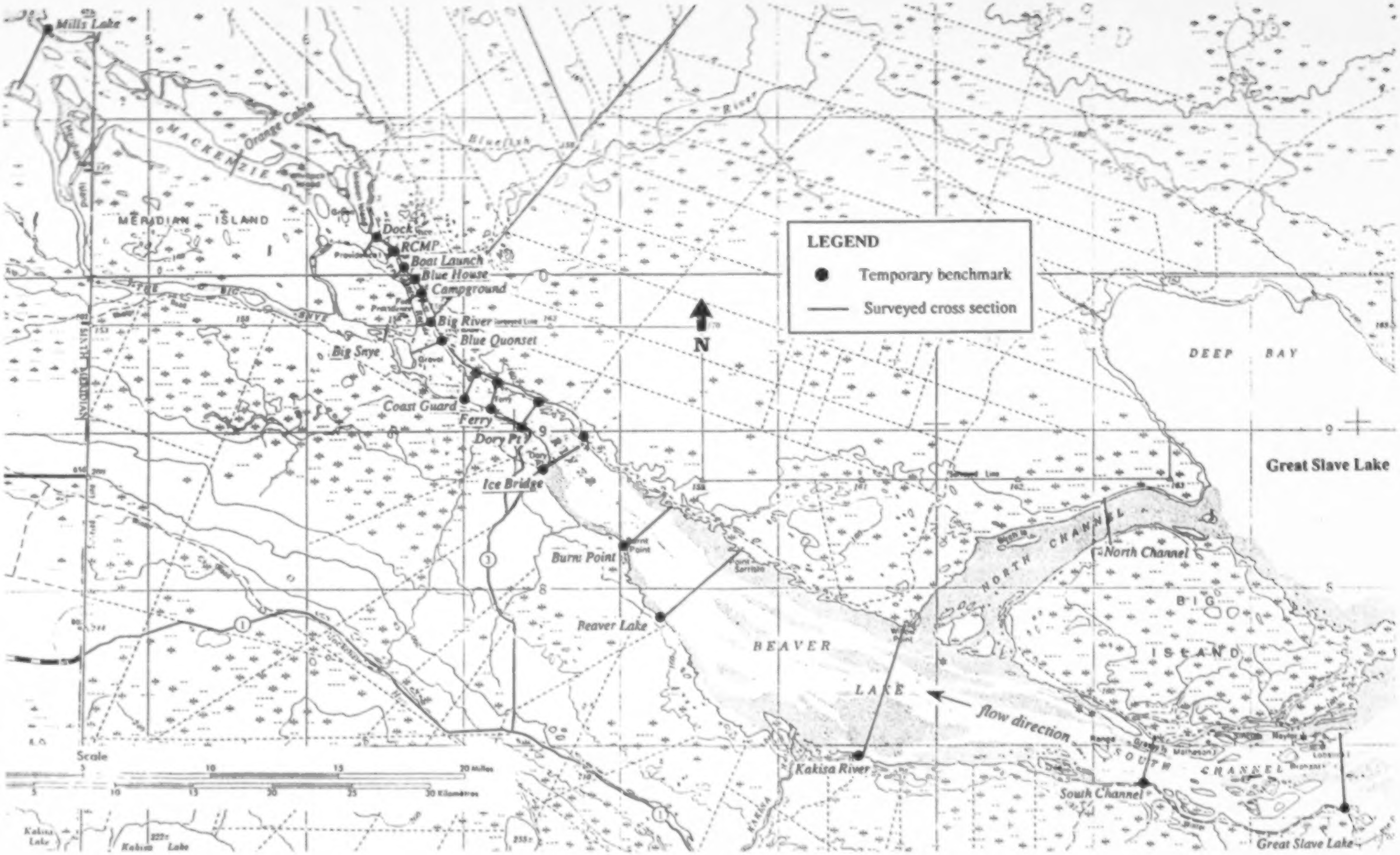
LEGEND
Temporary benchmark
Surveyed cross section
N
Mills Lake
MACKENZIE
Orange Cabin
MERIDIAN ISLAND
SIXTH MERIDIAN
Dock
RCMP
Boat Launch
Blue House
Campground
Big River
Blue Quonset
Big Snye
Coast Guard
Ferry
Dory Pt
Ice Bridge
Burnt Point
Reaver Lake
BEAVER
LAKE
flow direction
Kakisa River
NORTH CHANNEL
North Channel
BIG
ISLAND
SOUTH CHANNEL
South Channel
DEEP BAY
Great Slave Lake
Great Slave Lake
Scale
20 Miles
30 Kilomètres
Kakisa Lake

Figure 2.2 Location of cross sections and temporary benchmarks on the Mackenzie River near Ft. Providence.

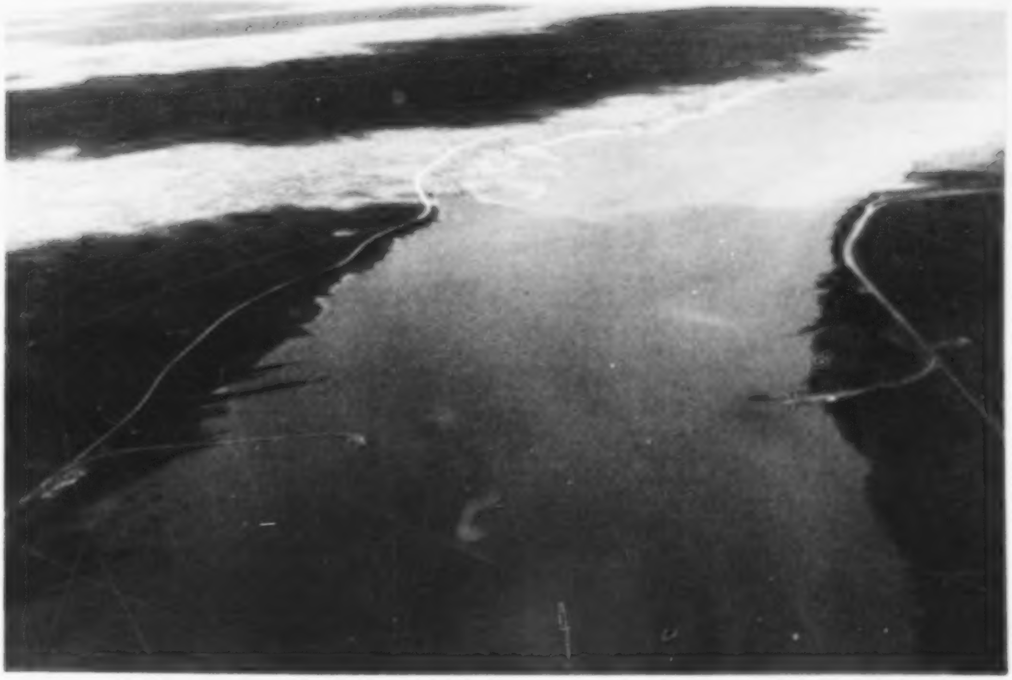

Figure 2.3 The Mackenzie River looking upstream to the Ft. Providence ferry crossing.

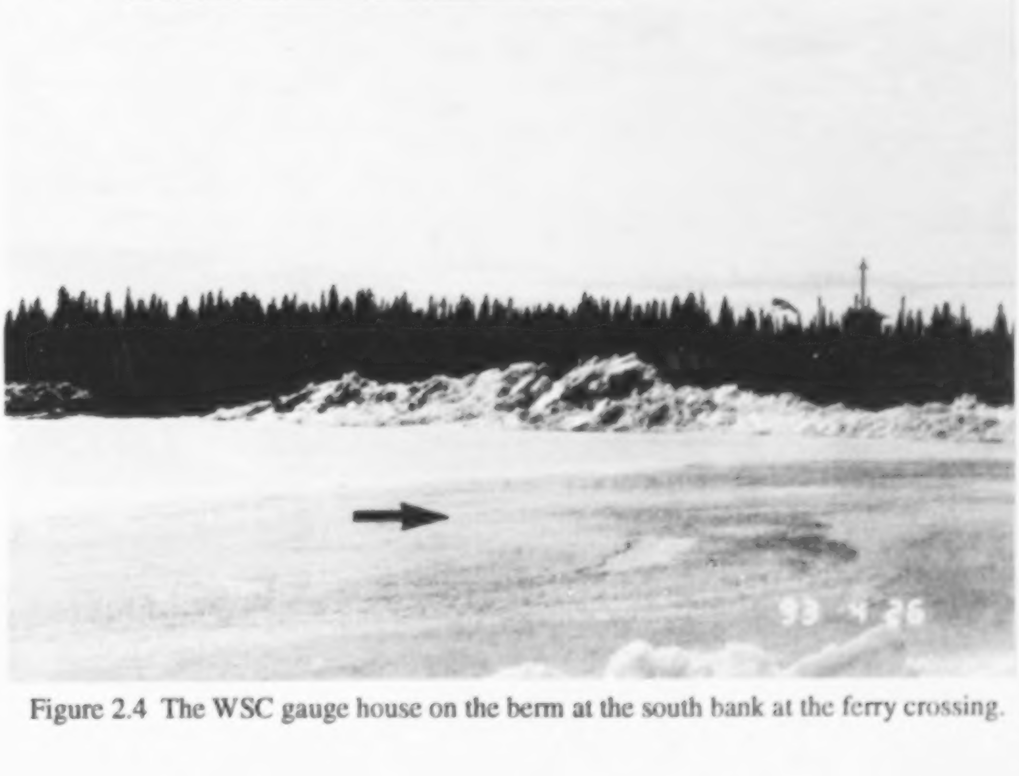

Figure 2.4 The WSC gauge house on the berm at the south bank at the ferry crossing.

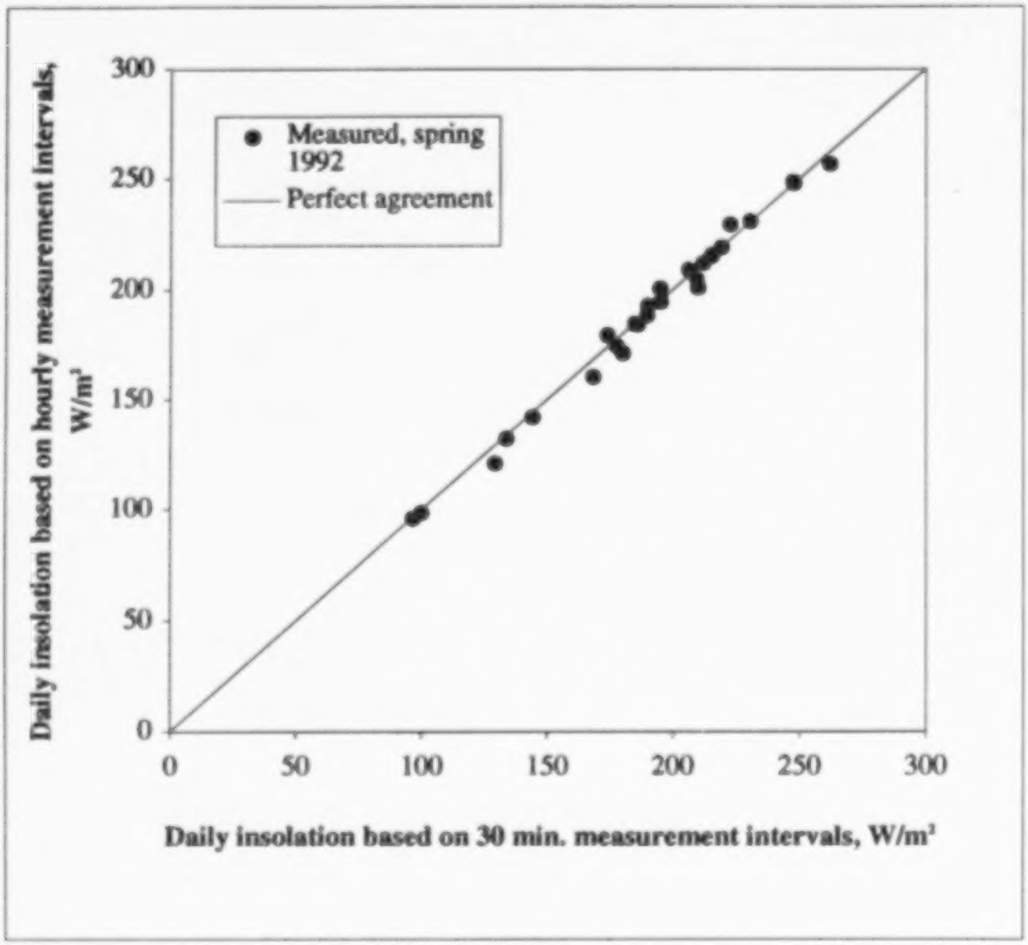

Figure 2.5 Comparison of daily insolation values obtained with hourly measurements to those based on a measurement interval of 30 minutes.

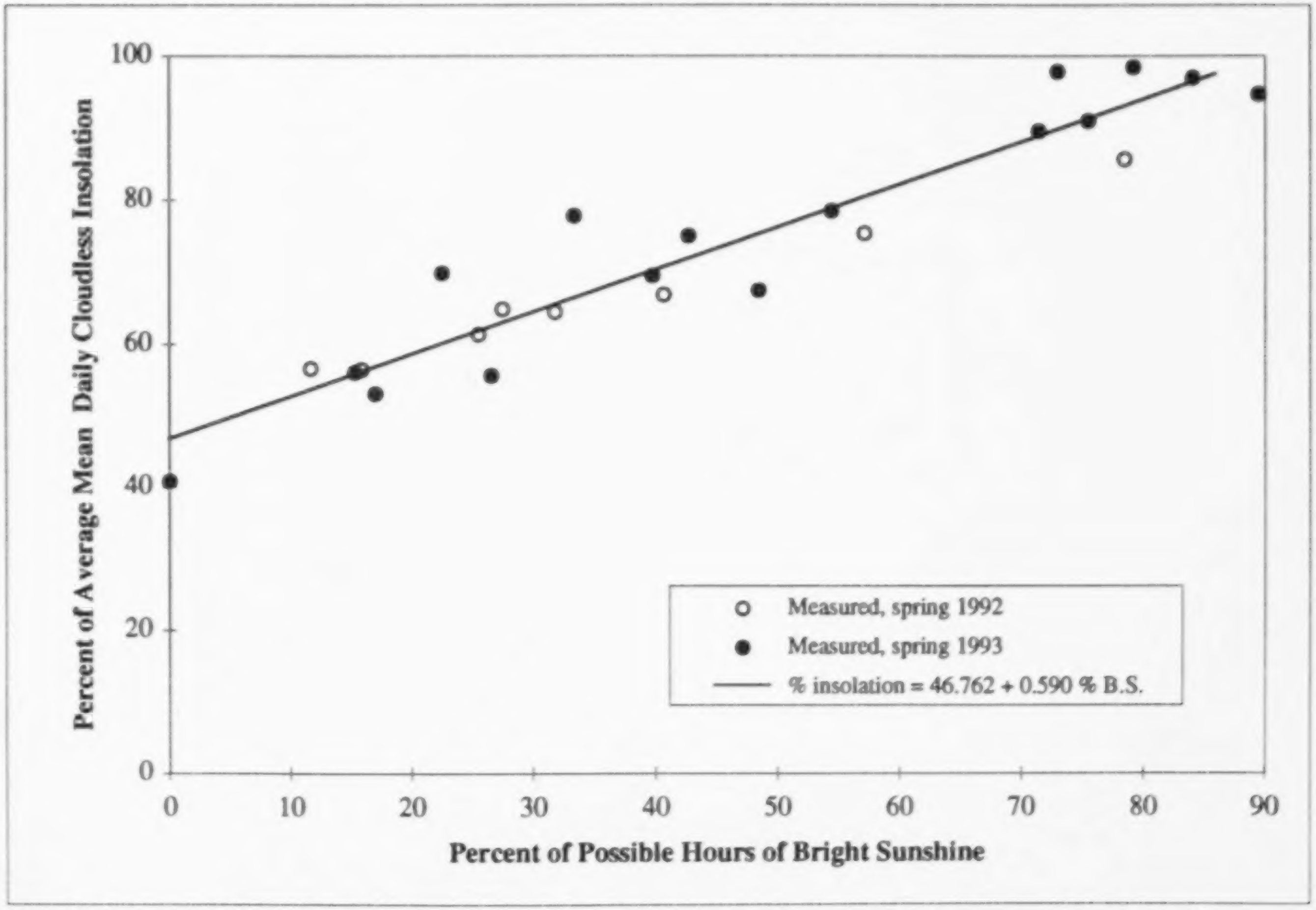

Figure 2.6 Duration of bright sunshine vs. daily insolation at Ft. Providence, spring 1992 and 1993.

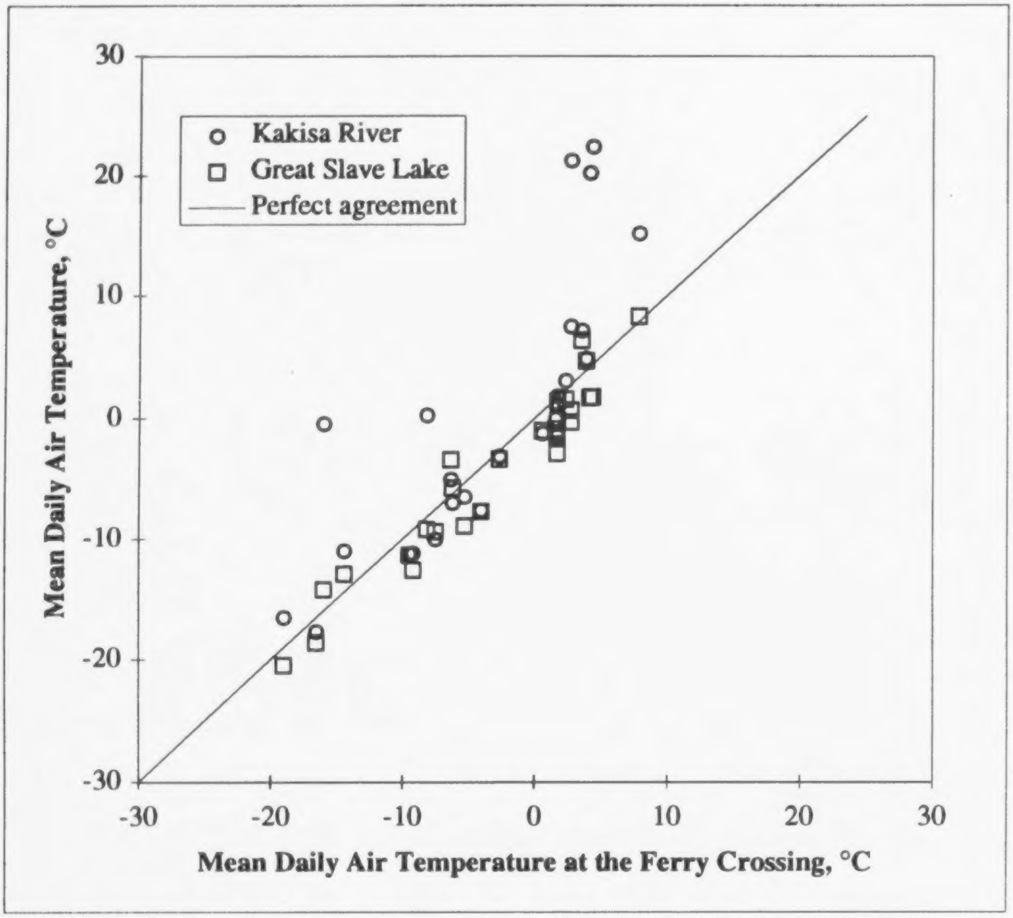

Figure 2.7 Comparison of mean daily temperatures measured at various sites near Ft. Providence, spring 1992.

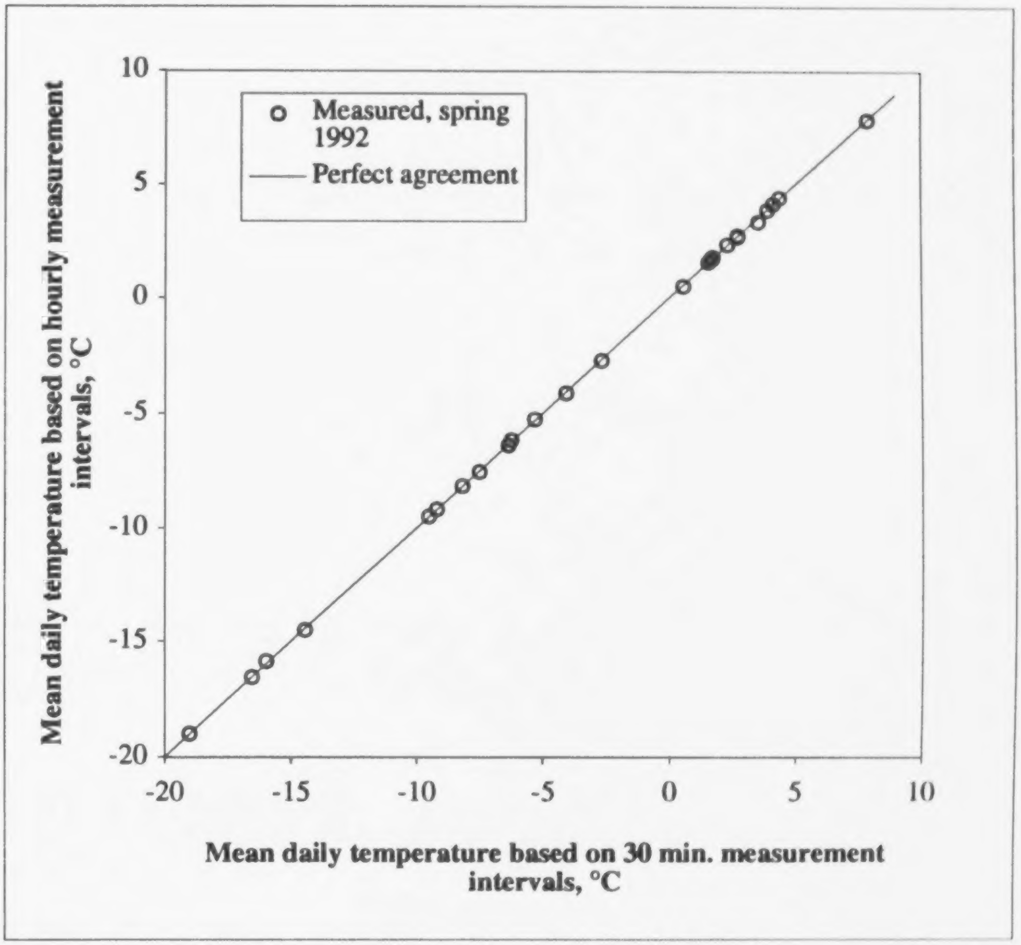

Figure 2.8 Comparison of mean daily temperatures obtained with hourly measurement to those based on a measurement interval of 30 minutes.

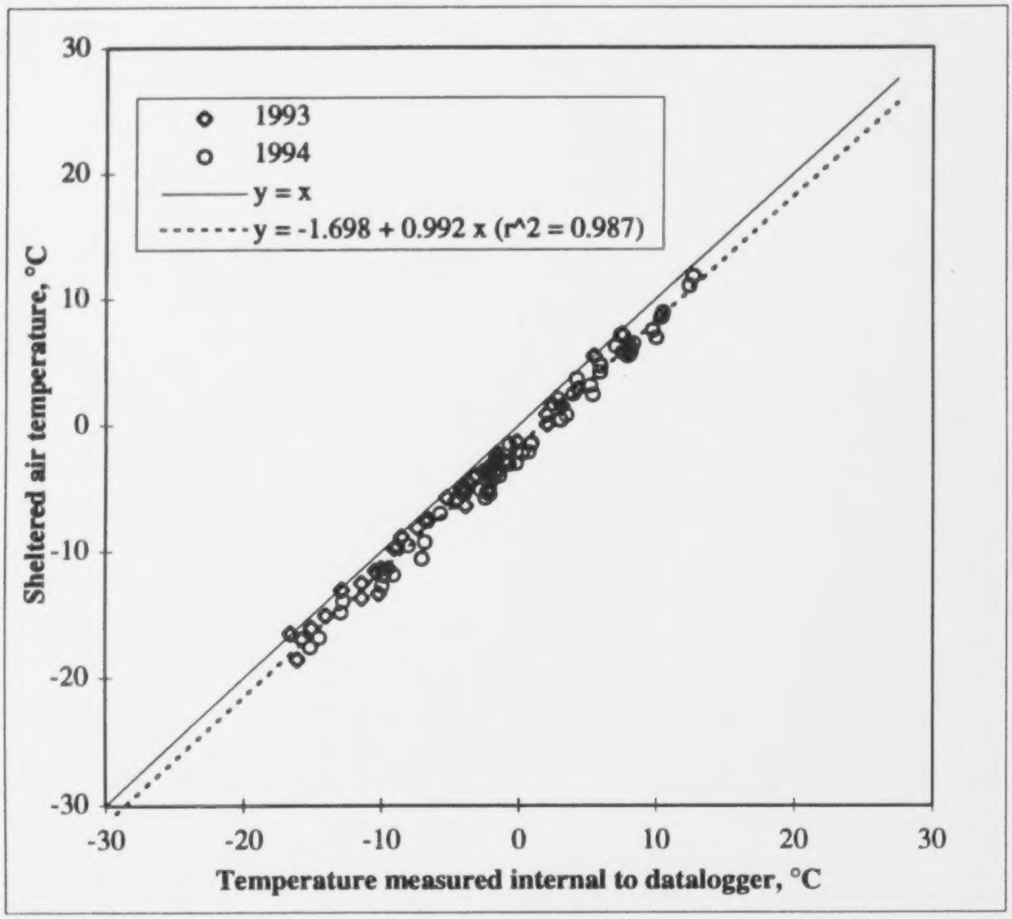

Figure 2.9 Comparison of mean daily temperatures obtained with the sheltered thermistor and those measured with the temperature sensor internal to the datalogger, spring 1993 and 1994.

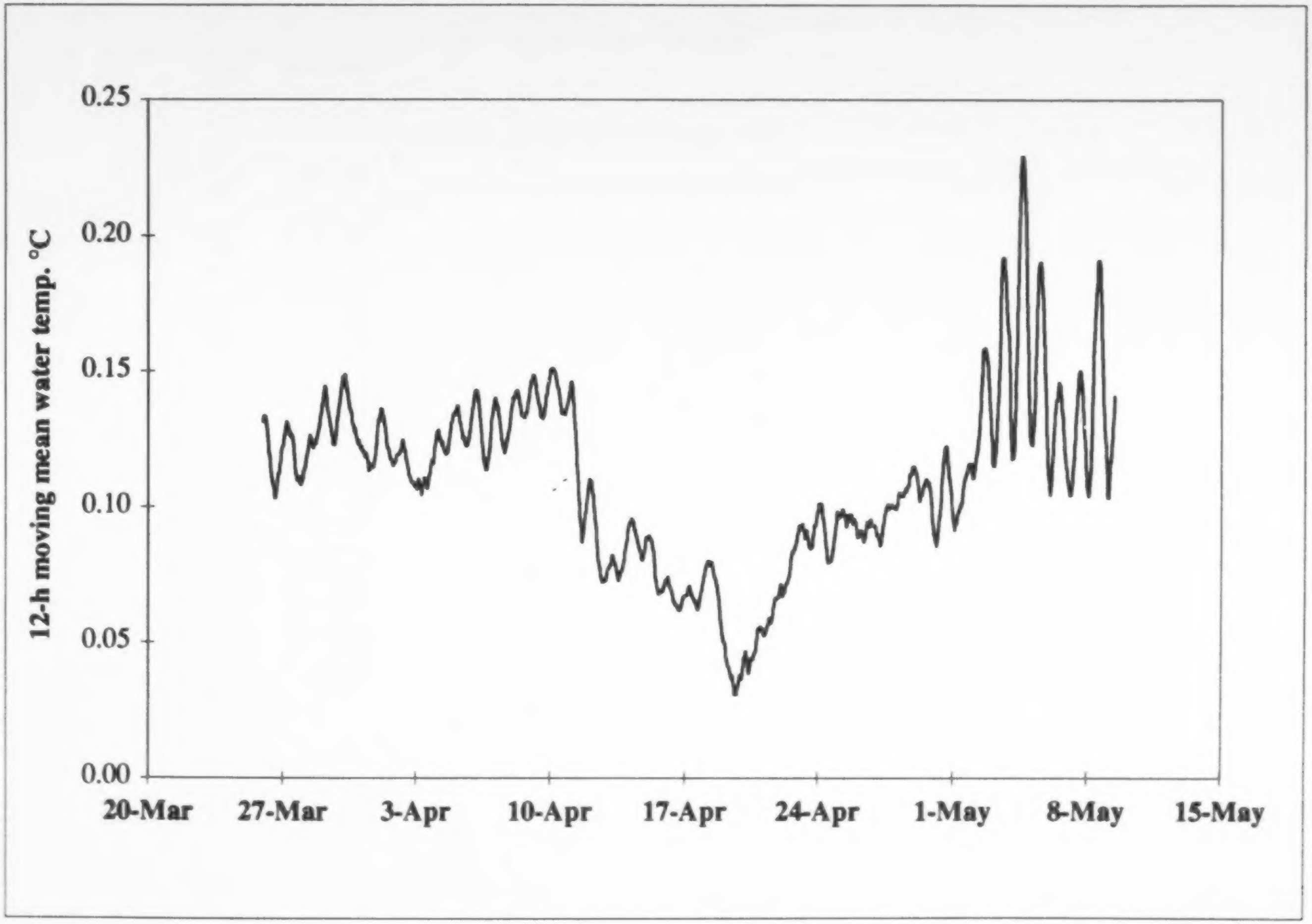

Figure 2.10 Automated water temperature measurements at the Great Slave Lake TBM, 1992.

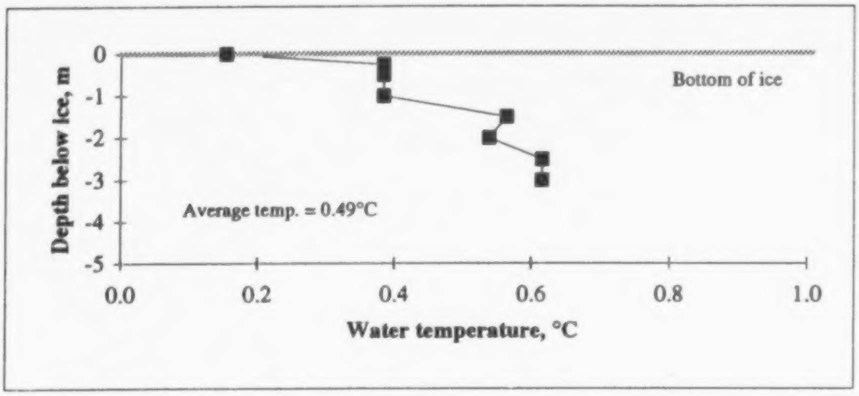

Figure 2.11 (a) Water temperature profile measured in Great Slave Lake, 7-Apr-93.

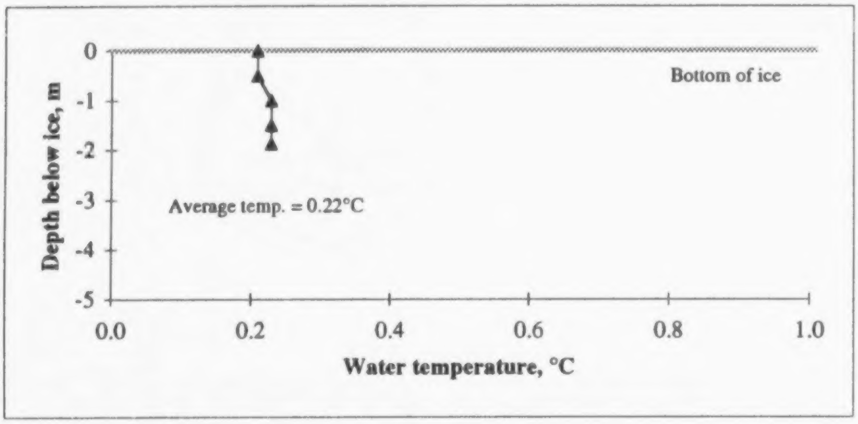

Figure 2.11(b) Water temperature profile measured in Great Slave Lake, 16-Mar-94.

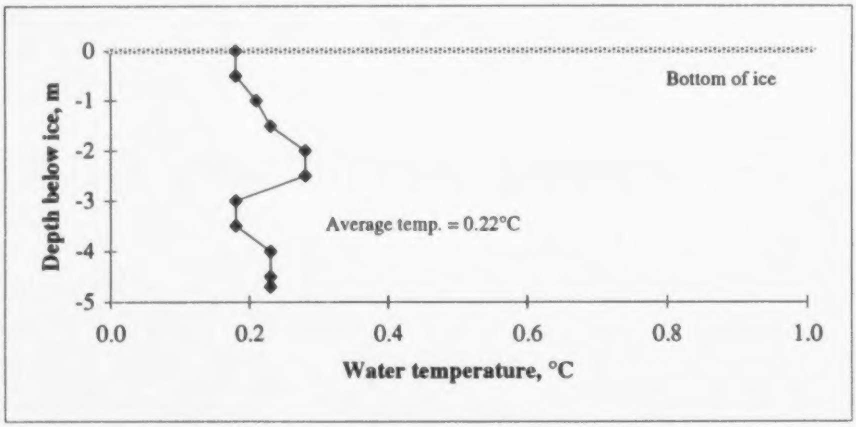

Figure 2.11(c) Water temperature profile measured in Great Slave Lake, 20-Apr-95.

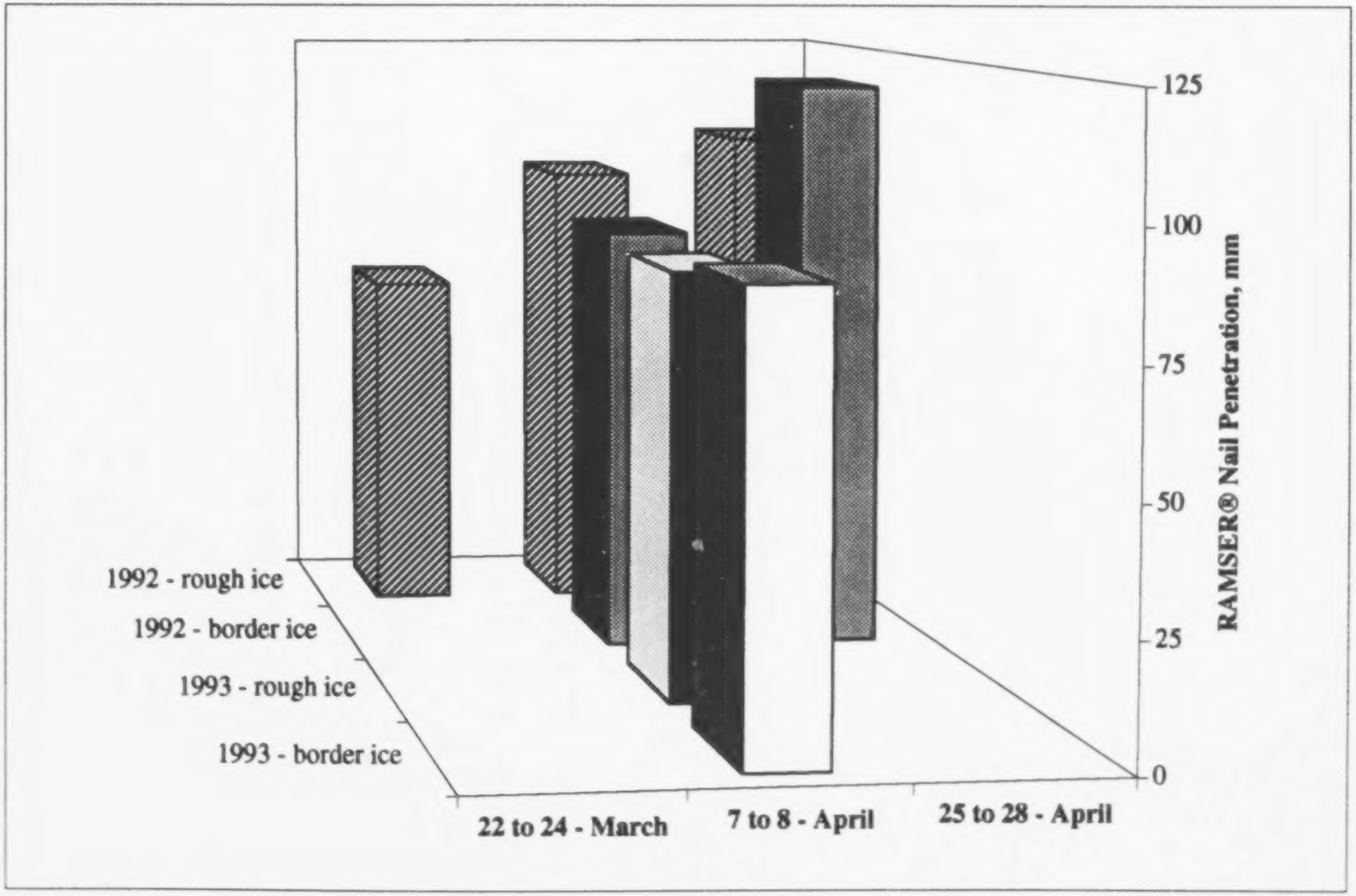

Figure 2.12 RAMSET® nail penetrations in the border and rough ice, 1992 and 1993.

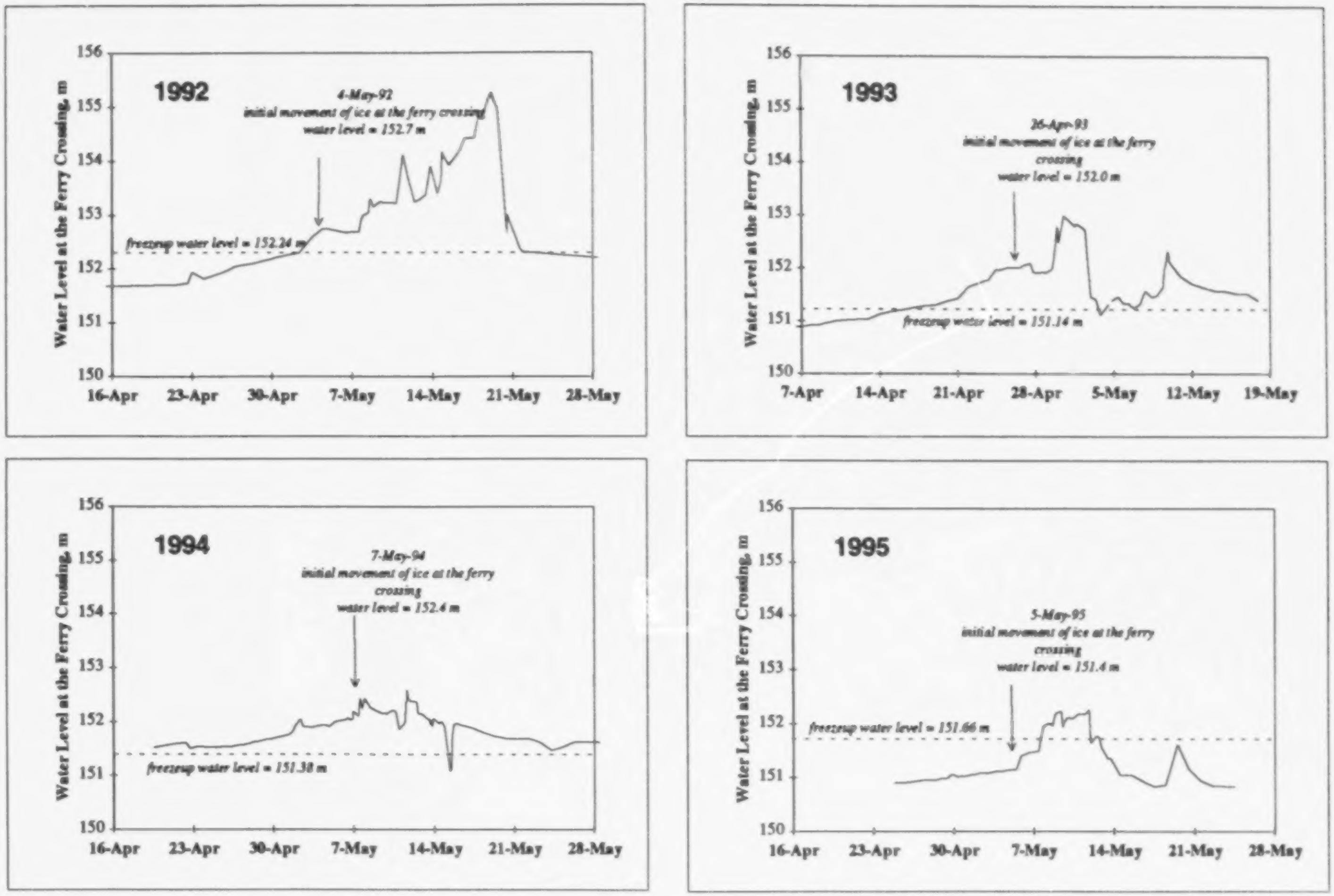

Figure 2.13 Stage hydrographs measured at the ferry crossing, 1991 to 1995.

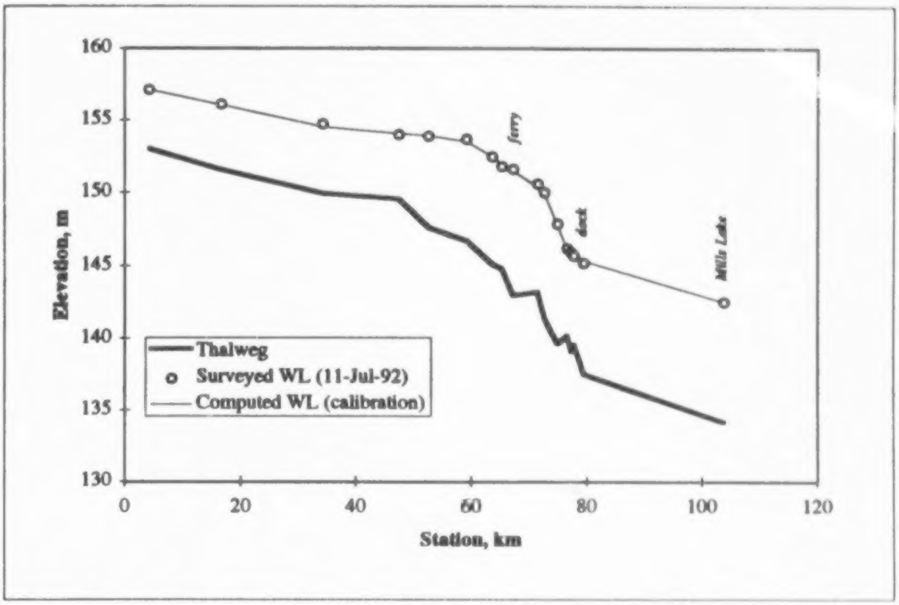

Figure 2.14 Calibration of hydraulic model for the Mackenzie River between Great Slave Lake and Mills Lake, 11-Jul-92.

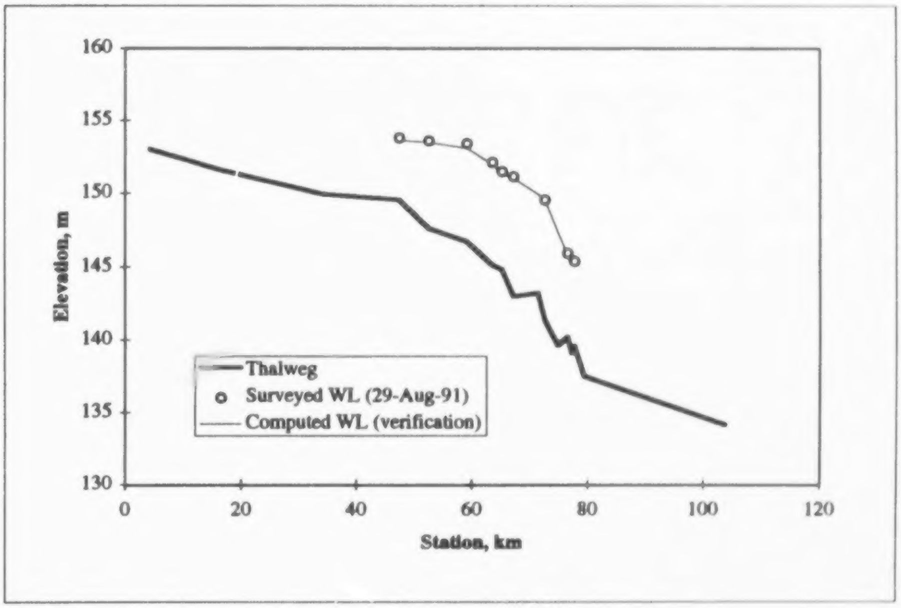

Figure 2.15 Verification of hydraulic model for the Mackenzie River between Beaver Lake and Ft. Prov., 29-Aug-91.

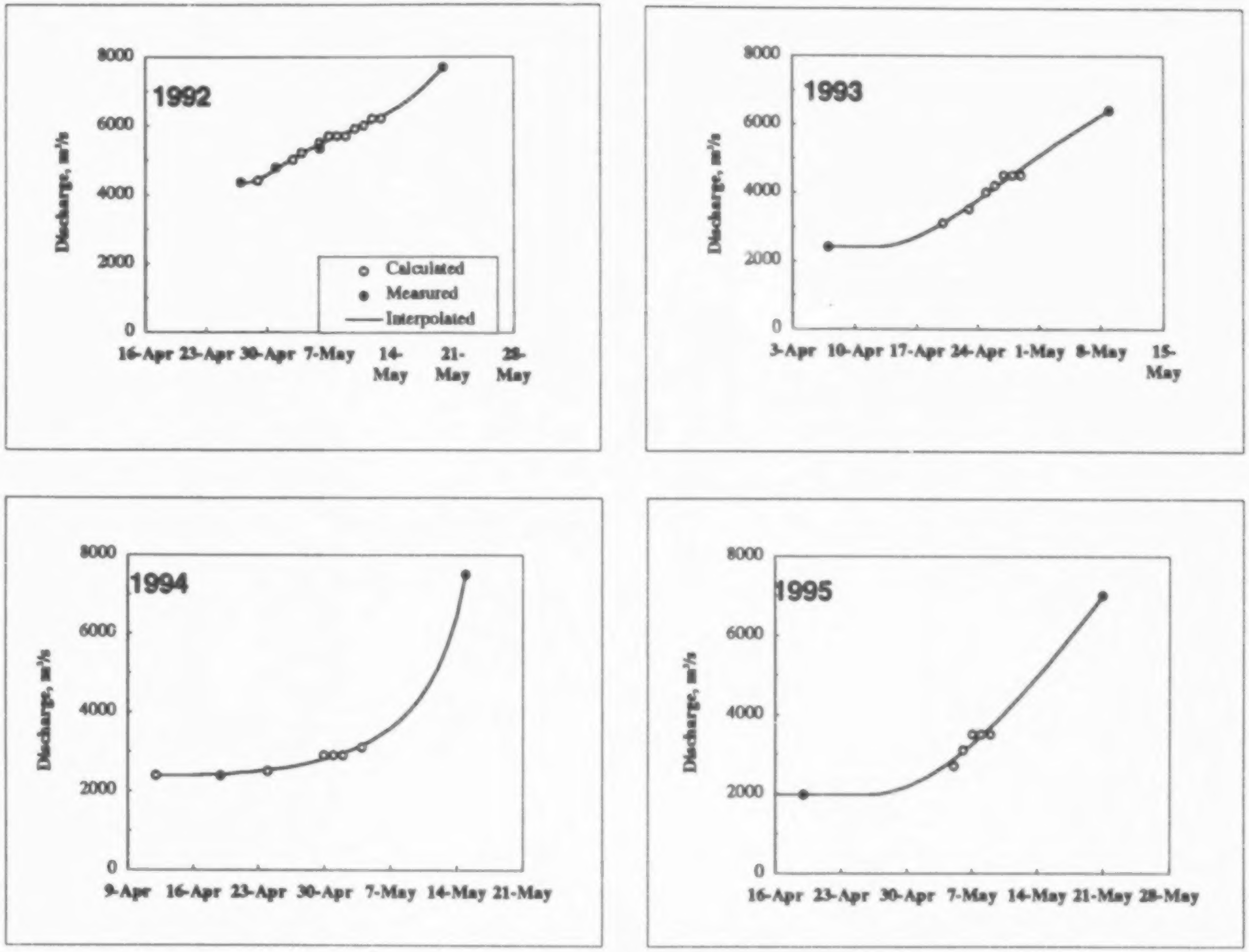

Figure 2.16 Measured and calculated discharges through the breakup period, 1992 to 1995.

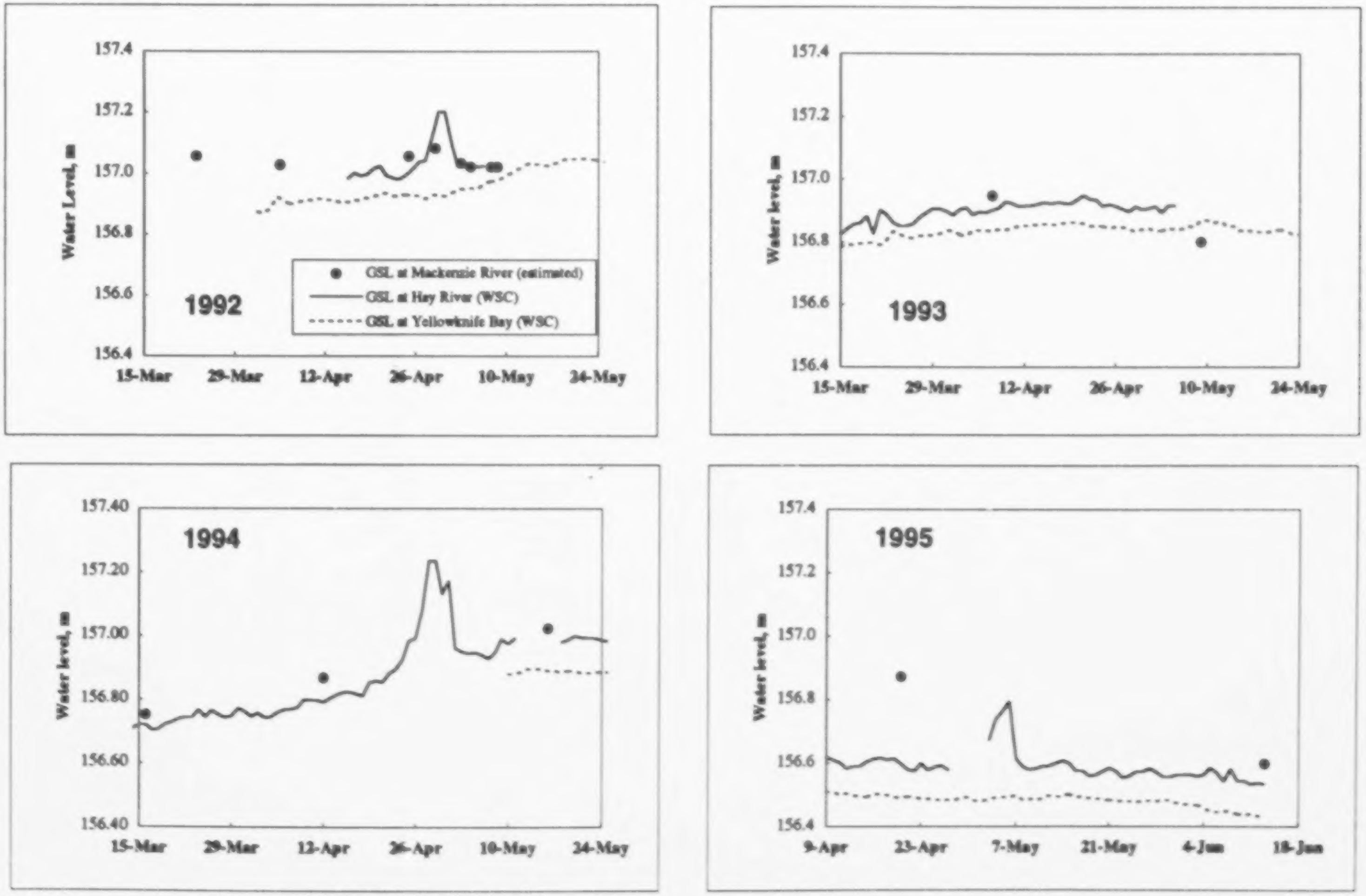

Figure 2.17 Great Slave Lake spring water levels, 1992 to 1995.

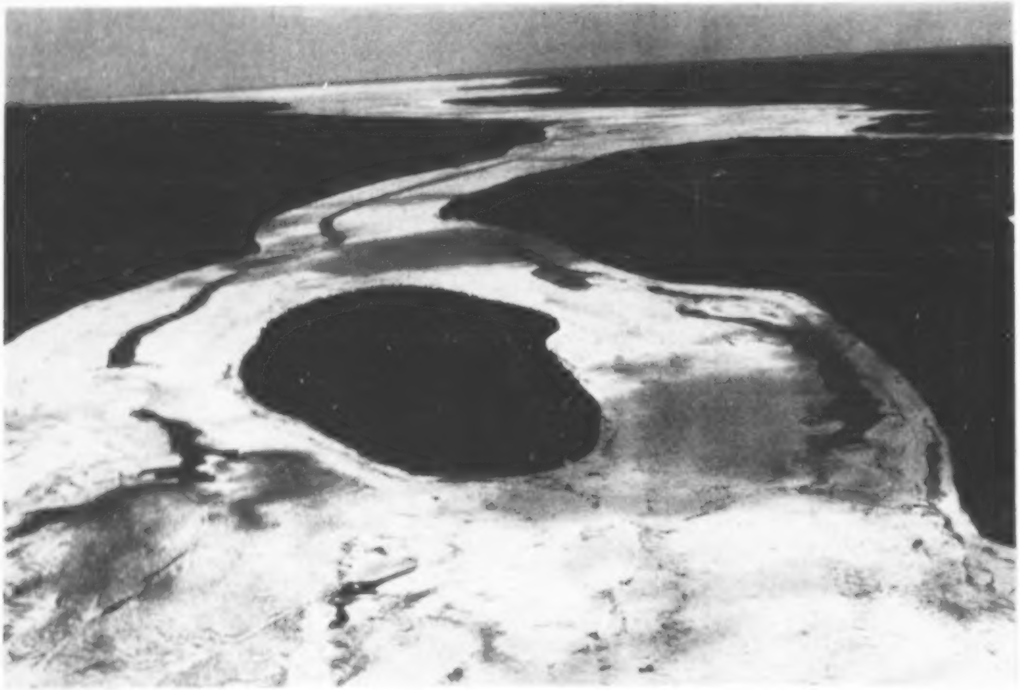

Figure 2.18 Overflow from open water leads, looking upstream to Providence Island.

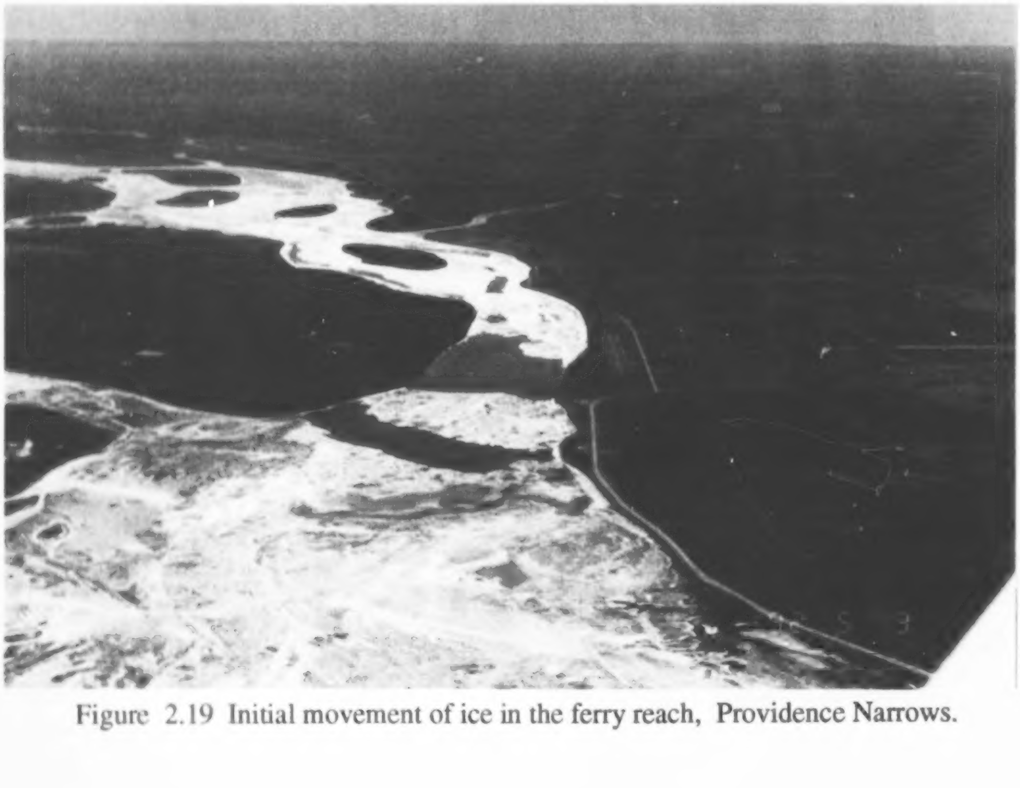

Figure 2.19 Initial movement of ice in the ferry reach, Providence Narrows.

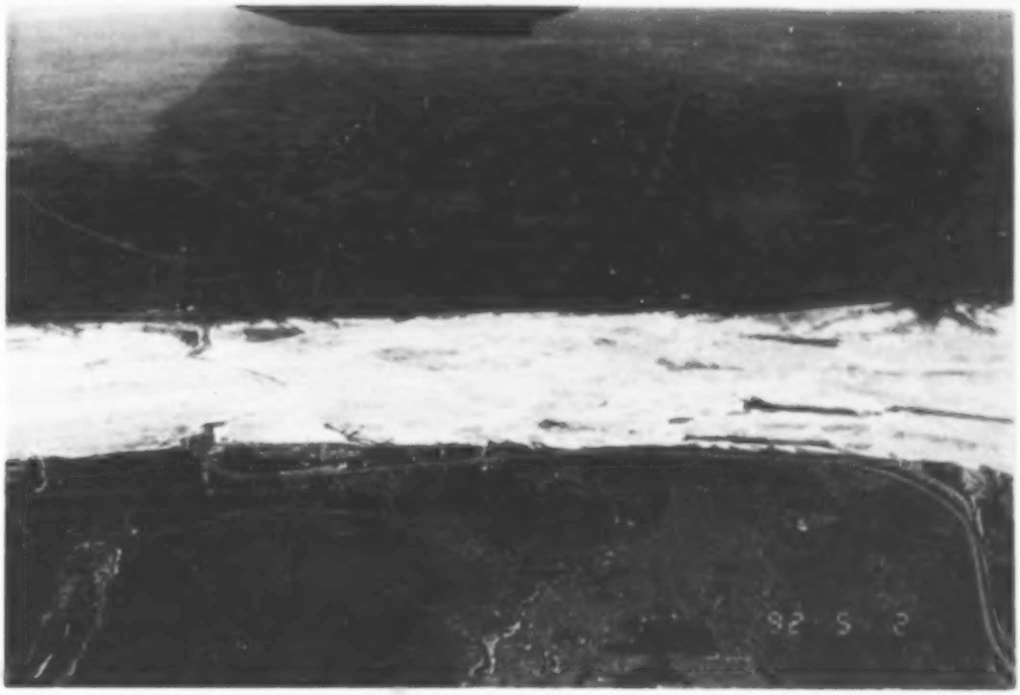

Figure 2.20 Looking north to the Mackenzie River at the ferry crossing. The path of the ferry passage channel is evident in the ice cover texture.

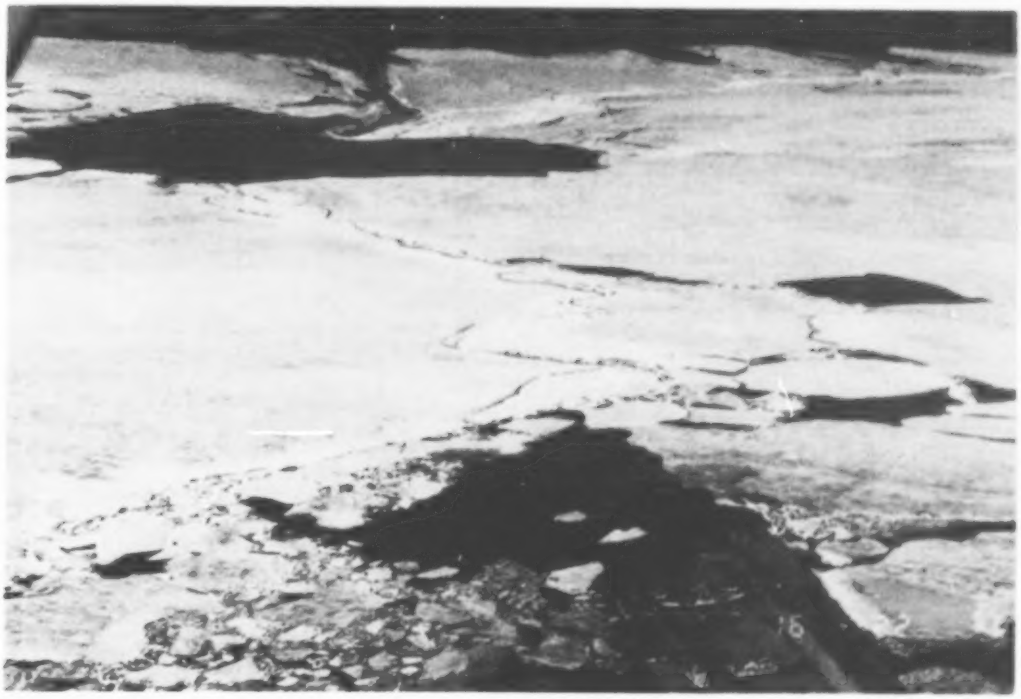

Figure 2.21 Looking north shortly after failure of the ferry passage channel, May 1992.

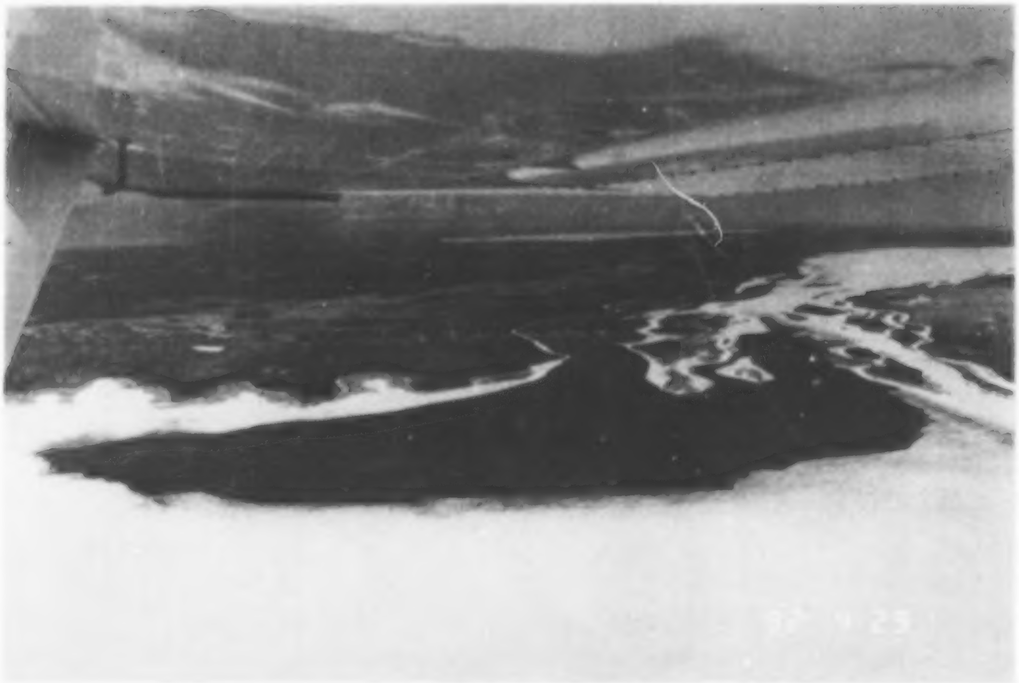

Figure 2.22 Typical pattern of open water development in the South Channel.

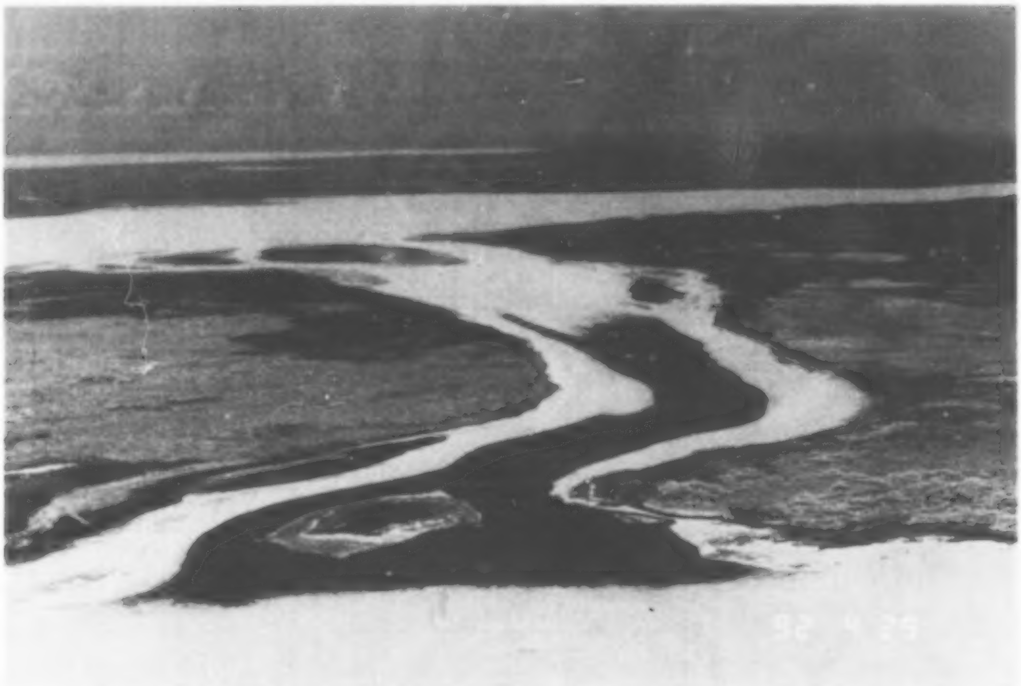

Figure 2.23 Typical pattern of open water development in the North Channel.

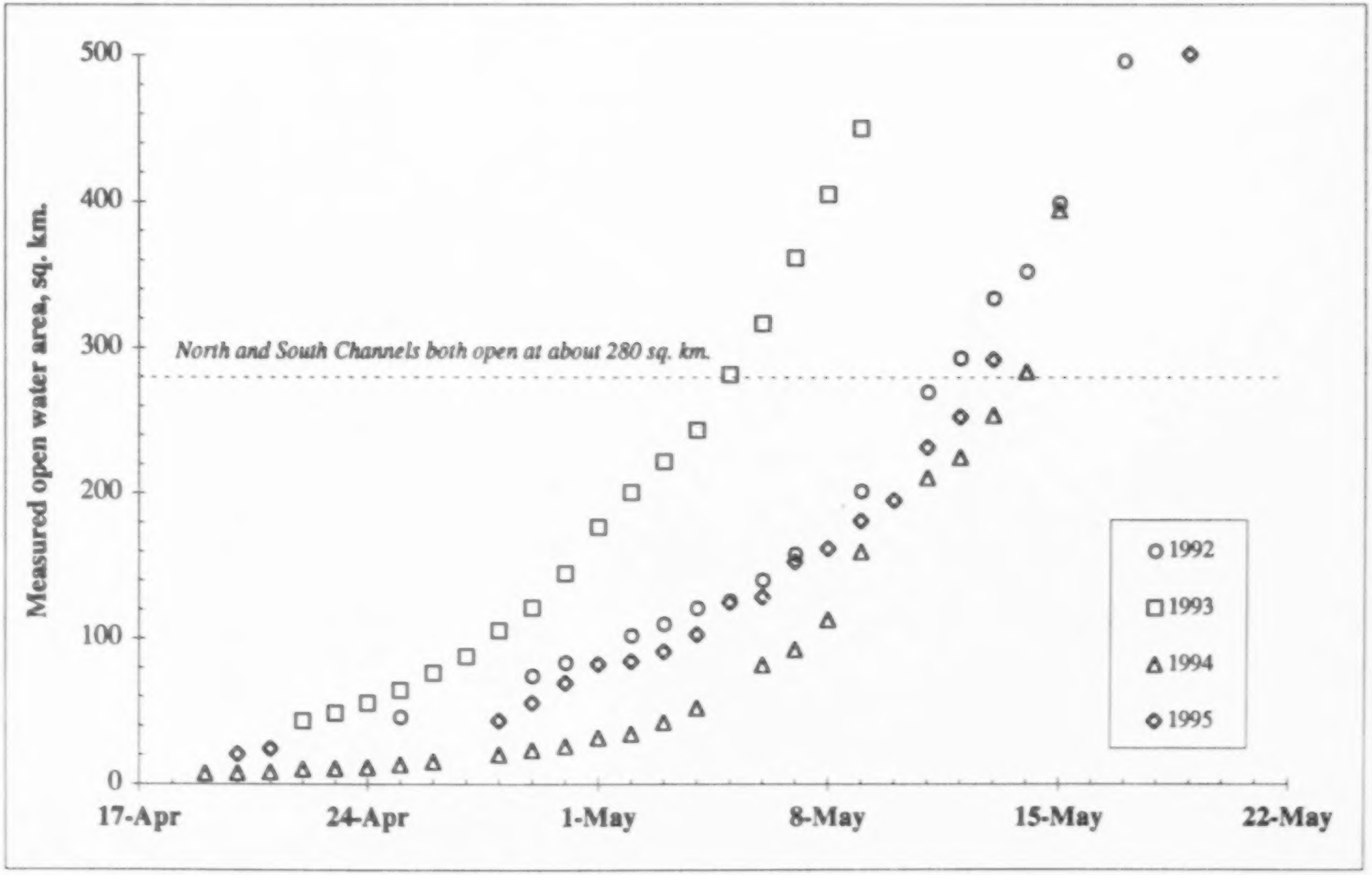

Figure 2.24 Development of open water area on the Mackenzie River upstream of Burnt Point, 1992 to 1995.

3.0 FORMULATION OF THE BREAKUP MODELS

3.1 Introduction

Based on the observations of breakup in the study reach to date, two key reaches have been identified based on the mode of breakup. One is the ferry reach, which extends upstream from the dock in Ft. Providence to the Ice Bridge section. Breakup in this reach would directly affect ferry operations as the ferry passage channel would be constructed within this reach. This second reach extends from Great Slave Lake, through the North and South Channels around Big Island, and downstream to Burnt Point. Breakup in this reach is of importance in this study because ice from Beaver Lake interrupts ferry service as it moves downstream through the ferry crossing.

As stated earlier, the mode of breakup in these two reaches is distinctly different. In the upstream reach breakup is predominantly thermal, with the development of open water progressing downstream from the thermal development of open water at the outlet of Great Slave Lake. In the ferry reach itself, the breakup is primarily mechanical, with the initial movement occurring as a result of reduced strength due to thermal deterioration and increased load of the ice cover due to increasing river discharge.

Despite the fact that the breakup in the ferry reach generally occurs before the completion of breakup of Beaver Lake, the latter will be addressed first for two reasons. First, being predominantly thermal, a breakup model for Beaver Lake has the potential to provide calibrated thermal parameters which could be used in the thermal components of the breakup model for the ferry reach. Second, although the completion of breakup for the ferry reach generally precedes that in Beaver Lake, open water development at the outlet of Great Slave Lake begins early in the spring and always prior to the initial movement of ice in the ferry reach.

3.2 Modelling the Development of Open Water at Great Slave Lake

3.2.1 Introduction

Thermal breakup occurs when the ice cover melts gradually and does not break up until its strength is nearly zero. Generally this occurs in situations where river stages do not increase rapidly during the breakup period as the water surface slope is relatively flat and, consequently, the forces acting on the ice cover are small.

In a thermal breakup, warm water flowing under the ice cover tends to thin the ice, resulting in the downstream propagation of a melting front. This is the type of breakup which is observed in the North and South Channels at Great Slave Lake each spring. Early breakup is primarily influenced by the outflow of water from Great Slave Lake which is slightly above 0°C. This leads to small open water areas at the upstream end of the north and south channels, which have been documented as early as the third week of March (Hicks *et al.*, 1994). Heat from the overlying air mass and from solar radiation is absorbed by the ice cover directly, first melting the snow on the ice cover and then deteriorating the ice cover itself. These sources of heat also warm the river water in open water areas supplementing the heat brought from Great Slave Lake.

In this section, two methods are employed in developing a thermal breakup model in the Beaver Lake reach.

3.2.2 Energy Budget Approach

3.2.2.1 Introduction

It is possible to develop a thermal model simulating the development of open water area just downstream of Great Slave Lake by considering all of the heat components both contributing to, and withdrawing heat from, the ice surface. One of the approaches is the Energy Budget approach. Figure 3.1 shows all of the heat components acting on an ice surface (which may or may not be covered with snow) floating on the river, as well as the heat components acting on the adjacent open water area. In the figure:

Q_{si} and Q_{sw} are the solar radiation heat incident to the ice (or snow) and water surfaces, respectively;

Q_{li} is the net longwave radiation heat exchange between the ice (or snow) surface and the atmosphere;

Q_{lw} is the net longwave radiation exchange between the water surface and the atmosphere;

Q_{ei} is the heat gain or loss due to condensation or evaporation from the ice (or snow) surface;

Q_{ew} is the heat of gain or loss due to condensation or evaporation from the water surface;

Q_{hi} is the sensible heat exchange between the ice (or snow) surface and the atmosphere due to convection (Ashton,1986). In this study, it is named as convective heat;

Q_{hw} is the sensible heat exchange between the water surface and the atmosphere due to convection. In this study, it is named as convective heat;

Q_{ai} is the heat advected to the ice (or snow) surface by snow or rain;

Q_{aw} is the heat advected to the water surface by snow or rain;

Q_{lake} is the heat energy carried by the warm water coming from upstream;

Q_f is the heat energy created by friction caused by flow under the ice cover; and

Q_g is the heat energy conducted from river bed to the river flow.

If all of the heat components directed toward the ice cover are considered positive, and those away from the ice cover are considered negative, the sum of the heat components is the heat available to melt the ice cover. This one dimensional approach neglects the effects of horizontal and vertical heat conduction.

In quantifying the energy budget, the heat components affecting the ice cover directly are considered in terms of a unit area of the ice cover. In quantifying the heat transfer to the river flow, through the open water area, the actual area must be considered.

3.2.2.2 Formulation

The energy budget method has been used to calculate evaporation (Anderson, 1954; Gray, 1970; Ponce,1989; and Shuttleworth, 1993). It can be applied to snow and ice melt problems as well, (Ashton,1986; and Gray and Prowse, 1993). This requires that the heat used for evaporation (or gained during condensation) be quantified by some other method.

Assumptions

To facilitate the application of the energy budget method to the determination of open water development in Beaver Lake, the following assumptions are applied:

1. *The warm water released from Great Slave Lake will transfer all of its heat to the ice cover.* This includes the additional heat that is received by the flow (from solar radiation and warm overlying air) in the open water area upstream of the melting front. Also, this amount of heat energy melts the ice cover and snow contiguous downstream of the open water. This is a reasonable assumption as water temperature measurements at the ice bridge and ferry sections show the water is close to 0°C during this period.

2. *The heat component from the river bed (Q_g) is negligible. This* heat flux is on the order of 1 to 4 W/m^2 (Ashton, 1986). The maximum value likely occurs in January while in April and May, a river bed's temperature is typically close to the water temperature (Ashton, 1986). Given the measured incoming solar radiation flux varies from 100 to 300 W/m^2, this assumption is reasonable.

3. *The heat created by friction due to the flow shear on the underside of ice cover is negligible.* This is justified by the fact that in the study reach the average water surface slope is 0.00007 and it is of the same order as the energy slope (Chen, 1993). Thus, at a typical spring discharge of 4000 m^3/s with the average width of the channel being 7000 m, the average heat flux created by flow friction is only 0.2 W/m^2.

4. *Heat advection by snow and rain negligible.* There was very little snow and rain measured at the site during the melting period in the four years of observations. For example, the maximum rain fall in 1992 was 2.4 mm on 18-May and the daily mean temperature was 2.5 C°. Under these conditions, the advective heat flux is only 0.3 W/m^2.

5. *The ice or snow surface temperature is assumed to be 0°C if the air temperature is above 0°C.* The ice or snow surface temperature is assumed to be equal to the air temperature if the air temperature is below 0°C, but the snow and ice body temperatures are still taken to be 0°C.

6. *The surfaces of the snow and ice are saturated.* This is probably true during the melting period because the melting volume is much more than evaporated volume.

7. *The snow and ice covers are homogeneous in their thermal properties . The snow and the ice thicknesses across the width are constant. The surface albedos and roughness es are also assumed constant with respect to location.* These are the necessary conditions for this one dimensional model.

8. *The ice mass transport from the open water area to the downstream reach is negligible.* Breakup observations showed that only a few broken ice sheets moved down from the area upstream of the open water area and most of the broken ice sheets were blocked in front of the ice cover at the downstream end of the open water area.

9. *The water temperature in the lake (T_{lake}) is constant during the breakup period.* This is because that the water temperature in the lake is expected to reach a minimum by late winter and there is almost no heat exchange between the ice cover and the water body in the lake during the melt season.

10. *Dynamic effects are negligible.* Although the breakup in this reach is dominated by thermal effects, dynamic effects are still involved to some extent. For example, under the effects of the water current, wind and waves, the ice cover could be broken and the broken ice sheets could move downstream. As discussed earlier, this effect is primarily seen in the latter part of the melt period, when the ice cover is porous and thin, because ice strength is weak. Neglecting this effect causes the simulated open water area to be smaller than that of the measurement.

11. *It is assumed that all of the heat received by the flow in the open water area (from solar radiation and warm air) will be transferred to the ice cover at the melting front, causing it to progress downstream.* This assumption neglects the fact that this heat source actually increases open water area by thinning the ice cover downstream of the melting front. This assumption may be reasonable early in the simulation when this heat component is small, as this thinning occurs in a zone very local to the melting front. However, once the open water area gets quite large, substantial amounts of heat can be absorbed, and the ice thinning process will occur over a greater distance downstream of the melting front. This is because there is a limit to the rate at which heat can be transferred from the flowing water to the ice. In this situation, one would expect an almost linear increase in open water area to follow, for a fairly constant flow rate and a fairly constant heat input (at least until the ice was so weak that the small dynamic forces could lead to breakup of the remaining ice cover). Neglecting this effect, would cause the simulated open water area to be larger than measured.

Data limitations

The ice thickness is the most important variable affecting the simulation results. Errors in the quantification of ice thickness result from natural variations in the ice cover and varying ice formation processes (rough ice versus border ice). Therefore, the six or eight point measurements of ice thickness obtained in this 500 km^2 of ice cover can, at best, only be considered an index of ice thickness. Given the two dimensional variability in the development of the open water area (as evidenced by the open water maps presented in the annual reports) such detailed ice thickness measurements would only be warranted if a two-dimensional model of thermal breakup were to be developed. However, it is neither economically or practically feasible (from a safety perspective) to facilitate such a modelling effort.

Heat component quantification

1. Net incoming short-wave radiation heat component

The net incoming short-wave radiation heat component on a unit area of the ice surface, E_{si}, can be obtained using:

$$E_{si} = (1 - \alpha_i)\, R_s\, \Delta t \qquad [3.1]$$

where: α_i is the albedo of ice;

R_s is solar insolation in W/m^2; and

Δt is time interval in seconds.

The value of the albedo depends upon surface conditions, weather conditions and solar altitude. Table 3.1 shows the typical ranges of albedo for a variety of surface types (Gray and Prowse, 1993). Snow cover albedo varies with grain size, surface conditions and age. As Table 3.1 indicates, Gray and Prowse report that new snow ranges in albedo from 0.80 to 0.90, while the albedo of old snow varies from 0.60 to 0.80. There is a lower limit for the albedo of an uncontaminated snow cover of 0.4 (US. Army, 1959). Bohren and Beschta (1976) measured snowpack albedo at the Ft. Valley Experimental Forest, Arizona during the month of February and found that for new snow (snow density of 50 to 200 kg/m^3) the albedo was 0.71 to 0.89 and for old snow (snow density of 300 to 450 kg/m^3) the albedo was 0.62 to 0.70. Gray and Prowse (Table 3.1) reports that snow ice ranges in albedo from 0.30 to 0.55, while black ice albedos of 0.10, 0.40 and 0.55, apply for undeteriorated, candled and granulated ice, respectively. Prowse and Marsh (1989) measured the albedo of black ice on the Liard River near Fort Simpson, N.W.T. (61° 53'N,121° 22'W) during the melting season and found that for candled black ice, the albedo was 0.39 and for granulated black ice, the albedo was 0.55.

As discussed in Chapter 2, the incoming solar radiation was measured at Ft. Providence. Mean daily values have been used in this study. The incident solar radiation measured during the early spring and breakup period was on the order of 100 to 300 W/m^2. The time interval is 86400 seconds when daily data are used.

The incoming short-wave radiation heat component on the water surface, Q_{sw} , can be obtained similarly:

$$Q_{sw} = (1 - \alpha_w) R_s \Delta t \ \tilde{A}_w \qquad [3.2]$$

where: Q_{sw} is solar radiation heat incident to water surface;
α_w is the albedo of the water surface; and
$\tilde{A}_w$ is the average open water area in m^2.

In this study, $\tilde{A}_w$ on day "j" is calculated by:

$$\tilde{A}_w{}^{j} = (A_w{}^{j-1} + A_w{}^{j}) / 2 \qquad [3.3]$$

where: $A_w{}^{j}$ is the open water area at the end of day "j"; and
$A_w{}^{j-1}$ is the open water area at the end of the previous day.

The value of the water surface albedo is generally between 0.05 to 0.15 with a value of 0.08 recommended (Gray and Prowse, 1993). Raphael (1962) presented a figure that gave the effect of solar altitude and cloud cover on the albedo of a horizontal water surface. He found that around April 10th (at the beginning of the breakup season when the solar altitude was about 23°) the water surface albedo was 0.08 under overcast conditions and 0.1 under clear conditions. He reported the albedo was 0.07 under both clear and overcast conditions around May 20th (at the end of breakup season when the solar altitude was about 34°). *For this study, a value of 0.08 was taken as the albedo of the water surface for all sky conditions throughout the simulation period.*

2. Longwave radiation heat components, E_{li} and Q_{lw}

Longwave radiation is a type of black-body radiation. It follows Stefan's Law, in that the radiation is proportional to the fourth power of body surface temperature (Brunt, 1934). An emissivity coefficient is introduced because ice, snow and water are not perfect black bodies. Therefore, the longwave radiation they issue can be presented as (Ashton, 1986):

$$R_l = \varepsilon\, \omega\, (273.2 + T_t)^4 \qquad [3.4]$$

where: ε is the emissivity;
ω is the Stefan-Boltzmann constant, in W/m^2°K^4; and
T_t is the body surface temperature, in °C.

The value of emissivity is 0.97 (Ashton, 1986) and the Stefan-Boltzmann constant is 5.67×10^{-8} W/m^2°K^4 (Anderson, 1954).

The longwave radiation reflected back from the atmosphere under a clear sky can be calculated by Brunt's formula (Brunt, 1934):

$$R_{lf\,clear} = (a + b\sqrt{e_a})\,\omega\,(273.2 + T_a)^4 \qquad [3.5]$$

where: a and b are empirical constants;
T_a is the air temperature measured at height of 2 metres above the surface, in °C;
and e_a is the vapor pressure in millibars.

The vapor pressure can be calculated by Tetens'(1930) equation (Shuttleworth, 1993):

$$e_a = 6.11\, exp\left(\frac{17.27\, T_a}{237.3 + T_a}\right)\frac{R_h}{100} \qquad [3.6]$$

where R_h is relative humidity expressed as a percentage.

Table 3.2 shows various investigators' values where it is seen that the coefficients a and b are vary considerably. Brunt (1934) recommended Dines' values of a and b be used. Anderson (1954) believed that the variations are probably related to the implied hypothesis concerning the relation between the local vapor pressure and the total water vapor content of the atmosphere. Snow investigations (US. Army, 1959) indicated that $(a + b\sqrt{e_a})$ is close to 0.757 when e_a is between 3 and 9 millibars. This value is very close to the values 0.742 ($e_a = 3$), and 0.788 ($e_a = 9$) that are calculated from Anderson's constants ($a = 0.68$, $b = 0.036$). Based on this, Anderson's coefficients were used for this study.

The longwave radiation reflected back from the sky increases under cloudy conditions. To account for this, Ashton introduces Bolz's (1949) formula (Ashton, 1986):

$$R_{lf} = (a + b\sqrt{e_a})\,\omega\,(273.2 + T_a)^4\,(1 + kC^2) \qquad [3.7]$$

where: R_{lf} is the longwave radiation reflected from atmosphere, in W/m^2;
k is an empirical constant; and
C is the fraction of the sky covered with cloud.

Wunderlich (1972) recommended the value of k to be 0.0017. The value of C is assumed to have a linear relationship with the percent of maximum possible solar insolation. C is 0 under clear sky conditions and is 10 under completet overcast conditions. In this study, C is estimated by means of measured solar radiation. When measured solar radiation is over 300, C equals 0. When When measured solar radiation is less than 300, C equals 10. Table 3.3 gives the values of C corresponding to the measured solar insolation values.

Finally, the net longwave radiation from the ice surface ice may be written as:

$$R_{li} = \varepsilon\,\omega\,(273.2 + T_{ti})^4 - (a + b\sqrt{e_a})\,\omega\,(273.2 + T_a)^4\,(1 + kC^2) \qquad [3.8]$$

where: R_{li} is net longwave radiation flux per unit area of the ice cover, in W/m^2; and
T_{ti} is the temperature at the ice surface, in °C.

The net longwave radiation flux from the water surface is:

$$R_{lw} = \varepsilon\,\omega\,(273.2 + T_{tw})^4 - (a + b\sqrt{e_a})\,\omega\,(273.2 + T_a)^4\,(1 + kC^2) \qquad [3.9]$$

where: R_{lw} is net longwave radiation flux per unit area of the water surface, in W/m^2;
T_{tw} is the temperature at the water surface in °C.

Based on equations [3.8] and [3.9] and the data collected at the site to date, the net longwave radiation from the water and ice surface is in the order of 10 to 100 W/m^2.

The longwave radiation heat energy from ice surface, E_{li}, is:

$$E_{li} = \left(\varepsilon\,\omega\,(273.2 + T_{tw})^4 - (a + b\sqrt{e_a})\,\omega\,(273.2 + T_a)^4\,(1 + kC^2)\right)\Delta t \qquad [3.10]$$

The longwave radiation heat energy from water surface, Q_{lw} , is:

$$Q_{lw} = \left(\varepsilon\,\omega\,(273.2 + T_{tw})^4 - (a + b\sqrt{e_a})\,\omega\,(273.2 + T_a)^4\,(1 + kC^2)\right)\Delta t\ \tilde{A}_w \qquad [3.11]$$

3. Evaporation heat components, E_{ei} and Q_{ew}

The evaporation heat component can be calculated by any one of a number of methods including the energy budget method, the water budget method, the mass transfer method or a combination method, such as Penman's equation (Ponce, 1991). In the context of this study, an energy budget approach is not possible because the energy budget is being used to quantify ice melt. Of the possible remaining methods, the mass transfer method is the only practical alternative, because of the available data.

The mass transfer method assumes that the amount of evaporation is proportional to the wind speed and the difference of vapor pressure between the body surface and the atmosphere. It is applicable in cases where the heat energy needed for evaporation is not limited, but rather available room for water vapour in the air layer over the evaporative surface is what limits the rate of evaporation. Dunne and Leopold (1978) recommended Kuzmin's formula to calculate the evaporation rate from a snow surface. It is adopted here to calculate the evaporation rate from both the snow and the ice surfaces:

$$\text{Evaporation Rate (cm/day)} = (0.018 + 0.00015\,u_2)\,(e_{ti} - e_a) \qquad [3.12]$$

where: u_2 is the wind speed measured at height of 2 metres above the surface, in km/day;
e_{ti} is the vapor pressure on the ice (or snow) surface, in mb.

The vapor pressure on the ice surface can be calculated by Tetens'(1930) equation (Shuttleworth, 1993):

$$e_{ti} = 6.11\,exp\left(\frac{17.27\,T_{ti}}{237.3 + T_{ti}}\right) \qquad [3.13]$$

the wind speed, u_2, is required in equation [3.12]. However, as discussed in Chapter 2, the wind anemometer used in this study was located at height of 6.4 metres. Based on the assumption that vertical distribution of wind speed obeys the logarithmic law, the wind speed at a height of 2 m can be calculated by the equation (Priestley, 1959):

$$\frac{u_z}{u^*} = \frac{1}{\kappa}\,ln\left(\frac{z}{z_o}\right) \qquad [3.14]$$

where: $u*$ is the shear velocity;
κ is von Karman's constant ($\kappa = 0.4$);
z is the height at which the wind speed is measured; and
z_o is the roughness height of the ground surface.

The wind speed at a height of 2 metres, u_2, can be determined from the measured wind speed, $u_{6.4}$, by the equation (Panodsky and Dutton, 1984):

$$u_2 = u_{6.4} \frac{\ln(z_2/z_o)}{\ln(z_{6.4}/z_o)} \qquad [3.15]$$

if the roughness height of the ground surface, z_o , can be quantified. Table 3.4 shows typical z_o values reported by Eagleson from a variety of sources. The ratio of u_2 to $u_{6.4}$ ($u_2/u_{6.4}$) is 0.91 when z_o is taken as 0.001 cm, and the ratio is 0.87 when z_o is taken as 0.1 cm. As the difference over this large range of z_o is less than 5 percent, the average of the two ratios (0.89) is used in this study for all surfaces. This corresponds to a value of z_o of 0.02 cm.

Calculation of the evaporation heat involves a number of steps. First, the evaporation rate must be converted from cm/day to m/day. Second, the total amount of mass evaporated from the ice cover surface must be calculated using:

$$\text{Mass evaporated} = \text{Evaporation rate} \times \rho_w \ \Delta t \qquad [3.16]$$

where ρ_w is density of water, in kg/m^3 (1000 kg/m^3 at 0 °C, Halliday and Resnick, 1988). Finally, the total heat energy used for evaporation per unit area of ice cover can be calculated as:

$$E_{ei} = (\,0.018 + 0.00015\ u_2)(e_{ti}\ - e_a\,)\,\rho_w\ \Delta t\ L_v \qquad [3.17]$$

where: E_{ei} is the total heat energy used for evaporation per unit area of ice cover, in J/m^2;
and L_v is latent heat of vaporization, in J/kg (2,500,000 J/kg, Ashton, 1986).

The evaporation rate from a snow and ice surface is different from that which occurs at a water surface. Therefore, two other mass transfer equations were used to calculate evaporation heat energy on the water surface in this study.

(a) Dunne's equation

Dunne and Leopold (1978) proposed the following equation:

$$\text{Evaporation Rate (cm/day)} = (\,0.013 + 0.00016\ u_2)(e_{tw} - e_a) \qquad [3.18]$$

where, e_{tw} is the saturation vapor pressure at the water surface temperature in millibars. The saturated vapor pressure on the water surface can be calculated by the equation:

$$e_{tw} = 6.11\, exp\left(\frac{17.27\, T_{tw}}{237.3\, +\, T_{tw}}\right) \qquad [3.19]$$

where: T_{tw} is the water temperature at the surface, in °C. In this study. T_{tw} is assumed equal to the average water temperature.

The total heat energy used for evaporation from the open water area, Q_{ew} , is then:

$$Q_{ew} = (\, 0.013 + 0.00016\, u_2)(e_{tw} - e_a)\, \tilde{A}_w\ \rho_w\ \Delta t\ L_v \qquad [3.20]$$

where: Q_{ew} , is the total heat energy used for evaporation from open water area, in J.

(b). Rimsha and Donchenko's formula

Ashton (1986) recommended an alternate formula for calculating evaporation heat flux (W/m^2) in winter which was originally presented by Rimsha and Donchenko (1957):

$$\text{Evaporation heat flux} = (\, 6.04 + 0.263\, (\, T_{tw} - T_a\,) + 2.95\, u_2\,)\, (e_{tw} - e_a\,) \qquad [3.21]$$

Using this equation, the total heat energy used for evaporation from open water area, Q_{ew} , becomes:

$$Q_{ew} = (\, 6.04 + 0.263\, (\, T_{tw} - T_a\,) + 2.95\, u_2\,)\, (e_{tw}\, - e_a\,)\, \Delta t\ \tilde{A}_w \qquad [3.22]$$

This will be referred to as Rimsha's approach in the ensuing text.

It is important to note that the estimates of evaporation obtained from these empirical equations are not very precise and the errors often exceed ± 25 percent (Dunne and Leopold, 1978). However, this potentially high error does not concern this analysis significantly because the total evaporation heat E_{ei} is in the range of -30 to 20 W/m^2, which is only about 10 percent of the typical net radiation heat energy.

4. Convective heat components, E_{hi} and Q_{hw}

Convective heat energy can be estimated by Bowen's ratio once the evaporation heat amount has been determined (Ponce, 1989). Bowen's ratio, R_{bo}, is given by

$$R_{bo} = \frac{E_{hi}}{E_{ei}} = \frac{Q_{hi}}{Q_{ei}} = \gamma \frac{(\, T_a - T_t\,)}{(\, e_a - e_t\,)} = c_1 \frac{p}{1000} \frac{(\, T_a - T_t\,)}{(\, e_a - e_t\,)} \qquad [3.23]$$

where: γ is a psychrometric constant;
c_1 is Bowen's constant;
P is atmospheric pressure in mb;
e_t is the saturation vapor pressure at the body surface temperature, in mb; and
T_t is body surface temperature.

The value of Bowen's constant varies from 0.57 for smooth surfaces to 0.66 for rough surfaces (Anderson, 1954). Bowen estimated the constant to be 0.6 (Ashton, 1986). It should be noted that Bowen's constant is different from the psychrometric constant, in that the latter incorporates the pressure term and, therefore, has the units of mb/°C (Ashton, 1986). The two are similar in magnitude, because the pressure term is close to one.

The atmospheric pressure, P, in the study area remains fairly constant during the melting period. Based on 20 years of observations at Hay River, Yellowknife and Fort Simpson, the average P value, is 1015 to 1017 mb during April and May (Department of Fisheries and Oceans, 1981) as summarized in Table 3.5. An average value of 1016 mb was used in this study.

The convective heat flux per unit area of the snow and ice cover, E_{hi} in J/m^2, may be calculated (based on Kuzmin's formula) as:

$$E_{hi} = 0.6\,P\,(\,0.018 + 0.00015\,u_2)(T_a - T_{ti})\,\rho_w\;\Delta t\;L_v\;/100000 \qquad [3.24]$$

When Dunne's formula is used, the convective heat transfer from the water surface, Q_{hw} in J, is:

$$Q_{hw} = 0.6\,P\,(\,0.013 + 0.00016\,u_2)(T_a - T_{tw}\,)\,\tilde{A}_w\;\rho_w\;\Delta t\;L_v\;/100000 \qquad [3.25]$$

And when Rimsha 's formula is used, the convective heat transfer from water surface, Q_{hw}, is:

$$Q_{hw} = 0.6\,P\;\;(6.04 + 0.263(T_{tw}\;-T_a\,) + 2.95u_2\,)\;(T_a - T_{tw}\,)\,\tilde{A}_w\,\Delta t\;/1000 \qquad [3.26]$$

5. Heat component carried by the warm water issuing from Great Slave Lake, Q_{lake}

The heat component carried by the warm water coming from Great Slave Lake as it approaches the open water area is a function of the water temperature in the lake and the discharge in the river:

$$Q_{lake} = Q\, T_{lake}\, \rho_w\, C_p\, \Delta t \qquad [3.27]$$

where: Q_{lake} is the heat carried by warm water from Great Slave Lake as it approaches the open water area, in J;

Q is the river discharge, in m^3/s,

T_{lake} is the water temperature the lake, in °C; and

C_p is specific heat of water, in J/kg°C.

Details of the measurements of lake temperature and the determination of the river's discharge throughout the breakup period are discussed in Chapter 2. The value of the specific heat of water used in this study is 4190 J/kg°C (Halliday and Resnick, 1988).

Snow effect

Snow cover was present on the ice surface at beginning of the melt period in three of the four years covered by this study. Therefore, the model had to be adapted to account for snow on the ice cover in the melting process. To simplify the formulation, the snow was simply converted to an equivalent depth of ice (t_{SIE}):

$$t_{SIE}\,(\mathrm{m}) = t_{sa}\,(\rho_s/\rho_i) \qquad [3.28]$$

where: t_{SIE} is the snow ice equivalent depth;

t_{sa} is the average snow depth at the simulation area, in metres,

ρ_s is the density of the snow, in kg/m^3 and

ρ_i is the density of the ice.

The average snow depth was calculated based on the measurements on both the border ice cover and the rough ice cover from the Great Slave Lake cross section to the Burnt Point cross section, which encompass the Beaver Lake portion of the study reach.

The density of snow varies depending upon the type and size of snow particles and also on the age of the snow. Table 3.6 shows typical values for the density of snow. In this study, the snow density was not measured in the field. Therefore, the snow density had to be estimated based on qualitative observations. Based on this, the snow density was taken as 200 kg/m^3. A sensitivity analysis was conducted to assess the validity of this choice.

The density of pure fresh ice is 917 kg/m^3 (Ashton,1986). Fortunately for this study, the Department of Transportation of N.W.T.(1992) measured the ice density at the Ice Bridge crossing in 1989 and 1991. These measurements were conducted both on the ice in the constructed ice bridge and in the natural ice adjacent to the ice bridge crossing. A summary of these measurements (for the natural ice) is presented in Table 3.7. The density of the natural ice throughout the study reach was taken as the average of these measured values, or 904 kg/m^3.

Taking the snow ice equivalent depth into consideration, the initial ice thickness used in the melt simulation is equal to:

$$t_{io} = t_{i\ \mathrm{measured}} + t_{SIE} \qquad [3.29]$$

where: t_{io} is the initial ice thickness used in simulation, in metres;

$t_{i\ \mathrm{measured}}$ is the ice thickness, in metres, measured on (or close to) the day the ice melt simulation began; and

t_{sa} is the average snow depth on the ice cover in the Beaver lake area measured on (or close to) the day the ice melt simulation began, in metres.

Open water area, $A_W{}^j$

Once all of the heat components acting on the ice cover have been determined, the changes of the ice cover thickness for day "j", $\Delta t_i{}^j$, can be calculated by:

$$\Delta t_i^j = \frac{E_{si}{}^j - E_{li}{}^j - E_{ei}{}^j + E_{hi}{}^j}{\rho_i L_m} \qquad [3.30]$$

where: $\Delta t_i{}^j$ is the ice cover deduction for day j; and

L_m is the latent heat of fusion, 333400 J/kg (Ashton, 1986).

The ice thickness at the end of day j, $t_i{}^j$ is

$$t_i{}^j = t_i{}^{j-1} - \Delta t_i{}^j \qquad [3.31]$$

The new open water area developed in day j, $\Delta A_w{}^j$, is

$$\Delta A_w^j = \frac{Q_{sw}{}^j - Q_{lw}{}^j - Q_{ew}{}^j + Q_{hw}{}^j + Q_{lake}{}^j}{\rho_i L_m t_{io}} \qquad [3.32]$$

where t_{ia} is the average value of the ice cover thickness, which is equal to:

$$t_{ia} = (t_i^{j-1} + t_i^{j})/2 \qquad [3.33]$$

Therefore, the total open water area at end of day j, A_w^j, is

$$A_w^j = A_w^{j-1} + \Delta A_w^j \qquad [3.34]$$

Water temperature in the open water area, T_W

As discussed in Chapter 2, the water temperature in Great Slave Lake (T_{lake}) is measured at beginning of melting season. Just after this water reaches the upstream end of open water area, its temperature begins to rise because it is heated by the solar heat and the warm air in direct contact with the river flow in the open water area. Once this water reaches the downstream end of the open water area (i.e. the melting front), it will have attained its highest temperature value. The increase in water temperature which occurs in the open water area can be calculated by:

$$\Delta T_w = \frac{Q_{sw} - Q_{lw} - Q_{ew} + Q_{hw}}{Q\rho_w C_p \Delta t} \qquad [3.35]$$

The water temperature at the upstream end of the open water area is likely something between the lake water temperature and 0 °C. If it is assumed that the water temperature at the upstream end of the open water area *is equal to* the lake water temperature, the average water temperature in the open water area, T_w, would be equal to:

$$T_w = \frac{Q_{sw} - Q_{lw} - Q_{ew} + Q_{hw}}{2Q\rho_w C_p \Delta t} + T_{lake} \qquad [3.36]$$

In this case, an iterative method must be used to calculate T_w because the terms on the right hand side of equation [3.36] include the average water temperature in the open water area.

The average water temperature in the channel is calculated in order to provide a reasonable boundary condition which is used in heat components quantification. The heat come from the lake is still calculated by using the lake water temperature (T_{lake}) and T_{lake} is not update anytime.

Summary

The heat fluxes acting on a unit area of the ice cover, (E_{si}, E_{li}, E_{ei} and E_{hi}) can be calculated by the following equations:

$$E_{si} = (1 - \alpha_i)\, R_s\, \Delta t \qquad [3.1]$$

$$E_{li} = \left(\varepsilon\, \omega (273.2 + T_{tw})^4 - (a + b\sqrt{e_a})\, \omega (273.2 + T_a)^4 (1 + kC^2) \right) \Delta t \qquad [3.10]$$

$$E_{ei} = (0.018 + 0.00015\, u_2)(e_{ti} - e_a)\, \rho_w\, \Delta t\, L_v \qquad [3.17]$$

$$E_{hi} = 0.6\, P\, (0.018 + 0.00015\, u_2)(T_a - T_{tw})\, \rho_w\, \Delta t\, L_v\, /100000 \qquad [3.24]$$

$$\Delta t_i^j = \frac{E_{si}^{\ j} - E_{li}^{\ j} - E_{ei}^{\ j} + E_{hi}^{\ j}}{\rho_i L_m} \qquad [3.30]$$

The ice thickness at the end of day j, t_i^j is then:

$$t_i^j = t_i^{j-1} - \Delta t_i^j \qquad [3.31]$$

The heat components acting on the open water area, can be calculated by the following equations:

$$Q_{sw} = (1 - \alpha_w)\, R_s\, \Delta t\, \tilde{A}_w \qquad [3.2]$$

$$Q_{lw} = \left(\varepsilon\, \omega (273.2 + T_{tw})^4 - (a + b\sqrt{e_a})\, \omega (273.2 + T_a)^4 (1 + kC^2) \right) \Delta t\, \tilde{A}_w \qquad [3.11]$$

$$Q_{ew} = (0.013 + 0.00016\, u_2)(e_{tw} - e_a)\, \tilde{A}_w\, \rho_w\, \Delta t\, L_v \qquad [3.20]$$

or

$$Q_{ew} = (6.04 + 0.263\, (T_{tw} - T_a) + 2.95\, u_2)\, (e_{tw} - e_a)\, \Delta t\, \tilde{A}_w \qquad [3.22]$$

$$Q_{hw} = 0.6\, P\, (0.013 + 0.00016\, u_2)(T_a - T_{tw})\, \tilde{A}_w\, \rho_w\, \Delta t\, L_v\, /100000 \qquad [3.25]$$

or

$$Q_{hw} = 0.6\, P\, (6.04 + 0.263(T_{tw} - T_a) + 2.95 u_2)\, (T_a - T_{tw})\, \tilde{A}_w\, \Delta t\, /1000 \qquad [3.26]$$

$$Q_{lake} = Q\, T_{lake}\, \rho_w\, C_p\, \Delta t \qquad [3.27]$$

The average value of the ice cover thickness, t_{ia} is equal to:

$$t_{ia} = (t_i^{j-1} + t_i^j)/2 \qquad [3.33]$$

The new open water area developed on day j, $\Delta A_w{}^j$ is:

$$\Delta A_w^j = \frac{Q_{sw}{}^j - Q_{lw}{}^j - Q_{ew}{}^j + Q_{hw}{}^j + Q_{lake}{}^j}{\rho_i L_w t_{ia}} \qquad [3.32]$$

and the total open water area at end of day j, $A_w{}^j$ is

$$A_w{}^j = A_w{}^{j-1} + \Delta A_w{}^j \qquad [3.34]$$

3.2.2.3 Model Application

The ice surface albedo is one parameter which must be calibrated in this model because it typically varies over a large range (Table 3.1) and because it was not practical, nor economical to measure it for this study. There are other coefficients in the simulation such as the constants in Brunt's formula, which could also be calibrated. However, practically speaking, only one or two parameters can be determined during a calibration without resorting to optimization techniques. Given the short period of record, four years, such techniques are not warranted in this study. Consequently, the ice albedo was selected as the only calibration parameter. This decision was confirmed through a sensitivity analysis of the effects of parameter variation, as it was determined that the ice surface albedo had a significantly higher effect on model results than any of the other parameters involved in the simulation. Table 3.8 gives the values of the constants and coefficients used in the simulation. As discussed earlier, the albedo of the water surface was taken as 0.08.

Because of the long period over which the thermal breakup in Beaver Lake occurs, and based on qualitative observations of ice surface albedo, two values of ice albedo were calibrated into the models developed for this study. The albedo used in the early melt period was higher than the value used in the latter part, with the day of change based on the documented date on which the ice cover in this reach first displayed a significantly darker surface appearance. These dates are summarized along with other key dates involved in the simulation, in Table 3.9. When there is a snow cover on the ice cover, the initial albedo should be close to the snow surface albedo. The initial conditions includes the date of modelling start, the initial open water area, the date of the surface albedo changed and the lake water temperature. These data are shown in the Table 3.9. The values of the open water area in following days (in Table 2.25) are also needed for evaluation of the fitted curve.

As stated in Chapter 2, ice thicknesses were measured in the border ice and rough ice as a part of the data collection program. Key data for this portion of the study are presented in Table 3.10. Based on the limited amount of data which could be obtained for the rough ice on Beaver Lake (due to safety considerations and given its vast surface area) the average rough ice thickness in this reach was consistently about 1.2 times the average border ice thickness. As it was desirable to minimize the subjectivity of determining representative ice thicknesses for input to the model based on measured data at varying sites, an assessment of the consistency of ice thicknesses compared to an index site (taken as the Great Slave Lake section) was undertaken. As the data shows, the average ice thickness at the South Channel cross section was consistently about 0.15 m thicker than the measured border ice thickness at the Great Slave Lake cross section. However, relative thicknesses were not quite so consistent between the Kakisa River section. Therefore, three different scenarios were examined for estimating the representative ice thickness at the Kakisa River cross section:

Case A

- the average ice thickness at Kakisa River cross section was taken to be equal to average ice thickness at the South Channel cross section (i.e. 0.15 m thicker than the measured border ice thickness at the Great Slave Lake section)

Case B

- the average ice thickness at Kakisa River cross section was taken to be equal to average ice thickness at the South Channel cross section plus 0.1 m (i.e. 0.25 m thicker than the measured border ice thickness at the Great Slave Lake section)

Case C

- the average ice thickness at Kakisa River cross section was taken to be equal to 1.2 times the average of border ice thicknesses measures from the South Channel cross section to the Burnt Point cross section

The three sets of initial ice thickness values used in the model are shown in Table 3.10. In all three cases the representative ice thickness at the Great Slave Lake section was taken as the measured border ice thickness, and the representative ice thickness at the South Channel section was taken as the Great Slave Lake value plus 0.15 m.

Wind speed and relative humidity measurement devices were incorporated into the Ft. Providence meteorological station in 1993. Although wind speed and relative humidity data were collected at the Natural Resources station in Ft. Providence in 1992, as mentioned in Chapter 2, these measurements only began on 5-May-92 which was too late to facilitate the simulation as there is no ice data corresponding to that day. Consequently, only the data from 1993, 1994 and 1995 could be used in the calibration of the energy budget model. With only three years of data, it was considered inappropriate to reserve one year of data for model verification.

In calibrating the model, some measure of the goodness of fit had to be devised to assess the comparative quality of various choices of the calibrated parameter (ice albedo). The quality of the simulation result was evaluated by a special variance, Δ^2 that was defined as:

$$\Delta^2 = \frac{1}{(n_m - 1)}[\sum_{1}^{n_m}(A_{w,calculated} - A_{w,measured})^2] \qquad [3.37]$$

where: n_m is the number of measurements of open water area;

$A_{w,calculated}$ is the open water area calculated by the model; and

$A_{w,measured}$ is the measured open water area.

This assessment of the goodness of fit was limited to those measurements involving open water areas less than 300 km^2. As stated in Chapter 2, the predominantly thermal breakup in Beaver Lake persists roughly until the open water in the North and South Channels joins downstream of Big Island (at an open water area of about 280 km^2). Beyond that point, dynamic effects often play a role in the clearing of the remaining ice upstream of Burnt Point.

The first step was to optimize the calibration of the ice surface albedo for each individual year. Taking into consideration the two approaches used in the calculation of the evaporation heat component for the open water area, and the three approaches used to handle the ice data, this results in six calibrations for each of the three years. Figures 3.2 to 3.4 illustrate the results for 1993, 1994 and 1995, respectively. Figure 3.5 shows the variances obtained in each case.

For the 1993 event (Figure 3.2), the calibrated ice surface albedo was 0.25 for the entire melt period. No improvement in fit to the measured data was obtained by varying ice surface albedo over time. For the 1994 event (Figure 3.3), the calibrated albedo was 0.50 during the early melt period and 0.45 later on. For the 1995 event (Figure 3.4), the calibrated ice surface albedo was 0.45 for the entire melt period. Again, as for 1993, no improvement in fit to the measured data was obtained by varying ice surface albedo over time. Overall, as Figure 3.5 illustrates, the model did not appear sensitive to the method used to calculate the evaporation heat component for the open water area, and of the three approaches to ice thickness data interpretation, Case B provided the best fit to the measured data.

Further calibration efforts were focused on determining whether representative values of the ice surface albedo for the early and late melt period could be obtained which would be applicable in all three years, as this is essential if the method is to be used for forecasting breakup. Figures 3.6 to 3.8 present the calibrated results for Cases A, B and C, respectively. The optimum values of the ice surface albedo were found to be 0.45 during the early melt period and 0.35 later on. Again, the quality of fit was not particularly sensitive to the method used to calculate the evaporation heat component for the open water area. However, as the figures illustrate, the overall fit is poor for all three years. Figure 3.9 shows the variances obtained in each case.

3.2.2.4 Discussion of Results

The calibration results by each individual year indicate that the ice surface albedo ranges from 0.25 to 0.50. These values are in the range of documented values for melting snow, snow ice and candled black ice. However, they seem low based on visual observation in the field. The value of albedo in 1993 is likely 20% lower than that in 1994 and 1995 because there was no snow on the ice cover in 1993. Unfortunately, though excellent results were obtained by this approach for the individual years, the method displayed no consistency from year to year. Consequently, it is unsuitable for forecasting the development of open water at this site.

Another factor to consider is that although the energy budget method is not difficult to apply, it is data intensive. Also, the daily averages of some of the data, such as wind speed and humidity, might not be representative of the average value over the whole area under investigation or over the day. Furthermore, relative humidity and wind speed are not straightforward to forecast. Therefore, the energy budget method is limited in its applicability as a forecasting model.

3.2.3 Conceptual (Radiation-Temperature Related) Approach

3.2.3.1 Formulation

Given the practical limitations of the energy budget approach, it was desirable to try an alternative modelling approach which assumes a simple linear relationship between temperature gradient and heat transfer (Andres, 1984). This conceptual approach uses only solar radiation, air temperature, discharge and lake water temperature as input data. An additional advantage of this approach was the fact that the 1992 data could be used in the conceptual model calibration along with the other three years' data, because wind speed and humidity are not required in this approach.

The heat components acting on the ice cover and the water surface considered in this conceptual model are:

Q_{sw} is the solar radiation heat incident to the water surface;
Q_{hw} is the convective heat exchange between the water surface and the atmosphere;
Q_{si} is the solar radiation heat incident to the ice (or snow) surface; and
Q_{hi} is the convective heat exchange between the ice (or snow) surface and the atmosphere.

Although these heat components are the same as some of those defined in the energy budget approach, either the equations for calculating these quantities are different or the same equations are used, but with different coefficients (since the approach has been simplified).

Assumptions

The assumptions that were required in the energy budget approach are also required for this conceptual model, except for assumption 6. Some additional assumptions are also required in this approach:

1. *The longwave radiation heat energy is a linear function of the difference between the air temperature and the ice, or water body, temperature.* Figure 3.10 (a) illustrates the validity of this assumption for temperature differences up to about 14 °C, by presenting the longwave radiation heat per unit area of the ice cover and the water surface as a function of temperature difference, calculated by the energy budget method using 1993, 1994 and 1995 data.

2. *The convective heat transfer is a linear function of the difference between the air temperature and ice, or water body temperature.* Figure 3.10 (b) illustrates the validity of this approach for temperature differences up to about 7 °C. The figure is plotted by using 1993 to 1995 data and was based on Rimsha's formula. As the figure shows, the suitability of this assumption decreases at higher temperature.

3. *The evaporation heat component is negligible.* The overall effect of the evaporation heat component is negative in that it decreases the rate of open water area development. In the application of the energy budget approach, it was determined that the average value of evaporation heat was less than 10 percent of the solar radiation heat. This effect is incorporated into the conceptual model through the calibrated coefficients.

Heat components acting on the ice cover and the water surface

1. Short-wave radiation heat components, E_{si} and Q_{sw}

The net incoming short-wave radiation heat on the unit area of ice surface can be obtained by equation [3.1], which is reproduced below for convenience:

$$E_{si} = (1 - \alpha_i)\, R_s\, \Delta t \qquad [3.1]$$

The net incoming short-wave radiation heat on the water surface can be obtained by equation [3.2]:

$$Q_{sw} = (1 - \alpha_w)\, R_s\, \Delta t\ \bar{A}_w \qquad [3.2]$$

The variables in equations [3.1] and [3.2] are the as same as defined earlier (in the section on the energy budget approach) but the values of albedo will be different because this parameter must now incorporate the effects of longwave radiation and evaporation.

2. Convective heat components, E_{hi} and Q_{hi}

The convective heat transfer from a unit area of the ice (or snow) cover is calculated using:

$$E_{hi} = h_i\, (T_a - T_i)\, \Delta t \qquad [3.38]$$

where h_i is the heat transfer coefficient between the air and the ice surface, in W/m² °C. This coefficient, h_i, has to be calibrated because it includes all of the effects that are based on temperature change, such as: conduction, convection, part of the longwave radiation, and the evaporation.

The convective heat transfered to the water surface can be calculated in a similar fashion by:

$$Q_{hw} = h_w\,(T_a - T_w)\,\Delta t\;\bar{A}_w \qquad [3.39]$$

where h_w is the heat transfer coefficient between air and water surface in W/m² °C. This coefficient has to be calibrated as well.

3. Heat component carried by warm water from Great Slave Lake, Q_{lake}

The heat carried by warm water issuing from Great Slave Lake can be obtained by equation [3.27]:

$$Q_{lake} = Q\,T_{lake}\,\rho_w\,C_p\,\Delta t \qquad [3.27]$$

Assuming the water temperature at the upstream end of the open water area is equal to the water temperature in the lake, the average water temperature in the open water area can be calculated as:

$$T_w = \frac{Q_{rw} + Q_{hw}}{2Q\rho_w C_p \Delta t} + T_{lake} \qquad [3.40]$$

Modelling the ice thickness and the open water area development

When all of the heat components acting on the ice cover have been determined, the ice cover deduction occurring on day j, Δt_i^j, can be calculated by:

$$\Delta t_i^j = \frac{E_{ri}{}^j + E_{hi}{}^j}{\rho_i L_m} \qquad [3.41]$$

The ice thickness at the end of day j, t_i^j is then:

$$t_i^j = t_i^{j-1} - \Delta t_i^j \qquad [3.31]$$

The new open water area developed on day j, ΔA_w^j is:

$$\Delta A_w^j = \frac{Q_{sw}{}^j + Q_{hw}{}^j + Q_{lake}{}^j}{\rho_i L_m t_{ia}} \qquad [3.42]$$

and the total open water area at end of day j, A_w^j is, therefore:

$$A_w^j = A_w^{j-1} + \Delta A_w^j \qquad [3.34]$$

Summary

The heat components acting on a unit area of ice cover, (E_{si} and E_{hi}) can be calculated by the following equations:

$$E_{si} = (1 - \alpha_i)\, R_s\, \Delta t \qquad [3.1]$$

$$E_{hi} = h_i\, (T_a - T_i)\, \Delta t \qquad [3.38]$$

The ice cover deduction in the day j, Δt_i^j , can be calculated by:

$$\Delta t_i^j = \frac{E_{si}{}^j + E_{hi}{}^j}{\rho_i L_m} \qquad [3.43]$$

The ice thickness at the end of day j, t_i^j is:

$$t_i^j = t_i^{j-1} - \Delta t_i^j \qquad [3.31]$$

The heat components acting on the open water area, (Q_{sw}, Q_{hw} and Q_{lake}) can be calculated by the following equations:

$$Q_{sw} = (1 - \alpha_w)\, R_s\, \Delta t\ \tilde{A}_w \qquad [3.2]$$

$$Q_{hw} = h_w\, (T_a - T_w)\, \Delta t\ \tilde{A}_w \qquad [3.39]$$

$$Q_{lake} = Q\, T_{lake}\ \rho_w\ C_p\, \Delta t \qquad [3.27]$$

The new open water area developed in day j, ΔA_w^j is

$$\Delta A_w^j = \frac{Q_{sw}{}^j + Q_{hw}{}^j + Q_{lake}{}^j}{\rho_i L_m t_{ia}} \qquad [3.42]$$

and the total open water area at end of day j, A_w^j is

$$A_w^j = A_w^{j-1} + \Delta A_w^j \qquad [3.34]$$

3.2.3.2 Model Application

As in the energy budget method, a constant water surface albedo was used. However, the water surface albedo was increased to 0.10 in this conceptual model, as it incorporates the effects of longwave radiation and evaporation, as well. The parameters to be calibrated were:

- the heat transfer coefficient between the air and the ice cover,
- the heat transfer coefficient between the air and the water surface, and
- the albedo of the ice cover.

Based on preliminary calibration runs, the value of the ice cover albedo was taken as 0.9 for the early melt period, and 0.7 after the ice surface darkened noticeably. These values are higher than that used in the energy budget approach, again because this parameter now includes the effects of longwave radiation and evaporation. During further calibrations, the ice cover albedo and the water surface albedo were not changed.

During some of the preliminary calibration runs, a constant value of the water temperature in the lake was tried. It was hoped that if the model was not sensitive to this variable, the need for annual measurements of lake water temperature could be avoided. However, it was determined that this data was essential to obtaining consistent results with the model.

As in the energy budget approach, three cases for the initial ice thickness were used. The values used were presented in Table 3.10.

The heat transfer coefficient between the air and the ice cover, h_i, and the heat transfer coefficient between the air and the water surface, h_w, generally range from of 10 to 20 (Andres, 1984). Based on preliminary calibration runs, nine different combinations were chosen:

$h_i = 4, h_w = 10$; $h_i = 4, h_w = 15$; $h_i = 4, h_w = 20$.
$h_i = 8, h_w = 10$; $h_i = 8, h_w = 15$; $h_i = 8, h_w = 20$.
$h_i = 12, h_w = 10$; $h_i = 12, h_w = 15$; $h_i = 12, h_w = 20$.

An assessment of the goodness of fit for each calibration run was determined by considering the variance as defined by equation [3.37]:

$$\Delta^2 = \frac{1}{(n_m - 1)}[\sum_{1}^{n_m}(A_{w,calculated} - A_{w,measured})^2] \qquad [3.37]$$

As in the energy budget method, this assessment of the goodness of fit was limited to those measurements involving open water areas less than 300 km². Table 3.11 shows the variances resulting for the different ice thickness scenarios and the different combinations of the heat transfer coefficients, for the four years of record. Based on consistency between years, and the overall magnitude of the variance, the best combinations of coefficients were found to be:

$h_i = 8$, $h_w = 20$ and $h_i = 12$, $h_w = 10$.

Figures 3.11 to 3.13 show the simulation curves and measured data for the three cases, A, B and C using these heat transfer coefficients, for 1992 to 1995, respectively.

3.2.3.3 Discussion of Results

In terms of the method of determining ice thickness, Case B provided the best results, when assessed based on the consistency of error between years, and minimized overall magnitude of the variance.

In all cases and for all combinations of the heat transfer coefficients, there was a conflict between the 1993 and 1995 data in that improving the fit for one could not be done without deteriorating the fit for the other. Similar difficulties were encountered with the energy budget method. However, overall, the optimal calibration of the conceptual model provided a reasonable fit for a single set of calibrated parameters, which is something that was not possible with the energy budget approach.

3.3 Modelling the First Movement of Ice at Providence Rapids

3.3.1 Introduction

In all of the four years of this study (1992 to 1995), the first movement of ice in the ferry reach occurred at Providence Narrows. The ice cover consolidated, or "shoved", in the upper portion of the Providence Rapids, and ice sheets broke away from the ice cover just upstream of Big River. The ensuing water level adjustments to the consolidation of the ice cover resulted in successive shoves and further water level fluctuations, setting up a cycle which cleared the ice in the ferry reach within 4 to 8 days. In all four years, also, this initial movement of ice preceded the initial movement of ice at the ferry crossing. As Figure 3.14 shows, this first, potentially threatening, movement of ice at the ferry crossing occurred 1 to 6 days following the initial movement of ice at Providence Narrows over the four years of investigations to date. Therefore, modelling the initial movement of ice at Providence Narrows is the objective of the breakup model for this reach.

As discussed in Chapter 2, breakup in the ferry reach is not thermal. Although heat is the agent of deterioration and strength reduction, the ice clears through a process of cracking, breaking and moving downstream. Therefore, in addition to the thermal aspects of breakup considered in the Beaver Lake model, the effects of the flow on the ice cover must be considered, as well. This includes the consideration of the effect of drag on the underside of the ice cover which is a function of the discharge in the channel, the energy gradient and the interactive effects of the ice on flow hydraulics. Also important is the strength or competence of the ice cover to resist the forces tending to fracture it. Finally, the mechanism of failure may vary; the ice cover may fail in bending, compression, shear or a combination of the three. Attempting to forecast a dynamic breakup deterministically involves consideration of the loads imposed on the ice cover and the resistance of the ice cover to failure or breaking, both of which vary in time. The rate of change of each depends upon initial conditions (ice thickness, snow depth on the ice cover, and late winter discharge) and on varying conditions through the pre-breakup period (discharge and water level fluctuations, and heat input to the ice). For the latter, it is the rate of change of these variables which dictates the rate at which breakup will progress.

The heat from the sun and the air is not only effective in initiating breakup by weakening the ice, it is also the mechanism for snow melt in the catchment. In many typical river cases, discharge increases rapidly in response to snowmelt in the upstream catchment. Thus, just as the ice strength begins to decrease during the early breakup period due to heat from the sun and air, stresses on the ice cover increase because of increasing discharge. When the load on the ice cover exceeds its strength, breakup will occur. Therefore, the more rapid the increase in discharge, the greater the potential for breakup to occur before significant thermal deterioration of the ice cover has occurred.

This study reach is different because of the effects of Great Slave Lake. As the majority of the catchment drainage area is upstream of Great Slave Lake, local inflow due to snowmelt runoff is small in comparison to the total river discharge. Therefore, although a distinct increase in river discharge occurs over the breakup period the increase is gradual and prolonged, as the runoff from the upstream catchment is routed through Great Slave Lake. Because of its early occurrence (typically around the last week of April) this initial movement of ice at Providence Rapids is not associated with dramatic increases in discharge, and the corresponding stresses on the ice cover. Consequently, this site should be more amenable than most to the consideration of simple failure mechanisms as a means of forecasting breakup.

In this section, several of the approaches proposed in the literature will be considered. First, the literature on thermal deterioration of ice is reviewed, including radiation absorption, radiation effect on porosity of a melting ice cover, and strength versus porosity relationships. Next, the loads acting on the ice cover are discussed and equations are developed to quantify these loads. Finally, four different models of mechanical breakup are considered, and applied to the study reach.

3.3.2 Quantifying Ice Deterioration

3.3.2.1 Introduction

A key component of any dynamic breakup model which considers the loads on the ice cover, and the ice resistance to those loads, is ice deterioration. The strength reduction which eventually causes the ice cover to succumb to imposed loads must be quantified. Two aspects of ice deterioration must be considered to quantify ice strength deterioration. The first is the thinning of ice (melting from the top down, or from the bottom up) as was considered in the thermal breakup models for the Beaver Lake reach. The second form of ice deterioration which must be considered is the decreasing porosity of the ice, due to intergranular melting. In this section, the literature on ice deterioration and strength reduction relationships is discussed.

3.3.2.2 Nature of Solar Radiation Absorption by an Ice Cover

The solar radiation absorbed by the ice cover melts the ice crystals at their boundaries (Knight, 1962). In thermal, or columnar, ice the crystal growth is in the vertical direction and melting in the interstices between crystals leads to the familiar porous "candle ice". Frazil ice has a more granular structure, and thus develops a different porosity pattern. Observations in this study, and in other studies, confirm that the melting does not occur uniformly over the depth, but rather primarily in the upper layers of the ice. Borisenkov (1970) introduced Koptev's empirical formula for estimating the amount of radiation absorbed by the ice at different depths, $I_a(z)$:

$$I_a(z) = I_o\left(1-\alpha_i\right)\left(1-\mu e^{-vz^{0.33}}\right) \qquad [3.44]$$

where: I_o is the incoming radiation at the ice surface;
α_i is the ice albedo;
e is the base of the natural logarithms; and
μ and v are empirical parameters which depend upon the physical properties of the ice and the nature of the incoming solar radiation.

Borisenkov (1970) reported typical values of μ and v, based on field measurements in the Russian Arctic. These are reproduced in Table 3.12. Figure 3.15 shows the curves which are obtained using these values in equation [3.44]. The measured data did not extend to the ice surface, and extrapolation of equation [3.44] to the ice surface produces negative numbers. Therefore, in Figure 3.15, the extrapolation to the ice surface has been approximated by forcing the curve through the origin.

Bulatov (1970) provided a summary of others' solar radiation penetration data from a number of lakes, reservoirs and rivers in the Russian. Based on this data, he presented the following equation for estimating the amount of solar radiation *penetrating* the ice at different depths, $I_p(z)$:

$$I_p(z) = I\left(e^{-cz^{0.6}}\right) \qquad [3.45]$$

where: I is the incoming solar radiation;

c is an empirical parameter which depends upon the physical properties of the ice; and, *z* is the depth below the ice surface, in cm.

Based on a regression of 13 data sets Bulatov recommended values of *c* for two ice types: 0.165 (Type I) and 0.074 (Type II). Type I was general crystalline ice with snow ice at the surface. Type II was quite transparent ice formed by pure water. For snow ice, Bulatov suggested a value of 0.25 for *c*, though he cautioned that this parameter could deviate widely from this value for various kinds of snow ice.

Ashton (1985) also presented an equation for calculating the solar radiation flux at different depths in ice, based on the data measured by Grenfell and Maykut (1977) in first-year blue sea ice under overcast skies:

$$I_p(z) = I_o\left(1-\alpha_i\right)\left(e^{-1.36\,z^{0.5}}\right) \qquad [3.46]$$

where *z* is the depth below the ice surface, in metres. Equations [3.45] and [3.46] are plotted in Figure 3.16.

Assuming that the difference in the amount of solar radiation penetrating at two different depths is equal to the radiation absorbed in the layer between those two depths, Ashton's equation can be converted to calculate absorbed radiation at different depths within an ice cover:

$$I_a(\,z)= I_o(1-\alpha_i)(1-\,e^{-1.36\,z^{0.5}}) \qquad [3.47]$$

In addition, assuming:

$$I = I_o\,(1 - \alpha_i) \qquad [3.48]$$

in Bulatov's equation, the absorbed radiation calculated by Bulatov's equation is:

$$I_a(\,z)= I_o(1-\alpha_i)(1-\,e^{-c\,z^{0.6}}) \qquad [3.49]$$

Figure 3.17 shows all of the absorbed radiation relationships based on equations [3.44], [3.47] and [3.49], for varying ice types, illustrating that highly transparent ice absorbs less radiation. Borisenkov's "ice with parallel-fiber structure" and Bulatov's "crystalline ice Type I" are closest to the type of ice in this study. As the figure illustrates, the curve for Borisenkov's "ice with parallel-fiber structure" under average sky conditions (based on the average values of μ and ν of 1.21 and 0.545, respectively) compares favorably to Bulatov's "crystalline ice Type I". From these two curves it is seen that about 75 % of the solar radiation is absorbed in top the 0.3 metres of the ice cover and about 10 % of the radiation passed through a one metre thick ice cover.

3.3.2.3 Quantifying the Porosity of Ice Cover

Porosity is defined as the ratio of the volume of voids in the melted ice to the total volume of the ice:

$$\Phi = \frac{V_{por}}{V_{total}} \qquad [3.50]$$

where: Φ is the porosity;
V_{por} is the volume of voids in the ice cover; and
V_{total} is the total volume of the ice.

At the same time that the ice porosity is increasing due to input solar radiation, the ice is thinning due to heat inputs from the warm water below and the warm air above. Thus the total volume of ice is changing in time and must be accounted for in the in porosity calculation.

Quantifying the increasing porosity of the ice cover is important to the development of a model of the first movement of ice in the study reach, as it is strongly correlated to ice strength reduction (Bulatov, 1970; Ashton ,1985). There are a number of possible approaches to apportioning the heat input in a porosity calculation, each based on different assumptions. Two, appropriate to the study site, are considered here.

In the first approach, it is assumed that 100% of the net incoming solar radiation is absorbed by the ice, increasing the porosity of the ice cover uniformly over the depth. The convective heat transfer from the warm overlying air causes the ice to melt on the top, thinning the ice cover. From water temperature measurements (Chapter 2), it has been observed that the water temperature is close to 0 °C during the early melt period (before the initial movement of ice at Providence Narrows). Therefore, the ice cover does not thin from the bottom up. Prior to any ice melt, any snow on the ice cover must first be melted. Both the solar radiation and the convective heat are used to melt this snow on the ice cover. Porosity calculations begin on the day that the computations indicate that the snow is fully melted. For this scenario the porosity can be calculated based on a unit area of the ice cover using:

$$V_{por} = \left(\frac{\sum E_{si}}{\rho_i L_m} \right) \times 1\ m^2 \qquad [3.51]$$

$$V_{total} = \left[t_o - \left(\frac{\sum E_{hi}}{\rho_i L_m} \right) \right] \times 1\ m^2 \qquad [3.52]$$

where t_o is the initial ice thickness, in metres, not including the equivalent ice thickness of the snow on the ice cover, t_{SIE}.

In the second approach, the fact that the solar radiation is absorbed in different quantities at different depths within the ice is considered. Based on an average of the two appropriate curves in Figure 3.15: Borisenkov's "ice with parallel-fiber structure" (for average sky conditions) and Bulatov's "crystalline ice Type I" the input solar radiation is apportioned such that the top 0.3 m of the ice cover absorbs 75%. In addition, 10% of the net incoming solar radiation is assumed to pass through the ice cover. For this scenario, the porosity in the top 0.3 m of the ice cover is greater than that calculated by the first approach, which means that thinning of the ice cover, due to convective heat transfer from the overlying air is increased. In addition, when the top layer melts, part of the porous volume is also gone. Consequently, the 0.3 m surface layer moves down at the thinning rate. For this approach, the porosity of the top 0.3 m of the ice cover is calculated using:

$$\Delta V^j_{por,\,top} = \left(\frac{0.75\ E^j_{si}}{\rho_i L_m} \right) \times 1\ m^2 - \Delta V^j_{total} \Phi^{j-1}_{top} \qquad [3.53]$$

where: $\Delta V^j_{por,\,top}$ is the porous volume of the top 0.3 m of the ice cover at the end of day j; and

ΔV^j_{total} is the total volume of the ice cover at the end of day j :

$$\Delta V^{j}_{total} = \frac{\left(\frac{E^{j}_{hi}}{\rho_i L_m}\right) \times 1\ m^2}{\left(1 - \Phi^{j-1}_{top}\right)} \qquad [3.54]$$

and $\Phi^{j-1}{}_{por}$ is the porosity of the top 0.3 m of the ice cover at the end of day j-1:

$$\Phi^{j}_{top} = \frac{\left(\sum \Delta V_{por,\,top}\right)}{0.3\ m^3} \qquad [3.55]$$

Gross porosity, per unit area of the ice cover, is then calculated using:

$$\Delta V^{j}_{por} = \left(\frac{0.9\ E^{j}_{si}}{\rho_i L_m}\right) \times 1\ m^2 - \Delta V^{j}_{total} \Phi^{j-1}_{top} \qquad [3.56]$$

where,

$$V^{j}_{total} = t_o \times 1\ m^2 - \left(\sum \Delta V_{total}\right) \qquad [3.57]$$

and,

$$\Phi^{j} = \frac{\left(\sum \Delta V_{por}\right)}{V^{j}_{total}} \qquad [3.58]$$

3.3.2.4 Ice Strength Reduction

It has been observed that ice strength varies with ice temperature and ice porosity. Ice at temperatures near the melting point, 0°C, exhibits less strength than ice at temperatures well below the melting point (Michel, 1978). This is the initial strength condition at the onset of ice melting. This initial ice strength varies with the type of ice. Data collected in this study (RAMSET® nail penetrations) indicate that this value is consistent within the study reach and from year to year. However, as discussed in Chapter 2, the RAMSET® device provides only an index of strength. Northwest Territories Transportation (1992) measured compressive ice strengths in the natural ice adjacent to the ice bridge during the ice bridge construction in 1989 and 1991. The measured ice strengths, shown in Table 3.13, range from 0.72 to 8.65 MPa. Because the data were measured while the ice bridge was being constructed, at a time when the temperature was lower than 0 °C, these measured values are higher than the near melting point ice strength required for this analysis.

Once heat input from the sun begins to increase the porosity of the ice through intergranular melting, the ice strength reduces rapidly. As stated earlier, a number of authors have presented relationships quantifying ice strength reduction as a function of increasing ice porosity. These will be discussed here.

Based on a cubic model of intergranular melt, Bulatov (1970) presented the following theoretical equation to evaluate the relationship between the strength reduction and the porosity of an ice cover:

$$\Phi = 0.645 \left(1 - \sqrt{\sigma/\sigma_o} \right)^2 \qquad [3.59]$$

where: Φ is the porosity of the ice cover;

σ is the reduced ice strength, in Pa; and

σ_o is the initial ice strength (at the time the ice starts to melt), in Pa.

This model assumes that the rate of melt at the cube corners, where three faces meet, would be 1.5 times great than the rate of melt at the edges, where two sides meet. Relating the accumulated radiation to the porosity, he obtained:

$$E_R = \Phi \rho_i L_m \qquad [3.60]$$

in which: E_R is the accumulated radiation absorbed per unit volume of ice, in J/m^3;

ρ_i is the density of the ice; and

L_m is the latent heat of fusion, 333400 J/kg (Ashton, 1986).

Substituting equation [3.59] into [3.60} Bulatov derived an expression relating the equivalent magnitude of the net solar radiation instead of the porosity to the strength reduction:

$$E_R = 0.645 \rho_i L_m \left[1 - \sqrt{\sigma/\sigma_o}\right]^2 \qquad [3.61]$$

defining a new variable, E_{Ro} :

$$E_{Ro} = 0.645\rho_i L_m \qquad [3.62]$$

where E_{Ro} is the accumulated amount of radiation absorbed per unit volume of ice at the time the ice strength reaches zero. This gives:

$$E_R = E_{R_o}\left[1 - \sqrt{\sigma/\sigma_o}\right]^2 \qquad [3.63]$$

Equation [3.62] would give a value for E_{Ro} close to 200 MJ/m^3 using the given values of ρ_i and L_m. Figure 3.18 shows Bulatov's curves relating strength reduction to the accumulated radiation absorbed per unit volume of ice by equation [3.63], and his comparison to field measurements. Based on this he gave the values of E_{Ro} for various types of ice:

Snow ice	230 MJ/m^3 (55 kcal/cm^3);
Slush ice	147 MJ/m^3 (35 kcal/cm^3);
Small-crystalline ice	113 MJ/m^3 (27 kcal/cm^3); and
Large-crystalline ice	67 MJ/m^3 (16 kcal/cm^3).

Combining equations [3.62] and [3.63]:

$$\Phi = \frac{E_{R_o}}{\rho_i L_m}\left[1 - \sqrt{\sigma/\sigma_o}\right]^2 \qquad [3.64]$$

yields an equation that can be used to calculate strength reduction in terms of porosity for different types of ice, given E_{Ro}. Bulatov (1970) suggested a value 184 MJ/m^3 (44 kcal/cm^3) for E_{Ro} for composite ice conditions.

Ashton (1985) presented the following equation based on uniform melting in Bulatov's cubic-grained model of intergranular melting:

$$\Phi = 0.645\left(1 - \sqrt{\sigma/\sigma_o}\right)^2 - 0.1674\left(1 - \sqrt{\sigma/\sigma_o}\right)^3 \qquad [3.65]$$

The last term in equation [3.65] approaches zero under the assumption that the cube corners melt at 1.5 times the rate of the cube edges (Ashton, 1985), and thus equation [3.65] reduces to equation [3.59].

Ashton (1985) also presented an equation to calculate the strength reduction (strength ratio) in terms of porosity based upon a hexagonal-grained model of internal melting:

$$\sigma/\sigma_0 = 1 - 2.813\sqrt{\Phi} \qquad [3.66]$$

which may be rearranged to obtain:

$$\Phi = 0.1264\left(1 - \sigma/\sigma_0\right)^2 \qquad [3.67]$$

In graphical comparisons between equations [3.65] and [3.67], and data for a variety of ice types measured by Shishokin, Korenkov and Butyagin (data reported by Bulatov, 1970), Ashton (1985) made an error in the presentation of equation [3.65]. This is illustrated in Figure 3.19 (a), where it is seen that the corrected curve for Ashton's adaptation of the cubic-grain internal melt model (equation [3.65]) is not significantly different from Bulatov's original cubic-grain internal melt model (equation [3.59]). More significantly, Ashton's hexagonal-grain melt model (equation [3.67]) is not consistent with either of the cubic-grain melt models. Ashton's model predicts a rapid decrease in strength as porosity increases, with the ice strength going to zero at a porosity of only 13%. For Bulatov's cubic-grain internal melt model (equations [3.59] and [3.65]), the porosity reaches 45 to 65% before the strength goes to zero.

Figure 3.19 (b) provides a comparison of the two internal melt models to field measurements for a variety of ice types (Shishokin, 1965, as reported by Bulatov, 1970). It is seen that Ashton's hexagonal-grain melt model (equation [3.67]) gives a lower envelope curve, while Bulatov's original cubic-grain internal melt model (equation [3.59]) approximates an upper envelop to the data.

In the application of strength versus porosity models there are two ways to determine the porosity. One would be to measure it in the field by cutting ice samples from the ice cover, measuring the weight of the ice sample, and dividing that weight by the weight of an equivalent volume of ice calculated based on the specific weight of ice for zero porosity (which could be determined from initial measurements before ice melt begins). The second, and much more common approach, is to calculate the increasing porosity using a thermal model, with input meteorological data. Equation [3.63] is very useful when the latter approach is used, because it gives the strength ratio directly from the meteorological data, rather than requiring the intermediate step of calculating porosity.

3.3.3 Forces Acting on the Ice Cover

3.3.3.1 Introduction

In a dynamic breakup, breakup is initiated once the loads on the ice cover exceed the resistance (strength) of the ice cover. The resistance to breakup is reduced due to thermal deterioration, but the increasing loads on the ice cover typically instigate failure long before zero strength is achieved. Therefore, in order to predict the initial movement of ice in a dynamic breakup situation, these loads must be quantified.

In this analysis a one-dimensional force balance will be considered. Before the initial movement of ice, the forces acting on an ice cover in the longitudinal direction include:

F_τ, the drag on the underside of the ice cover due to the river flow; and

F_W, the downslope component of the weight of ice cover.

The following discussion describes how each is quantified.

3.3.3.2 Shear Stress on the Underside of the Ice Cover

The shear stress exerted by the flow on a physical boundary can be calculated by (Chow, 1959):

$$\frac{\tau}{\rho_w} = g\ S_f\ R \qquad [3.68]$$

where: τ is the shear stress acting on the boundary due to flow drag, in Pa;

g is the acceleration due to gravity, in m/s^2;

R is the hydraulic radius, in metres; and

S_f is the slope of the energy grade line for the river.

For example, in the case of a free surface flow the only physical boundary to be considered is the bed and banks. The hydraulic radius is simply the total flow area (perpendicular to the flow) divided by the wetted perimeter, which is simply the perimeter of the cross section which is in contact with the flow. Many natural rivers have a high aspect ratio (width to depth ratio) such that the river banks form a negligible portion of the wetted perimeter. In these channels the wetted perimeter is well approximated by the channel topwidth and therefore the hydraulic radius is not significantly different from the mean flow depth. The surveyed cross sections in this reach (Hicks *et al.*, 1992) illustrate that this is a reasonable assumption here.

In the case when there is an ice cover floating on the water surface, there are two physical boundaries which are subjected to shear stress from the flow, and consequently the flow area must be apportioned appropriately. Here the objective is to consider the ice affected portion of the flow, for which:

$$\frac{\tau_f}{\rho_w} = g\ S_f\ R_i \qquad [3.69]$$

where: τ_f is the flow shear stress acting on underside of the ice cover, in Pa;

R_i is hydraulic radius for the ice affected portion of the flow, in metres; and

The slope of the energy grade line varies with both flow and ice conditions and must therefore be calculated. For the study reach, it could be obtained from the output of the hydraulic analysis done with the U.S. Corps of Engineers (HEC-2) program, in the calibration of the late winter ice profiles (Chen, 1993; Hicks *et al.*, 1992, 1994, 1995), as summarized in Chapter 2. However, based on that analysis it was observed that from the Big River section to the Water Intake section, the slope of the energy grade line was not significantly different from the measured slope of the water surface. Therefore, the water surface slope was used in the calculation since it is easy to obtain from the measured water levels.

The key problem in this analysis, therefore, is to quantify the hydraulic radius for the ice affected portion of the flow. Here a simple uniform flow model, based on Manning's equation, is used. If the flow area is divided into two zones, an average velocity can be calculated for each:

$$V_i = \frac{R_i^{2/3}\sqrt{S_f}}{n_i} \qquad [3.70]$$

where: V_i is the mean velocity within the ice affected portion of the flow area, in m/s; and
n_i is the ice roughness, (Mannings n).

$$V_b = \frac{R_b^{2/3}\sqrt{S_f}}{n_b} \qquad [3.71]$$

where: V_b is the mean velocity within the bed affected portion of the flow area, in m/s; and
n_b is the bed roughness.

Assuming V_i is approximately equal to V_b, (Ashton, 1986), then

$$R_i = R_b \left(\frac{n_i}{n_b}\right)^{3/2} \qquad [3.72]$$

This assumption is necessary to achieve a solution, and is a common one in quantifying the hydraulics of ice covered channels for this reason. However, it can be difficult to justify in some cases, particularly when the bed and ice roughnesses are dramatically different. Here, based on some crude velocity profiles measured in the study reach in 1992 (Chen, 1993) and a sensitivity analysis, it was concluded that this was not an unreasonable assumption for this site.

The gross hydraulic radius for the ice covered flow was approximated with the mean depth, computed using the flow area under the ice cover divided by the top width, based on tables of hydraulic geometry provided for each surveyed cross section by Chen (1993). If it is further assumed, since the channel aspect ratio is large, that this value is equal to the sum of the component hydraulic radii:

$$R = R_i + R_b \qquad [3.73]$$

Then equations [3.72] and [3.73] give:

$$R_i = \frac{R}{\left[1 + \left({}^{n_b}/_{n_i}\right)^{3/2}\right]} \qquad [3.74]$$

As discussed in Chapter 2, bed and ice roughnesses were calibrated based on measured channel geometry, ice characteristics, measured water surface profiles and measured discharges for each year of the study. The calibrated bed roughness for the Providence Rapids was, $n_b = 0.03$. Calibrated ice roughnesses varied from year to year because of varying ice conditions. As discussed in Chapter 2, for the Providence Rapids, $n_i = 0.05$, 0.07, 0.07 and 0.05 in 1992, 1993, 1994 and 1995, respectively.

Finally , the shear stress underside of the ice cover may be written:

$$\tau_f = \rho_w \; g \; S_w \; \frac{R}{\left[1 \; + \left(n_b/n_i\right)^{3/2}\right]} \qquad [3.75]$$

where S_w is the slope of the water surface. Based on this, the total force due to the shear stress on the underside of the ice cover is:

$$F_\tau = \int \tau_f \;\; \mathrm{d}A_i \qquad [3.76]$$

where: F_τ is the total force due to the shear stress, in Newtons; and
A_i is the area of the ice cover on which the shear stress is acting, in m^2.

3.3.3.3 Weight of the Ice Cover

The downslope component of the weight of the ice cover, per unit area of ice cover, w_i, can be calculated as:

$$w_i = \rho_i \; g \; S_w \; t_i \qquad [3.77]$$

where t_i is the ice thickness, in metres. The total force due to the weight of the ice cover:

$$F_w = \int w_i \;\; \mathrm{d}A_i \qquad [3.78]$$

where F_w is the total force due to the weight of the ice cover, in Newtons.

The ice thickness varies in the Providence Rapids, both from year to year and from location to location for any given year. Field measurements of ice thickness were used to determine an average ice thickness between the Big River and Water Intake sections.

In the load analysis, the water surface slope was calculated based on the difference in water levels between the Big River and Water Intake sections. The dates on which the initial movement of ice occurred in each of the four years were 3-May-92, 22-Apr-93, 1-May-94, and 4-May-95. In 1993 and 1995, the first water stage measurements were taken on the day after this initial movement occurred. Therefore, these values were used to approximate the conditions just prior to this initial movement. On intermediate days, if no water levels were available, linear interpolation was used to approximate these water levels. As the first movement of ice occurs prior to any significant water level fluctuations this is a reasonable assumption.

3.3.4 Compression Failure

3.3.4.1 Formulation

A compressive failure of the ice cover would occur if the loads on the ice cover were large enough to exceed the compressive strength of the ice cover. The following assumptions were made in the consideration of a compression failure:

1. When the first movement of ice occurs, the restraining forces on ice cover from the banks are negligible.
2. The ice cover failure occurs because the strength of ice cover is exceeded by the loads on the ice cover, and the ice cover fails by crushing.
3. The snow depth on the ice cover is uniform in thickness.
4. The ice cover has a constant thickness (equal to the average ice thickness) and has homogeneous mechanical properties.
5. The water is at 0°C. Therefore, the ice cover does not melt from the bottom up.
6. Wind drag on the ice cover is negligible.
7. The shear stress distribution on the underside of the ice cover is uniform.

Based on these assumptions, the compressive stress in the ice cover caused by the loads is:

$$\sigma_l = \frac{(\tau_f + w_i)LW}{t_i W} \qquad [3.79]$$

where: σ_l is the compression stress in the ice cover caused by the loads, in Pa;

L is the length of the free ice cover, in metres; and

W is the average width of the channel, in metres.

The length of the free ice cover is defined as the distance from the downstream end of the ruptured ice cover to the downstream end of the solid ice cover upstream. According to the breakup surveys, in each of the four years, the downstream end of the ruptured ice cover was in the rapids close to the Water Intake cross section and the upstream end of the solid ice cover was between the Big River and Blue Quonset cross sections. Therefore, the free length is close to 3000 metres. The average width of the channel in the rapids is about 600 metres.

Under the deteriorating effects of incoming solar radiation and the warm overlying air mass, the ice cover melts on the top (thins) and the ice strength decreases (due to intergranular melt). The strength ratio can be calculated by Bulatov's equation [3.63]:

$$E_R = E_{R_o}\left[1 - \sqrt{\sigma/\sigma_o}\right]^2 \qquad [3.63]$$

which may be rearranged to a more convenient form:

$$\frac{\sigma}{\sigma_o} = \left(1 - \sqrt{E_R/E_{R_o}}\right)^2 \qquad [3.80]$$

so that the compressive strength at any time during the melt period is:

$$\sigma = \sigma_o\left(1 - \sqrt{E_R/E_{R_o}}\right)^2 \qquad [3.81]$$

In general, the load on the ice cover increases with time and the strength of the ice cover decreases with time. Breakup is expected once the ratio of the ice strength, σ, over the load stress on the ice cover, σ_l, is less than one.

3.3.4.2 Model Application

As mentioned earlier, although compressive ice strengths were measured in the natural ice by GNWT staff during ice bridge construction in 1989 and 1991, these values would be expected to be much larger that the strength of ice at 0°C. Michel (1978) gave the compressive ice strength for different types of ice. His equations showed that the ice strength changes with ice temperature and crystal size as well. According to Michel's equations, the values of ice strength at 0 °C are: Snow ice from 1.39 to 2.79 MPa; Columnar ice from 0.54 to 1.33 MPa; and Frazil ice from 1.48 to 2.97 MPa (Michel, 1978).

In each year of the investigation, ice core samples were taken in the border ice and the rough ice to identify the component ice types. Photographs of some these core samples have been presented in the annual reports (Hicks et al., 1992, 1994). It was found that all of the samples contained layers of snow ice, columnar ice and frazil ice. The initial ice strength (σ_o) was taken as 1.2 MPa based on the mix of ice types observed in the ice cover.

In the calculation of ice strength deterioration, Bulatov's recommended value for E_{Ro}, the accumulated amount of radiation absorbed per unit volume of ice at the time the ice strength reaches zero, for composite ice types of 44 kcal/cm^3 (188 MJ/m^3) was used. The conceptual thermal model developed for Beaver Lake break-up prediction was used to calculate E_R, the accumulated radiation absorbed per unit volume of ice. The convective heat transfer coefficient used in this calculation was 8 W/m^2°C which is also from the thermal breakup model for Beaver Lake.

Ideally, calculations of the thermal deterioration of the ice cover would commence on the day the snow on the ice cover had fully melted, or in the absence of a snow cover, on the first day that the net incoming heat is greater than zero (given that the insolation from the sun could be larger than any heat loss to a cold overlying air mass). Unfortunately, snow melt on the ice cover is progressive and spatially variable, and it is difficult to determine an appropriate day in anything other than a subjective manner. Therefore, in this study, melt calculations commenced on the first day that the net incoming heat is greater than zero and the net incoming heat was first used to melt any snow on the ice cover. In this analysis, the initial albedo of the surface was taken as 0.9 and was decreased linearly to 0.7 as the snow melted, with 0.7 taken as the albedo of the ice cover once the snow was fully melted (according to the calculations). These albedo values were based on the Beaver Lake thermal model and a sensitivity analysis. On the day that the calculations indicate that all of the snow is gone from the ice cover, ice strength begins to decrease. These dates were calculated to be 29-Apr-92,12-Apr-93, 17-Apr-94 and 18-Apr-95, which compare favorably with a qualitative assessment of when the snow on the ice cover had melted.

As discussed in Chapter 2, the ice thickness and snow depths were measured at various locations. These data were shown in Tables 2.9 to 2.16. Based on these data, the snow ice equivalent and ice thicknesses used in the calculation were:

	1992	**1993**	**1994**	**1995**
t_{SIE} (m)	0.10	0.01	0.02	0.07
t_o (m)	1.20	1.90	1.00	1.40

t_o is the average ice thickness estimated based on the ice thicknesses in the rapids measured at the time before (or close to) the beginning of the ice strength simulation.

Figure 3.20 shows the reduction in the strength ratio based upon apportioning the solar radiation through the depth of the ice cover (as discussed in section 3.3.2.3). Table 3.14 shows the computed daily values which, at the time of the initial movement of ice at Providence Narrows, were between 8.4 and 47.5% of the initial strength for these four years.

Table 3.15 presents a summary of the load analysis. Table 3.16 shows the variation in this ratio with time. As the results show, the ratio between the reduced ice strength and the load on the ice cover at the time of the first movement of ice ranged from 0.8 to 7.8.

3.3.5 Shear Failure

3.3.5.1 Formulation

It is not uncommon to see sections of intact ice cover interspersed with open reaches when observing breakup on a long, straight reach of river. In the absence of a downstream cover, it is the shear along the banks which prevents the ice in these areas from moving downstream. Given this, and the fact that large open water leads develop in the Providence Rapids as a precursor to the initial movement of ice, it is possible that shear failure is the mechanism responsible for this initial movement of ice.

Two possible scenarios must be considered. The first is the case when the ice cover has lifted sufficiently (due to the increasing water levels resulting from increasing discharge) for hinge cracks to develop in the ice cover parallel to the banks. These hinge cracks occur because the ice is frozen to the ground at the banks and is not free to lift with the floating ice cover. In this case, the resistance of the ice cover to downstream movement is dependent upon the shear strength between discreet ice sheets, along these cracks. The second case is when the ice cover is intact, and the resistance is due to the shear strength of the ice itself (which may be reduced due to thermal deterioration).

In either case, some assumptions are required in the analysis:

1. When the initial movement of ice occurs, the restraining force on the ice cover from the downstream ice cover is negligible. The ice cover failure occurs because the shear resistance along the banks is exceeded by the load acting on the ice cover.
2. There are two shear interfaces which are parallel to the banks.
3. The snow depth on the ice cover is uniform in thickness.
4. The ice cover has a constant thickness (equal to the average ice thickness) and has homogeneous mechanical properties.
5. The water is at 0°C. Therefore, the ice cover does not melt from the bottom up.
6. Wind drag on the ice cover is negligible.
7. The shear stress distribution on the underside of ice cover is uniform.

The first shear failure condition, associated with shear resistance along hinge cracks, was examined by Ferrick (1989) and will be called the *crack shear resistance approach* in the following text. In this model, the difference between the applied forces and the bank reactions per unit length is given as:

$$F_n = W\left(\tau_f + w_i\right) - 2\,\tau_s\,t_i \qquad [3.82]$$

where F_n is the difference between the applied forces and the bank reactions per unit length, in N/m, and τ_s is the stress transmitted to the bank across each shore crack, in Pa. The ice cover is stable when the forces and reactions are in balance and the difference between the applied forces and the bank reactions per unit length is equal to zero. As the forces on the ice cover increase the stress transmitted to the bank, τ_s, reaches an upper limit: the maximum allowable stress corresponding to failure of the ice cover support, τ_m, which is the critical condition.

Based on a calibration of field data, Ferrick (1989) suggested that the maximum allowable stress corresponding to failure of the ice cover support ranges from 1500 to 2700 Pa. At the stable condition:

$$\tau_s = \frac{W\left(\tau_f + w_i\right)}{2\,t_i} \qquad [3.83]$$

and the criteria for failure in the crack shear resistance approach is:

$$\tau_s \geq \tau_m \qquad [3.84]$$

The crack shear resistance approach often gives an early prediction of the river breakup because the value of the maximum allowable stress corresponding to failure of the ice cover support is small. It assumes that there is a shear wall along the shore and the resistance on the wall is a crack shear resistance. This shear resistance is smaller than the shear strength of the intact ice cover. If it is assumed that the ice cover is intact along the shore the criteria for failure becomes:

$$\tau_s \geq \tau_t \qquad [3.85]$$

where τ_t is the shear strength of the ice cover. This ice shear strength, τ_t, decreases with time, due to thermal deterioration of the ice cover. In this study, it was assumed that the reduction in the shear strength occurs at the same rate as the reduction in the compression strength. Specifically, adapting Bulatov's equation [3.80]:

$$\frac{\tau_t}{\tau_o} = \left(1 - \sqrt{E_R/E_{R_o}}\right)^2 \qquad [3.86]$$

where τ_o is the initial shear strength of the intact ice cover (before any thermal deterioration).

3.3.5.2 Model Application

Crack Shear Resistance Approach

The ratios of the maximum allowable shear stress to the load stress on the day of the initial movement of ice are given in Table 3.17. The values range from 0.11 to 0.27 for the four years when 1500 Pa is taken as the value of the maximum allowable stress. If 2700 Pa is taken as the value of the maximum allowable stress, the ratios range from 0.21 to 0.49. Table 3.18 gives the ratios as a function of time during the melting season (when 2700 Pa is taken as the value of the maximum allowable stress). As Table 3.18 shows, these ratios are all less than one from the beginning of the melt calculation. This indicates that the crack shear resistance approach is not valid to predict the breakup at this site.

Reduced Ice Shear Strength Approach

Typical values of the shear strength range from 0.2 to 4.0 MPa (Ashton, 1986) and vary with the temperature, ice type, loading direction, loading rate and specimen size. In this study, the lowest value was used for the initial shear strength since the temperature is high, the loading rate is low and the specimen size (the ice cover) is large. The ratios of the shear strength to the load stress on the day of the initial movement of ice are given in Table 3.19, based on this initial ice shear strength. Table 3.20 gives the ratios as a function of time during the melting season. As the tables show, the values of this ratio range from 1.3 to 13.1 for the four years. Although the lower limit value of the initial shear strength was chosen, the ratio is still much higher than one for all years except 1994. These ratios are about 1.6 times those determined by the compressive failure approach.

3.3.6 Buckling Failure

3.3.6.1 Formulation

The third and final failure mechanism considered for this study was buckling failure. This is the failure of the ice sheet by bending under edge loads. The following assumptions were made in the consideration of a buckling failure:

1. When the first movement of ice occurs, the restraining forces on ice cover from the banks are negligible.
2. The ice cover failure occurs because the strength of ice cover is exceeded by the loads on the ice cover, and the ice cover fails by buckling.
3. The snow depth on the ice cover is uniform in thickness.
4. The ice cover has a constant thickness (equal to the average ice thickness) and has homogeneous mechanical properties.
5. The water is at 0°C. Therefore, the ice cover does not melt from the bottom up.
6. Wind drag on the ice cover is negligible.
7. The shear stress distribution on the underside of ice cover is uniform.

If the ice cover is assumed to act as a beam on an elastic foundation, then according to Hetenyi (1946), the limiting buckling force F_b for a semi-infinite ice bar is:

$$F_b = \sqrt{\frac{\rho_w g E t_i^3}{12}} \qquad [3.87]$$

where F_b is the buckling load in N/m and E is Young's modulus in Pascals.

Young's modulus decreases as porosity increases. Bulatov (1970) presented a linear relationship for Young's modulus as a function of porosity:

$$E/E_o = 1 - \xi\Phi \qquad [3.88]$$

where E_o is the value of Young's modulus associated with zero porosity and ξ is a coefficient which varies with the type of ice. Bulatov (1970) suggested the following values of ξ, based on field and experimental data:

large-crystalline ice	4.6
fine-crystalline ice	2.7
slush ice	2.1
snow ice	1.3
Bratsk reservoir ice	1.7

and he indicated that the magnitude of this coefficient would be expected to change over the duration of the melting period. Michel (1978) presented the same relationship in a slightly different form:

$$E/E_o = 1 - \Phi/\Phi_o \qquad [3.89]$$

where Φ_o is the porosity associated with a value of Young's modulus equal to zero. Combining equations [3.88] and [3.89], it is seen that:

$$\Phi_o = 1/\xi \qquad [3.90]$$

The value of the Young's modulus associated with zero porosity ranges from about 890 to 960 MPa (Michel, 1978) and the range of the porosities associated with a Young's modulus of zero is 22 to 77% (Bulatov, 1970). In this study, 900 MPa was taken as the value of Young's modulus associated with a porosity of zero. The appropriate value of the porosity associated with a Young's modulus of zero, was determined from Bulatov's equation, assuming that Young's modulus would go to zero at the same time as the compressive strength would go to zero (Bulatov, 1970). The value obtained was 0.61, which corresponds to a ξ value of 1.6.

The force caused by the loads acting on the ice cover due to flow drag and the downslope component of ice weight, F_l , can be calculated as:

$$F_l = (\tau_f + w_i)\, L \tag{3.91}$$

and the ratio of the buckling force to the load force is:

$$F_b/F_l = \sqrt{\frac{\rho_w g E t_i^{3}}{12(\tau_f + w_b)^2 L^2}} \tag{3.92}$$

3.3.6.2 Model Application

For this application the porosity can be calculated in terms of the strength ratio based on equation [3.64]:

$$\Phi = \frac{E_{R_o}}{\rho_i L_m}\left[1 - \sqrt{\sigma/\sigma_o}\right]^2 \tag{3.64}$$

This equation is used because it relates porosity and strength ratio and it is assumed that when the deteriorated ice strength reaches zero, Young's modulus reaches zero also. Therefore:

$$\Phi_o = \frac{E_{R_o}}{\rho_i L_m} \tag{3.93}$$

and

$$\frac{\Phi}{\Phi_o} = \left(1 - \sqrt{\sigma/\sigma_o}\right)^2 \tag{3.94}$$

Combining equations [3.68] and [3.93],

$$E = \left(2\sqrt{\sigma/\sigma_o} - \sigma/\sigma_o\right) E_o \tag{3.95}$$

The strength ratio results calculated in the compressive failure approach were used in this calculation.

The calculations of the ratios of the reduced buckling resistance to the imposed loads on the day of the initial movement of ice are shown in Table 3.21. Table 3.22 gives the varying ratios as a function of time over the melting season. As the tables show, on the day of the initial movement of ice, the values of the ratio ranged from 11.4 to 54.7 for the four years, all well in excess of one. This indicates that buckling failure is not a valid criterion for predicting the initial movement of ice.

3.3.7 Discussion of Results

3.3.7.1 Introduction

The consistency of the results depend to a large extent on the accuracy of the measured variables and the limitations of any assumptions made in quantifying the parameters in each model. In this section, these effects are discussed and the suitability of the various models is compared.

3.3.7.2 Variation in Measured Variables

The ice thickness at the Big River section is relatively consistent from year to year, but ice thickness varies considerably in Providence Rapids. The ice thickness in the rapids depends not only on the severity of winter but to an even greater extent on the nature of freezeup. If ice jams into the rapids at the time of freezeup, the ice thickness can be in excess of 2 m. In years when the freezeup is less dynamic, ice thicknesses of 1.0 to 1.2 metres are more likely. This variation has a large effect on the resistance because the edge area resisting the imposed loads increases linearly with ice thickness. Although the force due to the weight of ice will increase as well, due to the small water surface slopes involved the effect on the downslope component of ice weight is small.

The free length of the ice cover was estimated from the maps prepared documenting the ice cover locations and major ice movements throughout the breakup season each year. The value of the free length of the ice cover was about 2800 m in 1992, and 3500 m in 1993 and 1994. Despite this variation, the free length of ice cover was taken as a constant of 3000 m in the analysis, because the actual value would not be known in a forecasting situation.

The water stage and water surface slope were measured with great accuracy compared to the other parameters used in this analysis. However, one difficulty that was encountered was that data were not always available before the initial ice movement. For example, in 1993 and 1995, water levels were measured the day after the ice cover moved. However, water surface slopes were found to be very consistent from year to year and from day to day during the early melt season, averaging approximately 0.0006. Consequently the shear stress on the underside of the ice cover was consistent from year to year.

3.3.7.3 Failure Criteria

Four failure mechanisms were considered in this study, on the basis of ratios comparing the resistance of the ice to the imposed loads. Figure 3.21 illustrates a comparison of the computed ratios at the time of the initial movement of ice for each year. In an assessment of each failure mechanism, the following circumstances would be considered ideal:

1. the values of the ratio are higher than one at the time ice starts to melt;
2. the values of the ratio are close to one at the time of the initial movement of ice; and
3. the values of the ratio are consistent from year to year at the time of ice breakup.

The compression failure criterion can meet the first requirement, but not the other two as the ratios are not close to one in 1992 and 1993, and the values at the time of the initial ice movement vary by almost an order of magnitude. However, the value of the ratio is dependent upon the initial compressive strength used which can vary widely as a function of ice type, temperature and loading conditions. This variable had to be estimated for this study. The main limitation of this approach, therefore, is the range of values of the ratio (i.e. the lack of consistency). Measurements of the initial ice strength would not improve the consistency of this model unless it were found that it varied from year to year, something that the index strength tests did not indicate (Chapter 2).

The crack shear resistance failure criterion is considered unacceptable as the computed ratios are too small, varying from 0.21 to 0.48 at the time of the initial ice movement when the maximum value of crack resistance is used. In fact, the ratios were computed to be less than one at the time the ice started to melt. Again, the ratios obtained are a function of the estimated crack shear resistance. However, model consistency would not be improved unless this value were found to be different from year to year, and there is no direct measurement technique available.

The shear failure criterion, based on ice shear strength is consistent with the results of the compression failure approach. However, the values of the ratios obtained were about one and one half times that of compression failure criterion. Again, the magnitude of the ratio depends upon the estimate of the shear strength.

The results of the buckling failure analysis are also consistent with the results of the compression failure analysis. However, the ratios are extremely high, ranging from 11.4 to 56.6 at the time of the initial movement of ice. Buckling failure typically happens under conditions where the ice thickness is thin relative to the free length of the ice sheet. for example, it may occur when a long, thin ice sheet impacts on a structure or when a broad lake surface with a thin ice cover is subjected to high speed wind (Ashton, 1986). At this site, the ice thickness is thick relative to the free length, so that a buckling failure is not likely.

A key problem encountered in all four methods was determining the starting time for the model. This was primarily because of the fact that it was not possible to pinpoint the exact day the snow was completely melted from the ice cover, and therefore snowmelt had to be incorporated into the models. This might be an important reason for scattering of strength ratios.

Another parameter which might be expected to affect the consistency of results is the albedo of the ice surface, which may not be the same from year to year. However, from a practical perspective, this parameter must be taken as a constant (from year to year, and from location to location) in a forecasting model.

The application of any single criterion to the prediction of breakup should not necessarily be expected to give good results. For example, the assumption of zero shear strength in the compressive failure model, or the assumption of zero support from the downstream ice cover in the shear failure model each likely represents only part of a complex failure process which involves both failure mechanisms to some degree.

The open leads which develop in the Providence Rapids, prior to the initial movement of ice at Providence Narrows add a further level of complexity as it indicates that the flow turbulence under the ice cover represents a contributing heat component. Furthermore, the development of these open leads reduces the total shear force acting on the ice cover as well as the support capability of the ice cover. It may be reasonable to combine the crack shear resistance approach with the compressive failure approach and consider only part of the ice cover supporting the upstream ice cover because the open leads developed in the channel. This approach would require model detailed hydraulic information in the reach.

3.3.7.4 Summary

The best measure of model reliability at this stage would be based on an assessment of how well the limiting value of the ratio predicts the first movement of ice in each case. Figure 3.22 presents such a comparison, in terms of days, between the forecasted and actual date, based on the envelope (or largest) ratio determined. As the figure shows, none of the models perform well, with variations of up to two weeks in the worst of cases.

The study site was considered an ideal one for testing these various failure mechanisms, given the mitigating influence of Great Slave Lake on discharge increases through the breakup period, as the loads on the ice cover would not be expected to vary much over the breakup period. Therefore, for comparison purposes, the prediction based on the total heat received prior to the initial movement of ice is included in Figure 3.22 (as this is a common approach in current practice even for sites where the load increases significantly through the breakup period). The fact that this crude method appears to perform as well as any of the failure mechanisms is not surprising, given that it was found that the loads on the ice cover did not vary significantly.

Based on these results it must be concluded that none of the currently available failure models are adequate for forecasting the initial movement of ice, even in the case where loads on the ice cover are fairly consistent through the breakup period.

Table 3.1. Albedo of various surface for short-wave radiation (Gray and Prowse, 1993).

Surface	Typical range in albedo
New Snow	0.80 - 0.90
Old Snow	0.60 - 0.80
Melting snow-- porous---Fine-grained	0.40 - 0.60
Forests--conifers, snow	0.25 - 0.35
Forests--green	0.10 - 0.20
Water	0.05 - 0.15
Snow ice	0.30 - 0.55
Black ice: intact---- candled----granulated	0.10 --- 0.40 --- 0.55

Table 3.2. Various values of constants for Brunt's formula (Anderson, 1954).

Investigator	Place	*a*	*b*	Correlation coefficient
Dines	England	0.53	0.065	0.97
Asklof	Sweden	0.43	0.082	0.83
Angstrom	Algeria	0.48	0.058	0.73
Angstrom	California	0.50	0.032	0.30
Boutaric	France	0.60	0.042	---
Kimball	Washington, D.C.	0.44	0.061	0.29
Eckel	Austria	0.47	0.063	0.89
Raman	India	0.62	0.029	0.68
Anderson	Oklahoma	0.68	0.036	0.92

Table 3.3. Values of the fraction of sky cover used in this study.

Net short wave radiation, R_s	**Fraction of sky cover, C**
More than 300	0
281 - 300	1
261 - 280	2
241 - 260	3
221 - 240	4
201 - 220	5
181 - 200	6
161 - 180	7
141 - 160	8
121 - 140	9
120 or less	10

Table 3.4. Roughness heights on different surfaces (Eagleson, 1970).

Surface	**Wind speed, m/s**	**Roughness length, cm**
Open water	2.1	0.001
Smooth mud flats (ice)		0.001
Smooth snow on short grass		0.005
Snow on prairie		0.1
Wet soil	1.8	0.02

Table 3.5. Twenty year average atmospheric pressures for NWT sites (DFO, 1981).

Station	**April**	**May**
Yellowknife, 62°28'N, 114°27'	1017 mb	1016 mb
Fort Simpson, 61°52'N, 121°21'	1017 mb	1015 mb
Hay River, 60°51'N, 115°46'	1017 mb	1016 mb

Table 3. 6 Typical value of snow density (Gray and Prowse, 1993)

Situations	kg/m^3
Wild snow	10 - 30
New snow	50 - 65
Settling snow	70 - 190
Settled snow	200 - 300
Average wind-toughened snow	280

Table 3.7. Nature ice density at Ice Bridge crossing section
(Department of Transportation, NWT, 1992).

year	Value
1989	908
	906
	913
1991	899
	898
	890
	895
	906
	910
	913
Average value	904 kg/m^3

Table 3.8. The values of constants in simulation.

Constant	**Value**
a	0.68
b	0.036
k	0.017
c_1	0.6
k_1	0.4
ρ_s	200 kg/m3
ρ_i	904 kg/m3
P	1016 mb
ε	0.97
z_o	0.0002 m
L_m	333400 J/kg
L_v	2500000 J/kg

Table 3.9. Initial conditions in thermal break-up simulation.

Condition	**1992**	**1993**	**1994**	**1995**
Date of modelling start at GSL	25-April	9-April	19-April	20-April
A_w when modelling start at GSL	45.5 km^2	7.74 km^2	6.63 km^2	20.2 km^2
Date of the surface albedo changed	4-April	26-April	7-May	6-May
T_{lake}	0.39°C	0.49°C	0.22°C	0.22°C

Table 3.10 Measured late winter ice thicknesses and initial ice thicknesses used in simulation.

Ice thickness	Crossing section	1992		1993		1994		1995	
		Border	Rough	Border	Rough	Border	Rough	Border	Rough
Measured	Great Slave Lake	0.62		0.98		0.79		0.87	
	South Channel	0.78	0.45	1.12		0.88		1.03	1.20
	Kakisa River	1.04	1.26	0.92				0.91	0.86
	Beave Lake	1.10		0.80		0.91		0.79	
	Burnt Point	0.96		0.79		0.74		0.70	
	Average x 1.2	1.16		1.09		1.01		1.03	
Case A	Great Slave Lake	0.60		1.00		0.80		0.90	
	South Channel	0.75		1.15		0.95		1.05	
	Kakisa River	0.75		1.15		0.95		1.05	
Case B	Great Slave Lake	0.60		1.00		0.80		0.90	
	South Channel	0.75		1.15		0.95		1.05	
	Kakisa River	0.85		1.25		1.05		1.15	
Case C	Great Slave Lake	0.60		1.00		0.80		0.90	
	South Channel	0.75		1.15		0.95		1.05	
	Kakisa River	1.16		1.09		1.01		1.03	

Table 3.11 Variances of simulations under different h_i and h_w.

Ice thickness	h_i ; h_w	4 ; 10	4 ; 15	4 ; 20	8 ; 10	8 ; 15	8 ; 20	12 ; 10	12 ; 15	12 ; 20
Case A	1992	208	263	332	285	361	452	415	503	604
	1993	1439	1280	1036	1157	909	694	786	574	403
	1994	1267	611	264	694	293	122	242	216	370
	1995	848	366	164	318	279	687	443	932	2208
	range	1231	1017	872	872	629	572	544	716	1838
	max.	1439	1280	1036	1157	909	694	786	932	2208
Case B	1992	235	271	320	262	314	381	326	398	483
	1993	1454	1296	1052	1174	925	742	840	622	443
	1994	1282	622	291	710	324	87	254	107	302
	1995	889	415	146	345	185	444	300	768	1484
	range	1219	1025	906	912	740	655	586	661	1182
	max.	1454	1296	1052	1174	925	742	840	768	1484
Case C	1992	486	498	522	453	478	515	441	480	531
	1993	1429	1270	1026	1147	898	663	738	542	379
	1994	1276	618	280	704	311	93	246	132	226
	1995	839	357	175	317	275	755	503	1000	2412
	range	943	912	851	830	624	662	492	868	2186
	max.	1429	1270	1026	1147	898	755	738	1000	2412

Table 3.12 Values of μ and ν as functions of the state of ice

State of ice	Sky condition	μ	ν
Ice with parallel-fiber structure	clear	1.21	0.57
Ice with parallel-fiber structure	cloudy	1.21	0.52
Blue fresh ice	cloudy	1.21	0.36
Dirty ice	clear	1.04	1.07

Table 3.13 Ice strength measured in the natural ice adjacent to the ice bridge in 1989 and 1991.

1989		1991	
Sample	MPa	Sample	MPa
1	0.72	1	5.86
2	3.38	2	8.65
3	3.95	3	7.25
4	3.29	4	3.81
5	3.22	5	5.70
6	2.94	6	6.60
		7	5.39
Average	**2.92**	Average	**6.18**

Table 3.14 Strength ratio at Providence rapids, apportioned solar radiation used.

	$\alpha_i = 0.9/0.7$	h_i = 8 W/m² °C	E_{Ro} = 188 MPa/m³	
	t_i = 1.2/0.10	t_i = 1.9/0.01	t_i = 1.0/0.02	t_i = 1.4/0.07
Date	**1992**	**1993**	**1994**	**1995**
7-Apr	100.0		100.0	100.0
8-Apr	100.0	100.0	100.0	100.0
9-Apr	100.0	100.0	100.0	100.0
10-Apr	100.0	100.0	100.0	100.0
11-Apr	100.0	100.0	100.0	100.0
12-Apr	100.0	82.5	100.0	100.0
13-Apr	100.0	71.6	100.0	100.0
14-Apr	100.0	65.4	100.0	100.0
15-Apr	100.0	60.2	100.0	100.0
16-Apr	100.0	55.1	100.0	100.0
17-Apr	100.0	50.9	68.4	100.0
18-Apr	100.0	47.5	56.0	74.6
19-Apr	100.0	43.9	47.4	68.0
20-Apr	100.0	40.7	40.8	61.1
21-Apr	100.0	38.1	35.4	53.9
22-Apr	100.0	**36.4**	32.0	48.0
23-Apr	100.0	33.7	27.6	43.3
24-Apr	100.0	31.3	23.9	39.1
25-Apr	100.0	29.5	20.7	36.4
26-Apr	100.0		18.5	32.8
27-Apr	100.0		15.9	29.5
28-Apr	100.0		14.1	26.7
29-Apr	72.8		12.0	24.1
30-Apr	64.4		10.1	21.6
1-May	60.5		**8.4**	20.2
2-May	54.4		6.9	18.5
3-May	**47.5**			16.5
4-May	42.2			**14.7**
5-May				12.9

Table 3. 15 Compression force calculation

Year		**1992**	**1993**	**1994**	**1995**
Date		**3-May**	**22-Apr**	**1-May**	**4-May**
Stage at Big River	m	151.451	150.530	150.732	149.540
Stage at Blue House	m	148.800	148.123	148.516	147.290
Water surface slope		0.00066	0.00060	0.00055	0.00056
t_i	m	1.10	1.63	0.65	0.95
Elevation at Bottom of ice	m	147.806	146.649	147.928	146.431
n_b		0.03	0.03	0.03	0.03
n_i		0.05	0.07	0.07	0.05
R	m	5.81	4.7	5.93	4.53
R_i	m	3.97	3.67	4.63	3.09
τ_f	Pa	25.79	21.67	25.17	17.07
w_i	Pa	6.47	8.70	3.19	4.74
$\tau_f + w_i$	Pa	32.25	30.36	28.36	21.80
σ_i	Pa	87965	55886	130894	68857
σ / σ_o	%	47.5	36.4	8.4	14.7
σ_o	MPa	1.2	1.2	1.2	1.2
σ	Pa	570000	436800	100800	176400.00
σ / σ_i Ratio		**6.5**	**7.8**	**0.8**	**2.6**

Table 3.16 Compression strength and stress ratio, based on apportioned solar radiation.

Date	1992	1993	1994	1995
	t_i = 1.2/0.10	t_i = 1.9/0.01	t_i = 1.0/0.02	t_i = 1.4/0.07
7-Apr				
8-Apr				
9-Apr				
10-Apr				
11-Apr		28.0		
12-Apr		22.7		
13-Apr		19.2		
14-Apr		17.1		
15-Apr		15.6		
16-Apr		13.9	16.4	
17-Apr		12.6	11.0	26.2
18-Apr		11.5	8.8	19.5
19-Apr		10.3	7.3	17.8
20-Apr		9.2	6.1	15.7
21-Apr		8.4	5.1	13.6
22-Apr		**7.8**	4.5	11.8
23-Apr			3.8	10.5
24-Apr			3.2	9.3
25-Apr			2.7	8.5
26-Apr			2.3	7.5
27-Apr			1.9	6.5
28-Apr	19.9		1.6	5.7
29-Apr	14.3		1.3	5.0
30-Apr	12.6		1.0	4.3
1-May	11.9		**0.8**	3.9
2-May	10.7			3.5
3-May	**6.5**			3.0
4-May				**2.6**
α_i = 0.9/0.7	σ_o = 1.2 MPa	h_i = 8 W/m^2°C	E_{Bo} = 188 MJ/m^3	

Table 3.17 Shear force calculation by the crack shear resistance approach.

Year		**1992**	**1993**	**1994**	**1995**
Date		**3-May**	**22-Apr**	**1-May**	**4-May**
Stage at Big River	m	151.451	150.530	150.732	149.540
Stage at Blue House	m	148.800	148.123	148.516	147.290
Water surface slope		0.00066	0.00060	0.00055	0.00056
t_i	m	1.10	1.63	0.65	0.95
Elevation at Bottom of ice	m	147.806	146.649	147.928	146.431
n_b		0.03	0.03	0.03	0.03
n_i		0.05	0.07	0.07	0.05
R	m	5.81	4.7	5.93	4.53
R_i	m	3.97	3.67	4.63	3.09
τ_f	Pa	25.79	21.67	25.17	17.07
w_i	Pa	6.47	8.70	3.19	4.74
$\tau_f + w_i$	Pa	32.25	30.36	28.36	21.80
τ_s	Pa	8797	5589	13089	6886
$\tau_{m\ low}$	Pa	1500	1500	1500	1500
$\tau_{m\ high}$	Pa	2700	2700	2700	2700
τ_i / τ_s Ratio low		**0.17**	**0.27**	**0.11**	**0.22**
τ_i / τ_s Ratio high		**0.31**	**0.48**	**0.21**	**0.39**

Table 3.18 The ratio of the crack shear resistance to the shear stress.

Date	1992	1993	1994	1995
	t_i = 1.2/0.10	t_i = 1.9/0.01	t_i = 1.0/0.02	t_i = 1.4/0.07
7-Apr				
8-Apr				
9-Apr				
10-Apr				
11-Apr		0.63		
12-Apr		0.62		
13-Apr		0.60		
14-Apr		0.59		
15-Apr		0.58		
16-Apr		0.57	0.37	
17-Apr		0.56	0.36	0.59
18-Apr		0.54	0.35	0.59
19-Apr		0.53	0.35	0.59
20-Apr		0.51	0.34	0.58
21-Apr		0.50	0.32	0.57
22-Apr		**0.48**	0.32	0.55
23-Apr			0.31	0.54
24-Apr			0.30	0.53
25-Apr			0.29	0.53
26-Apr			0.29	0.51
27-Apr			0.27	0.50
28-Apr	0.45		0.26	0.48
29-Apr	0.44		0.24	0.47
30-Apr	0.44		0.23	0.45
1-May	0.44		**0.21**	0.43
2-May	0.44			0.42
3-May	**0.31**			0.41
4-May				**0.39**
α_i = 0.9/0.7	τ_m = 2700 Pa	h_i = 8 W/m^2°C	E_{Bo} = 188 MJ/m^3	

Table 3. 19 Shear force calculation by the reduced shear strength approach.

Year		1992	1993	1994	1995
Date		**3-May**	**22-Apr**	**1-May**	**4-May**
Stage at Big River	m	151.451	150.530	150.732	149.540
Stage at Blue House	m	148.800	148.123	148.516	147.290
Water surface slope		0.00066	0.00060	0.00055	0.00056
t_i	m	1.10	1.63	0.65	0.95
Elevation at Bottom of ice	m	147.806	146.649	147.928	146.431
n_b		0.03	0.03	0.03	0.03
n_i		0.05	0.07	0.07	0.05
R	m	5.81	4.7	5.93	4.53
R_i	m	3.97	3.67	4.63	3.09
τ_f	Pa	25.79	21.67	25.17	17.07
w_i	Pa	6.47	8.70	3.19	4.74
$\tau_f + w_i$	Pa	32.25	30.36	28.36	21.80
τ_s	Pa	8797	5589	13089	6886
τ_i / τ_o	%	47.5	36.4	8.4	14.7
τ_o	Pa	200000	200000	200000	200000
τ_i	Pa	95000	72800	16800	29400
τ_i / τ_s Ratio		**10.8**	**13.0**	**1.3**	**4.3**

Table 3.20 The ratio of shear strength and shear stress, based on apportioned solar radiation.

	1992	1993	1994	1995
Date	t_i = 1.2/0.10	t_i = 1.9/0.01	t_i = 1.0/0.02	t_i = 1.4/0.07
7-Apr				
8-Apr				
9-Apr				
10-Apr				
11-Apr		46.6		
12-Apr		37.8		
13-Apr		32.0		
14-Apr		28.6		
15-Apr		26.0		
16-Apr		23.2	27.4	
17-Apr		20.9	18.3	43.6
18-Apr		19.1	14.7	32.5
19-Apr		17.2	12.1	29.6
20-Apr		15.4	10.2	26.2
21-Apr		14.0	8.5	22.6
22-Apr		**13.1**	7.5	19.6
23-Apr			6.3	17.5
24-Apr			5.4	15.5
25-Apr			4.5	14.2
26-Apr			3.9	12.4
27-Apr			3.2	10.9
28-Apr	33.2		2.7	9.5
29-Apr	23.9		2.2	8.3
30-Apr	21.1		1.7	7.2
1-May	19.9		**1.3**	6.5
2-May	17.8			5.8
3-May	**10.8**			5.0
4-May				**4.3**
α_i = 0.9/0.7	τ_s = 0.2 MPa	h_i = 8 W/m^2°C	E_{fu} = 188 MJ/m^3	

Table 3. 21 Buckling failure calculation.

Year		**1992**	**1993**	**1994**	**1995**
Date		**3-May**	**22-Apr**	**1-May**	**4-May**
Stage at Big River	m	151.451	150.530	150.732	149.540
Stage at Blue House	m	148.800	148.123	148.516	147.290
Water surface slope		0.00066	0.00060	0.00055	0.00056
t_i	m	1.10	1.63	0.65	0.95
Elevation at Bottom of ice	m	147.806	146.649	147.928	146.431
n_b		0.03	0.03	0.03	0.03
n_i		0.05	0.07	0.07	0.05
R	m	5.81	4.7	5.93	4.53
R_i	m	3.97	3.67	4.63	3.09
τ_f	Pa	25.79	21.67	25.17	17.07
w_i	Pa	6.47	8.70	3.19	4.74
$\tau_f + w_i$	Pa	32.25	30.36	28.36	21.80
F_i	N/m	96762	91094	85081	65414
σ / σ_o	%	47.5	36.4	8.4	14.7
E_o	MPa	9000	9000	9000	9000
Φ / Φ_o		0.102	0.166	0.532	0.401
E	MPa	8082	7505	4208	5388
F_b	N/m	2965515	5154685	972005	1943299
F_b / F_i Ratio		**30.6**	**56.6**	**11.4**	**29.7**

Table 3.22 The ratio of the buckling resistance to the load forces.

Date	1992	1993	1994	1995
	t_l = 1.2/0.10	t_l = 1.9/0.01	t_l = 1.0/0.02	t_l = 1.4/0.07
7-Apr				
8-Apr				
9-Apr				
10-Apr				
11-Apr		87.2		
12-Apr		85.1		
13-Apr		82.0		
14-Apr		79.1		
15-Apr		77.0		
16-Apr		73.8	37.2	
17-Apr		70.9	35.3	69.3
18-Apr		68.4	33.6	68.7
19-Apr		65.2	31.9	68.2
20-Apr		61.8	30.0	66.1
21-Apr		58.7	27.8	63.3
22-Apr		**56.7**	26.3	60.1
23-Apr			24.9	57.8
24-Apr			23.6	55.3
25-Apr			22.1	53.5
26-Apr			20.9	50.6
27-Apr			19.2	47.7
28-Apr	49.5		17.4	44.9
29-Apr	48.0		15.4	41.8
30-Apr	47.0		13.5	38.6
1-May	46.8		**11.4**	36.5
2-May	45.7			34.7
3-May	**30.7**			32.5
4-May				**29.6**
$\alpha_l = 0.9/0.7$	$E_o = 900$ MPa	$h_l = 8$ W/m^2°C	$E_{Ro} = 188$ MJ/m^3	

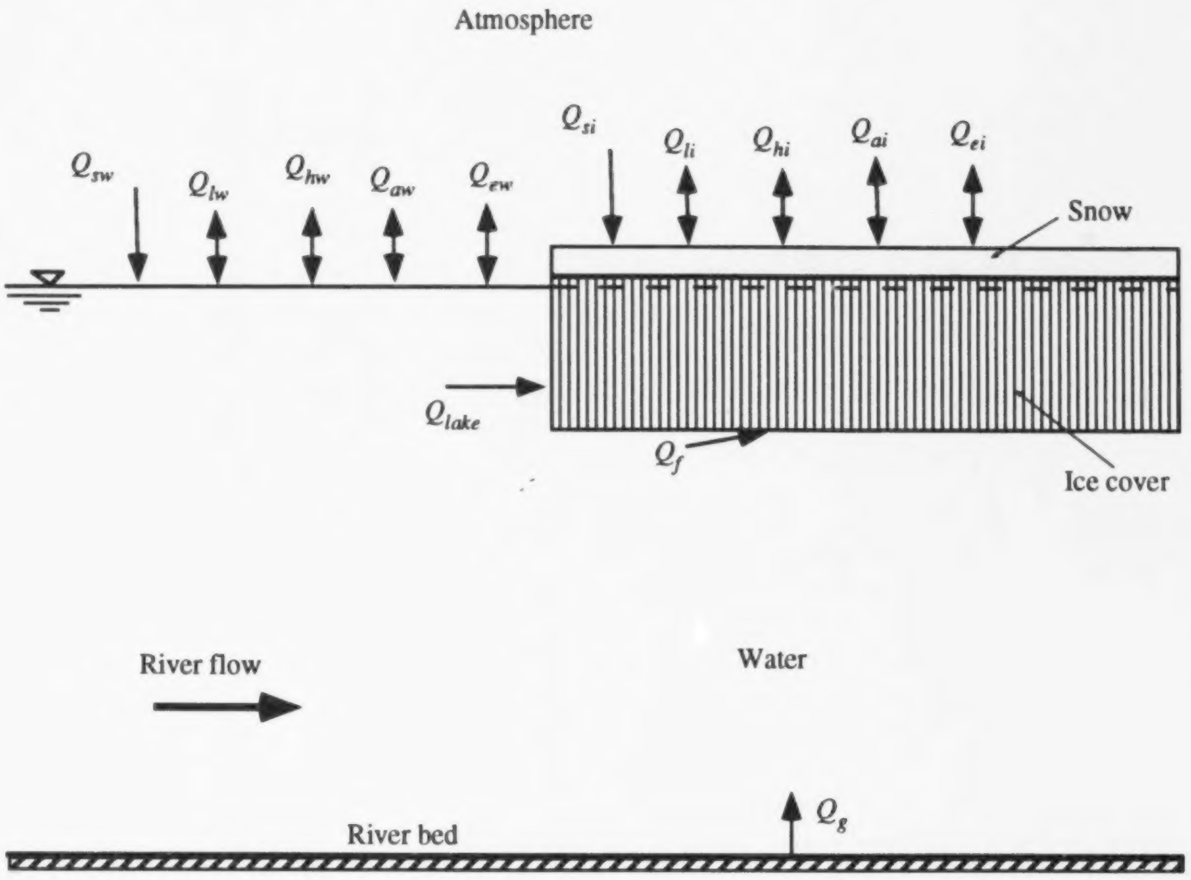
Atmosphere
Q_{sw}
Q_{lw}
Q_{hw}
Q_{aw}
Q_{ew}
Q_{si}
Q_{li}
Q_{hi}
Q_{ai}
Q_{ei}
Snow
Q_{lake}
Q_f
Ice cover
River flow
Water
Q_g
River bed

Figure 3.1 Heat components acting on ice surface and water body.

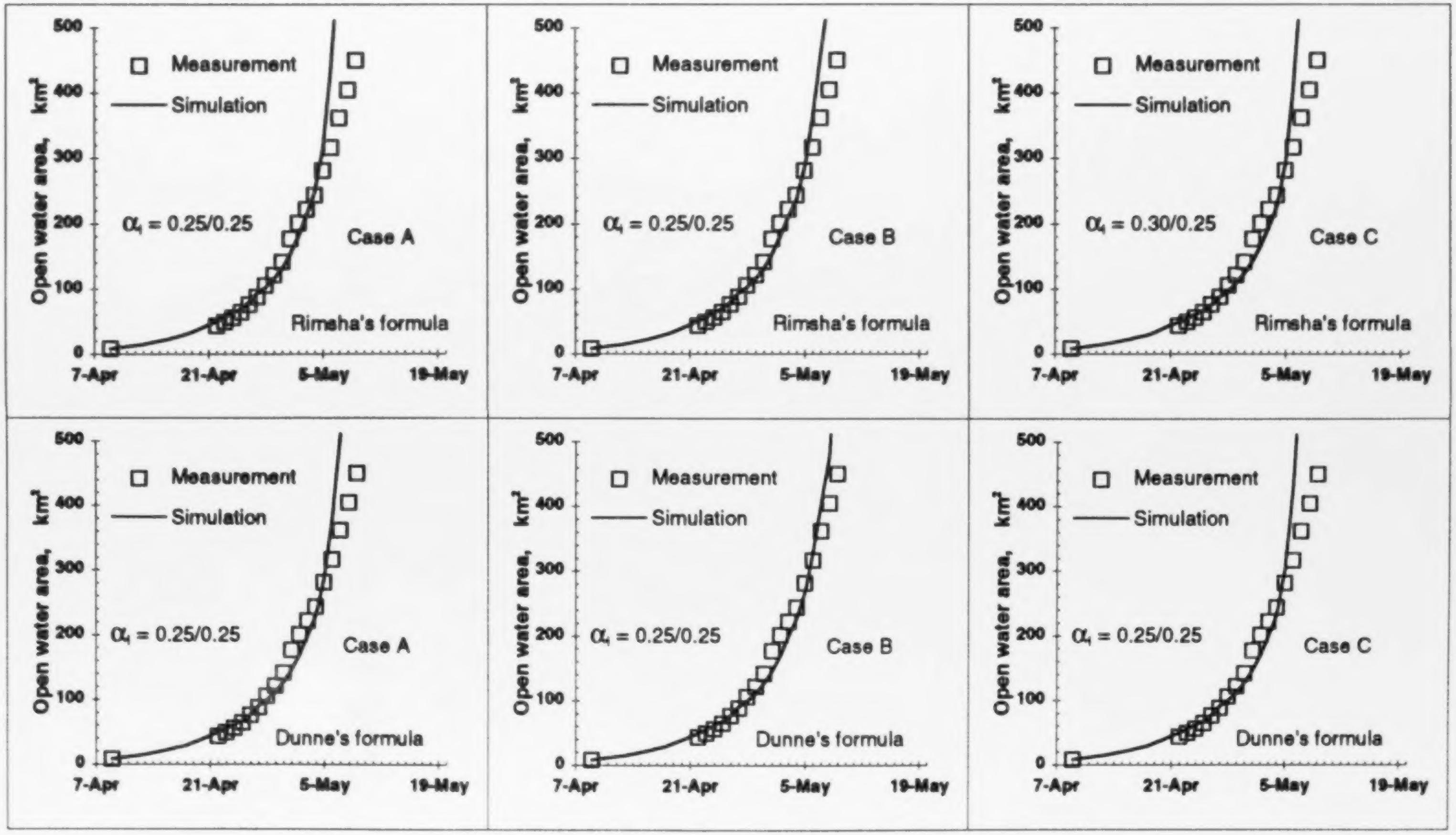

Figure 3.2 Surface albedo calibration of the Energy Budget approach by individual year, 1993.

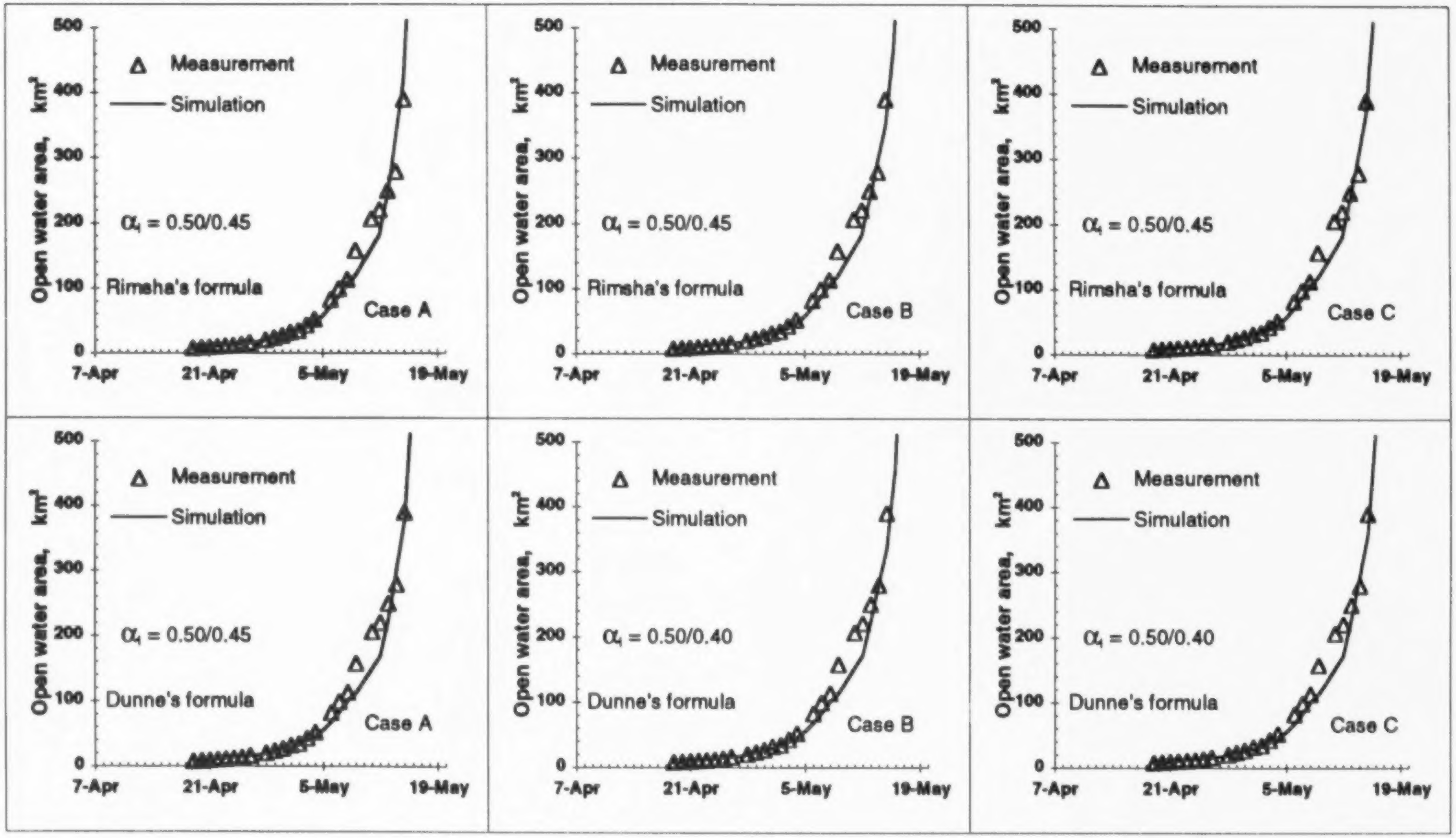

Figure 3.3 Surface albedo calibration of the Energy Budget approach by individual year, 1994.

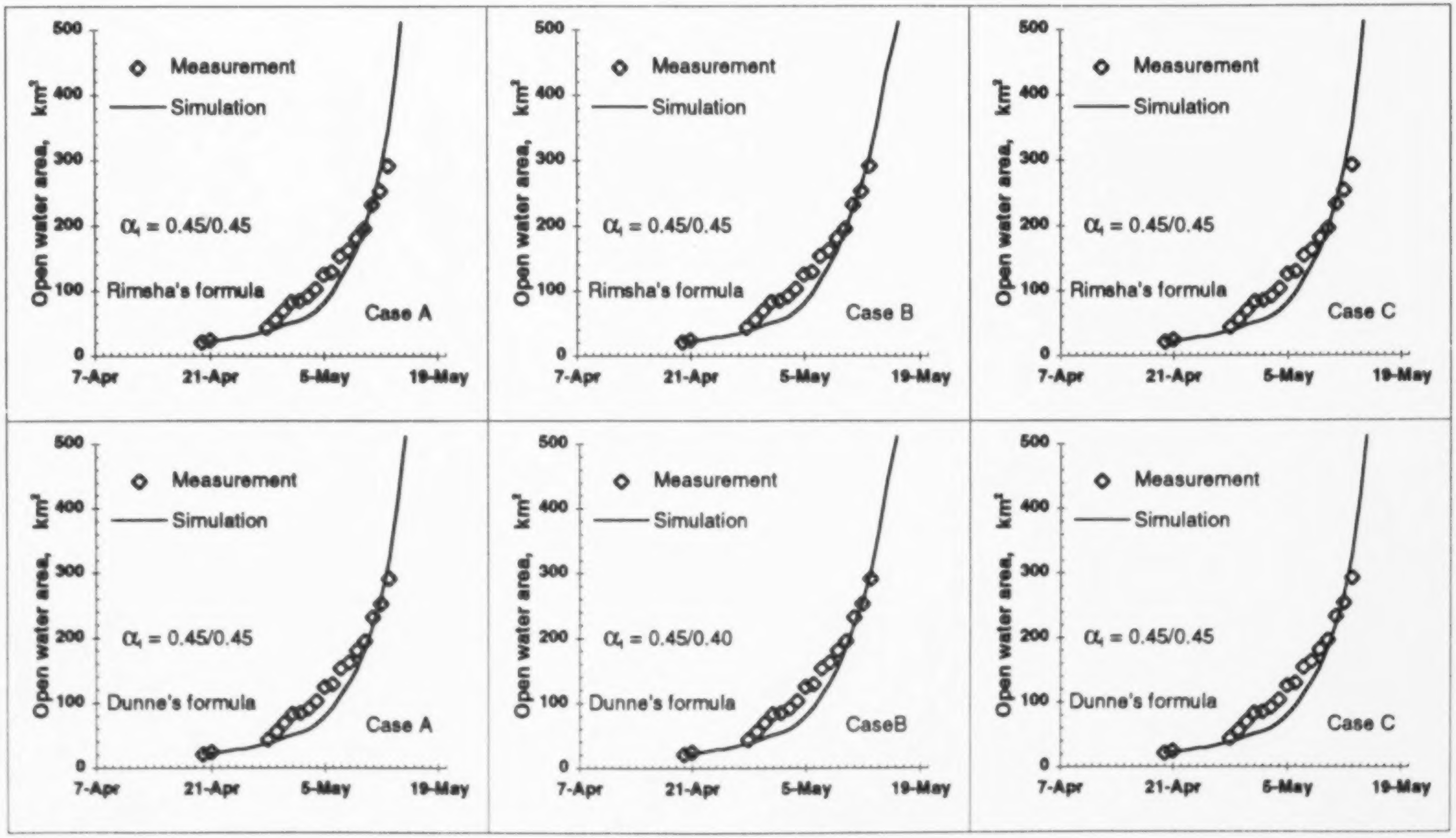

Figure 3.4 Surface albedo calibration of the Energy Budget approach by individual year, 1995.

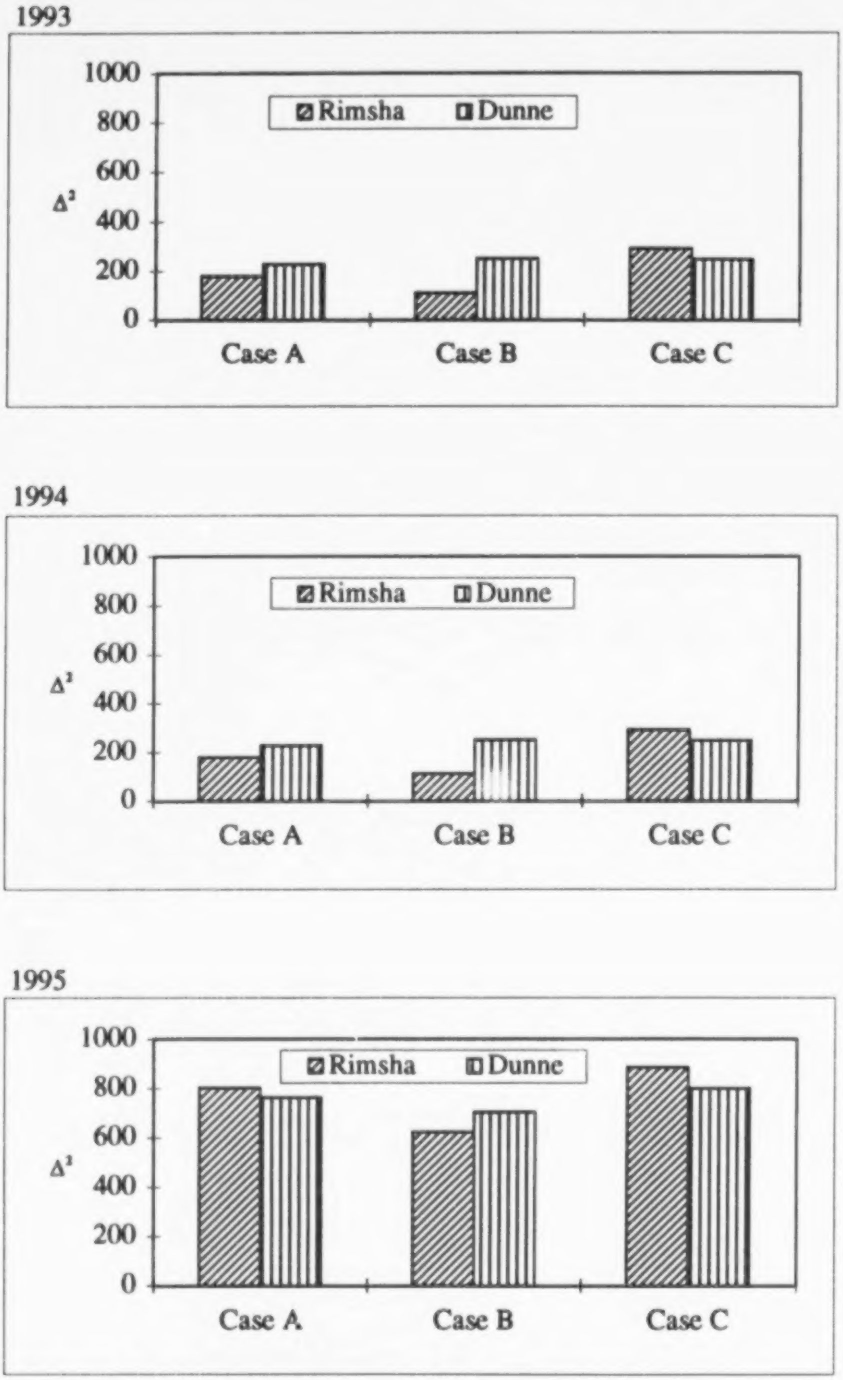

Figure 3.5 Variances, Δ^2, for the calibration of the Energy Budget method by individual year.

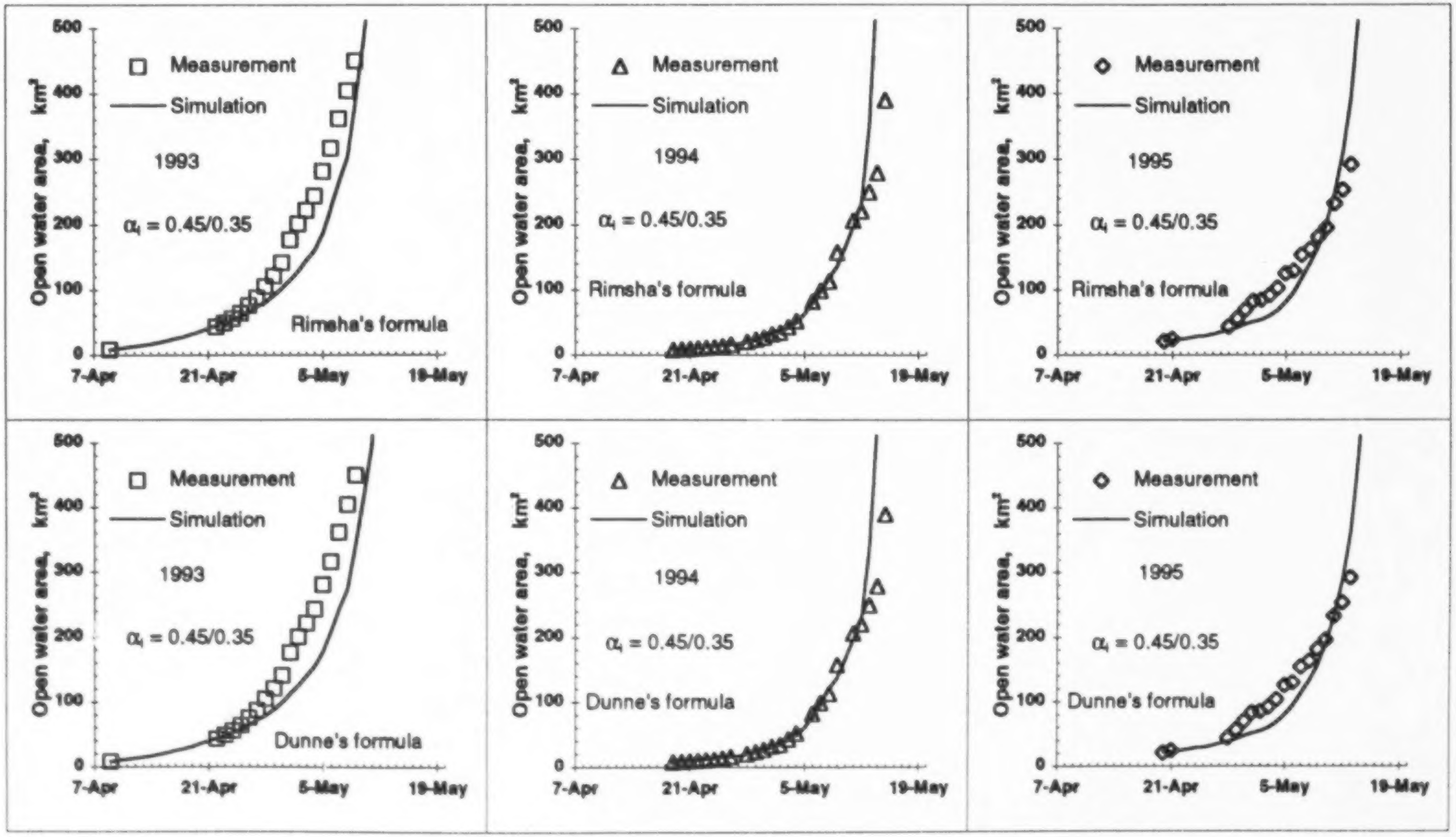

Figure 3.6 Typical surface albedo calibration, Energy Budget approach, Case A.

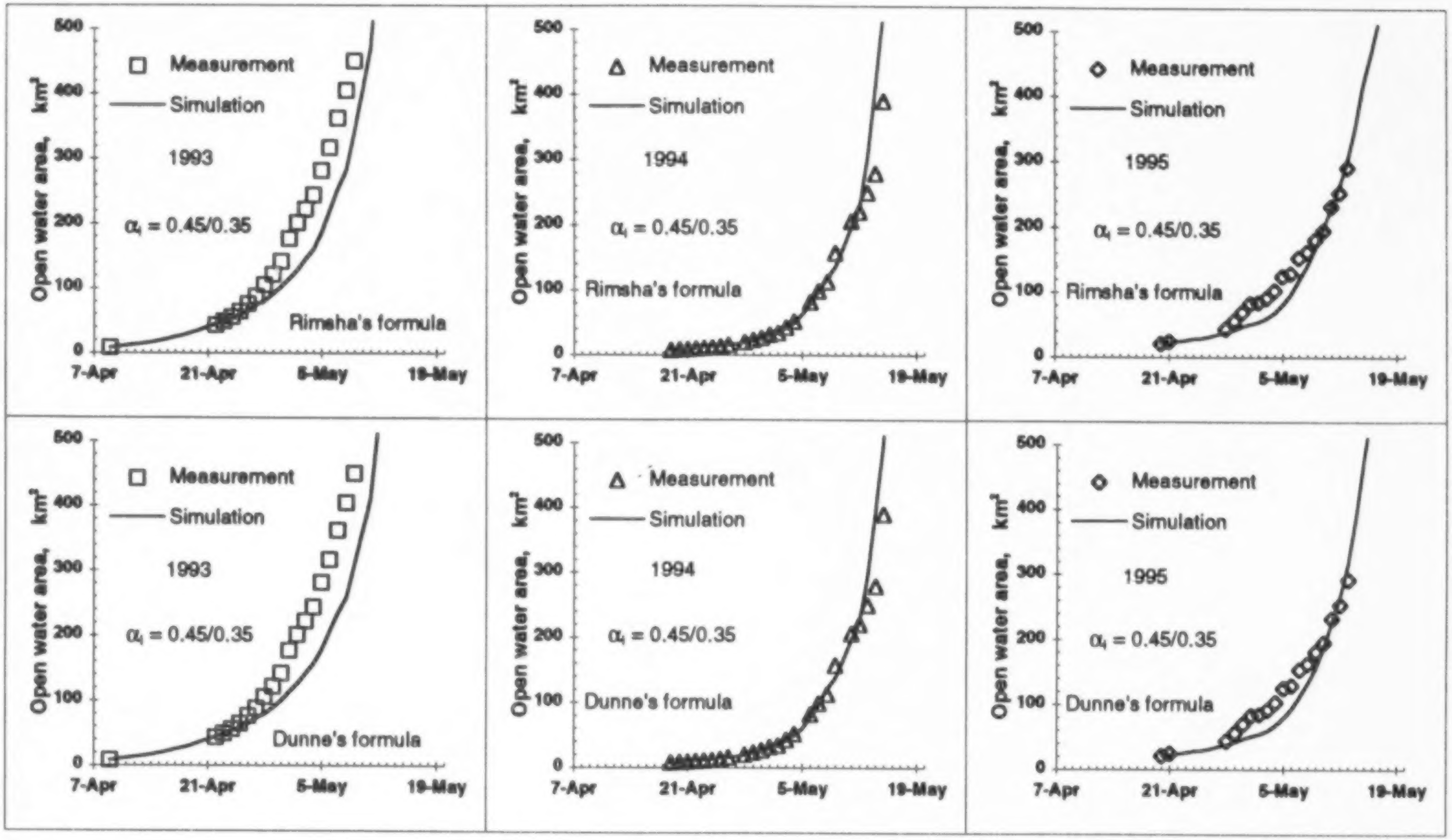

Figure 3.7 Typical surface albedo calibration, Energy Budget approach, Case B.

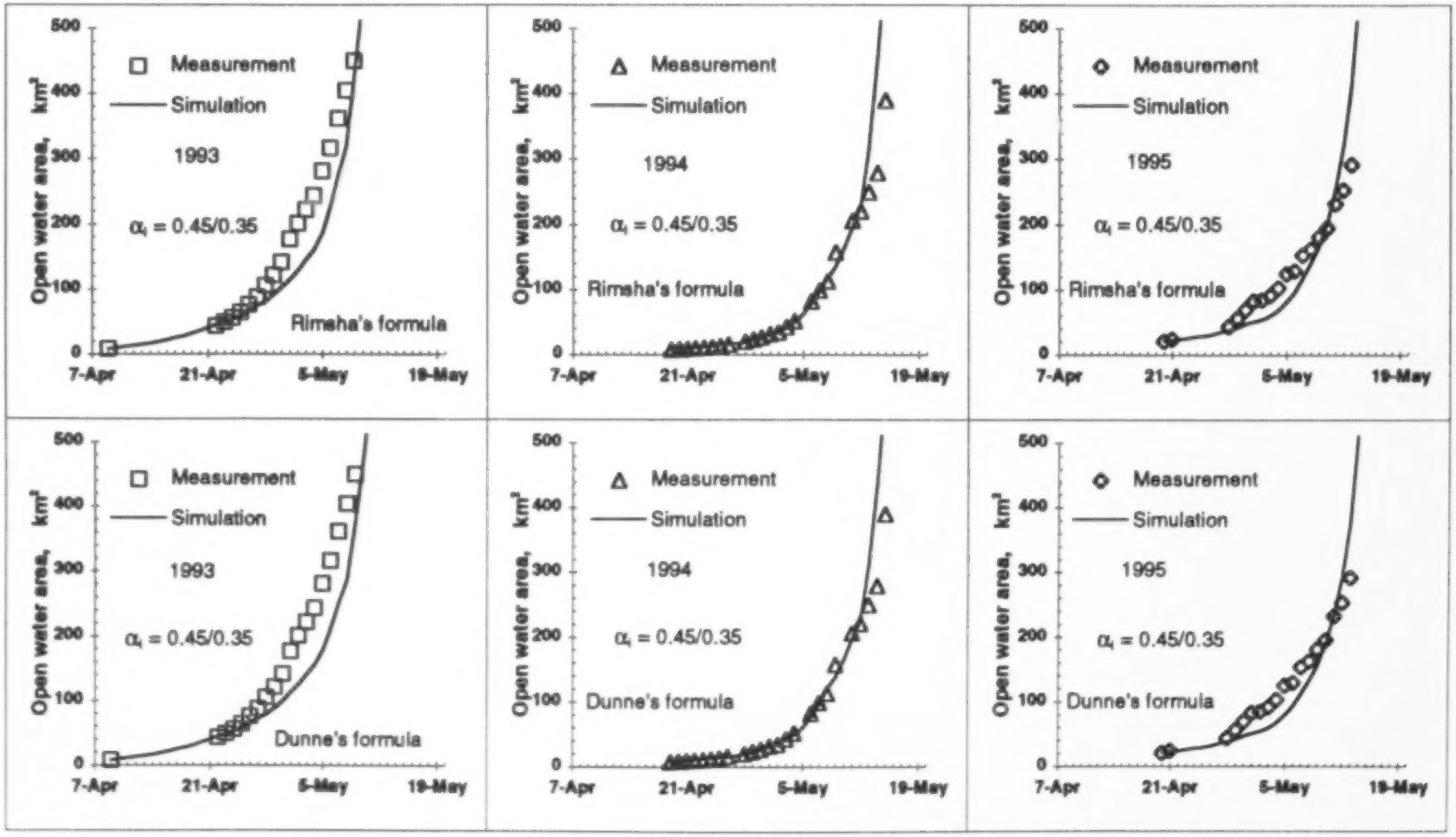

Figure 3.8 Typical surface albedo calibration, Energy Budget approach, Case C.

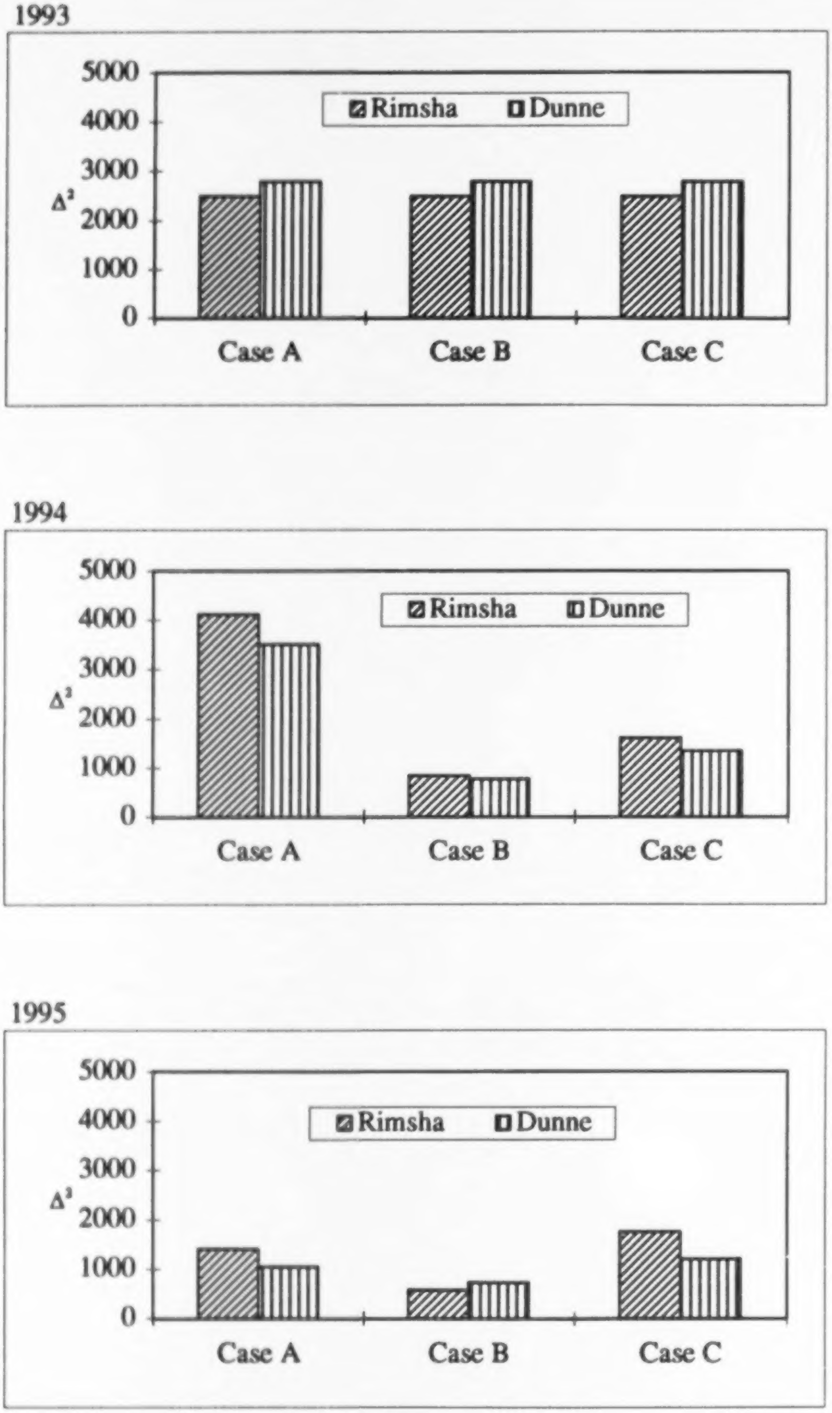

Figure 3.9 Variances, Δ^2, for the calibration of the E.B. method, albedo.

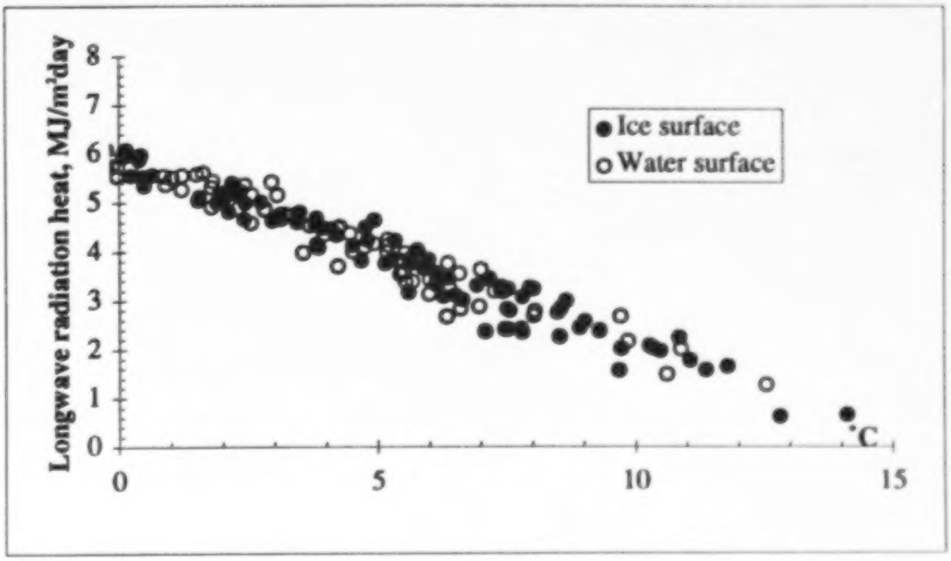

Figure 3.10(a) Longwave radiation heat change with the temperature difference between the air and the surface.

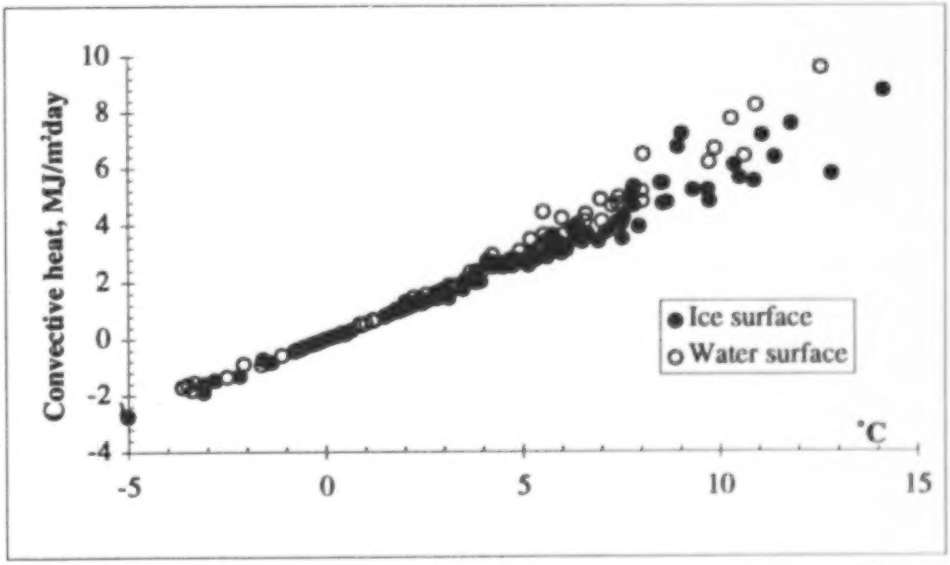

Figure 3.10(b) Convective heat change with the temperature difference between the air and the surface.

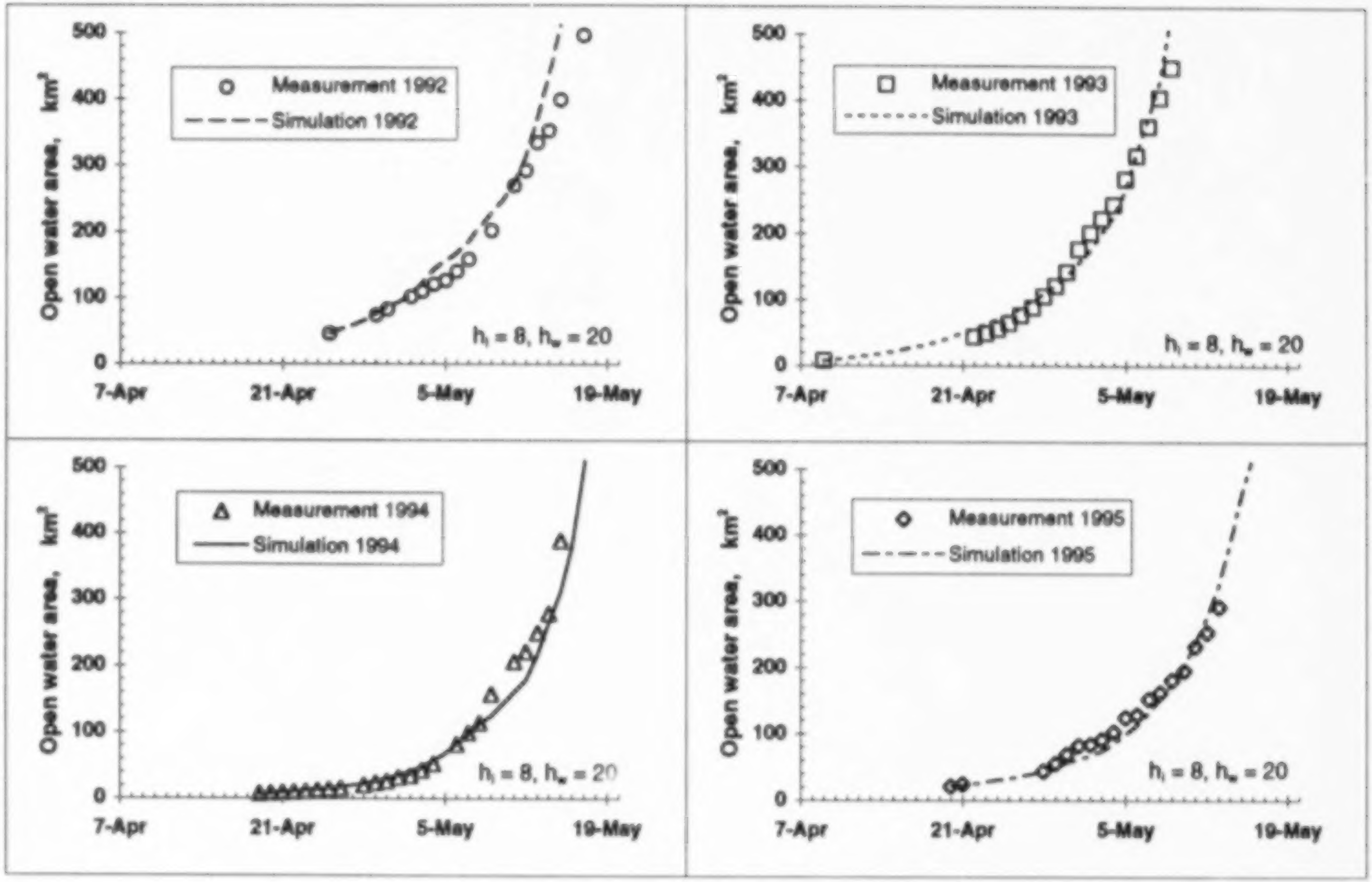

Figure 3.11 (a) Simulation of open water area development by conceptual model, Case A.

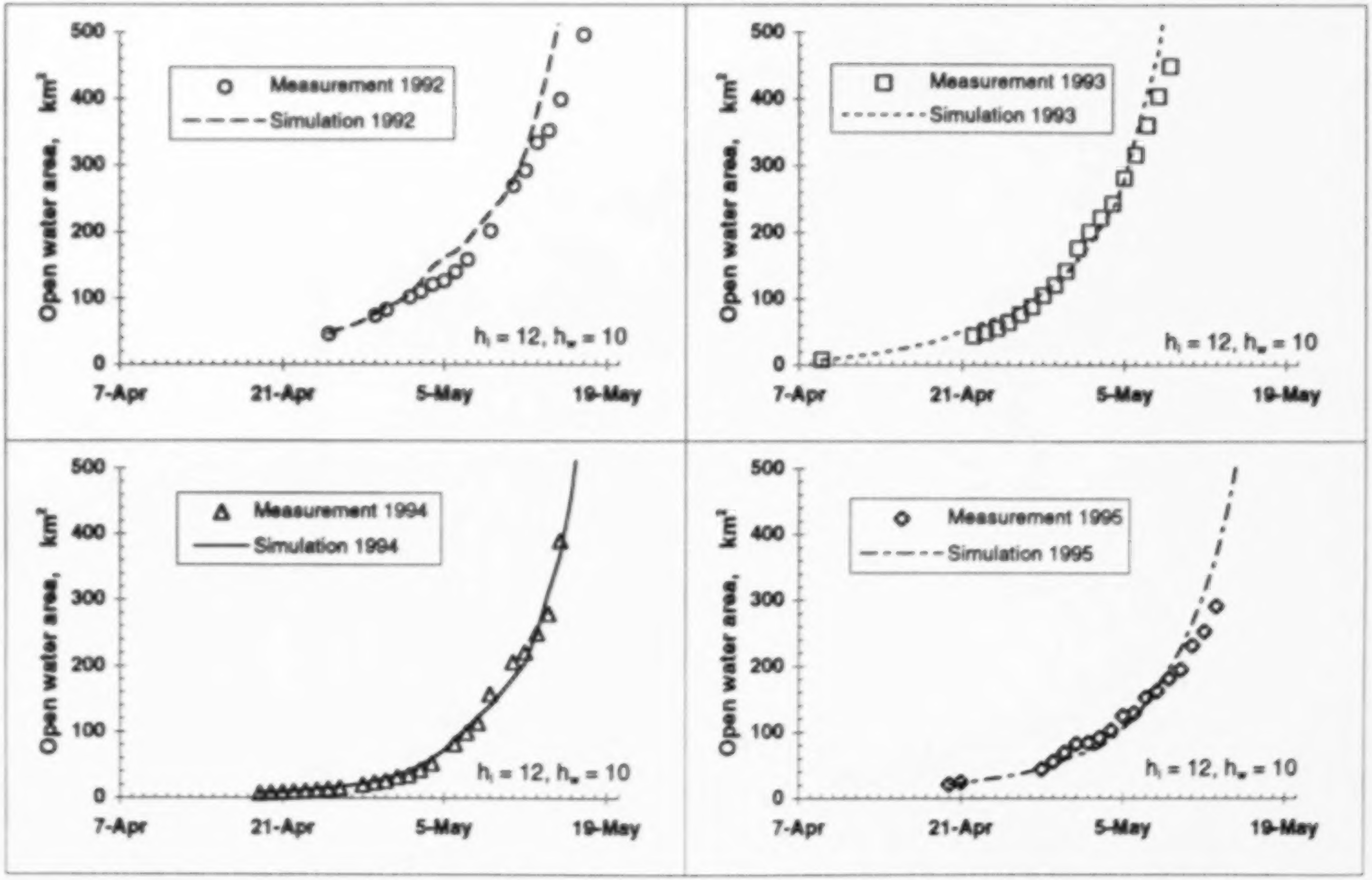

Figure 3.11 (b) Simulation of open water area development by conceptual model, Case A.

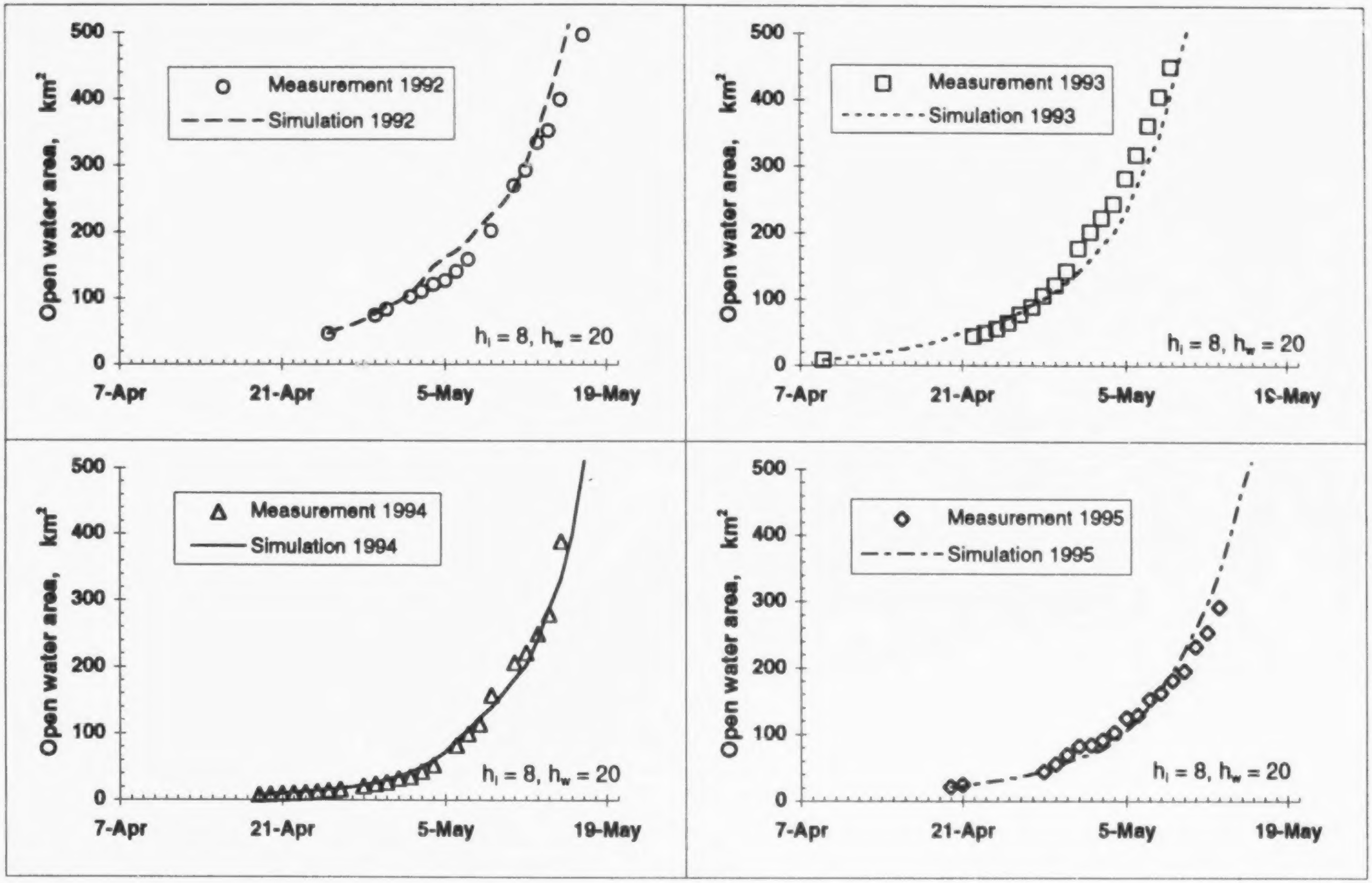

Figure 3.12 (a) Simulation of open water area development by conceptual model, CaseB.

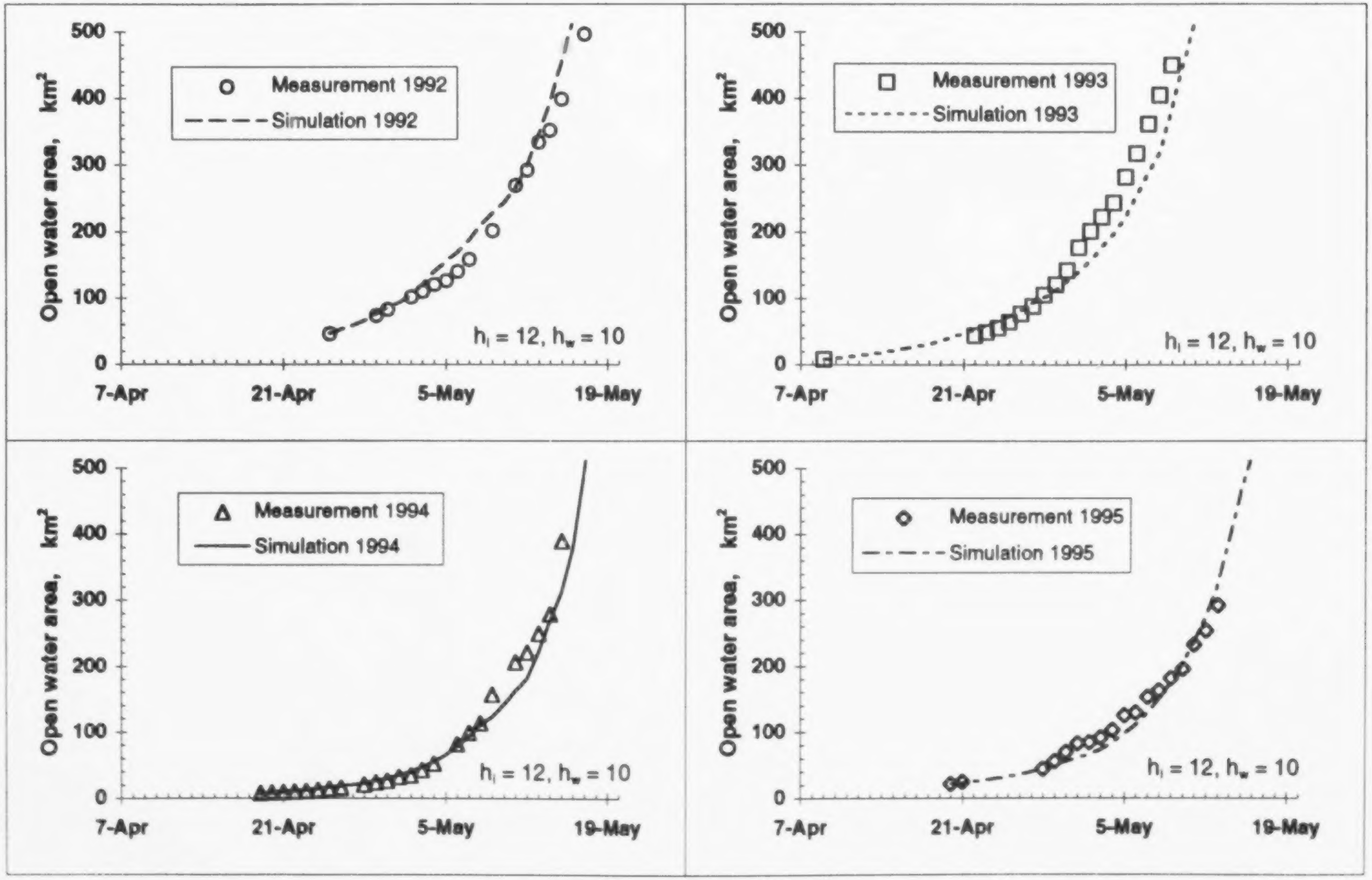

Figure 3.12 (b) Simulation of open water area development by conceptual model, Case B.

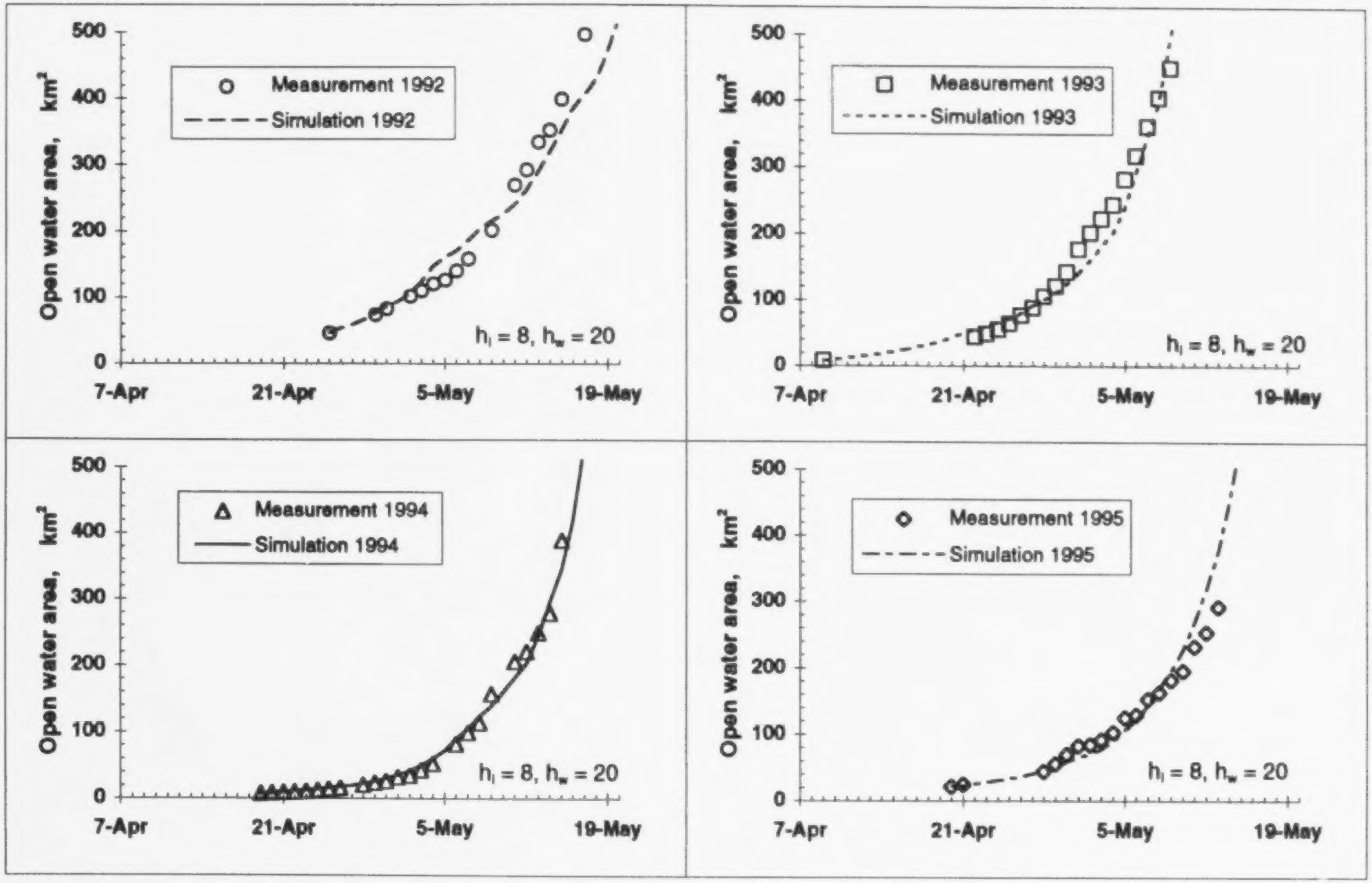

Figure 3.13 (a) Simulation of open water area development by conceptual model, Case C.

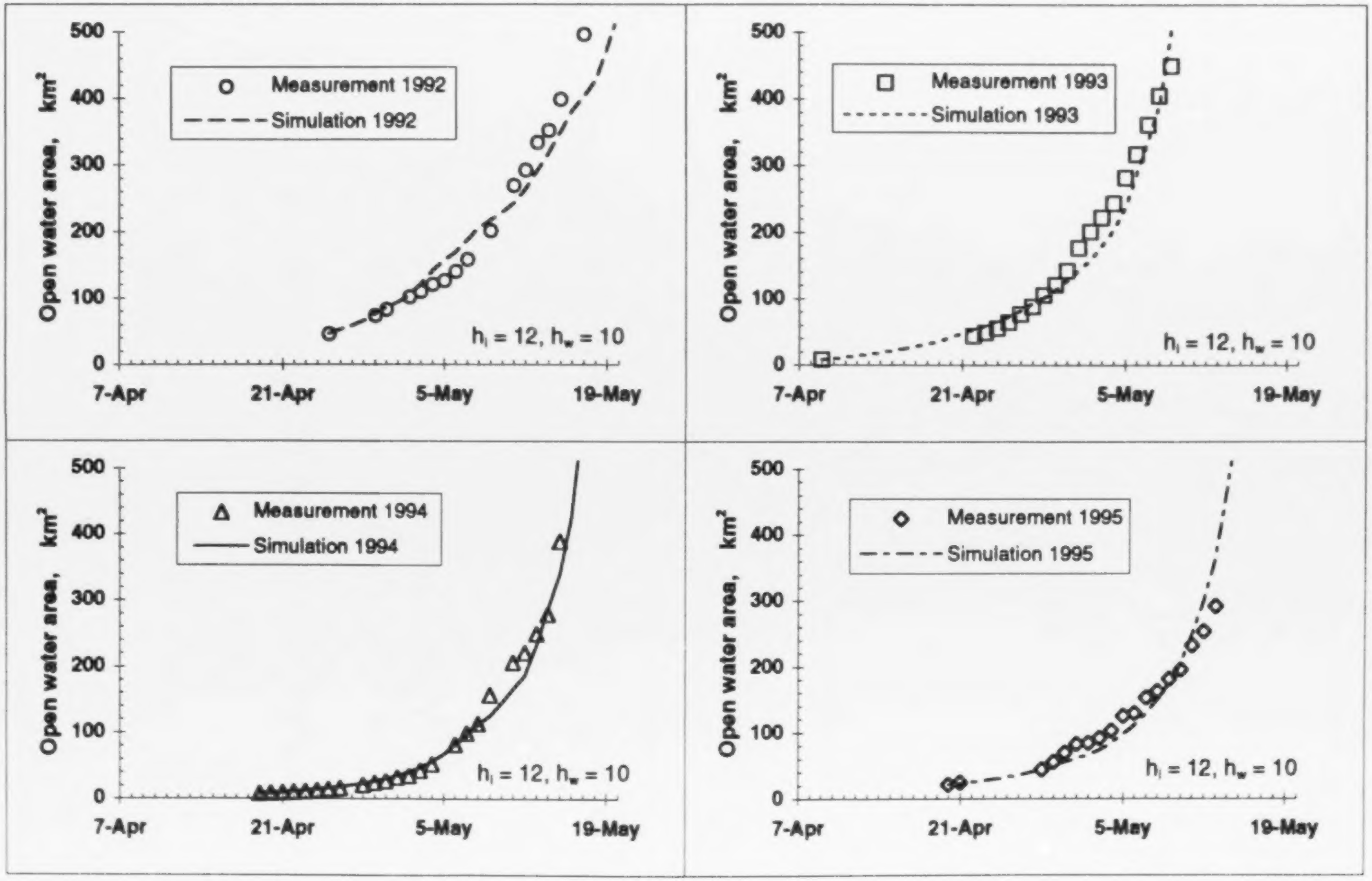

Figure 3.13 (b) Simulation of open water area development by conceptual model, Case C.

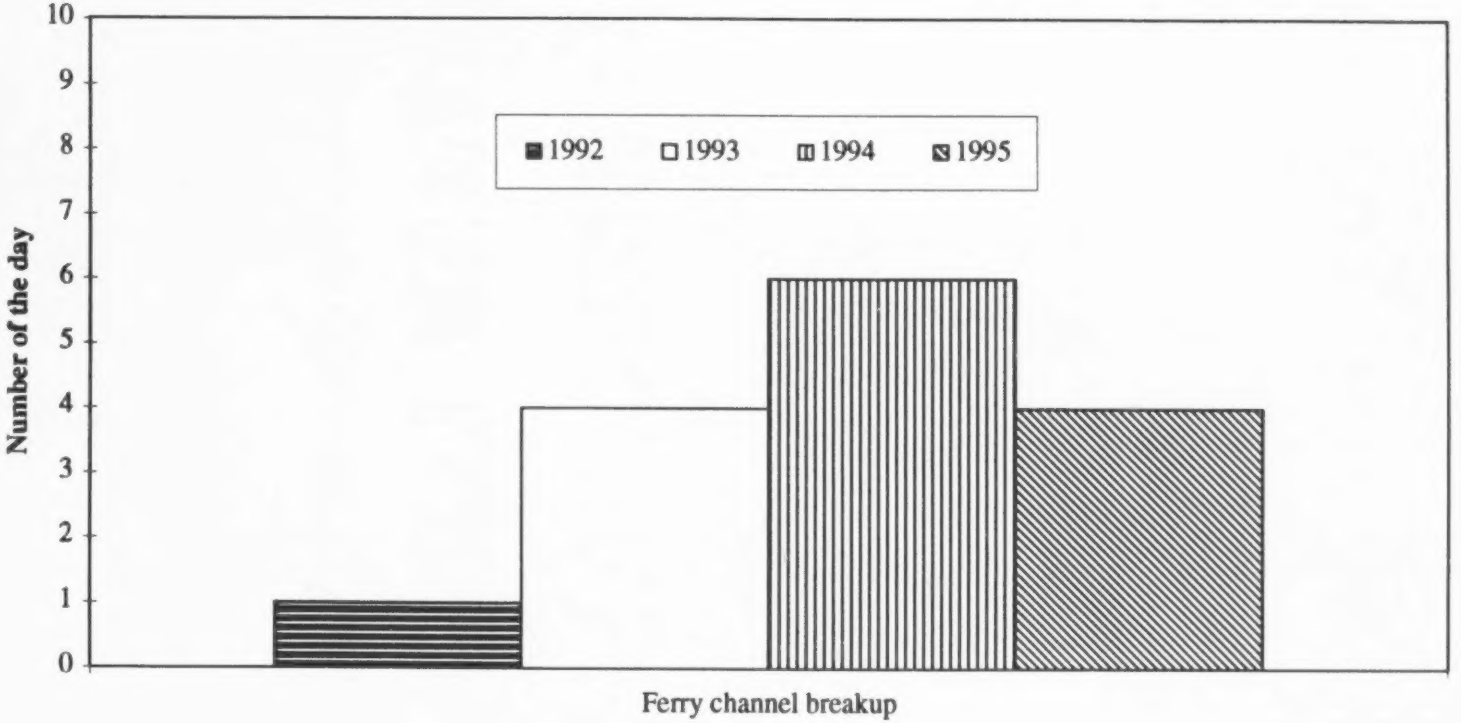

Figure 3.14 The relationship of Ferry channel breakup and Providence rapids breakup.

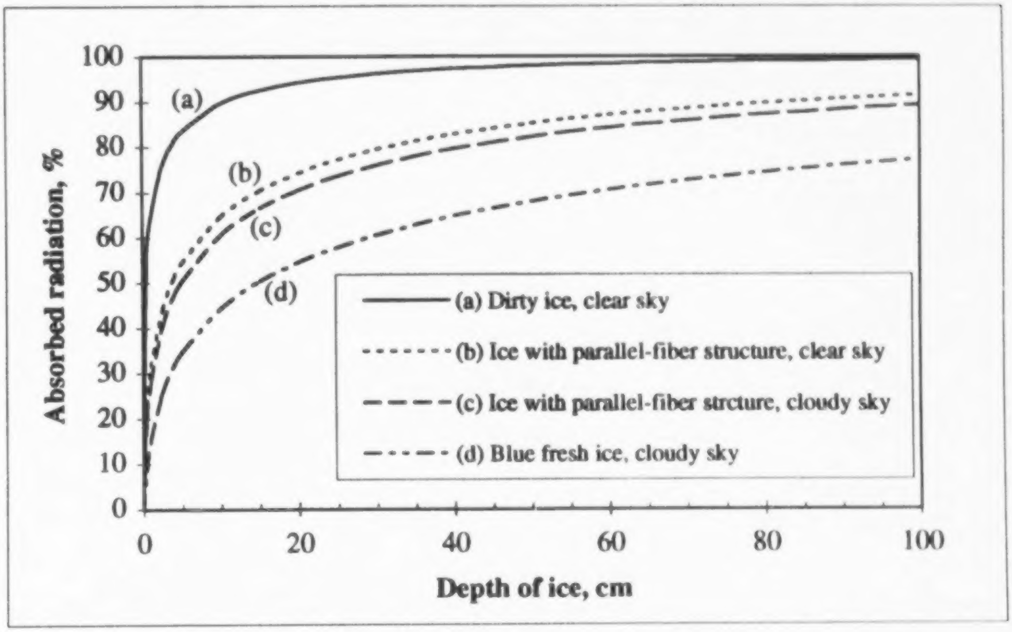

Figure 3.15 Solar radiation absorbed in an ice cover, Borisenkov (1970).

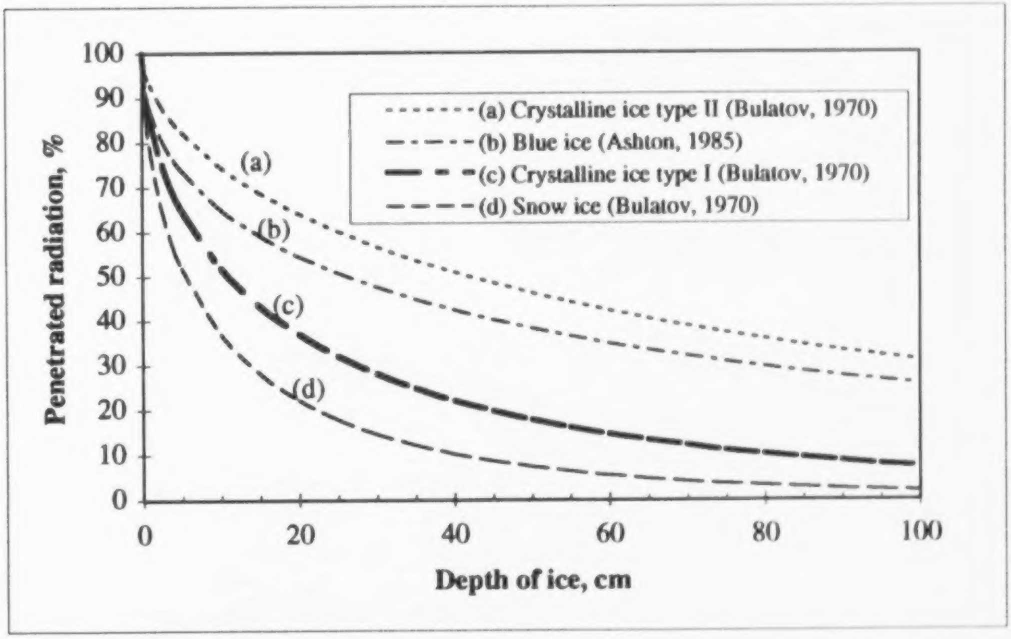

Figure 3.16 Solar radiation penetrating an ice cover, Bulatov (1970).

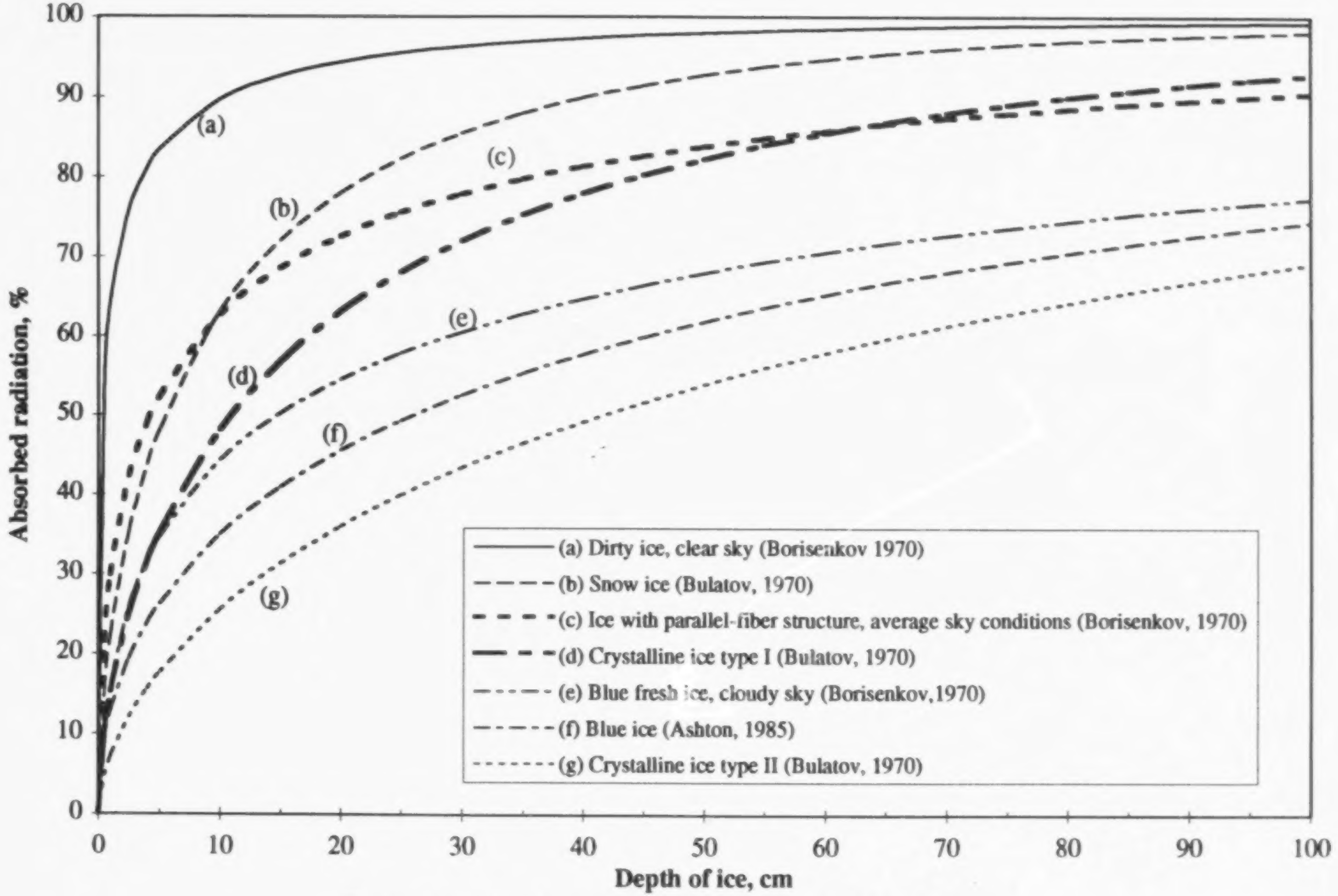

Figure 3.17 Absorbed radiation in different depth of ice cover.

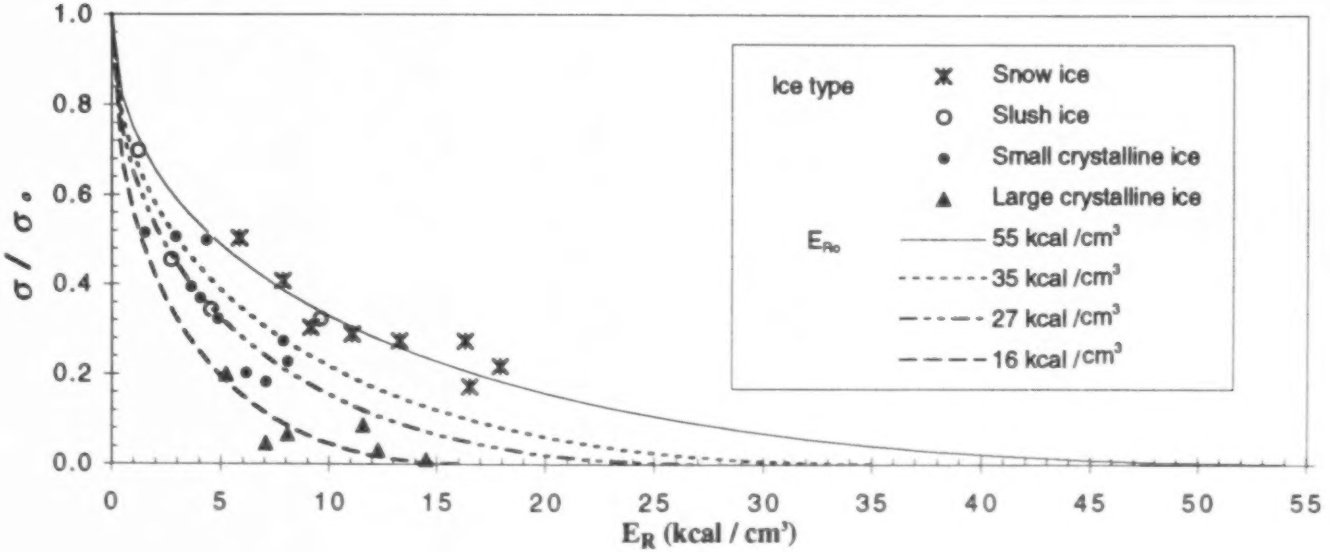

Figure 3.18 Strength reduction with increase in absorbed radiation (Bulatov, 1970).

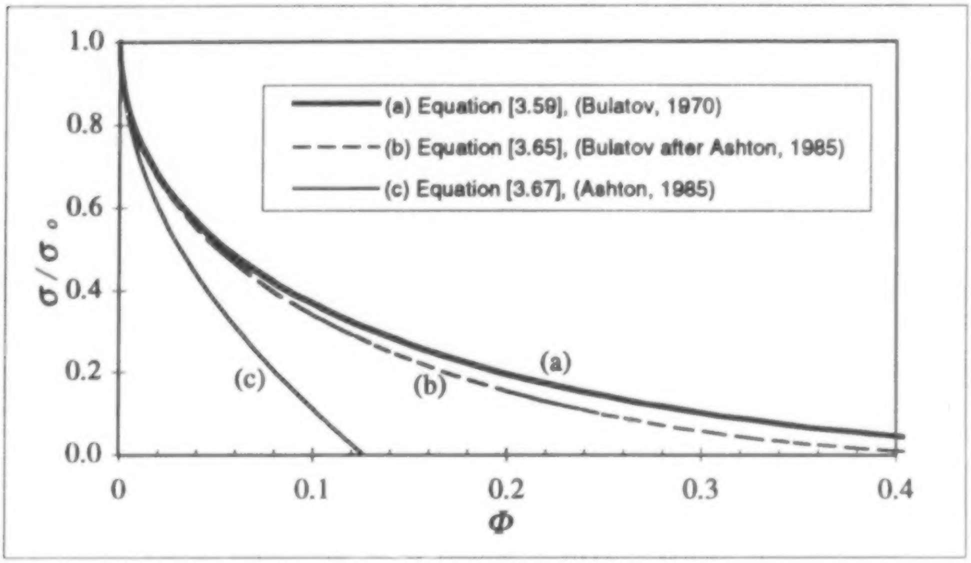

Figure 3.19 (a) Strength reduction with increase of porosity.

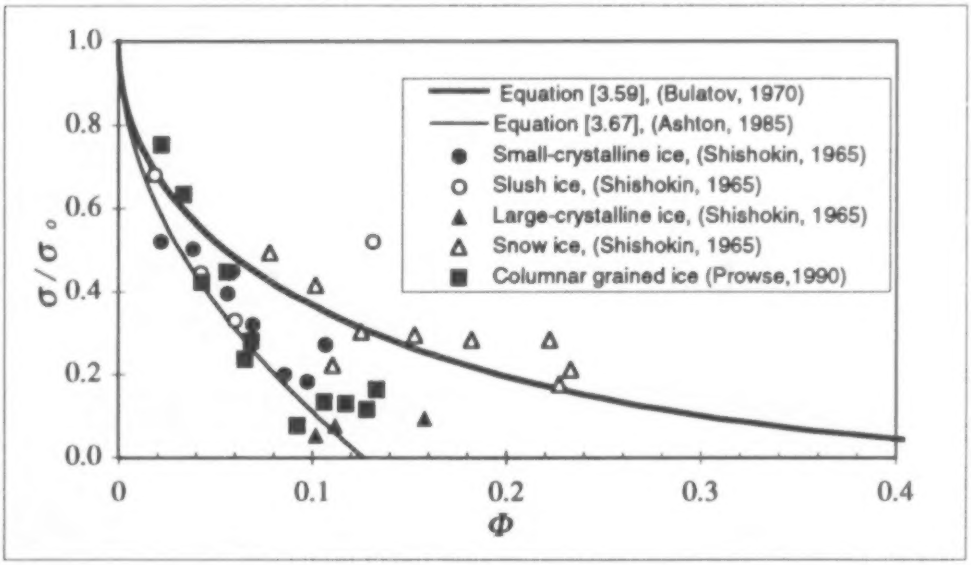

Figure 3.19 (b) Comparison of strength reduction models with field measurements.

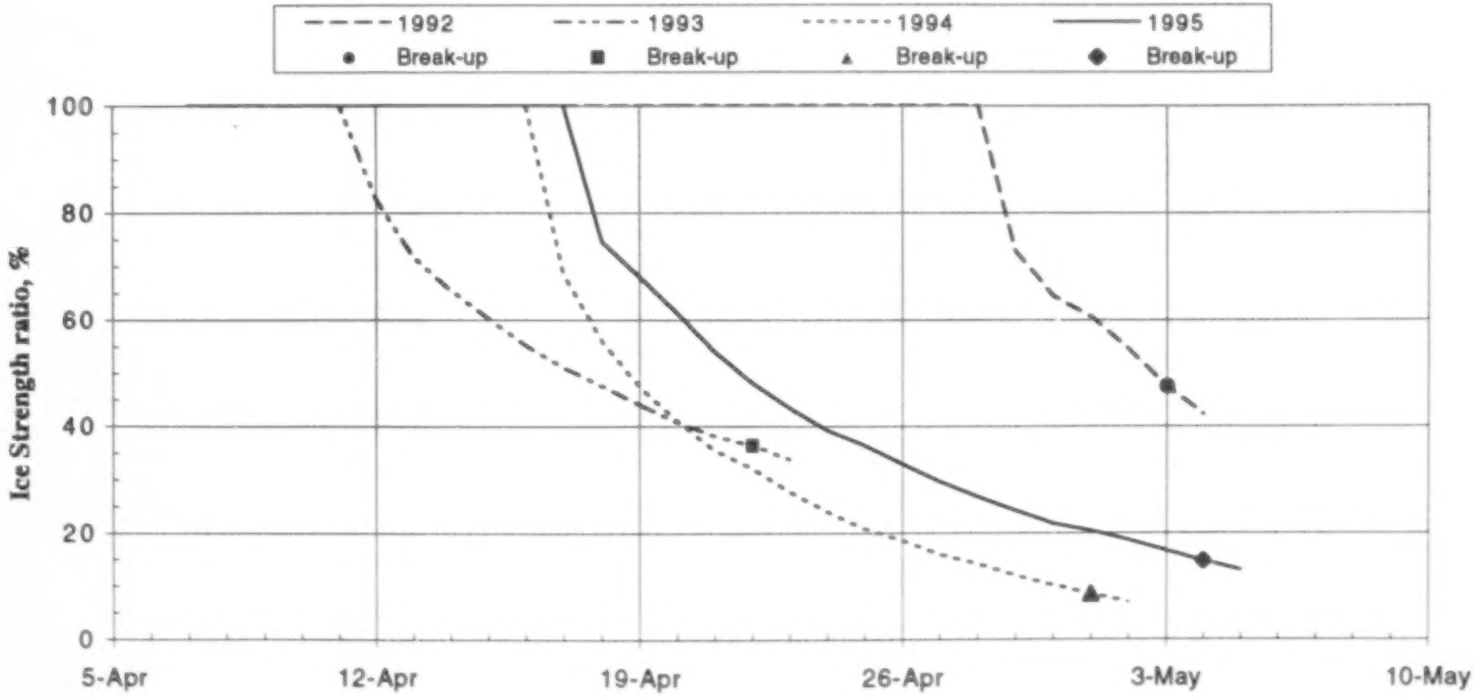

Figure 3.20 The reduction of the strength ratio, based on apportioned solar radiation.

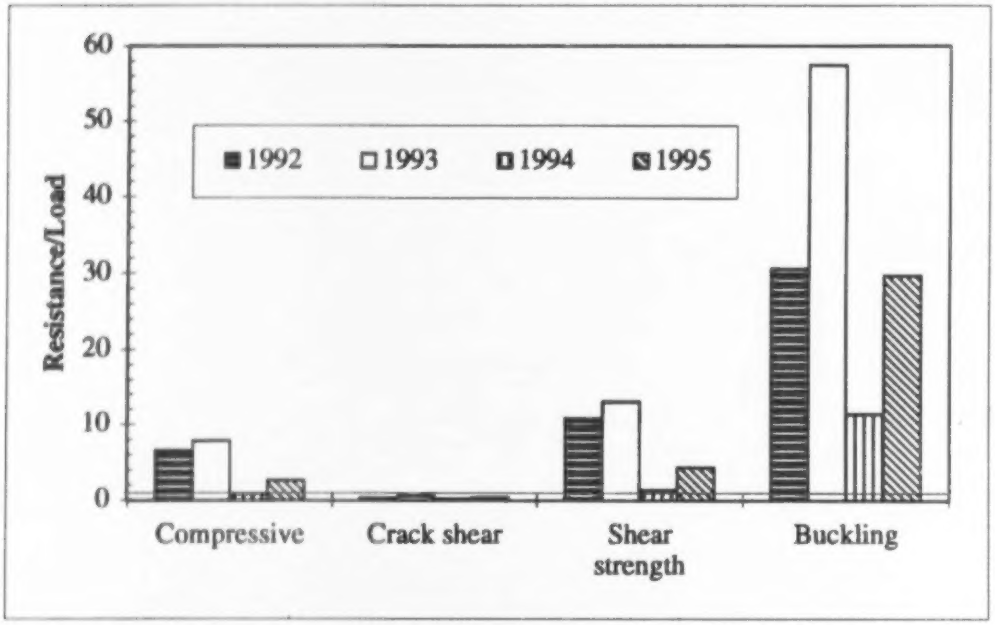

Figure 3.21 Comparison of the ratios obtained by the various failure mechanisms.

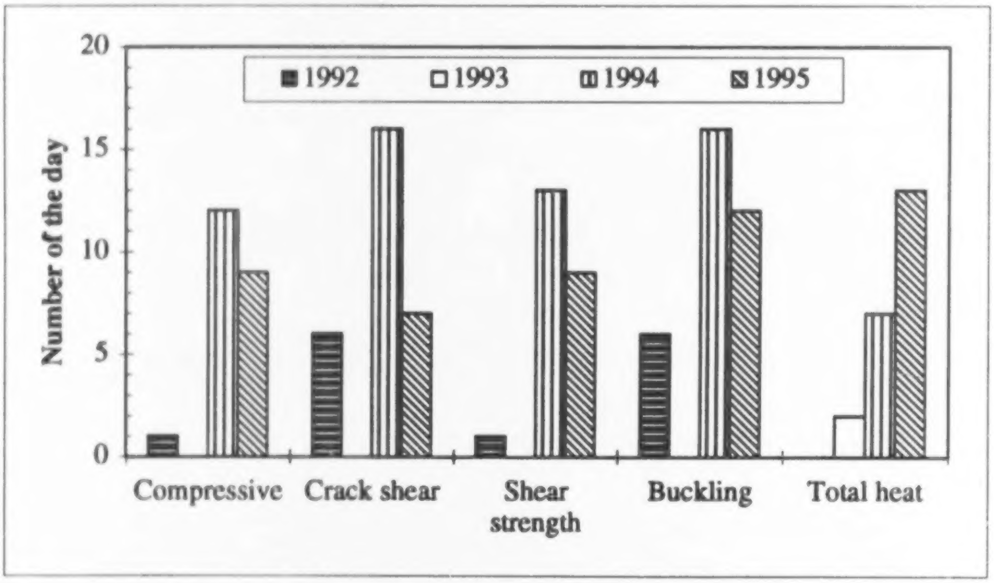

Figure 3.22 Lead time provide by the various approaches.

4.0 CONCLUSIONS AND RECOMMENDATIONS

Over the three years of this study, extensive observations of the sequence of ice deterioration and breakup were made. Together with the quantitative data collected, this facilitated the identification of two key sub-reaches, classified based on the mode of breakup: the *ferry reach* and the *Beaver Lake reach*. In the reach of the river where the ferry crosses the channel, breakup is predominantly dynamic. Upstream of this reach, breakup is predominantly thermal. The application of breakup modelling techniques began with the upstream reach, using two approaches: the energy budget approach and a linear heat transfer approach. Breakup modelling for the ferry reach was then examined, considering failure of the ice cover in compression, shear and buckling.

This study site provided an ideal situation for assessing current breakup modelling techniques. Results of the calibration of the breakup in the predominantly thermal upstream reach were used to help define the parameters in the thermal model of ice strength deterioration required for the dynamic breakup model in the ferry reach. As expected, discharge increases gradually through the breakup period, particularly in the early period prior to the initial movement of ice in the ferry reach. As a result, the loads on the ice cover were found to remain fairly constant over the breakup period, allowing for a more controlled examination of the strength deterioration and possible failure mechanisms.

4.1 Thermal Models of Breakup: Beaver Lake Reach

4.1.1 Energy Budget Approach

This approach considers all of the energy components providing or taking heat from the ice cover and, assuming that all can be accurately quantified, the net heat input to the ice cover is responsible for open water development. In this study, for practical reasons, the heat components from the river bed, flow drag and precipitation were assumed to be negligible. Additional assumptions were applied in order to satisfy a one-dimensional modelling approach and to provide necessary boundary conditions. The heat components considered in the model were: the net incoming short wave radiation heat; the long wave radiation heat; the heat expended for evaporation (or gained in condensation); the convective heat transfer between the air and the ice/water surfaces; and, the heat carried by the warm water coming from Great Slave Lake. Only three of the four years of data could be used to calibrate the model because the instruments used to measure humidity and wind speed were installed during the second year of the study.

Surface albedo was the only calibration parameter in the energy budget model. Because of the long period over which the thermal breakup in Beaver Lake occurs, two values of ice albedo were calibrated into the model. The albedo used in the early melt period was higher than the value used in the latter part, with the day of change based on the documented date on which the ice cover in this reach first displayed a significantly darker surface appearance. Although excellent results were obtained with the energy budget approach, in terms of the fit to the open water measurements, the calibrated albedos displayed no consistency from year to year, ranging from 0.25 to 0.50. These values are low based on a qualitative assessment of surface albedo in the field. The value of albedo obtained in 1993 was 20% lower than that in 1994 and 1995, likely because there was no snow on the ice cover at the beginning of the melt period in 1993.

Although the energy budget method is not difficult to apply, it is data intensive. Also, for data such as wind speed and humidity, daily averages of 24 discrete instantaneous measurements might not be that meaningful. Furthermore, relative humidity and wind speed are not straightforward to forecast. Given these factors and the variability in the calibrated surface albedo, the energy budget method is considered to be limited in its applicability as a forecasting model.

4.1.2. Conceptual Linear Heat Transfer Approach

In the conceptual modelling approach, a simple linear relationship between temperature gradient and heat transfer is assumed, and a simplified energy budget (neglecting longwave radiation and evaporation) is considered. This approach is more convenient than the full energy budget approach as it uses only solar radiation, air temperature, discharge and lake water temperature as input data.

In this approach, the parameters to be calibrated were: the heat transfer coefficient between the air and the ice cover; the heat transfer coefficient between the air and the water surface; and the albedo of the ice (snow) surface. Based on a preliminary series of calibration runs, consistent values of the ice surface albedo were established for the four years. The albedo of the ice cover was taken as 0.9 for the early melt period, and 0.7 after the ice surface darkened noticeably. These values were higher than those determined for the energy budget approach, because in the conceptual approach this parameter must account for the effects of longwave radiation and evaporation.

Nine different combinations of the two heat transfer coefficients were considered in the ensuing calibration. The values examined for the heat transfer coefficient between the air and the ice cover ranged between 4 to 12 W/m^2°C, and the values considered for the heat transfer coefficient between the air and the water surface ranged from 10 to 20 W/m^2°C.

The results of the calibration show that the best combinations of the coefficients were

$$h_i = 8\ \mathrm{W/m^2{}^\circ C},\ \ h_w = 20\ \mathrm{W/m^2{}^\circ C}\ \text{and}\ h_i = 12\ \mathrm{W/m^2{}^\circ C},\ \ h_w = 10\ \mathrm{W/m^2{}^\circ C}.$$

In all cases and for all combinations of the heat transfer coefficients, there was a conflict between the 1993 and the 1995 data, in that improving the fit for one could not be done without worsening the fit for the other. Despite this difficulty, it was still possible to obtain a good fit for a single set of calibrated parameters, something that was not possible with the energy budget approach. Therefore it was concluded that the conceptual approach is the preferred method for modelling the thermal development of open water.

4.2 Dynamic Models of Breakup: Ferry Reach

4.2.1 Models of Ice Deterioration

Ice strength reduction is caused mainly by solar radiation penetrating the ice cover, melting the ice crystals first at their boundaries and thus reducing strength by increasing the ice porosity. Previous researchers (Borisenkov, 1970; Bulatov, 1970; and Ashton, 1985) have shown that most of the solar radiation is absorbed in the top layer of the ice cover. For ice comprised of a combination of ice with a paralleled-fiber structure, crystallized (frazil) ice, and a surface layer of snow ice (basically the ice type in this study) they have determined that about 75 % of the net incoming solar radiation is absorbed in top 0.3 m of the ice cover, and 10 % of solar radiation passes directly through a one meter thick ice cover. Consequently the porosity in the top layer of a deteriorating ice cover is higher than that at the bottom. This effect has been observed in the broken ice cover at this site.

Bulatov (1970) and Ashton (1985) derived equations relating porosity and ice strength, based on simple intergranular melt models. Ashton's equation, based on a hexagonal-grain melt model, predicts that the strength of ice cover drops rapidly with increasing porosity producing a lower envelop to the available data (Shishokin, 1965, Prowse, 1990)which is too conservative to be used in practice. Bulatov's cubic-grain melt model provides a better fit to the available data and was therefore used in this study. Another attractive feature of Bulatov's model is that one can obtain the strength ratio directly from the net incoming solar radiation, eliminating the intermediate calculation of porosity.

4.2.2 Criteria for Ice Cover Failure

Four mechanisms of ice cover failure were considered in this study: failure due to crushing of the ice cover; failure in shear along hinge cracks parallel to the banks; shear failure of an intact ice cover along planes parallel to the bank; and buckling failure. The ratios of the resistance of the ice cover to the imposed loads were evaluated for each case, both for the period prior to the initial movement of ice, and at the time of the initial movement of ice. The ratio, which should decrease over time and approach one at the time of incipient failure varied as follows:

Type of Failure	**Ratio at the Time of the Initial Movement of Ice**
Compression	0.8 to 7.8
Crack shear	0.21 to 0.48
Internal shear	1.3 to 13.0
Buckling	11.4 to 56.6

The high ratios obtained for the buckling failure analysis indicate that this failure mechanism is not appropriate for this site. The values obtained in the analysis of crack shear were less than one from the commencement of melt, indicating that shear resistance along hinge cracks plays little or no role in preventing the initial movement of ice at this site. The values for the ratio obtained based on failure in compression and shear failure are consistent with each other in that they vary from each other by a consistent factor (about 1.6), which is to be expected, given that the same approach is used to calculate the deteriorated strength of the ice as a result of thermal influences.

Comparing the four criteria, compressive failure appears to be the most reasonable choice. However, the assumption that there is no shear restraining the ice cover parallel to the bank is not strictly accurate. If the compressive resistance and the crack shear resistance are combined, the ratio values vary from 0.97 to 8.3 for the four years of data. Unfortunately, taking the envelop (largest) value of the ratio as the conservative estimate would produce predictions of the initial movement of ice almost two weeks too early in the worst case. Thus none of these dynamic models of breakup can be considered suitable.

It was found that none of the four approaches were better that the simple cumulative heat input approach, which accounts only for total heat input. This is not unexpected, as loads on the ice cover would only be expected to increase through the breakup period in response to increasing discharge (which increases both the fluid drag on the underside of the ice cover and the slope of the water surface) and it has been determined that discharge increases only gradually here due to the storage effects of Great Slave Lake.

The lack of consistency from year to year can be attributed to a number of factors including non-uniformity in the ice thickness, open leads in the ice cover through Providence Rapids, and varying snowmelt conditions. These factors are of importance both in terms of the difficulties associated with obtaining representative data and in terms of the limitations of the one-dimensional modelling approach used here. Consequently, more detailed data collection is not sufficient. New models are required which take into account such two-dimensional effects. Therefore, in terms of forecasting breakup at this particular site, further research would be necessary to develop a reliable deterministic model of breakup at Providence Rapids.

Fortunately, it appears that this initial ice movement provides the physical mechanism for the initiation of breakup in the ferry reach (fluctuating water levels due to successive consolidation of the disturbed ice cover), and so from a practical perspective it provides a very reliable forecast of major ice movements at the ferry crossing (within 1 to 6 days). Unfortunately, given the simplicity of this particular case, it is not likely that the currently available modelling approaches have much potential. Until more sophisticated models of breakup are developed, forecasts will continue to be largely based on site specific breakup patterns, as in this case.

REFERENCES

Anderson, E.R., Energy Budget Studies, Geological Survey Professional Paper 269, United States Government Printing Office, Washington, 1954, pp 71-119.

Andres, D.D., Observation and prediction of the 1986 breakup on the Athabasca River upstream of Fort McMurray, Alberta, Alberta Research Council Report No. SWE-88/03, 1988.

Ashton, G.D., Deterioration of floating ice covers, Journal of Energy Resources Technology, Vol. 107, 1985, pp 177-182.

Ashton, G.D. (editor), River and Lake Ice Engineering, Water Resources Publications, Colorado, 1986, 485 pp.

Bohren C.F. and R.L. Beschta, Snowpack albedo and snow density, Cold Regions Science And Technology, 5, 1981, pp 119-125.

Borisenkov, E.P., (editor), Thermal interaction of the atmosphere and the hydrosphere in the Arctic, Gidrometeorologisheskoye Izdatel'stvo, Leningrad,1969. Translated from Russian, Israel Program for Scientific Translations, Jerusalem, 1970.pp 36-37.

Brunt, D., Physical and Dynamical Meteorology, Cambridge University Press, 1934, 411 pp.

Bulatov, S.N., Calculating the strength of thawing ice cover and the beginning of wind activated ice drift, Trudy Vypysk, 74, Gidrometeorologisheskoye Izdatel'stvo, Leningrad,1970. Translation by US Army CRREL, IR 799, 120 pp.

Canada Centre for Surveying, 1992 Guideline and Specifications for GPS Surveys. Geodetic Survey Division, Surveys, Mapping and Remote Sensing Sector, Release 2.1.

Chen, X, Ice effects of ice the hydraulics of the Mackenzie River at the outlet of Great Slave Lake, NWT, thesis submitted in partial fufillment of the degree of M Sc, Department of Civil Engineering, University of Alberta, 1993.

Chow, Ven Te., Open-Channel Hydraulics, University of Illinois, McGraw-Hill Book Company, 1959, 679 pp.

Department of Fisheries and Oceans, Great Slave Lake and Mackenzie River (Fifth edition), Minister of Supply and Services Canada, Ottawa, Canada, 1981, 159 pp.

Department of Transportation, N.W.T., Spray Ice - Program Evaluation and Review, 1992.

Dunne, Thomas and Leopold, L.B., Water in Environmental Planning, San Francisco: W. H. Freeman, 1978, 818 pp.

Eagleson P.S., Dynamic Hydrology, McGraw-Hill Book Company, 1970, 461 pp.

Ferrick, M.G. and D.N. Mulherin, Framework for control of dynamic ice breakup by river regulation, U.S. Army Corps of Engineers, CRREL Report 89-12, 1989, pp.1-14.

Foerstel, H. (secretary, Mackenzie River Basin Study Committee), 1981. Mackenzie River Basin Study Report, a report under the 1978-81 Federal-Provincial Study Agreement respecting the water and related resources of the Mackenzie River Basin, 233 pp.

Gerard, R., A simple field measure of ice strength, Proc. 3rd International Symposium on Ice Problems, Hanover, New Hanpshire, USA, 1975. pp. 589-600.

Gerard, R., D.C. Sego and T.M. Hrudey, Aspects of the use of spray ice in ice bridge construction, Mackenzie River at Ft. Providence, N.W.T., Water Resources Engineering Report, Department of Civil Engineering University of Alberta, Edmonton, Alberta, 1990, pp. 1-7.

Gray, D.M.(editor), Principles of Hydrology, Secretariat, Canadian National Commettee for the International Hydrological Decade, 1970.

Gray, D.M. and D.H. Male (editors), Handbook of Snow, Pergamon Press, Toronto, Canada, 1981, 776pp.

Gray, D.M. and T.D. Prowse, Snow and Floating Ice, Handbook of Hydrology, McGraw-Hill, Inc, New York, USA., 1993, pp. 7.1-7.58.

Grenfell, T.C. and Maykut, G.A., The optical properties of ice and snow in the Arctic basin, Journal of Glaciology, Vol. 18, No. 80, pp. 445-463.

Halliday, D. and Resnick, R., Fundamentals of Physics, John Wiley and Sons, Inc. New York, 1988. 977 pp.

Hetenyi, M. I., Beams on Elastic Foundation, The University of Michigan press; London, G. Cumberlege, Oxford university press, 1946, 255 pp.

Hicks, F.E. and D.D. Andres, 1992 breakup observations on the Mackenzie River at the Ft. Providence ferry crossing, Water Resources Engineering Report No. 92-5, Department of Civil Engineering, University of Alberta, Edmonton, Alberta, 1992.

Hicks, F.E. and D.D. Andres, 1993 breakup observations on the Mackenzie River at the Ft. Providence ferry crossing, Water Resources Engineering Report No. 94-H1, Department of Civil Engineering, University of Alberta, Edmonton, Alberta, 1994.

Hicks, F.E. and D.D. Andres, 1994 breakup observations on the Mackenzie River at the Ft. Providence ferry crossing, Water Resources Engineering Report No. 95-H1, Department of Civil Engineering, University of Alberta, Edmonton, Alberta, 1995.

Knight, C.A., Studies of Arctic lake ice, Journal of Glaciology, Vo. 4, No. 33, 1962, pp. 319-355.

Leick, A., 1990. GPS Satellite Surveying, Wiley-Interscience, Toronto.

Michel, B., Ice Mechanics, Les Presses de L'universite Laval, Quebec, 1978, 499 pp.

Nezhikhovskiy, R. A., Coefficients of roughness of bottom surface of slush-ice cover, Soviet Hydrology: Selected Papers, No. 2, 1964, pp. 127-150.

Panofsky, Hans A. and Huhn A. Dutton, Atmospheric Tubulence, The Pennsylvania State University, John Wiley & Sons, Inc. 1984, 397 pp.

Priestley C.H.B., Tubulent Transfer in the Lower Atmosphere, The University of Chicago Press, 1959, 130 pp.

Prowse, T.D. and P. Marsh, Thermal budget of river ice covers during breakup, Canadian Journal of Civil Engineering, Vol.16, 1989, pp 62-71.

Prowse, T.D., M.N. Demuth and H. A. M. Chew, Changes in the flexural strength of ice under radiation decay, Nordic Hydrology, 21, 1990, pp 341-354.

Shishokin, S. A., Ice deterioration under the influence of solar radiation, Enviroment Canada Translation 00ENV-2608: Trudy Koordinatsionnykh Soveshchanii Po Gidrotekhnike, Transactions of the Coordination Meetings on Hydraulic Engineering, 1965, 23: pp 137-143.

Shuttleworth, W. J., Evaporation, Handbook of Hydrology, McGraw-Hill, Inc, New York, USA., 1993, pp. 4.1-4.53.

U.S. Army Corps of Engineers, Snow Hydrology, North Pacifice Division, Corps of Engineers, U.S. Army, Portland Oregon, 1959, 437 pp.

Wunderlich, W.O., Heat and mass transfer between a water surface and the atmosphere, Tennessee Valley Authority Engineering Laboratory, Norris Tenn., Report no 14, 1972.